Structural and functional investigation of the organic anion transporting polypeptide 1B1 (OATP1B1)

Jennina Charlotte Taylor-Wells

Thesis submitted to Oxford Brookes University in partial fulfilment of the requirements of the award of Doctor of Philosophy

In collaboration with AstraZeneca

February, 2013

Dedication

I would like to dedicate this work to my parents and grandparents who have taught me to work hard and question the world, without you this work would not have been possible. Thank you.

Acknowledgements

Throughout this PhD I am truly grateful to many colleagues and friends who imparted their knowledge and supported me.

I would like to thank my supervisors David Meredith and Sarah Kelly for their constructive advice regarding the project and for reading many drafts of this thesis. I would like to thank Dan Caley and Ryan Pink for introducing me to cell culture and for answering my unending questions on the subject. Big thanks also to Katie Towers for teaching me immunofluorescence and John Runions for the essential training and advice on the microscope (as well as lending me his laptop when mine broke during the write up!). Thanks also to those who helped get my molecular biology skills on track, including Imogen Sparkes, Maria Shvedunova and Myrtani Pieri. Big thanks to Simon Giles who made me a fantastic aspirator that saved me lots of plate washing time and Michelle Rawlings who was a fantastic support and friend in the lab, I really appreciate all those last minute orders and autoclaving you helped me with!

I am really lucky to have worked alongside some fun and caring students and post-docs whose attitudes and advice have made the office a community. Thanks Anish Senan, Samantha Barry, Vidya Pawar-Menon, Petra Kiviniemi, Alessandra Rocchetti, Frances Tolmie, Louise Hughes and Katie Towers.

A very special thank you goes to Isabel Bermudez-Diaz, whose unbelievable work ethic and unwavering support for me has improved my confidence and helped me to face the final year of my PhD. I genuinely couldn't have done it without you! Thank you so much.

Finally thank you to all my friends and family who have supported me through the last four years of the emotional turmoil that is a PhD; Mum, Dad, Mike and my best friend and boyfriend Dan.

Abstract

Membrane transport proteins are the gatekeepers of the cell membrane, transporting compounds in and out of the cell. The organic anion transporting polypeptides (OATPs) are a family of transport proteins expressed in a variety of tissues, including absorptive / excretory cells of the liver and kidney. OATPs transport an array of endogenous and xenobiotic compounds including bile salts, thyroid hormones, statins and anti-cancer drugs. Therefore this protein family play an important role in cell homeostasis and drug disposition, and are implicated in disease and drug-drug interactions. However there is little information available regarding the structural properties of OATPs, which would reveal how the proteins fold and bind to substrates. To help further this understanding, the topology and signature sequence of the hepatocyte specific isoform OATP1B1 have been investigated using a HEK293T cell model.

OATP1B1 was expressed in HEK293T cells and transport assayed using the substrate estrone-3-sulfate. Topology prediction programs were employed to map the transmembrane domains (TMs), which predicted a consensus of 12TMs with internal amino (N) and carboxyl (C) termini. The topology was studied experimentally using a FLAG epitope system, whereby the FLAG epitope was inserted into the putative extracellular/intracellular and terminal regions of the protein. Detection of FLAG antibody binding was quantified by luminometry and visualised qualitatively using confocal microscopy. Results revealed that the predicted internal N and C termini of the protein were external, in contrast to the predictions and current literature. A novel model has been generated from this data, encompassing these results and the current literature.

All OATPs contain a conserved 13 amino acid signature sequence (D-X-RW-(I,V)-GAWW-X-G-(F,L)-L) which spans the putative extracellular loop 3 and TM6, the function of which is not known. Six conservative mutations were made using site-directed mutagenesis; D251E, R253K, W254F, W258/259F and N261A. Kinetic, luminometric and immunofluorescence analysis revealed

that all mutations except N261A reduced transport and expression on the membrane. The reduction in expression combined with the presence of structurally important arginine and tryptophan residues at the extracellular/TM interface indicate that this sequence may be important for membrane anchoring and/or protein folding. This knowledge of OATP structure and function is imperative to the understanding the role of these proteins in the binding of endogenous and xenobiotic compounds.

Table of contents

List of Figures

List of tables

List of appendices

List of abbreviations

ABC	ATP-binding cassette
ADME	Absorption, distribution, metabolism and excretion
AhR	Aryl hydrocarbon receptor
APC	Amino acid-polyamine-organocation
BCRP	Breast cancer resistance protein
BSA	Bovine serum albumin
BSEP	Bile salt export pump
BSP	Bromosulfophthalein
CAR	Constitutive androstane receptor
CCK-8	Cholecystokinin octapeptide
CHO	Chinese hamster ovary
CMV	Cytomegalovirus
CPA	Cation:proton antiporter/anion
CPM	Counts per minute
CYP	Cytochrome P450
DAPI	4',6-Diamidino-2-phenylindole dihydrochloride
DDI	Drug-drug interaction
DHEAS	Dehydroepiandrosterone sulphate
DMSO	Dimethyl sulfoxide
DPM	Disintegrations per minute
DT	Distal tubule
E17βG	Estradiol-17β-glucuronide
E3S	Estrone-3-sulfate
EC	Enzyme classification
EGTA	Ethylene glycol tetraacetic acid
FITC	Fluorescein isothiocyanate
Fmol	Femtomole
FXR	Farnesoid-X-receptor
GFP	Green fluorescent protein
HEK	Human embryonic kidney
HGNC	Human genome nomenclature committee
HIV	Human immunodeficiency virus
HMG-CoA	3-hydroxy-3-methyl-glutaryl-CoA reductase
HNF-1α	Hepatocyte nuclear factor-1α
HNF-3β	Hepatocyte nuclear factor-3β
HRP	Horseradish peroxidase
IFN-γ	Interferon γ
Il-1β	Interleukin-1β
Il-6	Interleukin-6
K_m	Michaelis constant
MCT	Monocarboxylate transporter
MDR	Multidrug-resistance protein
MFS	Major facilitator superfamily
MRP	Multidrug resistance-associated protein
NCBI	National center for bioinformatics information
NSAID	Non-steroidal anti-inflammatory drug

NTCP	Na^+ taurocholate cotransporting polypeptide
OAT	Organic anion transporter
OATP	Organic anion transporting polypeptide
OCT	Organic cation transporter
PBS	Phosphate buffered saline
PCR	Polymerase chain reaction
PepT1	Peptide transporter 1
Pgp	P-glycoprotein
PKA	Protein kinase A
PKC	Protein kinase C
Pmol	Picomole
PT	Proximal tubule
PXR	Pregnane-X-receptor
RLU	Relative light units
SDM	Site-directed mutagenesis
SE	Standard error
SLC	Solute carrier
SLCO	Solute carrier organic anion transporter
SNP	Single nucleotide polymorphism
SOAT	Sodium dependent organic anion transporter
SOC	Super optimal broth with catabolite repression
T3	Triiodothyronine
T4	Thyroxine
TBE	Tris-borate-EDTA
TC	Transport classification
TCDB	Transporter classification database
TM	Transmembrane domain
TNF-α	Tumour necrosis factor-α
UGT	UDP glucuronosyltransferase
V_{max}	Maximum rate
WT	Wild type

1 Introduction

1.1 Cell homeostasis and the plasma membrane

The plasma membrane is essential for the homeostasis of all cells, by maintaining the integrity of the cell and its organelles. The membrane also protects the cell from the extracellular environment by allowing the selective movement of molecules (Alberts *et al.*, 2002). These important features are achieved by a dynamic membrane structure, comprising of an amphipathic fluid bilayer (Singer and Nicolson, 1972). The bilayer consists of two layers of phospholipids which have hydrophilic heads and hydrophobic tails (figure 1.1). This arrangement naturally maintains the membrane as the hydrophobic tails are attracted to one another and the hydrophilic heads attracted to the polar outside environments. The combination of glycoproteins, glycolipids, cholesterol and transmembrane proteins forms an organised communication network between the inside and the outside of the cell.

Small molecules such as water and gases are able to diffuse across the membrane down a concentration gradient, without assistance from proteins or energy expenditure. However this process is slow and leads only to an equilibrium in concentration on either side of the membrane (Quastel, 1965). The transport process is therefore enhanced by a complex group of transmembrane proteins, known as transporters, which are responsible for the efficient and controlled transport of larger, more lipophilic molecules across the bilayer. In fact 30% of all human genes code for membrane spanning proteins (Sciara and Mancia, 2012), indicating their diversity and prevalence in the genome. Some transmembrane proteins transport molecules simply by facilitating their diffusion, in a process that does not require energy. These passive or facilitated transporters transport solutes such as glucose and urea (Hediger *et al.*, 2004). Other molecules may require ATP expenditure to drive the transport, often against the concentration gradient. This is known as primary active transport and is achieved by a combination of ATP-driven pumps and

channels. Transport can also be driven by electrochemical potential gradients such as H^+ and Na^+, a process known as secondary active transport (Hediger *et al.*, 2004).

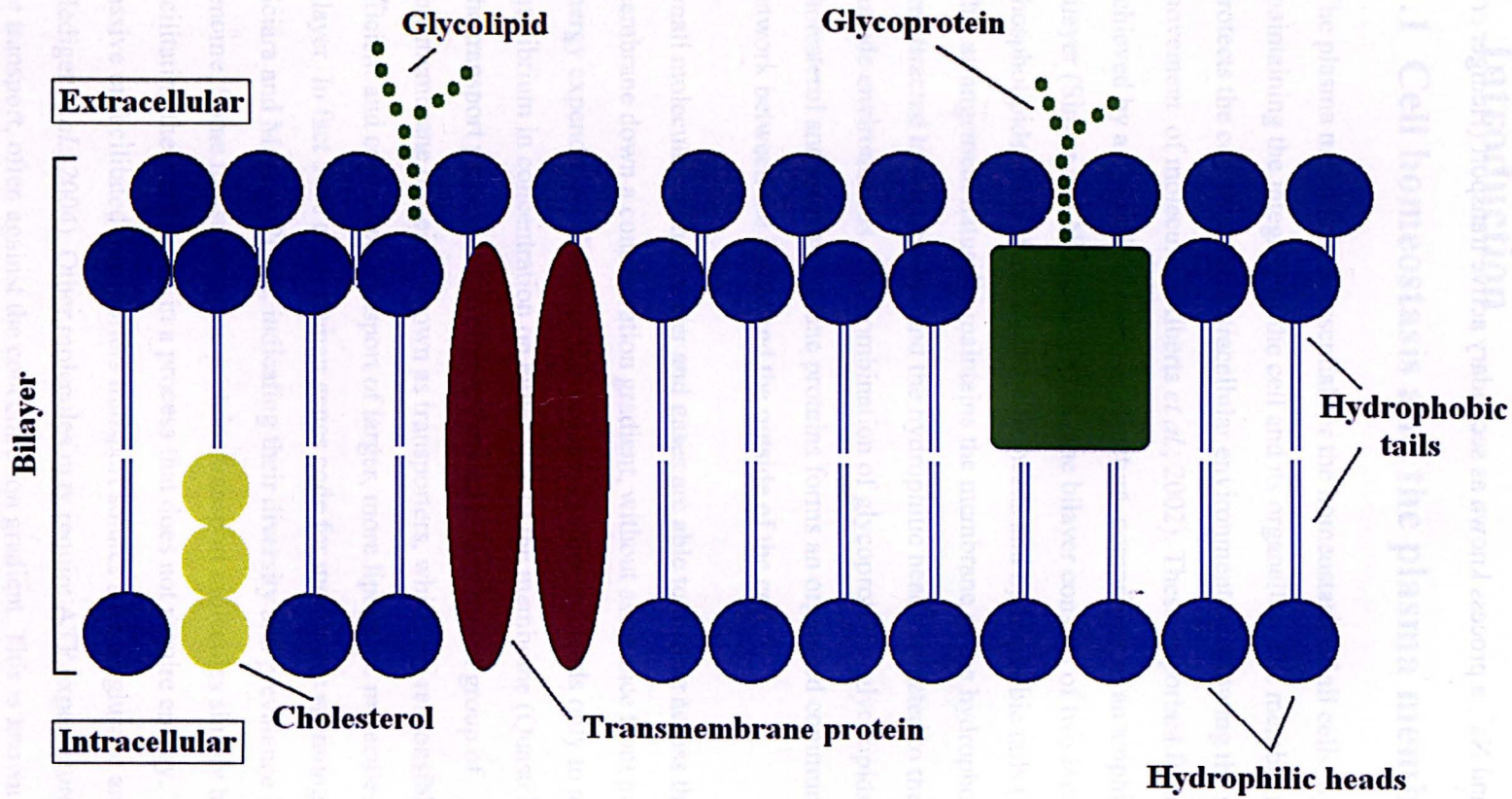

Figure 1.1 – Classical depiction of the cell membrane displaying the amphipathic phospholipid bilayer, containing cholesterol, transmembrane proteins and glycoproteins.

Transmembrane proteins are classified into channel proteins, transporters and ATP-powered pumps (figure 1.2). Channel proteins are characterised as channels or pores with a hydrophobic or hydrophilic lining, to which water or ions may pass through rapidly (up to 10^8 per second). Transporters, however, undergo a conformational change, moving one molecule at a time, resulting in a slower movement of approximately 10^4 molecules per second (Lodish *et al.*, 2000). ATP-powered pumps utilise ATP hydrolysis to drive molecules against their concentration gradient.

Transporters can function as uniporters; a single molecule transported down the concentration gradient, or as symporters; two or more molecules transported in the same direction, or as antiporters; exchange of one or more molecules for another (figure 1.2). Symporters and antiporters drive the molecule against the concentration gradient using various electrochemical gradients (Lodish *et al.*, 2000).

1.2 Transport protein classification

Transport proteins are classified by a transport classification (TC) system (Saier, 2000) similar to that of the enzyme classification (EC) system; however, unlike the EC system, the TC system is based upon both functional and phylogenetic information. This allows a classification based on many features, such as mechanism of transport, driving force and substrate specificities. The emergence of gene cloning combined with sequence analysis has revealed a number of transporter families that were previously unidentified. Transporter information is now compiled into a web based Transporter Classification Database (TCDB) which contains over 400 transporter families (Saier *et al.*, 2006), also including transmembrane receptors such as the G-protein-coupled receptors. The Solute Carrier (SLC) superfamily contains the Organic Anion Transporting Polypeptides (OATPs) under the classification TC #2.A.60; TC2: Electrochemical potential driven transporters; A: Uniporters, symporters,

antiporters; 60: OATP-family. The driving force for OATP transport is, however, still under debate, as described in section 1.3.3.

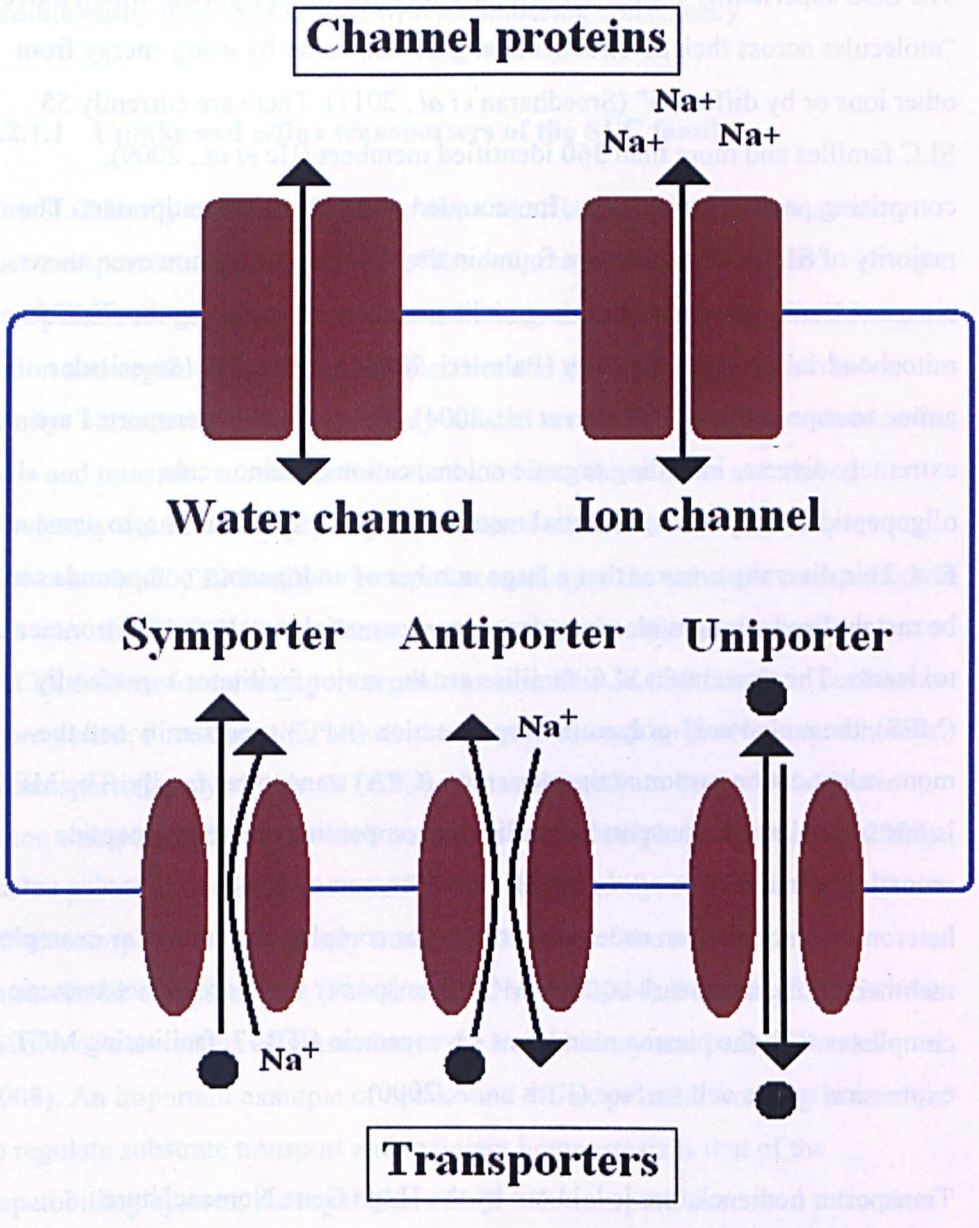

Figure 1.2 – Depiction of channel proteins and transporters with different types of transport, including uniport, symport and antiport.

1.2.1 The solute carrier (SLC) superfamily

The SLC superfamily contains a diverse collection of transporters which move "molecules across their electrochemical gradient, either by using energy from other ions or by diffusion" (Sreedharan *et al.*, 2011). There are currently 55 SLC families and more than 360 identified members (He *et al.*, 2009), comprising passive transporters, ion-coupled symporters and antiporters. The majority of SLC transporters are found in the cell membrane, however, there are some transporters present in organelle membranes, including the *SLC25* mitochondrial transporter family (Palmieri, 2004) and the *SLC18* vesicular amine transporter family (Eiden *et al.*, 2004). The substrates transported are extremely diverse, including organic anions, cations, amino acids, oligopeptides, fatty acids, essential metals, hormones and vitamins, to name a few. This diversity ensures that a large number of endogenous compounds can be metabolised, along with many drugs, non-essential metals and environmental toxicants. The three main SLC families are the major facilitator superfamily (MFS), the amino acid-polyamine-organocation (APC) superfamily and the monovalent cation:proton antiporter/anion (CPA) transporter family. The MFS is one of the largest transporter families, encompassing single polypeptide secondary carriers (Pao *et al.*, 1998). However, some MFS members also act as heteromers, requiring an accessory protein for complete function. For example members of the monocarboxylate (MCT) transporter family form heteromeric complexes with the plasma membrane glycoprotein CD147, facilitating MCT expression on the cell surface (Kirk *et al.*, 2000).

Transporter nomenclature is laid out by the Hugo Gene Nomenclature Committee (HGNC) (Seal *et al.*, 2011). Families are grouped according to at least 20% amino acid sequence identity (He *et al.*, 2009). The root SLC is followed by a number representing the family, a letter representing the sub-family and a number representing the isoform. The *SLCO* superfamily which codes for the OATPs is the only exception to this nomenclature system. The *SLCO* nomenclature stands for 'solute carrier organic anion transporter family,'

instead of *SLC21*, as proposed by Hagenbuch and colleagues in 2004 (Hagenbuch and Meier, 2004). This allows a species independent, evolutionarily divergent system with a numbering consistency.

1.2.1.1 Uptake and efflux transporters of the SLC family

The SLC family consists of both uptake and efflux proteins, i.e. transporters that transport into the cell and out of the cell, respectively. The uptake transporters for organic anions/cations include the *SLCO* family, *SLC22* organic cation and organic anion transport families and the *SLC10* Na^+ taurocholate family. These transporters are mainly located on the basolateral membrane of cells and transport substrates from the blood into the cell. As mentioned previously the *SLCO* family is grouped based on amino acid similarity. However the *SLC22* family is grouped according to the substrate transported. In this way, the *SLC22A1-3* isoforms transport organic cations, whereas the *SLC22A4-6* isoforms transport organic anions. The *SLC10* family in contrast is more varied; encompassing bile acid transporters such as the Na^+ taurocholate cotransporting polypeptide (NTCP) and also the sodium dependent organic anion transporter (SOAT) which transports steroid sulphates (Wu *et al.*, 2009). Efflux proteins are also present in the SLC superfamily, such as the *SLC30* zinc efflux transporters. This family transport zinc out of the cell and into intracellular compartments (Palmiter and Huang, 2004). Similarly, *SLC38A3* is involved in the efflux of glutamine in the liver, kidney and brain (Wendel *et al.*, 2008). An important example of uptake and efflux proteins working in unison to regulate substrate transport and maintain homeostasis is that of the hepatobiliary system; the regulation of bile salt transport, described in section 1.5.1.

1.3 The OATP superfamily

Oatp1a1 (*Slco1a1*), the first Oatp cloned, was isolated from rat liver in 1994 (Jacquemin *et al.*, 1994) and now more than 160 proteins have been predicted

in 25 species (Hagenbuch, 2010). Mammalian OATPs with identities greater than 40% are classified into families (e.g. OATP1-6) and those with greater than 60% similarity are grouped into subfamilies (e.g. OATP1A) (Hagenbuch and Meier, 2004). Human OATPs are depicted with upper case letters, animal Oatps with lower case letters; however, they will be collectively referred to here as OATPs. Human and mouse/rat orthologues are not exact, as amino acid identities vary from 60-75% and tissue distribution and transport features can differ. It is thought that OATP homologues probably emerged through gene duplication on divergence from a common ancestor (Pizzagalli *et al.*, 2002). This variation makes it difficult to examine cross species extrapolations and predict hepatic clearance.

The phylogenetic relationship between mouse, rat, bovine, dog and human OATPs is shown in figure 1.3. OATPs have not been located in plants, fungi or bacteria, indicating their evolution after the formation of the animal kingdom. However the OATPs are evolutionarily ancient, as an Oatp was identified in the liver of an ancient vertebrate, the small skate *Raja erinacea* (Cai *et al.*, 2002a). The following sections in this chapter serve to introduce the current knowledge relating to the structure, function and regulation of OATPs, as well as their role in disease and drug transport.

1.3.1 The human OATPs

1.3.1.1 Tissue distribution

There are 11 human OATP members divided into 6 subfamilies (Obaidat *et al.*, 2012), as shown in table 1.1. The OATP1 group is the largest and best characterised, containing the subfamilies OATP1A, OATP1B and OATP1C. OATP1A2 is expressed in many tissues and transports a large range of substrates, which along with the liver specific expression of OATP1B1 and OATP1B3, suggests a role for OATP1 in general detoxification. The other families have narrower substrate specificities; for example OATP1C and OATP4A transport thyroid hormone (Hagenbuch, 2007) and OATP2A

transports prostaglandins (Nomura *et al.*, 2004). The least functional information is available for OATP5A1 and OATP6A1. OATP1A2, OATP1B1, OATP1B3 and OATP2B1 are discussed in more detail in the following sections as they are the best characterised and most influential to drug interactions and disease.

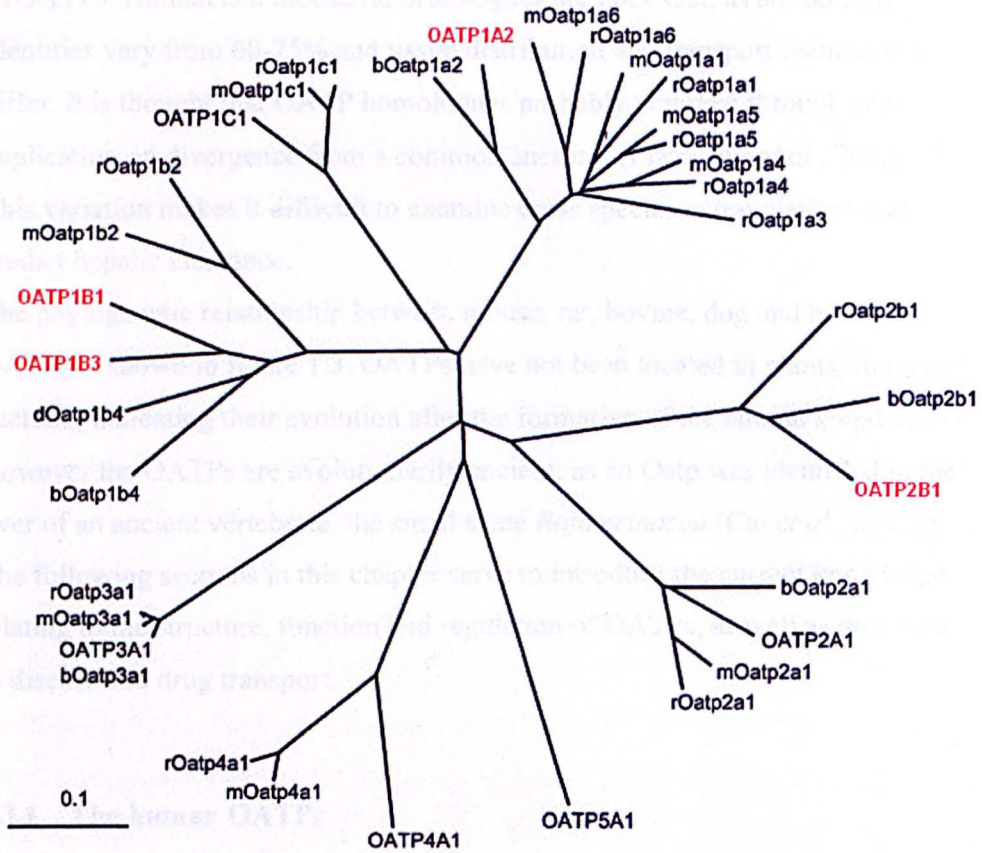

Figure 1.3 – Phylogenetic relationship between mouse (m), rat (r), bovine (b), dog (d) and human OATPs. Human hepatic OATPs are highlighted in red. Reproduced and adapted with permission of Elsevier Limited (Appendix VI) (Geyer *et al.*, 2004).

Table 1.1 – The six human OATP families and subfamilies with each member and tissue distribution

Family	Sub-family	Members	Tissue distribution	Reference
OATP1	OATP1A	OATP1A2	Ubiquitous	(Kullak-Ublick *et al.*, 1995)
	OATP1B	OATP1B1	Liver specific	(Hsiang *et al.*, 1999)
		OATP1B3	Liver specific	(Konig *et al.*, 2000a)
	OATP1C	OATP1C1	Brain, testis, ciliary body epithelium	(Gao *et al.*, 2005; Pizzagalli *et al.*, 2002)
OATP2	OATP2A	OATP2A1	Ubiquitous	(Schuster, 1998)
	OATP2B	OATP2B1	Ubiquitous	(Kullak-Ublick *et al.*, 2001)
OATP3	OATP3	OATP3A1	Testes, brain, heart, lung, spleen, peripheral blood leukocytes, thyroid gland	(Adachi *et al.*, 2003)
OATP4	OATP4A	OATP4A1	Heart, placenta, lung, liver, skeletal muscle, kidney and pancreas	(Fujiwara *et al.*, 2001; Hagenbuch, 2007)
	OATP4C	OATP4C1	Kidney-specific	(Mikkaichi *et al.*, 2004; Yamaguchi *et al.*, 2010)
OATP5	OATP5A	OATP5A1	Breast, fetal brain, prostate, skeletal muscle and thymus	(Bleasby *et al.*, 2006; Kindla *et al.*, 2011b)
OATP6	OATP6A	OATP6A1	Testes, spleen, brain, fetal brain and placenta	(Lee *et al.*, 2004; Obaidat *et al.*, 2012; Suzuki *et al.*, 2003)

1.3.1.2 OATP1A2

OATP1A2 (*SLCO1A2*, previously OATP, OATP-A, OATP1, *SLC21A3*) was the first human OATP to be cloned and consists of 670 amino acids (Kullak-Ublick *et al.*, 1995). The protein shares 67% and 81.7% amino acid identity with rat Oatp1a1 and bovine Oatp1a2 respectively. The gene *SLCO1A2* is located on chromosome 12p12, along with OATP1B1, OATP1B3 and OATP1C1 (Pizzagalli *et al.*, 2002).

OATP1A2 is considered ubiquitous (Franke *et al.*, 2009), however, expression is established primarily on apical membranes in the liver, kidney, intestine, lung, testes and blood-brain barrier (Hagenbuch and Gui, 2008). The highest expression has been detected in the brain capillary endothelial cells and microvessels (Gao *et al.*, 2000), suggesting an important role for the penetration of therapeutic drugs. In the kidney OATP1A2 is located in the distal tubule where it is most likely involved in the re-absorption of compounds (Lee *et al.*, 2005). Similarly the protein has a role in absorption from the duodenum, where it is co-localised with the ATP-binding cassette (ABC) efflux transporter ABCB1, at the apical membrane of villi (Glaeser *et al.*, 2007). In the liver OATP1A2 is expressed in cholangiocytes, forming part of the hepatobiliary system.

OATP1A2 transports the largest array of structurally diverse compounds including bile salts, steroid hormones, neutral and anionic peptides (van Montfoort *et al.*, 1999). It is also unique in the transport of bulky cations such as *N*-methylquinine (Kullak-Ublick *et al.*, 2001). This diversity combined with the location within excretory organs such as the liver and kidney suggest a general role in drug disposition and clearance.

1.3.1.3 OATP1B1

OATP1B1 (*SLCO1B1*, previously OATP2, OATP-C, LST-1, *SLC21A6*) is specific to the basolateral membrane of hepatocytes, where it mediates uptake of a number of amphipathic compounds from portal blood (Hsiang *et al.*, 1999).

OATP1B1 consists of 691 amino acids (Hsiang *et al.*, 1999) and shares 64% amino acid identity with mouse and rat Oatp1b2, which are also expressed only on the hepatocyte basolateral membrane (Chen *et al.*, 2008). OATP1B1 is the main basolateral bile salt transporter but also transports bilirubin, hormones, cyclic and linear peptides, toxins and many drugs. Such drugs include antibiotics, statins and anti-cancer drugs. The localisation of OATP1B1 within the liver, combined with the transport of a range of xenobiotic compounds, indicates a pivotal role in drug transport. Furthermore, a number of drug interactions have been associated with the transporter, particularly involving statins. This is further complicated by a number of single nucleotide polymorphisms (SNPs) which have also been associated with drug toxicity (discussed further in section 1.5).

1.3.1.4 OATP1B3

OATP1B3 (*SLCO1B3*, previously OATP8, LST-2, *SLC21A8*) is a 702 amino acid protein, also specific to the basolateral membrane of hepatocytes and shares an 80% amino acid identity with OATP1B1 (Konig *et al.*, 2000b). In addition, OATP1B3 shares 66% amino acid identity with rat Oatp1b2, also localised to the hepatocyte basolateral membrane (Meier-Abt *et al.*, 2004). The transport of amphipathic compounds by OATP1B3 is comparable to that of OATP1B1, while transporting bile salts and bilirubin to a lesser extent. OATP1B3 has a broad overlapping substrate specificity with OATP1B1, including the compounds phalloidin, valsartan and thyroxine (Hagenbuch and Gui, 2008). However in contrast to OATP1B1, OATP1B3 transports the intestinal peptide cholecystokinin octapeptide (CCK-8) (Letschert *et al.*, 2005) and the opioid peptide deltorphin II (Kullak-Ublick *et al.*, 2001). Transport of digoxin by OATP1B3 is controversial. Some groups have reported digoxin transport (Kullak-Ublick *et al.*, 2001; Reitman *et al.*, 2011) but others do not detect OATP1B3 mediated transport (Kimoto *et al.*, 2011; Taub *et al.*, 2011). Neither OATP1B1 nor OATP1B3 have so far demonstrated transport of organic cations. As well as having an important role in drug detoxification, OATP1B3

is up-regulated in many cancer cells, suggesting a role in cancer pathogenesis (section 1.4.2).

1.3.1.5 OATP2B1

OATP2B1 (*SLCO2B1*, previously OATP-B, *SLC21A9*) also consists of 702 amino acids with rat Oatp2b1 as the closest orthologue, containing 77% amino acid identity (St-Pierre *et al.*, 2004). Unlike OATP1A2, OATP1B1, and OATP1B3; OATP2B1 is located on chromosome 11q13 (Al Sarakbi *et al.*, 2006).

The highest expression of OATP2B1 is on the hepatocyte basolateral membrane, situated alongside OATP1B1 and OATP1B3. However, expression is also detected in spleen, placenta, kidney, ovary, lung, heart, small intestine and brain (Kullak-Ublick *et al.*, 2001). In relation to the other hepatocyte basolateral transporters, this protein has comparatively narrow substrate specificity; transport has only been shown for estrone-3-sulfate (E3S), bromosulfophthalein (BSP) and dehydroepiandrosterone sulphate (DHEAS) at pH 7.4. However it transports a number of additional substrates including taurocholate, statins and fexofenadine at acid pH (Hagenbuch and Gui, 2008). This suggests that pH affects the substrate and/or function of the protein, which is particularly relevant in the intestine where the local environment is around pH 6 (Fallingborg, 1999).

The broad distribution of this protein throughout the body suggests that OATP2B1 may have an important role in the general absorption and distribution of compounds.

1.3.2 OATP substrate specificity

The OATPs transport a wide range of solutes, both endogenous and xenobiotic. OATP substrates are generally amphipathic molecules with molecular weights greater than 350 Daltons (Roth *et al.*, 2011). The broad range includes bile acids, conjugated steroids,

thyroid hormones, linear and cyclic peptides, toxins as well as numerous drugs, including statins, sartans, antibiotics and anti-cancer drugs. Generally solutes are negatively charged, however some are neutral (digoxin) and even cationic (*N*-methylquinine) (Obaidat *et al.*, 2012). In addition, many solutes are substrates for several OATPs, such as E3S and estradiol-17β-glucuronide (E17βG) which are often used as model substrates. However, other substrates are unique to a single transporter, such as CCK8, which is specific to OATP1B3 (Ismair *et al.*, 2001). The transport of wide ranging endogenous and xenobiotic compounds indicates a pivotal role for OATPs in homeostasis and drug disposition.

1.3.3 OATP mechanism of transport

OATP transport has been established as chloride, sodium, potassium and ATP-independent (Roth *et al.*, 2011); however, the exact driving mechanism is still under debate. A central pore to which substrates physically translocate in a rocker–switch mechanism has been proposed (Meier-Abt *et al.*, 2005) and is discussed further in section 1.3.4.

OATPs transport bidirectionally and several studies have suggested that transport may occur via electroneutral exchange; whereby the uptake of organic anions is coupled to efflux. There is evidence for bicarbonate exchange in rat Oatp1a1, Oatp1a4 and OATP1A2, OATP1B3, OATP2B1 and OATP3A1 (Leuthold *et al.*, 2009; Satlin *et al.*, 1997). However glutathione exchange was also shown for rat Oatp1a1 and Oatp1a4 (Li *et al.*, 1998). In addition, OATP1B1 is not affected by bicarbonate (Leuthold *et al.*, 2009) and both OATP1B1 and OATP1B3 are not affected by glutathione (Mahagita *et al.*, 2007), suggesting that another mechanism is driving transport. This evidence is further supported by the amino acid identity the OATPs share with the MFS; a transport family which use an ion gradient to drive transport (Pao *et al.*, 1998) (see section 1.3.4).

The pH can also affect OATP mediated transport. Studies have revealed that many rat and human OATPs show increased transport activity when exposed to an acidic pH (Leuthold *et al.*, 2009). This is particularly interesting for OATP2B1, which is expressed in the small intestine, an organ that maintains a lower pH than other areas of the body. This may allow selectively increased transport of substrates and most likely affect drug absorption. Furthermore, the transport of some substrates is increased more than others when the pH is decreased (Nozawa *et al.*, 2004a). The increased transport is caused by the protonation of a conserved histidine residue at the extracellular end of transmembrane domain (TM) 3. This was shown in OATP1C1, an isoform which does not contain the histidine residue and is not pH dependent (Leuthold *et al.*, 2009), as mutating the corresponding residue to histidine restored the pH dependency.

Increasing the extracellular proton concentration will cause an outward driven flow of bicarbonate by its conversion into water and CO_2, thus in turn possibly causing increased bicarbonate exchange. This may be the cause of the increased transport in acidic conditions. The effect of pH was further demonstrated by Martinez-Becerra and colleagues, who recently revealed that OATP1B1 and OATP1B3 are electrogenic (Martinez-Becerra *et al.*, 2011). The group used ionophores to assess changes in membrane potential. This is the first evidence of its kind to show that OATPs are affected by membrane potential and may function via a proton pump. The group also confirmed that Oatp1a1 is not affected by membrane potential, therefore supporting the evidence that it is an electroneutral exchanger.

The current evidence for the driving force for OATPs is not clear and it is likely that different mechanisms are involved for different transporters. Further studies are required to confirm the electrogenicity of OATP1B1 and OATP1B3 and other human isoforms. However it is likely that pH is somehow involved in the facilitation of substrate transport, possibly through the induction of a conformational change or as a driving force for protons or bicarbonate efflux.

1.3.4 OATP protein structure

There is little high resolution structural knowledge of OATPs owing to the difficulties in purifying and crystallising transmembrane proteins. As a result, only 70 high resolution membrane protein structures exist compared to thousands of soluble protein structures (Nam *et al.*, 2009). As an alternative, protein structure predictions are made using homology modelling and hydrophobicity analyses, which provide a theoretical framework for experimental determination.

OATPs consist of 643-722 amino acids (Hagenbuch and Meier, 2004) and the majority expressed on plasma membranes of epithelial cells, however some OATPs are also expressed in T-lymphocytes (Janneh *et al.*, 2008). There is currently no crystal structure, and *in silico* modelling has revealed a putative topology of 12TMs with amino (N) and carboxyl (C) termini facing the cytoplasmic space (figure 1.4) (Hagenbuch and Meier, 2004; Hanggi *et al.*, 2006; Noe *et al.*, 1997; Roth *et al.*, 2011). However, the 12TM topology has only been studied in rat Oatp1a1 (Wang *et al.*, 2008) and the orientation of the N and C termini was not determined. The predictions are consistent with the notion that the OATPs are related to the MFS, which mainly have 12TMs. Evolutionary conservation has been shown between rat Oatp1c1 and the MFS (Westholm *et al.*, 2010) and OATP and MFS protein sequences share high sequence identity when compared using the protein domain database Prosite (Sigrist *et al.*, 2010) (data not shown).

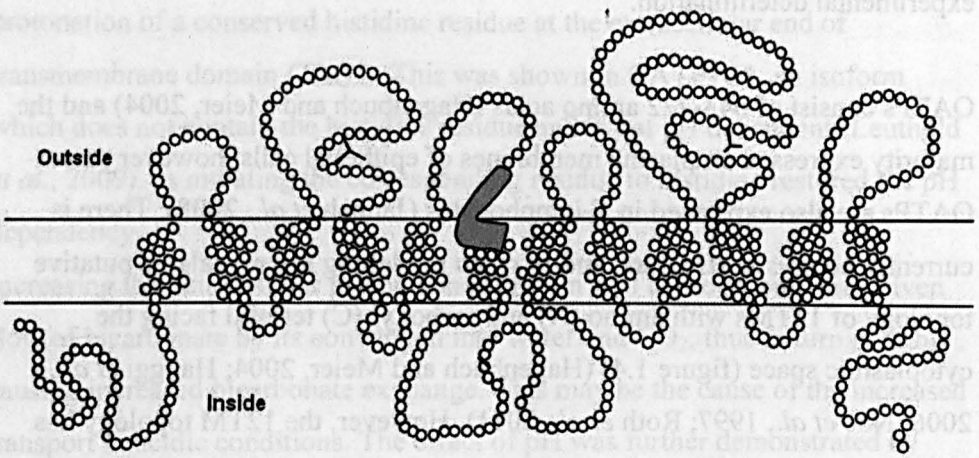

Figure 1.4 - Model of an OATP displaying the putative 12TM topology. The signature region (highlighted in grey) is at extracellular loop 3 and TM domain 6. *N*-glycosylation sites are indicated with a Y (Leuthold *et al.*, 2009) (Copyright permission not required, see Appendix VI).

The OATPs are characterised by a signature region (D-X-RW-(I,V)-GAWW-XG-(F,L)-L) located at the border between extracellular loop 3 and TM6 (figure 1.4) which is conserved across all species (Hagenbuch and Meier, 2004). Of particular interest are three unusual conserved tryptophans; tryptophan residues are rare in proteins, with only 2-3 residues often observed across an entire sequence (Samanta *et al.*, 2000). It is not known whether this sequence is required for functioning or membrane localisation.

The large extracellular loop 5 of OATP2B1 contains ten cysteine residues linked by disulphide bonds, found to be essential for OATP2B1 targeting to the cell surface (Hänggi *et al.* 2006). Mutations of just one residue resulted in the protein being retained intracellularly. These cysteine residues are conserved across many OATPs. Furthermore, the loop may not be positive (Meier-Abt *et al.*, 2005), suggesting a structural rather than substrate binding role. A homology has also been detected between this loop 5 and the kazal-2-type serine protease inhibitors, the role for which has not been elucidated. In fact, this homology was observed in 115 different OATPs (Barabote *et al.*, 2006). Remarkably, the OATPs are the only transmembrane proteins to show this homology (Svoboda *et al.*, 2011a). In humans, the kazal-type serine protease inhibitors are involved in many physiological processes such as inflammation and development, by regulating proteinase activity (Zheng *et al.*, 2006).

Glycosylation sites have been predicted for several rat and human OATPs, in extracellular loops 2 and 5 (figure 1.4). However, the sites have only been experimentally analysed in Oatp1a1 (Lee *et al.*, 2003; Wang *et al.*, 2008) and OATP1B1 (Yao *et al.*, 2012). Oatp1a1 also contains a PDZ sequence (Wang *et al.*, 2005a); a sequence known to interact with PDZ binding domain proteins. The 'PDZ' stands for the first letters of three proteins originally found to share the common structural domain (PSD95, Dlg1 and zo-1). Proteins containing the domains are known to interact with the C-terminal of transmembrane proteins, ensuring their localisation at the cell surface (Brone and Eggermont, 2005). However, not all OATPs contain a PDZ sequence and thus must use a different

mechanism for membrane localisation. Phosphorylation sites have also been detected in Oatp1a1, suggesting a possible mechanism for trafficking to the cell surface (Choi *et al.*, 2011). The role of glycosylation, membrane targeting and phosphorylation are further discussed in section 1.3.5.

The amino acids in various TMs are important for targeting to the cell membrane and substrate transport. In a comparison of mouse, rat and human OATPs, TMs 1-6 and 11 showed the most amino acid conservation (50-70%) (Cai *et al.*, 2002b). Four amino acids in TM2 of OATP1B1 when substituted, impaired the transport of E3S (Li *et al.*, 2012). More specifically, E74 may be involved in stabilising the protein through a salt bridge, and D70 is important for substrate recognition. Removing the charge from both amino acids also affected substrate transport, indicating that the charge is important for attracting anionic substrates to the protein. TMs 8 and 9 of OATP1B1 are also involved in E3S transport; as when substituted the membrane targeting was not affected, but transport kinetics were altered (Miyagawa *et al.*, 2009). Similar mutagenesis of OATP1B1 TM10 showed that four amino acids present in the domain are required for E3S transport, and substitution completely abolished function (Gui and Hagenbuch, 2009). DeGorter and colleagues went further to identify three amino acids in TM1, TM10 and extracellular loop 6 which are specific to the transport of CCK-8 by OATP1B3 (DeGorter *et al.*, 2012). This was shown by introducing the amino acids into OATP1B1, a transporter not previously capable of transporting CCK-8. Gui and colleagues also isolated amino acids in TM10 important for OATP1B3 mediated CCK-8 transport (Gui and Hagenbuch, 2008). Molecular modelling suggested that these amino acids form hydrogen bonds with the substrate.

It is clear that residues within certain TMs are essential for substrate transport. The layout of the TMs to form the tertiary structure was studied by Meier-Abt and colleagues, who put forward a model based on an alignment with the *E.coli* MFS proteins glycerol-3-phosphate and lactose permease (Meier-Abt *et al.*, 2005). The model, based on OATP1B3, revealed the protein to have a positive

electrostatic pore or 'binding pocket' formed by TMs 1, 2, 4, 5, 7, 8, 10 and 11 (figure 1.5). Charged residues were also identified and predicted to be involved in substrate interactions. The presence of a positive pore indicates a mechanism for facilitating the translocation of anionic compounds. A similar model with a putative pore was demonstrated for OATP1C1, also through MFS comparison (Westholm *et al.*, 2010). The positive residues predicted to be substrate exposed in this model have been studied by several groups. Amino acids R57, K361 and R580 are conserved within the OATP1 family and are solvent exposed within the pore. Mutation of these residues in OATP1B1 affected surface expression and transport kinetics (Weaver and Hagenbuch, 2010). Comparative results were seen with the mutation of R580 in OATP1B3 (Glaeser *et al.*, 2010). Gui and colleagues also predicted L545 in TM 10 of OATP1B1 to be substrate exposed, through helical wheel modelling (Gui and Hagenbuch, 2009). Substitution of this amino acid reduced transport function, suggesting that it is involved in substrate interaction.

OATPs are able to transport a wide range of chemical structures, which may be explained by the presence of multiple binding sites. Several groups have reported through the observation of biphasic kinetics, the presence of two E3S binding sites in OATP1B1 (Gui and Hagenbuch, 2009; Noe *et al.*, 2007; Sharma *et al.*, 2012). Atypical kinetics have also been shown for rat Oatp1c1 (Westholm *et al.*, 2009a) and OATP2B1 (Shirasaka *et al.*, 2012), suggesting multiple binding sites. The presence of multiple binding sites in OATPs of different subfamilies suggests that this may be an inherent property of OATPs. However the evidence is varying, as not all groups report biphasic properties. The presence of multiple binding sites is not unusual, as they have been found in other multispecific transporters, including Pgp (Aller *et al.*, 2009). This property, however, complicates drug disposition experiments; as a drug may inhibit one binding site but not another.

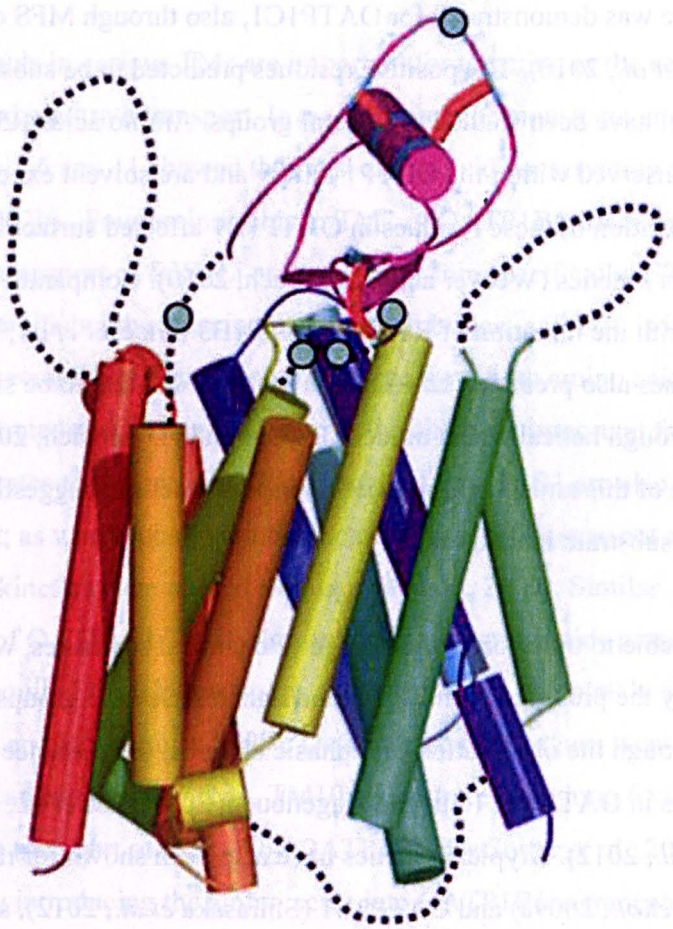

Figure 1.5 - Predicted tertiary structure of OATP1B3. TMs depicted as multi-coloured cylinders, extracellular loop 5 in magenta, black dotted lines depict other extracellular loops. Red bars represent disulphide bonds modelled on the kazal-2-type serine protease inhibitors. Cyan circles depict modelled cysteine residues. Reproduced with permission of Springer Science + Business Media (Appendix VI) (Meier-Abt *et al.*, 2005).

1.3.5 OATP regulation

OATP expression and function is tightly regulated by a complex network of transcription factors, cytokines and post-translational modifications. These regulate levels of expression and targeting of the protein to the membrane. Other factors can also indirectly affect regulation, including hormones, disease and xenobiotics. For example, sex steroid hormones are known to regulate the expression of mouse Oatps such as Oatp4c1, leading to gender specific expression patterns (Cheng and Klaassen, 2009). Disease is also known to affect expression, as shown by down-regulation of OATP1B1, OATP1B3 and OATP2B1 mRNA levels in hepatitis C patients (Ogasawara *et al.*, 2010). Therefore many factors and pathways influence OATP expression. The known transcriptional and post-translational regulation pathways are briefly discussed here.

1.3.5.1 Transcriptional regulation

Transcriptional regulation of OATPs allows protein expression to be adapted in response to the surrounding environment. OATPs have been associated with the cytokines and transcription factors; interferon-gamma (IFN-γ), interleukin-1-beta (Il-1β), interleukin-6 (Il-6), tumour necrosis factor alpha (TNF-α), hepatocyte nuclear factor-1α (HNF-1α), aryl hydrocarbon receptor (AhR), constitutive androstane receptor (CAR) and the farnesoid-X-receptor (FXR) (Svoboda *et al.*, 2011a).

The liver is under particular control by the hepatocyte nuclear factors (HNFs). OATP1B1 and 1B3 are under direct control by HNF-1α; a transcription initiation site was located eight nucleotides upstream from the start of the OATP1B1 sequence (Jung *et al.*, 2001). Furthermore, mutation of this site hinders OATP1B1 promoter activity, indicating that it is required for expression. Additionally, unconjugated hyperbilirubinaemia may be caused by reduction in HNF1α activity, leading to a reduction in OATP1B1 levels (Jung

et al., 2001). Interestingly OATP1A2, which is expressed in liver cholangiocytes, does not contain an initiation site for HNF1α, suggesting that this factor is involved only in hepatocyte specific regulation.

OATP expression can also be initiated by xenobiotics that are known ligand activators, as an important inductive response. Rifampicin is a ligand for the pregnane-X-receptor (PXR) and in the presence of rifampicin OATP1B1 expression is increased, suggesting that PXR affects *SLCO1B1* gene expression (Gui *et al.*, 2008). FXR is also implicated in hepatic OATP regulation through bile acid activation. For example, *SLCO1B3* is transactivated by FXR, causing an up-regulation in OATP1B3 (Eloranta and Kullak-Ublick, 2008). This may serve to ensure sufficient removal of endogenous and xenobiotic compounds, leading to decreased expression of other overlapping basolateral OATPs, such as OATP1B1 and OATP2B1.

1.3.5.2 Post-translational regulation

Post-translational regulation involving phosphorylation, glycosylation and protein-protein interactions ensures the correct targeting of transporters to the membrane. Protein phosphorylation is proposed to play a role in the targeting of OATP protein to the cell surface. Studies with rat Oatp1a1 have shown that the protein undergoes serine phosphorylation at S634 and S635 in the presence of extracellular ATP (Glavy *et al.*, 2000). This phosphorylation regulates the translocation of the protein between the plasma membrane and the intracellular vesicles, as mutation of the serines results in retention of the protein intracellularly (Choi *et al.*, 2011).

Protein kinase pathways allow for rapid regulation of OATP expression on the membrane. Rat Oatp1a1 (Guo and Klaassen, 2001), Oatp1a4 (Guo and Klaassen, 2001) OATP1A2 (Zhou *et al.*, 2011) and OATP2B1 (Kock *et al.*, 2010) are all controlled by protein kinase C (PKC). Down-regulation of the OATP protein by internalisation from the plasma membrane into endosomes is

induced by activation of PKC, in a clathrin-dependent process. The protein is then subjected to lysosomal degradation. OATP2B1 internalisation was further confirmed in an *ex vivo* placenta perfusion (Kock *et al.*, 2010). In contrast, protein kinase A (PKA) controls the membrane trafficking of OATP1B1 through the Golgi complex and the vacuolar H^+-ATPase vesicle mediated membrane sorting pathway, to ensure plasma membrane localisation (Sun *et al.*, 2008a).

The correct protein folding and localisation of OATPs is also regulated by *N*-glycosylation. *N*-linked glycosylation occurs at asparagines present in the following consensus sequence: Asn-Xaa-Thr/Ser, whereby Xaa can be any amino acid apart from proline or aspartic acid (Medzihradszky, 2008). OATPs are characterised by putative *N*-glycosylation sites at extracellular loops 2 and 5, which are conserved across most species (section 1.3.4). In rat Oatp1a1, function and membrane targeting are affected by the level of glycosylation (Lee *et al.*, 2003). These Oatp1a1 glycosylation sites were identified as N124, N135 and N492 (Lee *et al.*, 2003; Wang *et al.*, 2008). Absence of glycosylation in OATP1A2 also affects plasma membrane localisation (Lee *et al.*, 2005). Furthermore, glycosylation experiments with OATP1B1 (Konig *et al.*, 2000b), OATP1B3 (Konig *et al.*, 2000a) and OATP2B1 (Hanggi *et al.*, 2006) confirmed that all are glycosylated, and OATP1B1 sites have recently been identified as N134, N503 and N516 (Yao *et al.*, 2012). In addition, mutation in one of the three sites in OATP2B1 impairs transport function (Hanggi *et al.*, 2006).

The correct functioning of the OATPs also relies on the accurate binding of the protein within the plasma membrane. Members of PDZ domain containing proteins have been shown to regulate plasma membrane anchoring and modulate function. Several human, rat and mouse OATPs possess a C-terminal PDZ consensus sequence, and it has been demonstrated in rat Oatp1a1 that binding to PDZK1 is essential for plasma membrane localisation (Wang *et al.*, 2005a). PDZ proteins also interact directly with the C-termini of several human OATPs (table 1.2), however, whether the same mechanism is used for other OATPs that do not contain PDZ consensus sequences is yet to be elucidated.

Table 1.2 – Human OATPs known to contain a C-terminal PDZ sequence

OATP	C-terminal PDZ amino acid sequence	Reference
OATP1A2	KTKL	(Obaidat *et al.*, 2012)
OATP1C1	ETQL	(Kato *et al.*, 2004)
OATP2B1	DSRV	(Wang *et al.*, 2005a)
OATP3A1_v1	ESVL	(Kato *et al.*, 2004)

1.4 OATPs and disease

OATPs are vital for cell homeostasis, and thus it might be expected that disease would result from mutations disrupting their activity. Until very recently, however, there was no direct link between OATP impairment and disease, but a mutation in *SLCO2A1* (OATP2A1) has been linked to the genetic disease primary hypertrophic osteoarthropathy (Zhang *et al.*, 2012). The mutation inhibits OATP2A1 mediated prostaglandin E_2 transport, causing the rare bone disease. OATPs could be the cause of, or be affected by disease. For example inflammation caused by disease is linked to transporter impairment, as seen by the reduction of Oatp4a1 gene expression in adjuvant arthritis (Hanafy *et al.*, 2012). This is most likely caused by dysregulation. The main OATP linked diseases are hyperbilirubinaemia and cholestasis, which will be discussed in the following sections, as well as the role of OATPs during cancer pathogenesis.

1.4.1 Cholestasis and hyperbilirubinaemia

OATP1B1 and OATP1B3 are the major hepatocyte basolateral transporters for bile (see section 1.5.1 for the role of OATPs in the hepatobiliary system), and deficiencies in these OATPs are the cause of hyperbilirubinaemia and cholestasis.

Cholestasis is characterised by a reduction of bile flow and subsequent accumulation in hepatocytes, which eventually leads to cirrhosis and liver failure. This can be caused by an obstruction of bile flow or lack of secretion from hepatocytes and cholangiocytes (Paumgartner and Pusl, 2008). OATP transporter down-regulation is likely to be one of the causes of cholestasis. This was shown by a decrease in OATP1A2 and OATP1B3 expression during intrahepatic cholestasis of pregnancy (Wang *et al.*, 2012). This was also observed in rat Oatp1a1, which shares 67% amino acid identity with OATP1A2. The down-regulation of one transporter can also affect another, as observed in patients with primary sclerosing cholangitis. Patients with this disease have both down-regulation of OATP1B1 and the ABC transporter multidrug resistance-associated protein 2 (MRP2). Down-regulation of OATP1B1 is caused by the impaired canalicular transport by MRP2, as a mechanism to reduce the transport of more organic anions into the hepatocyte (Oswald *et al.*, 2001). This highlights the complex relationship between transporters and the importance of their regulation.

Un-conjugated bilirubin is transported into the hepatocyte by OATP1B1 and OATP1B3 where it is conjugated to make it soluble. Failure to transport bilirubin causes hyperbilirubinaemia, a build-up of bilirubin in the blood, leading to diseases such as jaundice. Mutations in OATP1B1 and OATP1B3 are the cause of human rotor syndrome, a genetically inherited hyperbilirubinaemia (van de Steeg *et al.*, 2012). SNPs in *SLCO1B3* similarly cause hyperbilirubinaemia, through the impairment of OATP1B3 function (Sanna *et al.*, 2009). Drug induced hyperbilirubinaemia is also caused through the inhibition of OATP1B1, for example by indinavir, saquinavir, rifamycin and/or cyclosporine A (Campbell *et al.*, 2004). It is likely this inhibition is also enhanced by the saquinavir and indinavir mediated inhibition of UDP glucuronosyltransferases (UGTs) (Zhang *et al.*, 2005). The UGTs are enzymes which catalyse the glucuronidation of bilirubin as part of the bilirubin elimination process, and thus inhibition causes bilirubin retention.

This evidence suggests a pivotal role of OATP1B1 and OATP1B3 in bilirubin transport and understanding their function may aid in understanding the pathogenesis resulting from transporter impairment.

1.4.2 Cancer

It is likely that OATPs play a role in, or are affected by cancer. The expression patterns of OATPs are altered in cancer tissue and expression can be up-regulated or down-regulated, as shown in table 1.3. Therefore transporters are expressed in cancer tissues that would not normally be associated with the transporter. This suggests a potential role for transporters maintaining or acting against cancerous tissues, possibly through a selective pressure in relation to drug resistance. However, there is still little evidence as to how OATP regulation is linked to cancer. It is speculated that altered post-translational regulation is involved, as increased cytoplasmic staining of OATP1A2 has been observed in breast cancer cells (Obaidat *et al.*, 2012). It is also speculated that the down-regulation of OATP1B3 in hepatocellular carcinoma is caused by hepatocyte nuclear factor-3β (HNF-3β), which is up-regulated (Vavricka *et al.*, 2004).

Transporters may also adversely facilitate hormone dependent cancers, by transporting hormone precursors to cancerous tissue. For example OATP1A2 and OATP1B3 are over expressed in breast cancer tissues and transport the estrogen precursor E3S, which is required by the estrogen dependent cancer. OATP1B3 is particularly prominent, as it is normally liver specific, but is expressed in many cancer tissues (table 1.3). A new cancer specific OATP1B3 mRNA isoform has even been identified; which contains a different transcription start site and an alternative promoter in intron 2 (Nagai *et al.*, 2012). OATP1B3 transports several anti-cancer drugs including methotrexate (Abe *et al.*, 2001), and by further understanding transport by this cancer isoform, cancers may be better targeted with chemotherapeutics.

Table 1.3 – OATP expression patterns and regulation during cancer

OATP	Cancer tissue	Up-regulated (↑) or down-regulated (↓)	Reference
OATP1A2	Prostate	↑	(Arakawa *et al.*, 2012)
	Pancreas	↑	(Kounnis *et al.*, 2011)
	Breast	↑	(Meyer zu Schwabedissen *et al.*, 2008)
	Bone	↑	(Liedauer *et al.*, 2009)
OATP1B1	Pancreas	↑	(Kounnis *et al.*, 2011)
	Liver	↓	(Pressler *et al.*, 2011)
	Colon	↑	(Pressler *et al.*, 2011)
	Ovarian	↑	(Svoboda *et al.*, 2011b)
OATP1B3	Pancreas	↑	(Kounnis *et al.*, 2011)
	Colorectal	↑	(Lockhart *et al.*, 2008)
	Gastroinestinal	↑	(Abe *et al.*, 2001)
	Breast	↑	(Muto *et al.*, 2007)
	Testicular	↑	(Pressler *et al.*, 2011)
	Ovarian	↑	(Svoboda *et al.*, 2011b)
	Liver	↓	(Vavricka *et al.*, 2004)
	Prostate	↑	(Hamada *et al.*, 2008; Yang *et al.*, 2011)
OATP1C1	Bone	↑	(Liedauer *et al.*, 2009)
OATP2A1	Bone	↑	(Liedauer *et al.*, 2009)
	Liver	↑	(Wlcek *et al.*, 2011)
	Breast	↑	(Wlcek *et al.*, 2008)
OATP2B1	Bone	↑	(Liedauer *et al.*, 2009)
	Liver	↓	(Pressler *et al.*, 2011)
	Pancreas	↓	(Pressler *et al.*, 2011)
	Prostate	↑	(Hamada *et al.*, 2008; Yang *et al.*, 2011)
	Thyroid	↑	(Pressler *et al.*, 2011)
OATP3A1	Bone	↑	(Liedauer *et al.*, 2009)

	Liver	↑	(Wlcek *et al.*, 2011)
	Breast	↑	(Kindla *et al.*, 2011b)
OATP4A1	Bone	↑	(Liedauer *et al.*, 2009)
	Liver	↑	(Wlcek *et al.*, 2011)
OATP4C1	Bone	↑	(Liedauer *et al.*, 2009)
OATP5A1	Bone	↑	(Liedauer *et al.*, 2009)
	Small cell lung	↑	(Olszewski-Hamilton *et al.*, 2011)
	Liver	↑	(Wlcek *et al.*, 2011)
	Breast	↑	(Kindla *et al.*, 2011b)
OATP6A1	Lung, bladder, oesophagus	↑	(Lee *et al.*, 2004)

1.5 OATPs and drug disposition

Xenobiotics require transport proteins to traverse cellular membranes, owing to their size, charge and lipophilicity. OATPs transport a broad range of xenobiotics, ranging from antibiotics such as penicillin (Tamai *et al.*, 2000), the antifungal caspofungin (Sandhu *et al.*, 2005) and many anti-retroviral protease inhibitors including saquinavir (Hartkoorn *et al.*, 2010; Su *et al.*, 2004), to chemotherapeutic agents including methotrexate (Badagnani *et al.*, 2006) and cardiac drugs such as the cardiac glycoside digoxin (Kullak-Ublick *et al.*, 2001). Numerous statins such as pitavastatin (Hirano *et al.*, 2006) are also transported by OATPs. The anti-histamine fexofenadine (Cvetkovic *et al.*, 1999), anti-diabetic drug glibenclamide (Satoh *et al.*, 2005b) and the opioid receptor agonist deltorphin II (Gao *et al.*, 2000) are also transported. Finally toxins including microcystin (Fischer *et al.*, 2005) and the poison arsenic (Lu *et al.*, 2006) are also processed through the liver by OATPs. In this way OATPs retain a selective barrier to different drugs and ensure that all compounds can be metabolised to maintain homeostasis.

Interestingly the preference for drug type can vary between transporters. For example, the angiotensin II receptor antagonists such as valsartan are taken up equally by OATP1B1 and OATP1B3 (Yamashiro *et al.*, 2006), however pitavastatin and rosuvastatin are transported preferentially by OATP1B1, even though they are also substrates for the other basolateral transporters (Hirano *et al.*, 2004). Similarly drugs belonging to the same class can be transported differently, for example valsartan and olmesartan can be transported by both OATP1B1 and OATP1B3 but telmisartan is only transported by OATP1B3, even though they are both angiotensin II receptor agonists.

The localisation of OATPs in a wide range of cell membranes and their ability to transport a wide selection of drug compounds indicates important roles in the absorption, distribution, metabolism and excretion (ADME) of xenobiotic compounds. For example, OATPs expressed in the intestine are involved in the

absorption of orally administered drugs and ubiquitously expressed OATPs are involved in the distribution of drugs to the site of action, such as the blood brain barrier. OATP1A2, OATP1B1, OATP1B3 and OATP2B1 are part of the hepatobiliary system and are their relationship with the ADME of drug compounds is the most characterised (section 1.5.1).

1.5.1 OATPs and hepatic drug disposition

1.5.1.1 The hepatobiliary system

Bile secretion is a process imperative to the excretion of waste compounds, including bilirubin and cholesterol, as well as many xenobiotics. Bile once produced in the liver is transported to the intestine, where it assists the breakdown and assimilation of lipids and lipid soluble nutrients (Zsembery *et al.*, 2000). This process, known as the enterohepatic circulation, is primarily controlled by transporters (Kullak-Ublick *et al.*, 2004).

Generation of bile flow is a vectoral, ATP driven process which requires a number of transport proteins in the canalicular and basolateral membranes of hepatocytes. Compounds including bile salts are transported from portal blood into the hepatocyte on the basolateral membrane (figure 1.6) by OATP1B1, OATP1B3, OATP2B1 and NTCP. NTCP mediates mainly Na^+-dependent conjugated and unconjugated bile salt transport into the hepatocyte. The non-bile salt substrates BSP, thyroid hormone (triiodothyronine T3 and thyroxine T4) and E3S are also transported among others (Meier *et al.*, 1997). OATP1B1 is the predominant Na^+-independent transporter of bile acids with OATP1B3 transport to a lesser extent. OATP2B1 transports a number of endogenous and xenobiotic compounds and the bile acid taurocholate. Additionally the organic anion transporters (OATs, *SLC22*) and organic cation transporters (OCTs, *SLC22*) transport organic anions and type 1 organic cations into the hepatocyte (Chandra and Brouwer, 2004). Once inside the hepatocyte, substrates may be

metabolised by enzymes through biotransformation and/or transported into the bile canaliculi by the ABC transporters.

Cholangiocytes are the epithelial cells of the bile ducts and also form a vital part of the hepatobiliary system. Cholangiocytes form only 3-5% of liver cells but they are responsible for up to 40% of the bile production, by adding fluid and electrolytes as well as reabsorbing substances (Arrese and Accatino, 2002). There is little experimental evidence to support the role of OATP1A2 in the liver; however its expression on apical membranes of cholangiocytes suggest a contributing role to bile production by transporting substrates across the membrane into the canalicular lumen.

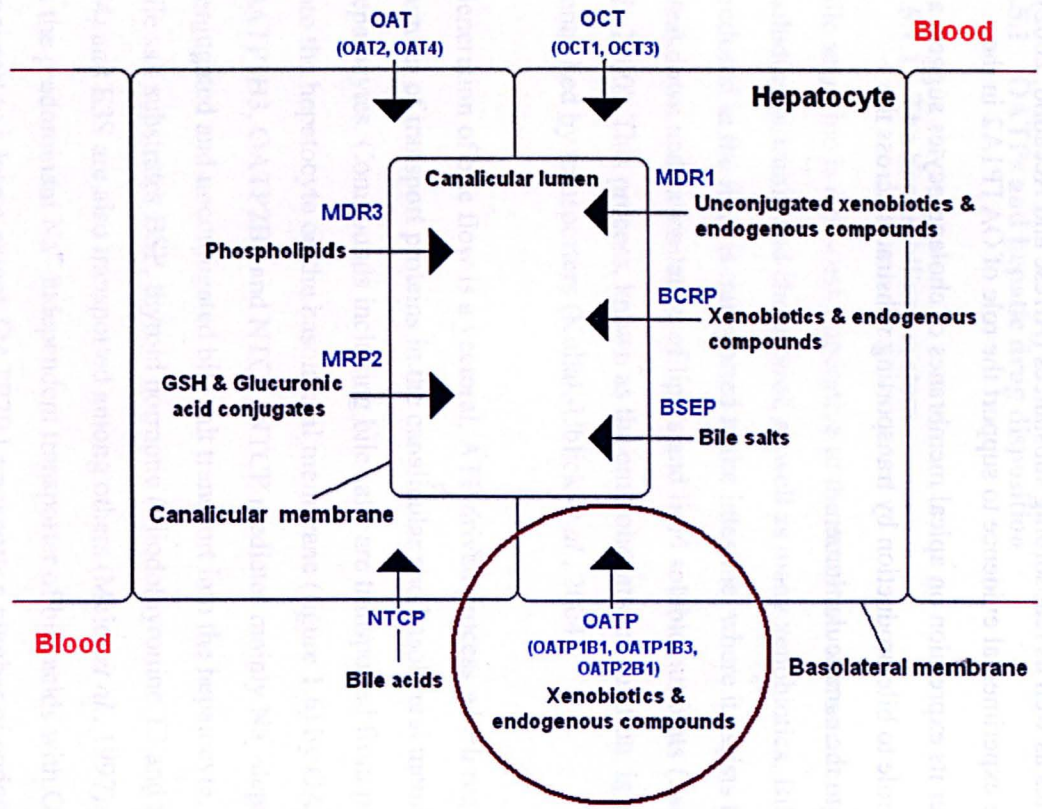

Figure 1.6 - Hepatocyte model displaying the major transporters involved in transport of solutes from portal blood into the hepatocyte and canalicular lumen. The OATPs are highlighted with a red circle. BSEP = Bile salt export pump, MDR = Multidrug-resistance protein, MRP = Multidrug resistance-associated protein, BCRP = Breast cancer resistance protein.

Biotransformation is the process whereby endogenous and xenobiotic compounds are chemically modified to make them more soluble for excretion (Boelsterli and Lim, 2007). The main studied enzyme group that catalyse phase I reactions through oxidation, reduction and peroxidation are the cytochrome P450 (CYP) enzymes (Gibson and Skett, 2001).

Biotransformation is central to determining the fate of a drug as the compound enters this process before reaching the systemic circulation. Until transporters were better understood it was thought that the CYP enzymes were major determinants of drug disposition, however it is more likely that disposition is influenced by a combination of transporter, CYP enzyme and other regulatory processes. It is claimed that the uptake of compounds into the hepatocyte can even be the rate limiting step in hepatic drug clearance; with the uptake of saquinavir, nelfinavir, and ritonavir into the hepatocyte exceeding their metabolism (Parker and Houston, 2008). These interactions between CYP enzymes and transporters are still not fully understood, particularly with regards to the OATPs. However, it is likely that there is an important relationship, as substrate specificities frequently overlap. For example the ABC multidrug-resistance protein 1 (MDR1) has an overlapping specificity with CYP3A for rifampicin. When MDR1 and CYP3A are both exposed to rifampicin *in vitro* and *in vivo*, levels of CYP3A are reduced (Schuetz *et al.*, 1996).

The hepatic OATPs have a major role in the bioavailability of drugs during first pass elimination. That is, increased uptake of drugs into the hepatocyte for biotransformation or bile production can decrease the availability of the drug in the systemic circulation. Conversely, decreased uptake results in systemic accumulation, causing toxicity. Owing to the position of OATP1B1, OATP1B3 and OATP2B1 on the hepatocyte basolateral membrane the majority of drug transporter interactions have been studied in these transporters, and a wealth of information has been gathered over the past decade.

1.5.2 OATP-drug interactions

Transporter-drug interactions alter the function of the transporter and are responsible for the hepatotoxicities associated with drug administration. These interactions can be caused by drug-drug interactions (DDIs), genetic variability and environmental factors such as diet. In addition, it is likely that interactions occur between compounds that are both substrates for the CYP enzymes and OATPs, as well as other transporters. For these reasons, the International Transporter Consortium was set up in 2007, for the purpose of investigating the role of transporters such as OATPs, in drug safety and efficacy (Huang *et al.*, 2010).

OATPs are inhibited by a wide array of xenobiotic compounds, such as the major OATP1B1 inhibitors displayed in table 1.4. These include anti-fungals, antibiotics, anti-cancer drugs and statins. Many are inhibitors for several OATPs, such as the immunosuppressant cyclosporine A, a potent inhibitor of OATP1B1, OATP1B3 and OATP2B1 function (Kalliokoski and Niemi, 2009). This transporter inhibition alters the pharmacokinetics of the drug, affecting the ADME properties and inducing toxicity and/or disease. For example, OATP1B1 is the main bilirubin transporter in the liver, and inhibition by indinavir, saquinavir, cyclosporine A and/or rifamycin causes drug induced hyperbilirubinaemia (Campbell *et al.*, 2004). One mechanism for the reduction of transporter expression may be through the drug induced modulation of regulation pathways. For example spironolactone and dexamethasone are PXR ligands, reducing the mRNA expression of several mouse Oatps (Cheng *et al.*, 2005). Inhibition may also be caused by the competitive inhibition of a substrate, by the inhibitor acting as a substrate itself (Westholm *et al.*, 2009b). Inhibition can however be to varying degrees, as shown by the varying IC_{50} values observed in table 1.4. The IC_{50} or half maximal inhibitory concentration is the concentration required to inhibit transporter activity by 50% (Sebaugh, 2011).A detailed review of the hepatic OATP inhibitors has been published recently (Karlgren *et al.*, 2012).

Table 1.4 – Major inhibitors of OATP1B1 with corresponding IC_{50} values. Reproduced and adapted with permission from John Wiley & Sons (Appendix VI) (Kalliokoski and Niemi, 2009)

Class	Inhibitor	IC_{50} (μM)	Reference
Angiotensin receptor II antagonists	Telmisartan	0.436	(Hirano *et al.*, 2006)
	Valsartan	8.96	(Hirano *et al.*, 2006)
Antibiotics	Clarithromycin	8.26 – 96	(Hirano *et al.*, 2006)
	Erythromycin	11.4 – 217	(Hirano *et al.*, 2006)
	Rifampicin	0.477 – 17	(Vavricka *et al.*, 2002)
	Rifamycin SV	0.171 – 2	(Vavricka *et al.*, 2002)
	Roxithromycin	153	(Seithel *et al.*, 2007)
	Telithromycin	121	(Seithel *et al.*, 2007)
Anti-cancer	Irinotecan	Unknown	(Nozawa *et al.*, 2005)
	SN-38	Unknown	(Nozawa *et al.*, 2005)
	Paclitaxel	0.03	(Gui *et al.*, 2008)
Anti-convulsants	Carbamazepine	188	(Gui *et al.*, 2008)
Anti-diabetics	Glibenclamide	0.746	(Hirano *et al.*, 2006)
	Pioglitazone	Unknown	(Nozawa *et al.*, 2004b)
	Repaglinide	2.2	(Bachmakov *et al.*, 2008)
	Rosiglitazone	6.0	(Nozawa *et al.*, 2005)
	Troglitazone	1.2	(Gui *et al.*, 2008)
	Troglitazone sulphate	Unknown	(Nozawa *et al.*, 2004b)
Anti-fungals	Caspofungin	Unknown	(Sandhu *et al.*, 2005)
	Clotrimazole	9.0	(Gui *et al.*, 2008)

	Ketoconazole	19.2	(Hirano *et al.*, 2006)
Anti-retrovirals	Indinavir	5.84 – 18.4	(Campbell *et al.*, 2004)
	Nelfinavir	0.93	(Tirona *et al.*, 2003)
	Ritonavir	0.71 – 0.781	(Tirona *et al.*, 2003)
	Saquinavir	1.2 – 1.56	(Campbell *et al.*, 2004)
Cardiac glycosides	Digoxin	31.7	(Hirano *et al.*, 2006)
Endocrine drugs	Metyrapone	Unknown	(Gui *et al.*, 2008)
	Mifepristone	3.3	(Gui *et al.*, 2008)
Immunosuppressants	Cyclosporine	0.2 - 2.2	(Shitara *et al.*, 2003)
	Tacrolimus	0.611	(Hirano *et al.*, 2006)
Lipid lowering	Atorvastatin acid	0.87	(Hsiang *et al.*, 1999)
	Atorvastatin lactone	2.6	(Chen *et al.*, 2005)
	Gemfibrozil	4.0 – 72	(Noe *et al.*, 2007)
	Gemfibrozil-1-*O*-glucuronide	22.6 – 24	(Shitara *et al.*, 2004)
	Lovastatin	6.1	(Hsiang *et al.*, 1999)
	Lovastatin acid	4.0	(Chen *et al.*, 2005)
	Lovastatin lactone	28	(Chen *et al.*, 2005)
	Pravastatin	Unknown	(Hsiang *et al.*, 1999)
	Simvastatin	Unknown	(Hsiang *et al.*, 1999)
	Simvastatin acid	3.6	(Chen *et al.*, 2005)
	Simvastatin lactone	9.7	(Chen *et al.*, 2005)
Other	Hyperforin	0.82	(Tirona *et al.*, 2003)
	Sildenafil	1.5	(Treiber *et al.*, 2007)

IC_{50} – Inhibitor concentration producing 50% inhibition by the transporter

1.5.2.1 Drug-drug interactions (DDIs)

DDIs are characterised by the effect of one drug on another, when administered concomitantly. This can be the competitive or non-competitive inhibition of a drug by the transport of another, or the induction of the transporter by another drug. For example, the OATP1B1 and OATP1B3 mediated transport of the endothelin receptor agonist bosentan is inhibited when co-administered with cyclosporine A and rifampicin (Treiber *et al.*, 2007). Transporter induction is less well characterised in the OATPs but has been observed in the ABC transporters and the P450 enzymes (Lin, 2003), suggesting it may also occur with the OATPs. In addition to direct inhibition/induction, allosteric induced modulation of transport may also assist in the mechanism of DDIs. This indirect modification of transport was shown recently, whereby non-steroidal anti-inflammatories (NSAIDs) inhibited the mediated transport of OATP1B1 and OATP1B3, even though they themselves were not substrates of the transporters (Kindla *et al.*, 2011a).

Herbal and other alternative non-prescribed medicines also have DDI effects. Alternative medicines are popular and past clinical studies have quoted >50% of participants using at least one non-prescribed alternative medicine (MacLennan *et al.*, 2002). A number of herbal compounds have been studied to observe their potential inhibitory effects on OATP2B1. Bilberry, echinacea, green tea, banaba, grape seed, ginkgo, and soybean potently inhibited OATP2B1 mediated uptake of E3S (Fuchikami *et al.*, 2006). OATP2B1 is expressed in intestinal epithelial cells as well as hepatocytes, suggesting that herbal medicines of this nature may reduce OATP2B1 mediated oral drug absorption as well as metabolism and excretion.

DDIs are further enhanced by the multispecific overlapping nature of the OATPs, ABCs and CYP enzymes for substrates. Many compounds that are inhibitors for the OATPs are also inhibitors for the ABC transporters and the CYP enzymes. Therefore the vectoral process of drug transport, metabolism

and elimination is affected by interactions associated with each step. For example, OATP1B1 mediated transport of the anti-cancer drug gimatecan is completely inhibited by the breast cancer resistance protein (BCRP) inhibitor valspodar (Oostendorp *et al.*, 2009). This increases the level of complexity when assessing the effects of drugs administers concomitantly. There are several important OATP DDIs associated with the cholesterol lowering drugs statins, which are discussed below.

1.5.2.1.1 Statin interactions

The hepatic OATPs are crucial determinants of statin clearance, as the site of action is within the hepatocyte, through the inhibition of 3-hydroxy-3-methyl-glutaryl-CoA (HMG-CoA) reductase. Therefore the inhibition of statin transporting OATPs on the hepatocyte membrane reduces the cholesterol lowering effect of the statin. A number of DDIs have been associated with statins; whereby another drug inhibits the transporter mediated uptake of the statin. This has led to clinically relevant cases of myotoxicity, a condition characterised by muscle breakdown from the toxicity of statin accumulation. OATP1B1 is the most studied and main hepatocyte basolateral transporter for statins. The most potent is the inhibition of OATP1B1 mediated cerivastatin transport by cyclosporine A (Shitara *et al.*, 2003) and gemfibrozil (Shitara *et al.*, 2004). Cyclosporine A is also an inhibitor of MDR1 and CYP3A4 (Kalliokoski and Niemi, 2009). Therefore uptake and efflux transporters as well as metabolising enzymes are inhibited, resulting in a damaging effect on the disposition of other drugs. Cyclosporine A inhibition of pravastatin (Regazzi *et al.*, 1993) and simvastatin (Vlahakos *et al.*, 2002) transport was also confirmed *in vivo*. In fact cerivastatin was removed from the market in 2001 owing to cases of rhabdomyolysis, a condition causing severe muscle breakdown and kidney failure from toxic products in the blood (Psaty *et al.*, 2004). The consequences of these DDIs highlight the detrimental effects of these interactions on patient health.

1.5.3 Environmental drug interactions

It is well established that fruit juices have an impact on orally absorbed drugs by enhancing the systemic exposure during first pass metabolism. The furanocoumarins in citrus juices inhibit the CYP3A4 enzymes (Paine *et al.*, 2006) and fruit juices also affect transporter function. Juices from grapefruit, apple and orange inhibited the OATP2B1 (Satoh *et al.*, 2005a) and OATP1A2 (Adachi *et al.*, 2003; Dresser *et al.*, 2002) mediated absorption of E3S and fexofenadine respectively. This inhibition was most likely caused by flavonoids, which are present in many fruit juices and herbal medicines. Flavonoids were found to directly inhibit OATP1B1 uptake of DHEAS (Wang *et al.*, 2005b) and OATP1A2 and OATP2B1 mediated uptake of atorvastatin (Mandery *et al.*, 2010). As these transporters are expressed in the intestine and the liver, there is the strong potential for altered ADME of drugs in the presence of fruit juices.

1.5.4 Genetic variation and drug transport

SNPs in the *SLCO* gene sequence alter the OATP protein sequence, often reducing transport function and affecting the ADME of xenobiotic compounds. Influential SNPs can be in coding and non-coding regions (Trevino *et al.*, 2009). Many polymorphisms that reduce transport function have been identified in OATP1A2 (Lee *et al.*, 2005), OATP1B1 (Chigutsa *et al.*, 2011), OATP1B3 (Chew *et al.*, 2011) and OATP2B1 (Nozawa *et al.*, 2002). However the *in vitro* and *in vivo* associations with drug interactions have been most extensively studied in OATP1B1.

Initially 14 non-synonymous SNPs were located in OATP1B1 (Tirona *et al.*, 2001); eight of which conferred decreased transport activity. Now more than 40 have been located (Niemi *et al.*, 2011) (figure 1.7). These variations can affect protein expression on the membrane (Kameyama *et al.*, 2005) or the functional processes of the transporter (Iwai *et al.*, 2004). The variations are widely

distributed around the world and haplotypes (frequently occurring collections of SNPs) are associated with populations in Africa, Middle East, Americas, Europe and Oceana (Chigutsa *et al.*, 2011; Pasanen *et al.*, 2008). The SNP 521T>C is one of the most prevalent and associated with altered pharmacokinetics of several drugs. One such altered is lopinavir, an anti-retroviral drug used in combination for the treatment of human immunodeficiency virus (HIV). Individuals with the SNP were shown to have significantly higher plasma concentrations of lopinavir, suggesting that impaired transport of the drug into the hepatocyte was the cause (Hartkoorn *et al.*, 2010; Kohlrausch *et al.*, 2010; Schipani *et al.*, 2012). This SNP also has implications for statin clearance. SNP 521T>C reduced the hepatic uptake of atorvastatin, pitavastatin, pravastatin, rosuvastatin (Romaine *et al.*, 2010) and simvastatin (Brunham *et al.*, 2011), also elevating plasma levels.

Genetic variation is another important mechanism for the adverse effects associated with drug ADME. It is attractive to consider that this knowledge of genotype may in the future indicate a patient's response to drug therapy.

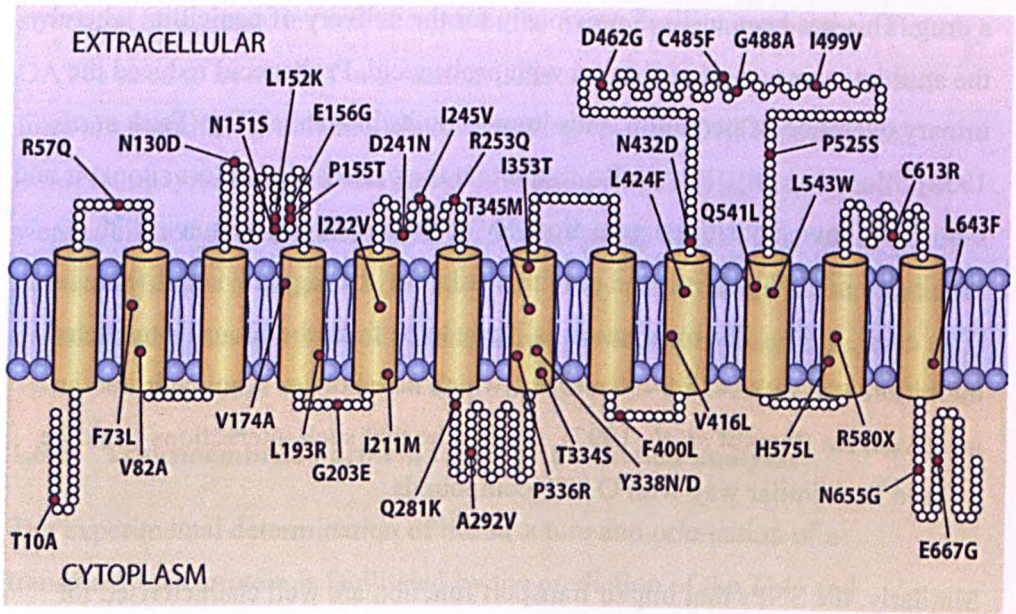

Figure 1.7 – Predicted topology of OATP1B1 highlighting the broad range of SNPs. Reproduced with permission from the American Society for Pharmacology and Experimental Therapeutics (Appendix VI) (Niemi *et al.*, 2011).

The presence of the many drug interactions associated with OATPs highlights the importance of characterising these transporters for future drug development studies. OATPs are part of a complex network of transporters and enzymes which work together to move and metabolise drugs. Furthermore, interactions associated with each of these components can have a detrimental or synergistic effect on another component.

DDIs could, however, be used advantageously to improve the bioavailability of a drug. This has been utilised previously for the delivery of penicillin, whereby the antibiotic was co-administered with probenecid. Probenecid reduced the urinary excretion of penicillin, thus improving its bioavailability (Frisk *et al.*, 1952). More recently, it was also found that the protease inhibitors ritonavir and saquinavir have a positive interaction. By co-administering ritonavir with saquinavir in HIV patients, the oral bioavailability of saquinavir was increased (Hsu *et al.*, 1998). The mechanism is likely to be from the ritonavir mediated inhibition of CYP3A4; a P450 enzyme which metabolises saquinavir into an inactive form (Kempf *et al.*, 1997). It could be that such interactions could be utilised in a similar way with OATP compounds.

Similarly, the SNPs that impair transport function are well characterised for OATP1B1 but less so for the other hepatic OATPs. Analysis of genetic variation in this manner may in the future change the way drugs are administered, by assessing an individual's genotype prior to administration. Understanding the structural and functional characteristics of OATPs is fundamental to understanding the properties of drug disposition.

1.6 Choice of model system

The choice of model system for studying the characteristics and kinetics of transport proteins is crucial to gaining an accurate insight to transporter function. There is literature to support the use of several systems for OATP

transport, including *Xenopus laevis* oocytes (St-Pierre *et al.*, 2002), primary hepatocytes (Nakai *et al.*, 2001), mammalian cell lines (Gui and Hagenbuch, 2008) and cell line membrane vesicles (St-Pierre *et al.*, 2002).
Primary human hepatocyte studies are useful for studying the entire cellular environment as they maintain cellular characteristics and regulatory pathways. Influx and efflux by transporters has been demonstrated this way (Jigorel *et al.*, 2005). However, by analysing a complete endogenous cell, specific families or individual transporter characteristics cannot be isolated. In order to study the structural characteristics and because of the overlapping substrate specificities, OATPs need to be studied in isolation. Therefore *X. laevis* oocytes and cell lines are more favourable models for studying specific OATP properties.
X. laevis oocytes and a human embryonic kidney 293T (HEK293T) cell line were evaluated as potential models for investigating the OATPs, which is discussed further in chapter 3. Primary rat kidney membrane vesicles were also investigated as a novel method for measuring endogenous Oatp transport.

1.6.1 Transmembrane protein topology prediction analysis

The experimental determination of the structure and orientation of a transmembrane protein is facilitated by the prediction of the TMs and extracellular loops. This is known as the 'topology;' defined by the orientation of the N and C termini within the membrane, as well as the number and orientation of TMs (Sonnhammer *et al.*, 1998). There are various topology prediction programs available to predict these features with algorithms based on hydrophobicity analysis, statistical models and multiple sequence alignment (Zhou and Zhou, 2003). Hydrophobicity analysis is the most frequently utilised tool for topology prediction and is based on the hydrophobicity of amino acids. Amino acids present within the cell membrane are hydrophobic to match the hydrophobic phospholipid tails, and thus collections of hydrophobic amino acids can be predicted as intramembrane domains. The hydrophobicity of amino acids is organised into a scale; the more hydrophobic the amino acid, the

more positive on the scale it becomes. This can be displayed on a hydropathy plot, as shown in figure 1.8.

1.6.2 Site directed mutagenesis

Site directed mutagenesis (SDM) is a useful tool for assessing the structural and functional properties of a protein, when a crystal structure is not available. A single amino acid is mutated to determine the importance for protein folding, membrane targeting and/or substrate binding, which can be identified by quantifying levels of protein on the membrane and altered transport kinetics. The method is used frequently for the structural analysis of transmembrane proteins, including the OATPs. For example the positive amino acids within the putative pore of OATP1B1 (Weaver and Hagenbuch, 2010) and the cysteine residues in loop 5 of OATP2B1 (Hanggi *et al.*, 2006) were characterised using this method.

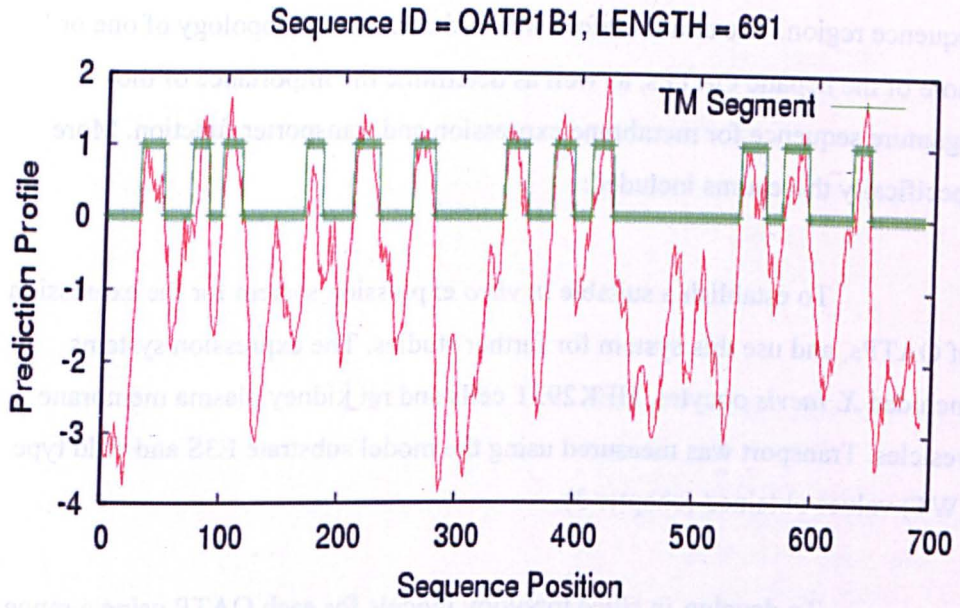

Figure 1.8 – Hydropathy plot of OATP1B1 displaying 12 predicted TM segments; regions of hydrophobic amino acids show as positive on the hydrophobicity scale (green bars). Obtained from the SVMtm protein prediction server (Nugent and Jones, 2009).

1.7 Aims

The aim of this thesis was to further elucidate the structure and function of any/all of the functionally influential OATPs; OATP1A2, OATP1B1, OATP1B3 and OATP2B1. These four hepatic OATPs have important roles in the ADME of compounds and have been implicated in disease and clinically relevant DDIs. Little is known about the exact topology of the OATPs and the function of their structural features, such as the 13 amino acid signature sequence region. The aim therefore was to determine the topology of one or more of the hepatic OATPs, as well as determine the importance of the signature sequence for membrane expression and transporter function. More specifically these aims included:

- To establish a suitable *in vitro* expression system for the expression of OATPs, and use this system for further studies. The expression systems included *X. laevis* oocytes, HEK293T cells and rat kidney plasma membrane vesicles. Transport was measured using the model substrate E3S and wild type (WT) values obtained (chapter 3).

- To develop *in silico* topology models for each OATP using a range of topology prediction programs, to predict the amino acid locations of the TMs, extracellular loops, N and C termini and signal peptide sequence (chapter 4).

- To experimentally determine the number of TMs and orientation of the N and C termini, by inserting FLAG epitope tags into the predicted extracellular loops and termini, based on the topology predictions. The tagged proteins were to be detected on the membrane quantitatively using luminometry and qualitatively using confocal microscopy. Maintenance of function would be confirmed by comparing transport kinetics for E3S with the WT protein (chapter 4).

- To determine the importance of residues within the signature sequence region for substrate transport and membrane expression using SDM of one of the previously tagged isoforms. The effect of the mutation was to be determined through transport experiments, luminometry and confocal microscopy. Values would be compared to those of the tagged WT protein (chapter 5).

2 Materials and Methods

2.1 Materials

2.1.1 Chemicals

All chemicals were purchased from Sigma Aldrich (Dorset, UK) unless stated otherwise

.

2.1.2 Bacterial cells

Escherichia coli: XL1-Blue Subcloning Grade Competent Cells (Agilent Technologies, Stockport UK; cat # 200130).

2.1.3 Mammalian cells

Human Embryonic Kidney 293T/17 cells (LGC Standards, Middlesex UK; ATCC # CRL-11268).

2.1.4 cDNA clones

SLCO1A2: Source Bioscience, Nottingham UK; Accession # BC042452, ATCC Image clone # 4820050
SLCO1B1: Autogen Bioclear, Wiltshire UK; Accession # BC114376, ATCC Image clone # 40037364
SLCO1B3: Invitrogen, Paisley UK; Accession # BC141525, ATCC Image clone # 100014510
SLCO2B1: Source Bioscience, Nottingham UK; Accession # BC041095, ATCC Image Clone # 5752976

2.1.5 Vectors

pGem-T (Ampicillin resistance): Promega, Southampton UK; cat # A3600
pXT7 (Ampicillin resistance): Gift from S.L Alper (Kurschat *et al.*, 2006)
pcDNA3.1/Hygro(-) (Ampicillin resistance): Life Technologies Ltd, Paisley UK; cat # V875-20
pCI-neo (Ampicillin resistance): Promega, Southampton UK; cat # E1841

2.1.6 Enzymes

All restriction enzymes were purchased from New England Biolabs (Hitchin, UK)
Pfu DNA polymerase (Promega, Southampton UK)
Easy-A high-fidelity PCR cloning enzyme (Agilent Technologies, Stockport UK)

Antarctic phosphatase (New England Biolabs, Hitchin UK)
T4 DNA ligase (New England Biolabs, Hitchin UK)
T7 enzyme mix (Life Technologies, Paisley UK)
Turbo DNase solution (Life Technologies, Paisley UK)

2.1.7 Antibiotics

Ampicillin sodium salt (Sigma, Dorset UK)
Gentamycin sulphate (Sigma, Dorset UK)
Penicillin/Streptomycin solution (Sigma, Dorset UK)
Amphotericin B (Sigma, Dorset UK)

2.1.8 Antibodies

Monoclonal ANTI-FLAG M2-Peroxidase (HRP) mouse antibody (Sigma, Dorset UK; cat # A8592)
Monoclonal ANTI-FLAG M2 mouse antibody (Sigma, Dorset UK; cat # F1804)
Anti-mouse IgG-FITC rabbit antibody (Sigma, Dorset UK; cat # F9137).

2.1.9 Isotopes

[^{3}H] E3S (54.3Ci/mmol, Perkin Elmer, MA USA; cat # NET203250UC)
[^{3}H] D-phenylalanyl-L-glutamine (17.4Ci/mmol custom synthesised, Cambridge Research Biochemicals, Stockton-on-Tees UK)

2.2 Molecular biology methods

2.2.1 Polymerase chain reaction (PCR)

2.2.1.1 Primer design

Primers were designed in order to sequence a region of a gene, flank the gene for amplification or mutate a region of interest (mutagenic primers). Mutations included single base pair mutations and FLAG epitope tag insertions. Flanking and sequencing primers were designed to conform to a length of 18-22 base pairs, minimum 40% GC content, 55-60°C T_m and terminate in one or more C or G bases where possible. Mutagenic primers were between 30-60 base pairs and T_m >78°C. The mutation was contained in the middle of the primer with

approximately 20 base pairs of gene sequence each side of the mutation. Primers were constructed with a restriction site before the start/after the stop codons with at least 3 bases each side for efficient restriction digestion. Restriction sites in sequences were located using NEBcutter (Vincze *et al.*, 2003). Primers were checked for hairpins, dimers and complementarity using OligoCalc (Kibbe, 2007) and efficient alignment checked using GeneDoc (Nicholas *et al.*, 1997). Primers were ordered from Fisher Scientific (Loughborough UK).

2.2.1.2 PCR reaction

Polymerase chain reactions (PCRs) were facilitated with the high fidelity enzyme *Pfu* DNA polymerase (Promega, Southampton UK) unless otherwise stated. Reactions were prepared according to the product datasheet and summarised in table 2.1. Aliquots of assembled dNTPs were stored at -20°C prior to reaction assembly. Primers were reconstituted in nuclease free dH_20 to 50 picomoles (pmol) according to the manufacturer's instructions and also stored at -20°C.

Table 2.1 – Reaction components for a single PCR reaction using *Pfu* DNA polymerase

Reaction components	Volume (µl)
DNA template (50-100ng/µl)	1
Pfu 10X reaction buffer	5
dNTPs (10nM each)	1
Forward primer (~50pmol)	1
Reverse primer (~50pmol)	1
Pfu DNA polymerase (2-3U/µl)	0.5
Nuclease free dH_20	40.5
TOTAL	**50**

Temperature and cycling conditions were based on a 'ramp' approach (personal communication, Dr Imogen Sparkes, Oxford Brookes University, Oxford UK), whereby the annealing temperature was gradually decreased every 5 cycles to

provide a range of temperatures for different primers to anneal. This reduced the level of annealing temperature optimisation for each primer designed. The thermal cycling conditions are summarised in table 2.2. The extension temperature is optimal for the polymerase used (68-72°C) and extension time depends on the size of the gene to be amplified (1 min per kb).

Table 2.2 – Thermal cycling conditions for *Pfu* polymerase reaction utilising a 'ramp' based approach

Step	Temperature (°C)	Time (mins)	Number of cycles
1	95	1	1
2	94	0.2	- 5
	63	1	
	72	1/kb	
3	94	0.2	5
	55	1	
	72	1/kb	
4	94	0.2	5
	45	1	
	72	1/kb	
5	4	∞	-

2.2.2 Purification of PCR and template DNA

The QIAquick PCR purification kit (Qiagen, Hilden Germany) was used to purify PCR products and restriction enzyme digested DNA (section 2.2.3) up to 10kb. Purification was performed according to the manufacturer's instructions. Briefly, 5 volumes of buffer PB supplied in the kit were added to 1 volume of DNA. The total volume was added to a purification column and DNA bound to the membrane by centrifuging at 13,000rpm for 1 minute. All further centrifugation steps were performed at 13,000rpm. The eluate was discarded and 750µl buffer PE supplied with the kit added to the column. The column was centrifuged as above. The eluate was discarded and column centrifuged once more to remove residual ethanol. The column was then transferred to a clean 1.5ml tube and 50µl nuclease free dH_20 added directly to the membrane. The

membrane was left for 1 minute before centrifuging. Purified DNA was stored at -20°C.

2.2.3 Restriction digestion

Restriction digests were performed to create compatible cohesive/blunt ends for a gene/vector ligation. A generic restriction digest is displayed in table 2.3. Typically, 1µg DNA was digested for 1 hour at 37°C. Bovine serum albumin (BSA) was required for specific enzymes described by the manufacturer and prevented adhesion of the enzyme to tubes and pipette surfaces.

Double digests were also performed with two restriction enzymes simultaneously. High fidelity enzymes were purchased where possible for this purpose, which displayed 100% activity in the same buffer. Digests with incompatible enzymes were conducted sequentially, by digesting with one enzyme at a time and purifying the template in between.

Table 2.3 – Typical single enzyme restriction digest reaction

Reaction components	**Volume (µl)**
Template DNA (1µg/µl)	1
10X NEBbuffer	5
100X BSA (if required)	0.5
Restriction enzyme	0.5
Nuclease free dH_20	43
TOTAL	**50**

2.2.4 Agarose gel electrophoresis

Agarose gel electrophoresis was used to separate nucleic acids by size following a PCR or restriction digest reaction. Typically, 1% agarose gels were prepared with Hi-Pure Low EEO agarose (Biogene Ltd, Cambridge UK), Tris-Borate-EDTA (TBE) buffer (Invitrogen, Paisley UK) and ethidium bromide solution (10mg/ml) (Sigma, Dorset UK). Approximately 100ng DNA was

combined with 6X blue/orange loading dye (Promega, Southampton UK) and loaded one sample per well. A 1kb ladder (Promega 1kb DNA ladder, Southampton UK or NEB 1kb DNA ladder, Hitchin UK) was loaded 1:5 with blue/orange loading dye (Promega, Southampton UK) in the first and last wells. Gels were run in TBE buffer at ~95V for 45 minutes or until the ladder had separated thoroughly. Gels were visualised using a UV transilluminator (UVP, Cambridge UK) and photographed using a Uvitec camera with hood (Cambridge, UK). When DNA band excision was required, gels were run at ~75V to avoid shearing of DNA ends. The DNA bands were then quickly removed from the gel by scalpel, to avoid the introduction of mutations by the UV light.

2.2.5 DNA gel extraction

Specific DNA bands were excised from 1% agarose gels and purified using a QIAquick gel extraction kit (Qiagen, Crawley UK). Briefly, 3 volumes of buffer QG supplied with the kit was added to 1 volume of excised gel slice (100mg gel ~ 100µl buffer QG). The tube was heated to 50°C and vortexed to dissolve the agarose. The solution was then added to a spin column and centrifuged for 1 minute at 13,000rpm. The eluate was discarded and the column was washed by adding 750µl buffer PE supplied with the kit and centrifuging as above. The eluate was discarded and the column centrifuged for an additional minute to remove residual ethanol. The column was transferred to a clean tube and 50µl nuclease free dH_20 added for 1 minute. The tube was centrifuged to elute the DNA and was stored at -20°C.

2.2.6 Vector dephosphorylation

DNA vectors were dephosphorylated with antarctic phosphatase (NEB, Hitchin UK) following restriction enzyme digestion, to remove 5' phosphates and prevent vector re-ligation. Antarctic phosphatase can be 100% heat inactivated in 5 minutes and thus requires no further purification prior to ligation.

Reactions were assembled as per table 2.4 and incubated for 15 minutes at 37°C. The enzyme was then heat inactivated for 5 minutes at 65°C.

Table 2.4 – Reaction components for antarctic phosphatase treatment of DNA vectors

Reaction components	Volume (µl)
Purified vector DNA (~1µg)	44
10X reaction buffer	5
Antarctic phosphatase (5µl)	1
TOTAL	**50**

2.2.7 DNA ligation

Vector and gene restriction fragments were ligated using T4 DNA ligase (NEB, Hitchin UK). Gene (insert) fragments were routinely ligated 3:1 with vector fragments as recommended in the manufacturer's instructions. The amount of insert DNA required for a ligation was calculated with the equation displayed in figure 2.1.

$$\text{Insert (ng)} = N \times \left(\frac{\text{Length of insert (bp)}}{\text{Length of vector (bp)}} \right) \times \text{vector (ng)}$$

Figure 2.1 – Equation for calculating the amount of insert DNA required for a particular insert to vector ratio (N).

Reactions were assembled according to table 2.5. Negative controls contained vector DNA and dH_20 in place of gene fragments to assess for vector re-ligation. Reactions were incubated overnight at 16°C then stored at 4°C until transformation into *E. coli* cells (section 2.2.8).

Table 2.5 – Components of a DNA ligation reaction

Reaction components	Volume (µl)
Vector DNA	4*
Insert DNA	4*
10X T4 DNA ligase reaction buffer	1
T4 ligase (400U/µl)	1
TOTAL	**10**

* Volumes were calculated according to molar ratios and varied per reaction.

2.2.8 Transformation of DNA into *E. coli* cells

XL1 blue subcloning grade *E. coli* cells (section 2.1.2) were used to transform whole plasmid and ligated plasmid DNA. Cells were thawed on ice and 50µl aliquots made per transformation reaction. Approximately 50ng plasmid DNA or 5µl of ligation reaction (section 2.2.7) were added to the cells followed by heat shocking at 42°C for 45 seconds. Tubes were incubated on ice for 2 minutes prior to the addition of 900µl Super Optimal Broth with Catabolite repression (SOC) medium (Invitrogen, Paisley UK), prewarmed to 42°C. Tubes were incubated at 37°C while shaking for 30 minutes. Cells were centrifuged at 3500rpm, 25°C for 5 minutes and the supernatant replaced with 100µl fresh SOC medium. The total volume was spread on LB agar (Sigma, Dorset UK) plates containing 100µg/ml ampicillin (section 2.1.7). Plates were incubated overnight at 37°C and transformants screened by cracking method (section 2.2.9). Positive colonies were grown overnight at 37°C in 5ml LB broth (Sigma, Dorset UK) followed by the generation of glycerol stocks (section 2.2.10). DNA was isolated and purified by a miniprep (section 2.2.11). DNA was quantified using a spectrophotometer (section 2.2.12) and stored at -20°C.

2.2.9 DNA cracking

E.coli bacterial colonies were screened to check for positively ligated DNA. The DNA cracking method (Personal communication, Dr Isabel Bermudez-Diaz, Oxford Brookes University, Oxford UK) allows for rapid screening of

colonies prior to miniprep and sequencing. The method involves the lysis of bacterial cells to release the plasmid DNA, which is then visualised immediately using agarose gel electrophoresis (section 2.2.4). Approximately 12 colonies were screened per plate. Cracking buffer stock was made according to table 2.6 and stable at room temperature for 6 months. The stock was assembled by dissolving sucrose in the dH_20 by heating to 65°C (without boiling), followed by the addition of the other components. Lysis buffer was prepared fresh by combining cracking buffer stock with 6X loading dye (Promega, Southampton UK) in a 1 in 10 dilution.

Table 2.6 – Components of the cracking buffer stock

Components	Amount/volume
Sucrose	25g
5M NaOH	5ml
10% SDS	2.5ml
dH_20	42.5ml
TOTAL	**50ml**

Individual colonies were collected from agar plates with a pipette tip and placed in 20µl dH_20 by pipetting up and down 10-20 times. The tip was then transferred to a corresponding tube containing 200µl LB broth with 100µg/ml ampicillin. Following this 7µl lysis buffer was added to the bacterial/dH_20 solution and the total volume immediately loaded on a 1% agarose gel. The sample DNA band patterns were compared with that of negative (vector only) and positive (vector with insert) controls. Sample bands that matched the pattern of the positive control were chosen as positive colonies and the bacterial/LB broth solutions grown while shaking overnight in 5ml LB broth with 100µg/ml ampicillin at 37°C. Glycerol stocks were then made; the DNA purified by miniprep and sent for sequencing to confirm the presence of the insert.

2.2.10 Plasmid glycerol stocks

Glycerol stocks are a reliable method for long term storage of bacterial cells which contain a specific plasmid of interest. Stocks were generated by combining 1ml *E. coli* overnight culture with 250µl autoclaved 80% glycerol in dH_20 and stored immediately at -80°C. Stocks were regenerated by placing a sample of the stock in 5ml LB broth with antibiotic and grown overnight at 37°C while shaking.

2.2.11 Isolation and purification of DNA from *E. coli*

Overnight cultures were prepared by picking *E. coli* colonies from agar plates, from DNA cracking or from glycerol stocks and placing in 5ml LB broth plus antibiotic. Cultures were grown overnight at 37°C while shaking. Following incubation 1ml culture was reserved for glycerol stocks if required (section 2.2.10). DNA was isolated from the remaining culture using the miniprep purification system (section 2.2.11.1). High quality and highly concentrated DNA required for cell transfections was isolated using a maxiprep purification system (section 2.2.11.2). Purified DNA was visualised using agarose gel electrophoresis and quantified by spectrophotometer.

2.2.11.1 Miniprep DNA purification

DNA was isolated from *E. coli* cultures using the Wizard Plus SV Minipreps DNA Purification System (Promega, Southampton UK) which yielded ~1.5µg total purified DNA. This DNA was used for PCR reactions and restriction digestions.

Overnight culture was centrifuged at 3500rpm for 10 minutes to generate a cell pellet. All further centrifugation steps were conducted at 13,000rpm and all solutions were provided in the kit. The supernatant was discarded and the pellet thoroughly resuspended in 250µl resuspension solution. The total volume was transferred to a 1.5ml tube, 250µl cell lysis solution added and the tube inverted

several times. This was followed by the addition of 10µl alkaline protease solution, the tube inverted and then incubated at room temperature for 5 minutes. Then 350µl neutralisation solution was added, the tube inverted and centrifuged for 10 minutes. The supernatant was placed in the supplied columns and centrifuged for 1 minute. The eluate was discarded and 750µl column wash solution added to the column. This was centrifuged for 1 minute and the eluate discarded. The column was then centrifuged for a further 2 minutes to remove any residual ethanol.

The column was transferred to a clean 1.5ml tube and 100µl sterile dH_20 placed directly on the membrane. The column was centrifuged for a further minute to elute the DNA. It was then stored at 4°C for ~3 days or -20°C for long term storage.

2.2.11.2 Maxiprep DNA purification

The Pureyield™ plasmid maxiprep system (Promega, Southampton UK) was used to isolate DNA for HEK293T cell transfections, as the system produces DNA of a high yield and quality. It also includes an endotoxin removal wash step which reduces the amount of protein, RNA and endotoxins in the sample.

An *E. coli* cell sample containing the plasmid of interest was taken from a glycerol stock and grown overnight at 37°C in 5ml LB broth with 100µg/ml ampicillin. The total volume was added to 245ml LB broth with antibiotic in a 500ml conical flask overnight at 37°C whilst shaking. The culture was centrifuged at 20,000rpm for 10 minutes at room temperature to pellet the cells. The supernatant was discarded and the pellet thoroughly resuspended with 12ml resuspension solution. This was followed by the addition of 12ml cell lysis solution and the tube inverted several times. The solution was incubated at room temperature for 5 minutes. Then 12ml neutralisation solution was added and the tube inverted 10-15 times. The tube was then centrifuged for 30 minutes at 20,000 rpm. A blue column was placed in a white column supplied with the kit and placed on a Vac-Man® laboratory vacuum manifold (Promega,

Southampton UK). Vacuum was applied to the manifold using a Laboport vacuum pump (KNF Neuberger Inc, Witney UK). The supernatant was dispensed into the blue column and drawn through the blue and white column using the vacuum. The blue column was discarded and 5ml endotoxin removal wash drawn through the white column by vacuum. Then 20ml column wash was drawn through the white column. The vacuum was applied for a further 5 minutes to remove any residual ethanol from the membrane. A sterile 1.5ml tube was placed in the supplied elution device and placed on the manifold under the column to elute the DNA. 1ml nuclease free dH_20 was placed directed on the membrane and drawn through the column. The purified DNA was sent for sequencing and stored in aliquots at -20°C.

2.2.12 DNA quantification

DNA and RNA were quantified using the NanoDrop ND 1000 spectrophotometer (Thermo Fisher Scientific, Loughborough UK) at the 260nm absorbance. The spectrophotometer was normalised with 2µl dH_20 before measuring 2µl DNA sample. Units were reported as ng/µl and purity was assessed using the 260/280nm ratio.

2.2.13 DNA sequencing

Purified miniprep/maxiprep DNA was sequenced by Sanger sequencing, conducted by the Oxford division of Source Bioscience (Nottingham, UK). DNA at a concentration of ~100ng in 5µl aliquots were sent with 3.2pmol custom primers. The beginning of the gene was sequenced using the stock T7 primer, the centre and end of the gene were sequenced with custom primers (table 2.8), to ensure the gene was completely sequenced. Resultant sequences were aligned using ClustalW2 (Larkin *et al.*, 2007).

2.2.14 DNA constructs

DNA cloning was required to sub-clone genes into different vectors, introduce FLAG epitope tags and make single base mutations. An overview of the cloning method is displayed in figure 2.2, with a list of constructs generated in table 2.7. Primers are listed in table 2.8. The molecular biology methods employed in section 2.2 are those described previously unless otherwise stated.

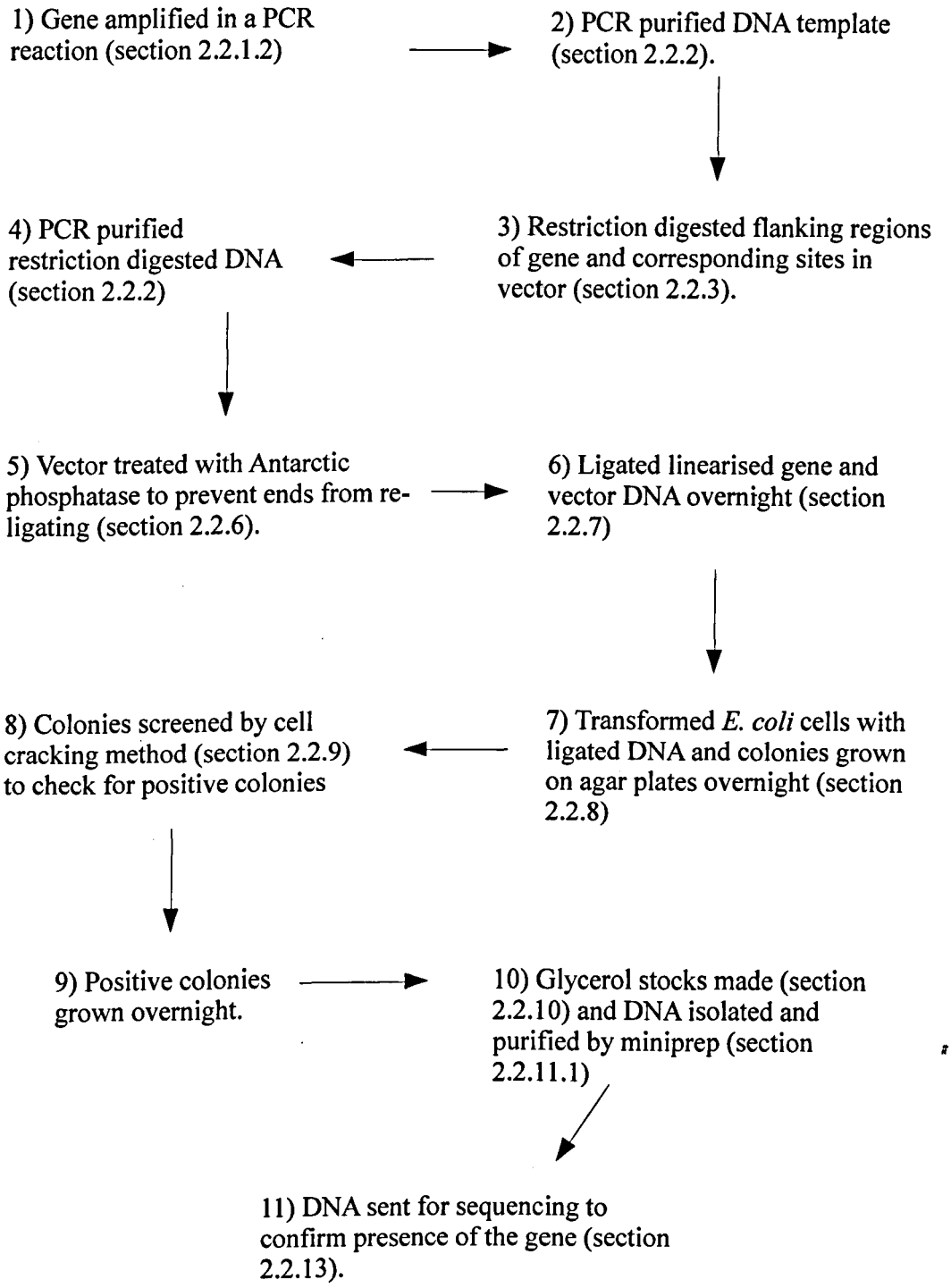

Figure 2.2 – Flow chart displaying procedures for sub-cloning a gene from one vector to another

Table 2.7 – Plasmid constructs generated

Plasmid	Vector	Gene	Epitope
pGem vector sub-cloning			
pGem-T/*SLCO1A2*	pGem-T	*SLCO1A2*	None
pGem-T/*SLCO1B1*	pGem-T	*SLCO1B1*	None
pGem-T/*SLCO1B3*	pGem-T	*SLCO1B3*	None
pGem-T/*SLCO2B1*	pGem-T	*SLCO2B1*	None
pXT7 vector sub-cloning			
pXT7/*SLCO1A2*	pXT7	*SLCO1A2*	None
pXT7/*SLCO1B1*	pXT7	*SLCO1B1*	None
pXT7/*SLCO1B3*	pXT7	*SLCO1B3*	None
pXT7/*SLCO2B1*	pXT7	*SLCO2B1*	None
pCI-neo vector sub-cloning			
pCI-neo/*SLCO1A2*	pCI-neo	*SLCO1A2*	None
pcDNA3.1/Hygro(-) vector sub-cloning			
pcDNA/*SLCO1A2*	pcDNA3.1/Hygro(-)	*SLCO1A2*	None
pcDNA/*SLCO1B1*	pcDNA3.1/Hygro(-)	*SLCO1B1*	None
pcDNA/*SLCO1B3*	pcDNA3.1/Hygro(-)	*SLCO1B3*	None
pcDNA3.1/Hygro(-) FLAG cloning			
pcDNA/*SLCO1B1*-F1-F13	pcDNA3.1/Hygro(-)	*SLCO1B1*	FLAG 1-13 (F1-F13)
pcDNA3.1/Hygro(-) mutagenesis cloning			
pcDNA/*SLCO1B1*-F4-D251E	pcDNA3.1/Hygro(-)	*SLCO1B1*	F4
pcDNA/*SLCO1B1*-F4-R253K	pcDNA3.1/Hygro(-)	*SLCO1B1*	F4
pcDNA/*SLCO1B1*-F4-W254F	pcDNA3.1/Hygro(-)	*SLCO1B1*	F4
pcDNA/*SLCO1B1*-F4-W258/259F	pcDNA3.1/Hygro(-)	*SLCO1B1*	F4
pcDNA/*SLCO1B1*-F4-N261A	pcDNA3.1/Hygro(-)	*SLCO1B1*	F4

Table 2.8 - List of primers used in sequencing, sub-cloning and mutagenesis: highlighting the restriction enzyme (yellow), Kozak sequence (pink), FLAG epitope insertion (blue) and site-directed mutation (green)

Key:
Restriction enzyme
Kozak sequence
FLAG epitope insertion
Site-directed mutation

Primer	Restriction enzyme	Sequence (5'-3')
DNA sequencing primers		
SLCO1A2 central gene primer	-	AGATGATCTGATCATAACTCCCA C
SLCO1A2 end of gene primer	-	GGACTAGAGACTAATGCTGACA
SLCO1B1 central gene primer	-	CCTTGTGTCTGGACTATTCTCC
SLCO1B1 end of gene primer	-	GTCTCCAGAACAGAAATTACTC
SLCO1B3 central gene primer	-	CACTATCATTGCATGTGCTG
SLCO1B3 end of gene primer	-	GTAACTGGTCTCCAGAACAG
SLCO2B1 central gene primer	-	GAAAGGTCTTAGCAGTCAC
SLCO2B1 end of gene primer	-	TTCTACACCAACTGCAGC
pXT7 vector sub-cloning		
pXT7/*SLCO1A2*-F	*KpnI*	TTTTTTGGTACCAACATGTTTCT GTTGGC
pXT7/*SLCO1A2*-R	*EagI*	AAAAAACGGCCGTCATTAGAAA ACAACATAC
pXT7/*SLCO1B1*-F	*KpnI*	TTTTTTGGTACCCAATCATGGAC CAAAATCAAC
pXT7/*SLCO1B1*-R	*EagI*	AAAAAACGGCCGTCCCTTAACA ATGTGTTTC
pXT7/*SLCO1B3*-F	*AvrII*	TTTTTTCCTAGGACCATGGACCA AC
pXT7/*SLCO1B3*-R	*XbaI*	AAAAAATCTAGACTAGTTGGCA GCAGCAT

pXT7/*SLCO2B1*-F	*AvrII*	TTTTTTCCTAGGGTCATGGGAC
pXT7/*SLCO2B1*-R	*EagI*	AAAAAACGGCCGAGCTCACA
pcDNA3.1/Hygro(-) vector sub-cloning		
pcDNA/*Slc15a1*(PepT1)-FLAG-F	*XhoI*	TTTTTTCTCGAGGCCACCATGGGAATGTCTAAGTCACTGAGC
pcDNA/*Slc15a1*(PepT1)-FLAG-R	*KpnI*	AAAAAAGGTACCTCACATCTGTGTCTG
pcDNA/*SLCO1A2*-F	*XhoI*	TTTTTTCTCGAGGCCACCATGTTTCTGTTG
pcDNA/*SLCO1A2*-R	*KpnI*	AAAAAAGGTACCTCATTAGAAAACAACATACCCTTC
pcDNA/*SLCO1B1*-F	*XhoI*	TTTTTTCTCGAGGCCACCATGGACCAAAATCAAC
pcDNA/*SLCO1B1*-R	*KpnI*	AAAAAAGGTACCTCCCTTAACAATGTGTTTC
pcDNA/*SLCO1B3*-F	*XhoI*	TTTTTTCTCGAGGCCACCATGGACCAACATCAAC
pcDNA/*SLCO1B3*-R	*KpnI*	AAAAAAGGTACCCTAGTTGGCAGCAGCATTGTC
***SLCO1B1* FLAG cloning**		
pcDNA/*SLCO1B1*-F1 (N terminal) primer 1 – F	-	GACGACGACAAGGACCAAAATCAACATTTGAATA
pcDNA/*SLCO1B1*- F1 (N terminal) primer 2 – F	*XhoI*	ATATATCTCGAGGCCACCATGGATTATAAGGACGACGACGACAAGGACC
pcDNA/*SLCO1B1*-F2 – F	-	ATTCATATAGAACGGAGAGATTATAAGGACGACGACGACAAGTTTGAGATATCCTCTTCTCT
pcDNA/*SLCO1B1*-F2 – R	-	AGAGAAGAGGATATCTCAAACTTGTCGTCGTCGTCCTTATAATCTCTCCGTTCTATATGAAT
pcDNA/*SLCO1B1*-F3 – F	-	GTTACTTTGGATCCAAACTACATGATTATAAGGACGACGACGACAAGAGACCAAAGTTAATTGGAAT
pcDNA/*SLCO1B1*-F3 – R	-	ATTCCAATTAACTTTGGTCTCTTGTCGTCGTCGTCCTTATAATCATGTAGTTTGGATCCAAAGTAAC
pcDNA/*SLCO1B1*-F4 – F	-	CAACATCAACCTTATCCACTGATTATAAGGACGACGACGACAAGTGTTTAATTAATCAAATTTTATC
pcDNA/*SLCO1B1*-F4 – R	-	GATAAAATTTGATTAATTAAACACTTGTCGTCGTCGTCCTTATAATCAGTGGATAAGGTTGATGTTG

pcDNA/*SLCO1B1*-F5 – F	-	GTATTTAGGTATATTGAATGCAG ATTATAAGGACGACGACGACAA GATAGCAATGATTGGTCCAATC
pcDNA/*SLCO1B1*-F5 – R	-	GATTGGACCAATCATTGCTATCT TGTCGTCGTCGTCCTTATAATCT GCATTCAATATACCTAAATAC
pcDNA/*SLCO1B1*-F6 – F	-	GGTGGCTTAATTTCCTTGTGGAT TATAAGGACGACGACGACAAGT CTGGACTATTCTCCAT
pcDNA/*SLCO1B1*-F6 – R	-	ATGGAGAATAGTCCAGACTTGT CGTCGTCGTCCTTATAATCCACA AGGAAATTAAGCCACC
pcDNA/*SLCO1B1*-F7 – F	-	CCCCTGTATGTTATGTTTGTGGA TTATAAGGACGACGACGACAAG CTTTTGACGTTGTTACAAG
pcDNA/*SLCO1B1*-F7 – R	-	CTTGTAACAACGTCAAAAGCTT GTCGTCGTCGTCCTTATAATCCA CAAACATAACATACAGGGG
pcDNA/*SLCO1B1*-F8 – F	-	CTAAGGCTAACATCTTATTGGAT TATAAGGACGACGACGACAAGG GAGTCATAACCATACCTAT
pcDNA/*SLCO1B1*-F8 – R	-	ATAGGTATGGTTATGACTCCCTT GTCGTCGTCGTCCTTATAATCCA ATAAGATGTTAGCCTTAG
pcDNA/*SLCO1B1*-F9 – F	-	TTTTTCATACTCTGTGAAAACGA TTATAAGGACGACGACGACAAG AAATCAGTTGCCGGACTAAC
pcDNA/*SLCO1B1*-F9 – R	-	GTTAGTCCGGCAACTGATTTCTT GTCGTCGTCGTCCTTATAATCGT TTTCACAGAGTATGAAAAA
pcDNA/*SLCO1B1*-F10 – F	-	GCAAATCTTCAAGTGGCAATGA TTATAAGGACGACGACGACAAA AAGCCTATAGTGTTTTACAAC
pcDNA/*SLCO1B1*-F10 – R	-	GTTGTAAAACACTATAGGCTTTT TGTCGTCGTCGTCCTTATAATCA TTGCCACTTGAAGATTTGC
pcDNA/*SLCO1B1*-F11 – F	-	TGATTGTTAAAATTGTTCAAGAT TATAAGGACGACGACGACAAGC CTGAATTGAAATCACTTGC
pcDNA/*SLCO1B1*-F11 – R	-	GCAAGTGATTTCAATTCAGGCTT GTCGTCGTCGTCCTTATAATCTT GAACAATTTTAACAATCA
pcDNA/*SLCO1B1*-F12 – F	-	GTAGGACATATAATTCCACAGA TTATAAGGACGACGACGACAAG TCATTTTCAAGGGTCTACTT

pcDNA/*SLCO1B1*-F12 – R	-	AAGTAGACCCTTGAAAATGACT TGTCGTCGTCGTCCTTATAATCT GTGGAATTATATGTCCTAC
pcDNA/*SLCO1B1*-F13 (C terminal) – Primer 1 R	-	GTCCTTATAATCACAATGTGTTT CACTATCTGCCCCAGC
pcDNA/*SLCO1B1*-F13 (C terminal) – Primer 2 R	*KpnI*	CGATCAGGTACCTTACTTGTCGT CGTCGTCCTTATAATCACAATGT GTTTCAC
***SLCO1B1* signature sequence mutagenesis**		
pcDNA/*SLCO1B1*-F4-D251E – F	-	GGATAACTCCTACTGAGTCTCGA TGGGTTGG
pcDNA/*SLCO1B1*-F4-D251E – R	-	CCAACCCATCGAGACTCAGTAG GAGTTATCC
pcDNA/*SLCO1B1*-F4-R253K – F	-	ACTCCTACTGATTCTAAATGGGT TGGAGCTTGG
pcDNA/*SLCO1B1*-F4-R253K – R	-	CCAAGCTCCAACCCATTTAGAAT CAGTAGGAGT
pcDNA/*SLCO1B1*-F4-W254F – F	-	CTACTGATTCTAAATTTGTTGGA GCTTGGTGG
pcDNA/*SLCO1B1*-F4-W254F – R	-	CCACCAAGCTCCAACAAATTTA GAATCAGTAG
pcDNA/*SLCO1B1*-F4-W258/259F – F	-	CGATGGGTTGGAGCTTTCTTCCT TAATTTCCTTGTG
pcDNA/*SLCO1B1*-F4-W258/259F – R	-	CACAAGGAAATTAAGGAAGAAA GCTCCAACCCATCG
pcDNA-*SLCO1B1*-F4-N261A – F	-	TTGGAGCTTGGTGGCTTGCTTTC CTTGTGTCTGGACTATTCTC
pcDNA/*SLCO1B1*-F4-N261A – R	-	GAGAATAGTCCAGACACAAGGA AAGCAAGCCACCAAGCTCCAA

F = forward primer, R = reverse primer

2.2.14.1 Cloning *SLCO* genes into pXT7 vector

The *SLCO* genes were sub-cloned into the pXT7 vector (section 2.1.5) to facilitate expression in *X. laevis* oocytes.

The genes were cloned either side of *X. laevis* untranslated beta globin regions which were recognised by the *X. laevis* translation machinery (figure 2.3). *SLCO1A2*, *SLCO1B1*, *SLCO1B3* and *SLCO2B1* were first cloned into a pGem-T vector before sub-cloning into pXT7. Primers were generated to include flanking restriction enzymes, which could be used to digest the gene out of the pGem vector and into pXT7. *SLCO1A2* and *SLCO1B1* were cloned with *KpnI* and *EagI*. *SLCO1B3* was cloned with *AvrII* and *XbaI*, *SLCO2B1* with *AvrII* and *EagI* (table 2.8). The DNA template was amplified by PCR using the Easy-A polymerase (Agilent Technologies, Stockport UK). This high fidelity enzyme generated 3'-A overhangs which facilitated cloning into the pGem vector with T-overhangs. The reaction was assembled as per table 2.9 and cycling conditions as per table 2.10.

Table 2.9 – Components for the Easy-A PCR reaction

Reaction components	Volume (µl)
SLCO DNA template (100ng/µl)	1
Easy-A 10X reaction buffer	5
dNTPs (10nM each)	1
Forward primer (~50pmol)	1
Reverse primer (~50pmol)	1
Easy-A DNA polymerase (5U/µl)	0.5
Nuclease free dH_20	40.5
TOTAL	**50**

Table 2.10 - Thermal cycling conditions for Easy-A DNA polymerase based PCR

Step	Temperature	Time	Number of cycles
1	95°C	2 min	1
2	95°C	40 sec	30
	(T_m–5°C)	30 sec	
	72°C	1 min / kb	
3	72°C	7 min	1

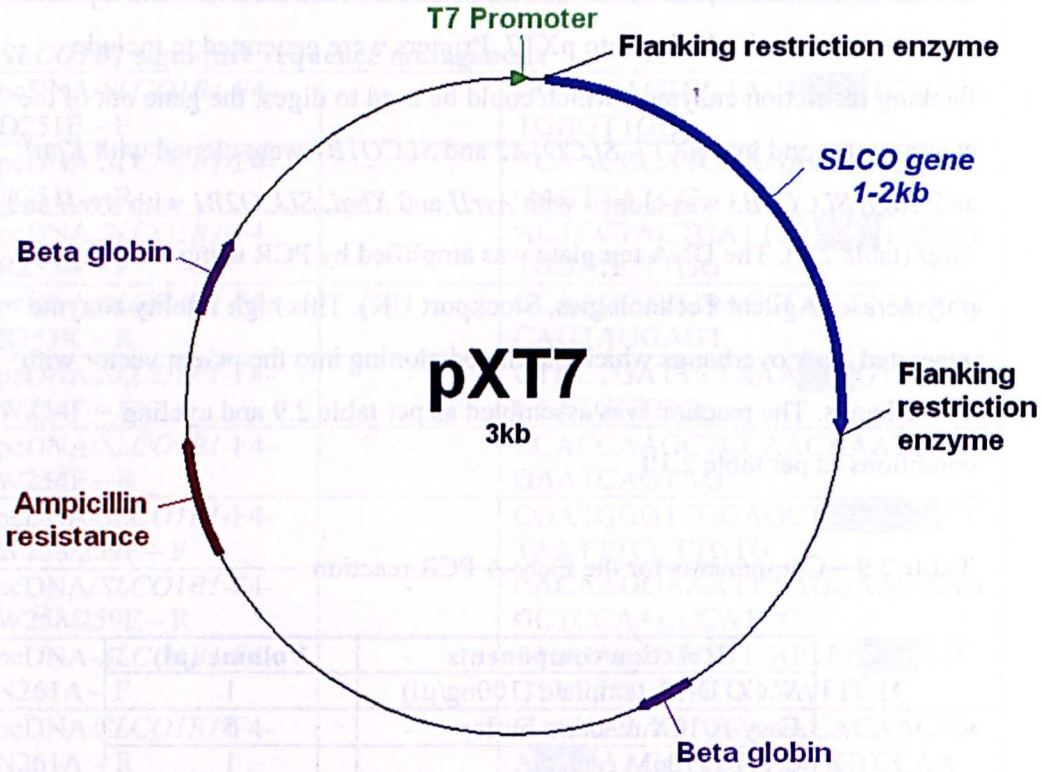

Figure 2.3 – pXT7 vector with *SLCO* gene sub-cloned and displaying the *X. laevis* beta globin regions. Designed with 'A Plasmid Editor' (Davis, 2012).

The PCR product was confirmed on an agarose gel, then purified before ligating into the pGem-T vector (table 2.11). Ligated products were transformed into *E. coli* cells and positive colonies identified by cracking. Glycerol stocks were then made and the DNA isolated by miniprep. Positive colonies were further confirmed by sequencing.

The four *SLCO* genes were sub-cloned from pGem-T into pXT7 by restriction digestion and ligation. Digests with *KpnI* and *EagI* were performed sequentially as the buffers were not compatible. The template was PCR purified between digests. The other digests were performed as double digests. 1µg pXT7 vector DNA was also digested with corresponding enzymes. The *SLCO* and pXT7 digested DNA bands of the correct size were then excised from an agarose gel and purified. The vector was dephosphorylated before ligation of the gene into the vector. The ligation was transformed into *E. coli* cells and plated on agar overnight. Glycerol stocks were made and plasmid DNA isolated by miniprep. Plasmids containing the gene were confirmed by restriction digestion with *NdeI*, an enzyme which cut once within pXT7 but not in the gene. Those visualised as the correct size on an agarose gel were confirmed by DNA sequencing (all methods as described in section 2.2).

Table 2.11 – Reaction assembly for a pGem-T ligation reaction

Reaction components	Volume (µl)
2X Rapid ligation buffer	5
PCR product	3
pGem-T vector (50ng/µl)	1
DNA ligase (3U/µl)	1
TOTAL	**10**

2.2.14.2 Cloning *SLCO* genes into pcDNA3.1/Hygro(-) vector

SLCO1A2, *SLCO1B1*, *SLCO1B3* and rabbit *Slc15a1*(PepT1)-FLAG (positive control) were cloned into pcDNA3.1/Hygro(-) (section 2.1.5) to facilitate expression in HEK293T cells. The vector contains the human cytomegalovirus immediate-early (CMV) promoter which allows high level constitutive

expression in mammalian cells. The primers were designed with a flanking restriction enzyme followed by the Kozak consensus sequence (GCCACC) upstream of the start codon, which is known to initiate translation in eukaryotes (Kozak, 1991) (table 2.8). *SLCO1A2*, *SLCO1B1*, *SLCO1B3* and *Slc15a1*-FLAG were cloned individually into the vector with the restriction enzymes *XhoI* and *KpnI* (figure 2.4).

The genes were amplified with *Pfu* polymerase in a PCR reaction then confirmed on an agarose gel. The product was PCR purified before digesting the total volume with both enzymes in a double digest as displayed in table 2.12.

Table 2.12 - Components of a double restriction digest for cloning *SLCO* genes into pcDNA3.1/Hygro(-)

Reaction components	Volume (µl)
PCR product	43.5
10X NEB buffer 4	5
100X BSA	0.5
XhoI (20U/µl)	0.5
KpnI High fidelity (20U/µl)	0.5
TOTAL	**50**

The pcDNA3.1/Hygro(-) vector was digested simultaneously; 1µg DNA in a double digest as above. The PCR product and vector were then PCR purified and the vector dephosphorylated. The product was ligated into the vector before transforming into *E. coli* cells. Positive colonies were screened by cracking, confirmed by DNA sequencing and stored as glycerol stocks. Large quantities of DNA were isolated by maxiprep and used for HEK293T cell transformations (all methods as described in section 2.2).

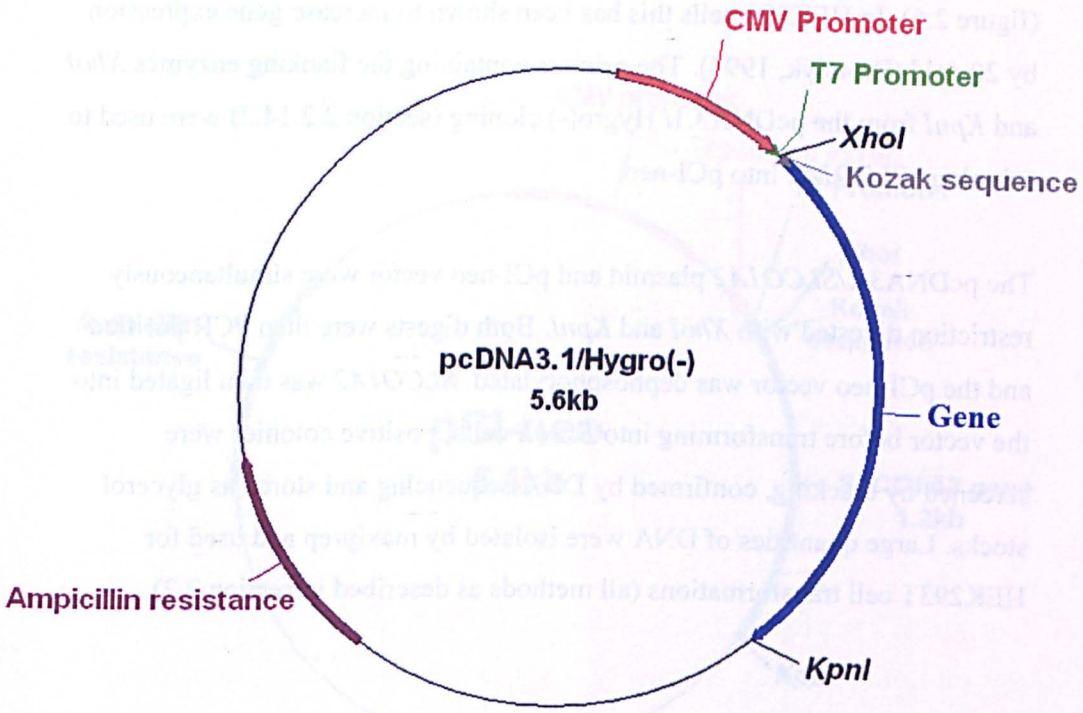

Figure 2.4 – pcDNA3.1/Hygro(-) vector containing a gene with *XhoI* and *KpnI* flanking restriction enzymes, displaying the features of the vector. Designed with 'A Plasmid Editor' (Davis, 2012).

2.2.14.3 Cloning *SLCO1A2* into the pCI-neo vector

The *SLCO1A2* gene was cloned into the pCI-neo vector (section 2.1.5) following poor expression of pcDNA/*SLCO1A2* in HEK293T cells. The pCI-neo vector is a similar mammalian expression vector containing the mammalian CMV promoter but also contains a chimeric intron which flanks the gene (figure 2.5). In HEK293 cells this has been shown to increase gene expression by 20-fold (Brondyk, 1994). The primers containing the flanking enzymes *XhoI* and *KpnI* from the pcDNA3.1/ Hygro(-) cloning (section 2.2.14.2) were used to sub-clone *SLCO1A2* into pCI-neo.

The pcDNA3.1/*SLCO1A2* plasmid and pCI-neo vector were simultaneously restriction digested with *XhoI* and *KpnI.* Both digests were then PCR purified and the pCI-neo vector was dephosphorylated. *SLCO1A2* was then ligated into the vector before transforming into *E. coli* cells. Positive colonies were screened by cracking, confirmed by DNA sequencing and stored as glycerol stocks. Large quantities of DNA were isolated by maxiprep and used for HEK293T cell transformations (all methods as described in section 2.2).

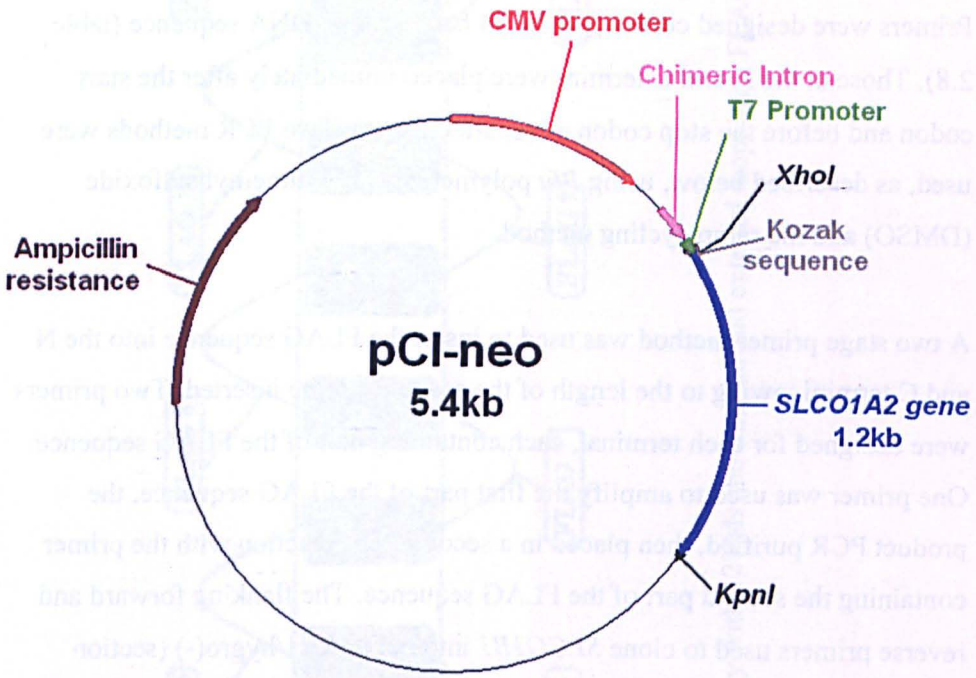

Figure 2.5 – pCI-neo vector containing *SLCO1A2* with *XhoI* and *KpnI* flanking restriction enzymes and displaying the features of the vector. Designed with 'A Plasmid Editor' (Davis, 2012).

2.2.14.4 Cloning FLAG epitope regions into *SLCO1B1*

The FLAG epitope consisting of 8 amino acids (DYKDDDDK) was cloned separately into the N-terminus, C-terminus and putative internal and external loops of pcDNA/*SLCO1B1* (figure 2.6). The epitope regions once cloned could be detected using luminometry (section 2.5.2.3) and immunofluorescence (section 2.5.2.4).

Primers were designed containing the 24 base epitope DNA sequence (table 2.8). Those at the N and C termini were placed immediately after the start codon and before the stop codon as separate clones. Two PCR methods were used, as described below, using *Pfu* polymerase, 10% dimethyl sulfoxide (DMSO) and the ramp cycling method.

A two stage primer method was used to insert the FLAG sequence into the N and C termini, owing to the length of the sequence to be inserted. Two primers were designed for each terminal, each containing half of the FLAG sequence. One primer was used to amplify the first part of the FLAG sequence, the product PCR purified, then placed in a second PCR reaction with the primer containing the second part of the FLAG sequence. The flanking forward and reverse primers used to clone *SLCO1B1* into pcDNA3.1/hygro(-) (section 2.2.14.2) were used for the opposite end of the gene.

An overlap-PCR method (Heckman and Pease, 2007) was used for cloning the FLAG epitope into all other internal and external loops. Two fragments were generated; from the beginning of the gene to the end of the FLAG epitope, and the beginning of the FLAG epitope to the end of the gene (figure 2.7).

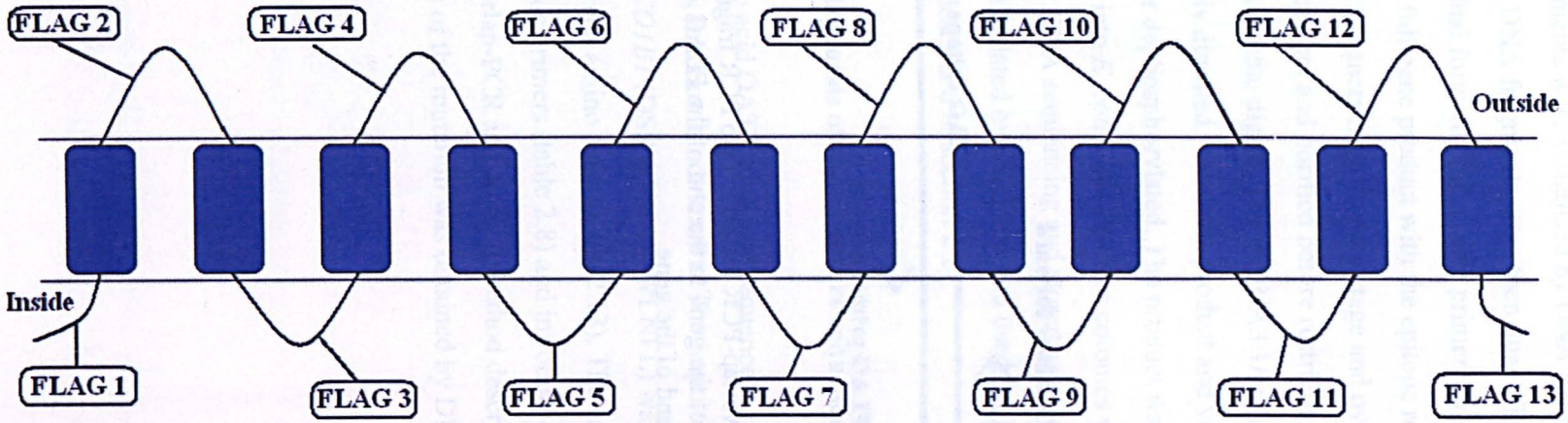

Figure 2.6 – Depiction of OATP1B1 predicted topology with 12TMs and internal and external loops with FLAG epitope insertions.

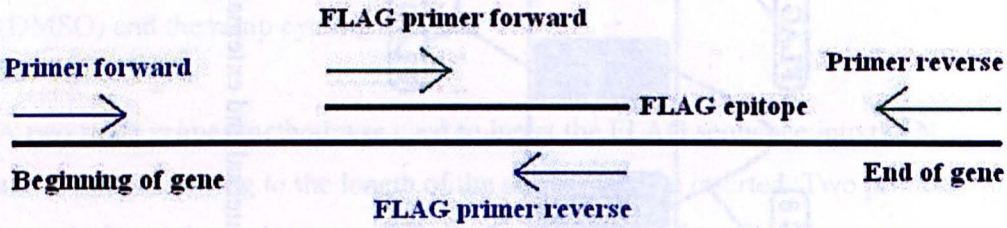

Figure 2.7 – Principle of the overlap-PCR method. Two PCR fragments were generated, from the beginning of the gene to the end of the FLAG, and from the beginning of the FLAG to the end of the gene.

The two fragments were visualised by DNA gel electrophoresis then PCR purified. The DNA fragments were then quantified and 50ng each combined with the original forward and reverse primers in another PCR reaction. This produced the full gene product with the epitope region in the correct location. The full gene products from the two stage and overlap PCR were then excised from an agarose gel and purified before restricting the total volume with *XhoI* and *KpnI* in a double digest. The pcDNA3.1/hygro(-) vector was simultaneously digested. The PCR product and vector were then PCR purified and the vector dephosphorylated. The product was ligated into the vector before transforming into *E. coli* cells. Positive colonies were screened by cracking, confirmed by DNA sequencing and stored as glycerol stocks. Large quantities of DNA were isolated by maxiprep and used for HEK293T cell transformations (methods as described in section 2.2).

2.2.14.5 Mutagenesis of the signature sequence region in *SLCO1B1*

The 13 amino acid OATP signature sequence is highly conserved between species but its function is not known. The importance of the signature sequence region in *SLCO1B1* (DSRWVGAWWLNFL) was determined by SDM of the highly conserved amino acids (table 2.13). The amino acid changes were made with mutagenic primers (table 2.8) and introduced to pcDNA/*SLCO1B1*-F4 using the overlap-PCR and cloning method described in section 2.2.14.4. Confirmation of the mutation was obtained by DNA sequencing (section 2.2.13).

Table 2.13 – Site-directed mutations in the signature sequence of *SLCO1B1*. The amino acids in bold were mutated

Name	Original protein sequence	Mutated protein sequence
D251E	**D**SRWVGAWWLNFL	**E**SRWVGAWWLNFL
R253K	DS**R**WVGAWWLNFL	DS**K**WVGAWWLNFL
W254F	DSR**W**VGAWWLNFL	DSR**F**VGAWWLNFL
W258/259F	DSRWVGA**WW**LNFL	DSRWVGA**FF**LNFL
N261A	DSRWVGAWWL**N**FL	DSRWVGAWWL**A**FL

2.3 *Xenopus laevis* oocyte methods

The *X. laevis* oocyte model is an established method for expressing transport proteins. Oocytes were removed from frogs and prepared before micro-injection with cRNA for the transport protein of interest. Transport function was assessed by radioactive substrate transport experiments.

2.3.1 Preparation and maintenance of oocytes

Oocytes were harvested from female African clawed *X. laevis* frogs (European *Xenopus* Resource Centre, Portsmouth University, Portsmouth, UK) as approved by the Oxford Brookes University Animal Research Committee, in accordance with the guidelines of the 1986 Scientific Procedures Act of the United Kingdom. Frogs were anesthetised on 1:1 ice/water mix for 30-45 minutes before sacrificing by decapitation. An incision was made on the posterior ventral side and ovary lobes were removed, by sterile scalpel and forceps.

Ovaries once removed were treated to remove the follicular membrane (section 2.3.1.1). Oocytes were stored pre and post-injection in Barths's solution (table

2.14) at 17.5°C. The solution was stored at 4°C and 0.4μM sterile filtered before use.

Table 2.14 – Composition of Barth's solution for *X. laevis* oocytes

Component	Concentration
NaCl	88 mM
KCl	1 mM
$MgSO_4$	0.82 mM
$CaNO_3$	0.33 mM
$NaHCO_3$	2.4 mM
$CaCl_2$	0.41 mM
HEPES (adjusted to pH 7.6 with 10M NaOH)	15 mM
Sodium Pyruvate*	5 mM
Gentamycin sulphate salt*	50μg/ml

* Added after the pH of the solution had been set.

2.3.1.1 Oocyte defolliculation

Oocytes were defolliculated to facilitate micro-injection. Ovary lobes were separated into approximately 5mm sections using forceps, then incubated in 1mg/ml collagenase from *Clostridium histolyticum* (Sigma, Dorset UK), in calcium free solution (table 2.15) on a tube roller. The oocytes were incubated at room temperature for 45 minutes then fresh collagenase solution exchanged and incubated for a further 45 minutes. Following defolliculation oocytes were washed five times with calcium free solution and then five times with Barth's solution (table 2.14). Oocytes were maintained in Barth's solution at 17.5°C for 24 hours prior to micro-injection. Barth's solution was exchanged daily and dead oocytes removed.

Table 2.15 – Components of calcium free solution

Component	Concentration (mM)
NaCl	80
KCl	2
$MgCl_2$	1
HEPES (adjusted to pH 7.6 with 10M NaOH)	5

2.3.2 cRNA synthesis

cRNA was synthesised in preparation for oocyte micro-injection. The pXT7 vector DNA containing the *SLCO* gene of interest was grown fresh from a glycerol stock and isolated using the miniprep method (section 2.2.11.1). The plasmid was linearised and purified (section 2.3.2.1) then used as template DNA for cRNA synthesis (section 2.3.2.2). The newly synthesised cRNA was further purified using an RNA specific clean up kit prior to micro-injection.

2.3.2.1 Plasmid linearisation and purification

The pXT7/*SLCO* plasmid was linearised with *NdeI* (NEB, Hitchin UK), a restriction enzyme present only in the vector, downstream of the gene to be transcribed. This process ensured that specifically the gene and not the entire plasmid were transcribed into cRNA. The restriction digest was assembled as shown in table 2.16, overnight at 37°C.

Table 2.16 – Components of a restriction digest in preparation for cRNA synthesis

Reaction components	Volume/amount
Template DNA	10µg
10X NEBbuffer	10µl
NdeI (20U/µl)	1µl
Nuclease free dH_20	Up to 100µl
TOTAL	**100µl**

The linearised DNA was purified using the Qiagen PCR purification kit (section 2.2.2) and then assembled into a cRNA synthesis reaction (section 2.3.2.2).

2.3.2.2 cRNA synthesis reaction

cRNA synthesis was performed using the Ambion® mMessage mMachine T7 kit (Life Technologies, Paisley UK). All RNA experiments were conducted in a dedicated RNA work area and the area and equipment cleaned for RNases using RNaseZap (Life Technologies, Paisley UK). All reactions were performed with Ambion® RNase free consumables (Life Technologies, Paisley UK). The reaction was set up as listed in table 2.17. All components except for the 10X reaction buffer were thawed on ice and the reaction buffer and NTP/CAP were vortexed before use. The reaction was assembled at room temperature and incubated for 3 hours at 37°C.

Table 2.17 – Components of a cRNA synthesis reaction

Reaction components	Volume (µl)
Purified template DNA	6
2X NTP/CAP	10
10X Reaction buffer	2
T7 Enzyme Mix	2
TOTAL	**20**

Following cRNA synthesis 1µl TURBO DNase solution (2U/µl) was added to the reaction to remove any remaining DNA template. The tube was incubated for a further 15 minutes at 37°C.

2.3.2.3 cRNA purification

The newly synthesised cRNA was purified using the RNeasy Mini Kit (Qiagen, Crawley UK). Purification was conducted at room temperature and all mixing steps were performed by pipetting rather than vortexing. In addition, all

centrifugation steps were performed at 13,000rpm. The cRNA was adjusted to 100µl with 80µl Ambion® nuclease free dH_20 (Life Technologies, Paisley UK) and 350µl buffer RLT was added to the tube. Then 250µl 100% molecular grade ethanol (Sigma, Dorset UK) was added and mixed. The entire volume was transferred to an RNeasy mini spin column placed in a collection tube and centrifuged for 15 seconds. The collection tube was replaced after each centrifugation step to reduce contamination. Then 500µl buffer RPE was added and the column centrifuged for 15 seconds. A further 500µl buffer RPE was added to the column before centrifuging for 2 minutes. The column was then centrifuged for a further 1 minute to remove residual ethanol before placing in an RNase free 1.5ml tube and 30µl DNase free water added directly to the membrane. The column was incubated for 1 minute before centrifuging for 1 minute to elute the RNA.

RNA was quantified using a spectrophotometer (section 2.2.12). Typical cRNA recoveries were between 1-3µg/µl. The RNA was visualised on a 1% agarose gel (section 2.2.4). RNA was stored at -80°C and maintained on ice throughout use.

2.3.3 Oocyte micro-injection

Oocytes following collagenase treatment at approximately 1mm diameter and with a healthy appearance were selected for micro-injection. Injections were achieved with a Nanoject II injector (Drummond Scientific, c/o Alpha Laboratories Ltd, Eastleigh UK) under a Leica MZ6 light microscope (Wetzlar, Germany). Oocytes were injected using disposable glass capillary needles made with a PC-10 puller (Narishige, London UK). Needles were filled with mineral oil before filling with cRNA to facilitate injection. Approximately 30 oocytes per experimental condition were injected with 27ng cRNA into the vegetal pole of the oocyte (figure 2.8). The animal pole was avoided to reduce the likelihood of damaging the nucleus. Water-injected and/or non-injected oocytes were used as controls. Injected oocytes were transferred to a new dish with fresh Barth's

solution. Oocytes were incubated for 72 hours at 17.5°C, with Barth's solution changed and dead oocytes removed daily.

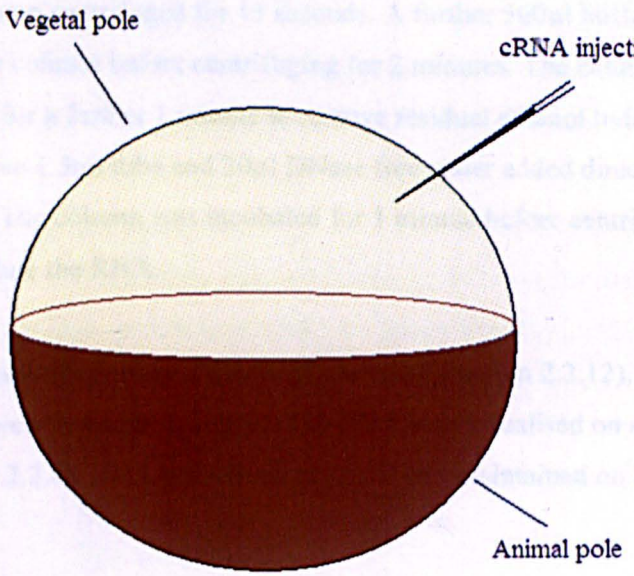

***X. laevis* oocyte**

Figure 2.8 – Schematic diagram of a *X. laevis* oocyte displaying the vegetal and animal poles. cRNA was injected into the vegetal pole.

2.3.4 Oocyte transport experiments

Transport by OATP expressing oocytes was determined by measuring the radioactive substrate [^{3}H]E3S. At 72 hours post-injection 5 healthy oocytes per experimental condition (including control non-injected and water-injected oocytes) were selected and placed in freshly made uptake solution (table 2.18). All stages of the experiment were conducted at room temperature.

Table 2.18 – Components of uptake solution for oocyte transport experiments

Component	Concentration (mM)
NaCl	95
Kcl	2
$CaCl_2$	1
$MgCl_2$	1
HEPES (adjusted to pH 7.4 with 0.5M TRIS)	20

After approximately 30 minutes in uptake solution the oocytes were transferred to uptake solution containing 37nM [^{3}H] E3S (Perkin Elmer, MA USA), 5 oocytes per 100µl. Oocytes were incubated for various time points. Individual oocytes were then washed sequentially five times in 1ml 0.12M NaCl before being transferred individually to a flexible 96 well microplate (Perkin Elmer, Cambridge UK). Oocytes were lysed with the addition of 50µl 2% SDS and placed on a plate shaker for 1 hour at room temperature. Following lysis 200µl scintillation fluid (Optiphase Supermix, Cambridge UK) was added per oocyte/well and a plate sealer added (Perkin Elmer, Cambridge UK). The plate was placed on a plate shaker for 1 hour before counting in a Microbeta Trilux 1450 liquid scintillation and luminometry counter (Perkin Elmer, Cambridge UK). [^{3}H]E3S was detected as counts per minute (cpm) at 1 minute per well. The counting protocol was standardised to radioactive controls to account for quenching agents. The efficiency was 41.4% which resulted in 49.9 cpm/femtomol (fmol). Sample counts were converted to fmol and reported as

fmol/oocyte. Data were expressed as the mean ± standard error (SE) and data analysis were performed as discussed in section 2.7.

2.4 HEK293T cell culture methods

HEK293T cells were also utilised for OATP expression. Cells were transiently transfected with the *SLCO* gene using an electroporation method and transport function was assessed by radioactive substrate transport experiments.

2.4.1 Maintenance of HEK293T cells

HEK293T cells (section 2.1.3) were routinely grown in 75cm^2 flasks with 10ml complete media (table 2.19) and incubated at 37°C with 5% CO_2. Fresh media was exchanged every 2 days or when the media changed colour. Cells were grown in complete media unless stated otherwise.

Table 2.19 – Components of complete media for HEK293T cells

Components	Volume (ml)
Dulbecco's modified eagles media (Life Technologies, Paisley UK)	500
Fetal bovine serum (Heat inactivated) (Life Technologies, Paisley)	50
Penicillin-Streptomycin solution, 100X	5
L-Glutamine, 200mM	5
Non-essential amino acid solution, 100X	5
Amphotericin B solution, 250µg/ml	0.5

2.4.1.1 Routine sub-culturing of HEK293T cells

HEK293T cells were sub-cultured after ~3 days or when cells reached 70% confluence. Cells were not grown further than passage 15 to ensure maintenance of phenotype and high protein expression. The media was removed and the flask washed with 10ml cell culture grade phosphate buffered saline (PBS) (Sigma, Dorset UK). This PBS was used for all further cell culture

methods unless stated otherwise. Cells were detached from the plate by incubating with 5ml 0.05% trypsin-EDTA (Life Technologies, Paisley UK) in PBS for 5 minutes at 37°C. The flask was then knocked by hand to dislodge cells and confirmed by visualising on a Motic AE31 inverted light microscope (Wetzlar, Germany). 5ml pre-warmed complete media was added to the cell suspension and the total volume was centrifuged at 1300rpm for 5 minutes. The supernatant was discarded and the pellet resuspended in 10ml complete media. This was split 1/10 (~$1x10^7$ cells/75cm^2 flask) between 75cm^2 flasks containing 10ml pre-warmed complete media.

2.4.1.2 Cryopreservation of HEK293T cells

Cell stocks at passage numbers ~2-6 were maintained in liquid nitrogen for long term storage. Stocks were prepared by growing HEK293T cells until confluent and sub-cultured as described in section 2.4.1.1. The cell pellet was resuspended in 1ml complete media including 5% DMSO (Sigma, Dorset UK) as a cryoprotective agent. The cell suspension was placed immediately in a sterile cryogenic vial and stored in an isopropanol chamber overnight at -80°C. The vials were then transferred to liquid nitrogen for long term storage.

2.4.1.3 Thawing cryopreserved HEK293T cells

Working HEK293T cell stocks at low passage number were generated from cryopreserved stocks stored in liquid nitrogen. Individual cryovials were removed from liquid nitrogen and thawed rapidly in a water bath pre-warmed to 37°C. Immediately after all ice in the solution had thawed the vial was transferred to a 50ml tube and centrifuged for 5 minutes at 1300rpm. The supernatant was removed and the pellet resuspended in 1ml pre-warmed media. The total volume was then transferred to a 25cm^2 flask with 5ml pre-warmed media. Cells were sub-cultured into 75cm^2 flasks after 24 hours or when the cells were attached and ~60-80% confluent. Once in 75cm^2 flasks cells were

sub-cultured once more to ensure the working stocks were stable before conducting experiments.

2.4.2 HEK293T cell experiments

2.4.2.1 HEK293T cell transfections

Cell transfection experiments were conducted in order to deliver the *SLCO* gene into cells. Cells transfected with the *SLCO* gene then translated the gene into protein on the membrane. Transfection was achieved using the Amaxa® cell line nucleofector® kit V (Lonza, Preston UK), specific for HEK293T cells. The kit is based on an electroporation method and is compatible with the Amaxa nucleofector II device (Lonza, Preston UK; model # AAB-1001). The method involved removing the cells from the flask, electroporating the cells, then plating the cells in plates or dishes specific to the experiment required. Before electroporation, plates and/or dishes were required to be coated with poly-D-lysine (section 2.4.2.1.1).

2.4.2.1.1 Coating plates with poly-D-lysine

Transport experiments were conducted in 12 well cell culture plates (Appleton Woods Ltd, Birmingham UK), immunofluorescence experiments were conducted in 12 well plates with 15mm glass coverslips (Bioquote, York UK) and luminometry experiments were conducted in 35mm x 10mm dishes (Corning, Ewloe UK). Cover slips were prepared by individually soaking in 100% ethanol for 1 minute before air drying and placing in 12 well plates with sterile tweezers. Before plating cells, each surface required coating with poly-D-lysine to facilitate cell adherence. Poly-D-lysine solution (Millipore, Watford UK) was used at a concentration of 0.1mg/ml diluted in PBS. For 12 well plates 800µl/well was added, for 35mm dishes 1ml/dish was added. Plates/dishes were incubated at 4°C for 3–72 hours then washed once with PBS before use.

2.4.2.1.2 HEK293T cell transfection method

The cell transfection method using the kit and device mentioned in section 2.4.2.1 is the same for transport, immunofluorescence and luminometry experiments. The plates/dishes previously coated with poly-D-lysine (section 2.4.2.1.1) were prepared by adding transfection media (table 2.20) then sealed with micropore surgical tape for sterility. Volumes are stated in table 2.21. The plates/dishes were then pre-warmed to 37°C in the incubator.

Table 2.20 - Components of transfection media for HEK293T cells

Components	Volume (ml)
Dulbecco's modified eagles media (Life Technologies, Paisley UK)	500
Fetal bovine serum (Heat inactivated) (Life Technologies, Paisley)	50
L-Glutamine, 200mM	5
Non-essential amino acid solution, 100X	5

Table 2.21 – Volumes of HEK293T transfection media and cell suspension required per plate/dish type

Plate type	Volume of transfection media required (ml)	Final volume of cell suspension added to plate/dish (µl)	Number of wells per cuvette
12 well plate	3	100	6
12 well plate with cover slips	3	100	6
35mm dish	2	150	4

A 75cm^2 flask containing cells at 80-90% confluence was washed with 10ml PBS. The flask was then incubated with 10ml accutase (Millipore, Watford UK) for 5 minutes at 37°C. Accutase is a cell detachment solution found to cause less stress to cells before transfection than trypsin. Cells were dislodged as described in section 2.4.1.1. 5ml pre-warmed 37°C transfection media was added to the cell suspension and the total volume was centrifuged at 1300rpm at room temperature for 5 minutes. The supernatant was discarded and the pellet

resuspended in 500µl transfection media. The cell density was measured by removing 10µl and combining with 10µl 0.4% trypan blue solution (Sigma, Dorset UK) then counted using a standard glass haemocytometer.
The cells were then divided into aliquots of 1 x 10^6 cells as required per cuvette. Each aliquot was centrifuged 1646rpm at room temperature for 10 minutes. The supernatant was completely removed and the pellet resuspended in 100µl nucleofector solution provided in the kit. Then 5µg maxiprep purified plasmid DNA was added to each cell aliquot and the total volume added to a cuvette. Each cuvette was electroporated under program Q-001 of the nucleofector device. Following electroporation 500µl transfection media was added directly to the cuvette and the entire volume transferred to a 1.5ml tube. Aliquots of the cell suspension were transferred to the prepared plates. The volumes required per plate type and number of wells filled per cuvette are displayed in table 2.21. Micropore tape was placed around the edges of the plates before incubating for 72 hours. Transfection media was exchanged 50% for complete media after 24 hours.

2.4.2.2 HEK293T cell transport experiments

OATP radioactive transport experiments were conducted using [^{3}H]E3S. HEK293T cells transfected with the *SLCO* gene or vector alone in 12 well plates were removed from the incubator at 72 hours post-transfection (approximately 80% confluence). The media was aspirated and the wells washed three times with 1ml freshly made uptake solution (table 2.22) pre-warmed to 37°C.

Table 2.22 – Composition of uptake solution for HEK293T cell transport experiments

Component	Amount (mM)
NaCl	142
KCl	5
KH_2PO_4	1
$MgSO_4$	1.2
$CaCl_2$	1.5
Glucose	5
HEPES (Adjusted with TRIS to pH 7.3)	12.5

Cells were then incubated in 0.1μM [^{3}H]E3S (Perkin Elmer, Witney UK) in 300μl uptake solution for 3 minutes at 37°C. The transport was stopped by the addition of 1ml ice cold uptake solution per well. Each well was washed a further three times with ice cold uptake solution before the addition of 200μl 1% SDS/0.5M NaOH. The plate was then placed on a plate shaker at room temperature for 1 hour. Transport experiments were quantified by liquid scintillation counting and protein quantification. For liquid scintillation counting 50μl of the cell/SDS/NaOH solution was removed and placed in a flexible 96 well microplate (Perkin Elmer, Witney UK). Then 200μl scintillation fluid (Optiphase Supermix, Perkin Elmer, Witney UK) was added per well and a plate sealer added (Perkin Elmer, Witney UK). The plate was placed at room temperature on a plate shaker for 1 hour before counting in a Perkin Elmer 1450 Microbeta Trilux liquid scintillation and luminometry counter (Witney, UK).

Cell transport experiments were performed with at least 3 well replicates and [^{3}H]E3S detected by liquid scintillation counting as disintegrations per minute (dpm) at 20 minutes per well. The protocol was standardised to radioactive controls to account for quenching agents and determine the efficiency of the counter. The efficiency was 35.5% which resulted in 42.8 dpm/fmol. Sample counts were converted to fmol/pmol, then adjusted to (fmol/pmol)/mg protein in the sample using a BCA protein quantification method (section 2.4.2.2.1).

Data were displayed as mean ± SE. Data analysis and transport kinetics were performed as discussed in section 2.7.

2.4.2.2.1 Protein quantification

HEK293T protein was quantified using a BCA protein assay kit (Merck, Feltham UK), conducted in a 96 well flat bottom plate. BSA (BDH Biochemicals, Poole UK) standards were calculated as shown in table 2.23, with 1% SDS/0.5M NaOH as diluent. The standards were added in triplicate, 25µl/well. As a blank control 25µl diluent was also added in triplicate. 25µl of each sample was also added to the plate, diluted if necessary to ensure the absorbance results were within the range of that of the standards.
Working BCA reagent was prepared by adding 4µl 4% cupric sulphate to 200µl BCA reagent per sample. A mastermix was made and 200µl working reagent added per well. The plate was mixed on a plate shaker at room temperature for 1 minute then incubated at 60°C for 15 minutes.
The plate was left to cool to room temperature then measured on a Benchmark microplate reader (Biorad, Hemel Hempstead UK) at 490nm. Absorbances were corrected for interactions by the diluent through subtracting the blank absorbances from the sample and standard absorbances. A standard curve was generated by plotting the corrected standard absorbances against BSA concentration. Sample protein amounts were calculated from the equation generated from the standard curve.

Table 2.23 – BSA standards required for BCA protein quantification

Tube	Volume of BSA (µl)	Volume of diluent (1% SDS/0.5M NaOH) (µl)	Final concentration (mg/ml)
1	100 (from 10mg/ml stock)	900	1
2	800 (from tube 1)	200	0.8
3	750 (from tube 2)	250	0.6
4	666 (from tube 3)	334	0.4
5	500 (from tube 4)	500	0.2

2.4.2.3 HEK293T cell luminometry

Luminometry was used to detect OATP protein present in the membranes of HEK293T cells. To summarise; the FLAG epitope was cloned into putative extracellular and intracellular regions of the protein (section 2.2.14.4) and an anti-FLAG antibody was used to detect the epitope on the membrane. Cells expressing OATPs with putative internal FLAG epitopes were pemeabilised to allow the antibody into the cell. The antibody was HRP conjugated and thus with the addition of a substrate light was produced, which could be detected quantitatively using a luminometer.

The following method is adapted following personal correspondence with Dr Kevin Paavola, Emory University, USA (Paavola *et al.*, 2011). OATP transfected HEK293T cells grown in 35mm dishes as described in section 2.4.2.1.1 and 2.4.2.1.2 were used for experiments 72 hours post-transfection, or when the cells reached 100% confluence.

The dishes were placed on ice, media removed and washed twice with PBS. Cells were then fixed to the dishes at room temperature with 1ml 4% paraformaldehyde (Agar Scientific, Essex UK) in PBS for 30 minutes. For cells requiring permeabilisation, the above fix solution was supplemented with 0.25% Triton-X100 (Sigma, Dorset UK). Dishes were then washed twice with PBS.

Blocking was performed with 2% Marvel skimmed milk (Premier Foods, Herts UK) buffer in PBS for 30 minutes at room temperature. Primary monoclonal mouse HRP-conjugated anti-FLAG antibody (Sigma, Dorset UK) was immediately added, 1ml at 1:1000 dilution in milk buffer. Dishes were incubated for 2 hours at room temperature. Cells were then washed twice with milk buffer and once with PBS. The PBS remained in the dish ready for luminometry experiments.

PBS was replaced with 1ml substrate (Pierce Protein Research Products, Loughborough, UK), which was added to the dish for 15 seconds before analysing in a TD-20/20 luminometer (Turner Designs, c/o R.S Aqua Ltd,

Alton UK). Luminometry readings were taken with a 5 second delay and 30 second measurement. Protein was quantified using the BCA protein assay kit as described in section 2.4.2.2.1. Substrate was removed and the dishes washed once with PBS. 1ml 1% SDS / 0.5M NaOH was added per dish and the fixed cells removed from the bottom of the dish by scraping with a plate scraper. The cells were lysed using a plate shaker overnight, then 25µl of each sample was removed for protein quantification.
Luminescence was displayed as luminescence/mg protein in relative light units (RLU) by normalising raw luminescence values to the protein content in each dish. Sample values were displayed as mean ± SE and data analysis performed as described in section 2.7.

2.4.2.4 HEK293T cell immunofluorescence

An immunofluorescence technique was used to visualise OATP protein in the membranes of HEK293T cells, under a confocal microscope. Detection was achieved using an anti-FLAG antibody which recognised the external FLAG eptiope region in the protein, coupled to a fluorescein isothiocyanate (FITC) secondary antibody which fluoresced at 488nm. The nuclei were also stained for visualisation. Cells expressing OATPs with putative internal FLAG epitopes were pemeabilised to allow the antibody into the cell. The following method is optimised from the anti-FLAG antibody manufacturer's instructions (Sigma, Dorset UK).

SLCO transfected HEK293T cells grown on cover slips in 12 well plates as described in section 2.4.2.1.1 and 2.4.2.1.2 were used for experiments 72 hours post-transfection. All steps were performed at room temperature with coverslips remaining within the wells unless otherwise stated.
Wells were washed with 1ml PBS then cells fixed by the addition of 1ml 4% paraformaldehyde, 4% sucrose (BDH Biochemicals Ltd, Poole UK) in PBS for 15 minutes. For cells requiring permeabilisation, the above fix solution was

supplemented with 0.25% Triton-X100 (Sigma, Dorset UK) in PBS. Wells were then washed with 1ml PBS twice at 5 minute intervals.
Wells were blocked with 1ml 10% BSA in PBS for 30 minutes at 37°C. The blocking solution was removed and 1ml primary monoclonal mouse anti-FLAG antibody (Sigma, Dorset UK) at 1:2000 dilution in 5% BSA/PBS was added to the wells. Incubation was for 2 hours at 37°C. Wells were washed with 1ml PBS three times at 5 minute intervals. Then 1ml anti-mouse IgG-FITC rabbit secondary antibody (Sigma, Dorset UK) in a 1:1000 dilution with 5% BSA/PBS was incubated for 45 minutes at 37°C. Wells were washed three times with 1ml PBS at 5 minute intervals.
Before mounting, wells were incubated with 4',6-Diamidino-2-phenylindole dihydrochloride (DAPI) (Sigma, Dorset UK), a nucleic acid stain that fluoresces at 504nm. Wells were incubated with 1ml 1µg/ml DAPI in dH_20 for 2 minutes. Wells were then washed three times with 1ml PBS and the last wash left on the plates. The cover slips were then removed from the wells with tweezers and mounted face down over a drop of polyvinyl alcohol mounting media containing 1,4-diazabicyclo[2.2.2]octane (DABCO) (Sigma, Dorset UK) on a standard glass slide. Nail varnish was used to seal the edges of the cover slip and the slides stored in the dark overnight at 4°C. Slides were visualised on a confocal microscope within 7 days of mounting.

A Zeiss LSM 510 META was used for confocal microscopy. The blue fluorescence of DAPI was excited with a 405 nm diode laser and detected after passing through a 420-480 nm band-pass filter. The green fluorescence of FITC was excited with the 488 nm line of an argon ion laser and detected after passing through a 505-530 nm band-pass filter. Pinhole diameter and gain settings varied based on brightness of stain emission on a sample-to-sample basis.

2.5 Membrane vesicle methods

Membrane vesicles are useful for studying the overall transport and inhibition of endogenously expressed membrane proteins. This method has been adapted from a personal communication with Dr David Meredith (Oxford Brookes University, Oxford UK). Rat kidney membrane vesicles were used to study endogenous Oatp transport.

2.5.1 Preparation of membrane vesicles

Kidneys were removed from female Wistar rats (Harlan UK Ltd, Oxon UK) following euthanasia in house and placed on ice. The connective tissue, fat and medulla were removed with a scalpel and the remaining cortex tissue cut into small pieces. Suspension solution (table 2.24) was heated until the ethylene glycol tetraacetic acid (EGTA) was dissolved and cooled to 4°C before use. The tissue was transferred to 100ml suspension buffer and homogenised on ice using an IKA T10 basic homogeniser (IKA, c/o Labsource, Manchester UK).

Table 2.24 - Components of suspension solution for membrane vesicles

Component	Concentration
Mannitol	300mM
EGTA	5mM
TRIS-HCl	12mM
KOH (Adjust pH to 7.4)	10M

Once fully homogenised 12mM $MgCl_2$ was added to the solution and the volume incubated for 15 minutes on ice. A series of centrifugation steps were then conducted, as described in figure 2.9. Suspension buffer was diluted two fold with dH_20 and the membrane pellet re-suspended in experimental buffer (table 2.25) was stored at -80°C.

Table 2.25 - Components of the experimental buffer for membrane vesicle experiments

Component	Concentration (mM)
NaCl	100
Mannitol	20
$MgSO_4$	0.1
HEPES (Adjusted with TRIS to pH 7.4)	80

Membrane aliquots were thawed on the day of vesicle uptake experiments. The protein in the sample was quantified using a Bradford's assay (Bradford, 1976). BSA standards were assembled as shown in table 2.26. Absorbance was measured by adding 2.9ml protein assay dye (Biorad, Hemel Hempstead UK) to 100µl sample/standard and read at 595nm in a Jenway 6505 UV spectrophotometer (Bibby Scientific Limited, Staffordshire UK). Blank control absorbances were measured with 100µl dH_20 and 2.9ml Bradford's reagent.

Table 2.26 - BSA standards required for Bradford's protein quantification

Tube	Volume of BSA (µl)	Volume of diluent (dH_20) (µl)	Final concentration (µg/ml)
1	50 (from 10mg/ml stock)	950	500
2	500 (from tube 1)	500	250
3	400 (from tube 2)	600	100
4	500 (from tube 3)	500	50
5	200 (from tube 4)	800	10

Each membrane preparation yielded ~200µg/ml protein. The membrane sample was diluted to allow for 50µg/well protein. The total volume was drawn through a 1ml syringe with a 25 gauge needle (Terumo Medical Corporation, Renfrewshire UK) 15 times to form the membrane vesicles.

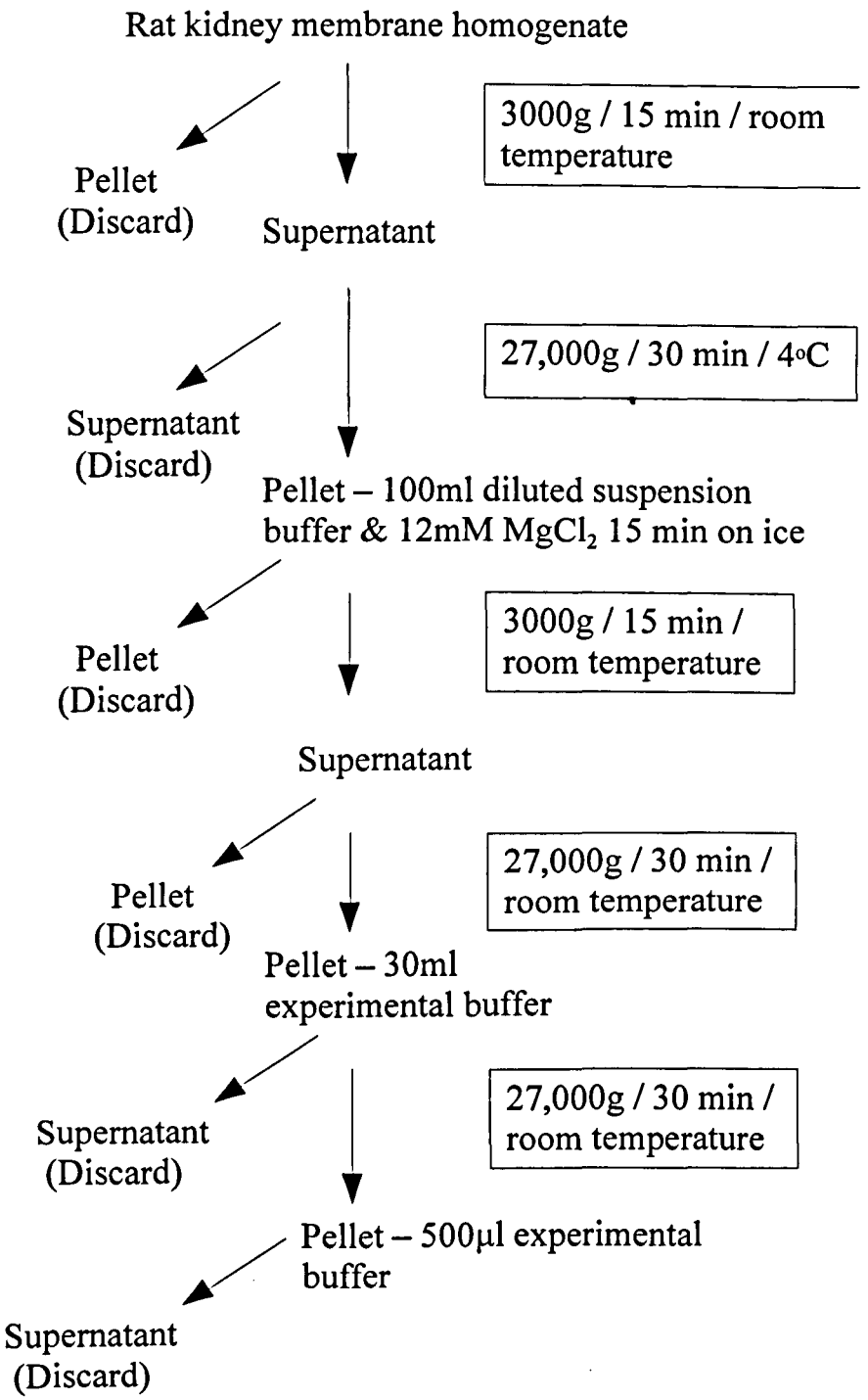

Figure 2.9 - Flow chart representing the centrifugation steps required to isolate membrane vesicles.

2.5.2 Membrane vesicle transport experiment

The transport of [^{3}H]E3S into rat kidney vesicles endogenously expressing rat Oatp1a1 and Oatp4c1 was quantified using a membrane vesicle uptake experiment. This involved incubating the vesicles with [^{3}H]E3S, capturing the vesicles on a filter membrane and measuring the radioactivity contained within them.

A Multiscreen HTS filter plate (Millipore, Watford UK) was prepared by adding 100µl experimental buffer (table 2.25) per well and incubating the plate on ice. Experimental buffer was pre-warmed to 37°C. 50µg membrane vesicles were combined with 37nM [^{3}H]E3S or 37nM [^{3}H]E3S + 200µM E3S (control) in experimental buffer to a total of 50µl (table 2.27). The plate was incubated for 30 minutes at 37°C. The reaction was stopped by the addition of 200µl ice cold wash solution (table 2.28) per well.

Table 2.27 - Layout of the membrane vesicle assay plate

	Time	1	2	3	4	5	6	7	8	9	10	11	12
A	0 min	Vesicles + 37nM [^{3}H]E3S						Vesicles + 37nM [^{3}H]E3S + 200µM E3S					
B	1 min	Vesicles + 37nM [^{3}H]E3S						Vesicles + 37nM [^{3}H]E3S + 200µM E3S					
C	5 min	Vesicles + 37nM [^{3}H]E3S						Vesicles + 37nM [^{3}H]E3S + 200µM E3S					
D	10 min	Vesicles + 37nM [^{3}H]E3S						Vesicles + 37nM [^{3}H]E3S + 200µM E3S					
E	20 min	Vesicles + 37nM [^{3}H]E3S						Vesicles + 37nM [^{3}H]E3S + 200µM E3S					
F	30 min	Vesicles + 37nM [^{3}H]E3S						Vesicles + 37nM [^{3}H]E3S + 200µM E3S					
G	n/a	n/a						n/a					
H	n/a	37nM [^{3}H]E3S control			37nM [^{3}H]E3S + 200µM E3S control			n/a					

Table 2.28 - Components of wash solution for membrane vesicle uptake experiments

Component	Concentration (mM)
NaCl	150
$MgSO_4$	50
Mannitol	30
TRIS (Adjusted with MES to pH 5.5)	5

The total volume was transferred to the prepared filter plate and the solution filtered using a Multiscreen HTS vacuum manifold (Millipore, Watford UK). The wells were washed a further 5 times with 200µl ice cold wash solution before drying at 50°C for 15 minutes. The vesicles were released from the filters by incubating with 200µl scintillation fluid (Optiphase Supermix, Perkin Elmer, Witney UK) for 10 minutes at room temperature. The vesicle solution was filtered into a 96 flexible well plate (Perkin Elmer, Witney UK) and a plate sealer added (Perkin Elmer, Witney UK). Radioactivity was counted using a Perkin Elmer 1450 Microbeta Trilux liquid scintillation counter (Witney UK). Vesicle experiments were performed with 6 well replicates and [^{3}H]E3S detected by liquid scintillation counting as counts per minute (cpm) at varying time points (table 2.27). The protocol was standardised to radioactive controls to account for quenching agents and determine the efficiency of the counter. The efficiency was 35.5% which resulted in 42.8 cpm/fmol. Sample counts were converted to fmol, then adjusted to fmol/mg membrane protein. Data was displayed as mean ± SE and data analysis was performed as discussed in section 2.7.

2.6 *In silico* modelling

2.6.1 Topology modelling

Protein sequences corresponding to the cDNA clones described in section 2.1.4 were obtained from the National Center for Biotechnology Information (NCBI)

website (http://www.ncbi.nlm.nih.gov). Sequences were submitted to 16 topology prediction programs and 9 signal peptide prediction programs online (section 4.2.1 and appendix I-V for the list of programs and results).

2.6.2 OATP1B1 homology modelling

Homology modelling was performed by submitting the OATP1B1 protein sequence (obtained as described in section 2.6.1) to the Phyre2 protein fold recognition server (www.sbg.bio.ic.ac.uk/phyre2).

2.7 Data analysis

Sample values for transport and luminometry experiments were displayed as mean ± SE, with outliers removed using a Grubb's test (Graphpad Prism 5, Version 5.04 for Windows, California USA, www.graphpad.com). Statistical significance ($P<0.05$) between controls and sample data were determined using a two tailed unpaired Student's t-test (Graphpad Prism 5) and a two tailed one sample t-test for normalised values (Sigmaplot 11.0, Systat Software, San Jose, CA). The data was tested for normality using the D'Agostino-Pearson omnibus K2 normality test (Graphpad prism 5). Transport kinetics calculations were performed as described in section 2.7.1.

2.7.1 Transport kinetics

OATP1B1 transport in HEK293T cells was characterised using Michaelis-Menten kinetics. The Michaelis constant or K_m denotes the affinity of a substrate for a transporter and is defined as the substrate concentration at which the transport rate is half of the maximum (Simon, 1998). The maximum rate at a saturating substrate concentration is known as the maximum rate, or V_{max}. This is a useful measure of the rate at which a substrate is transported. These features are calculated by the Michaelis-Menten equation, as shown in figure

2.10. In this way, v is the initial rate of reaction, [S] is substrate concentration, V_{max} is the maximum rate of reaction and K_m is the Michaelis constant (Stenesh, 1998).

An apparent K_m and V_{max} for OATP transport was derived by inhibiting a set concentration of [^{3}H]E3S substrate with increasing concentrations of unlabelled E3S substrate. Therefore the transport of [^{3}H]E3S into the oocyte/cell was inhibited by the unlabelled substrate, although the total concentration of substrate entering the system was increased. Only the OATP mediated transport was used to determine the kinetics, by the removal of background non-injected oocyte / pcDNA vector uptake. The Michaelis-Menten equation was rearranged to account for the total fraction of substrate entering the cell (figure 2.11), as only the radioactive fraction was measured. In the equation V_{tot} is the total velocity and [S*] is the radioactive substrate concentration. The V_{tot} was calculated for each concentration and the residual squares calculated by subtracting the V_{tot} from the V, then squared. The sum of the residual squares was then used to calculate best fit values to determine an apparent K_m and V_{max} (Sakoda and Hiromi, 1976). The equation was then used to plot the values as a Michaelis-Menten curve (Sigmaplot 11.0, Systat Software, San Jose, CA). WT OATP transport kinetics were compared to mutant OATPs to determine any change in affinity following SDM.

$$v = \frac{V_{max}[S]}{(K_m + [S])}$$

Figure 2.10 – Michaelis-Menten equation, describing the relationship between the initial rate of reaction (v), substrate (S), K_m and V_{max}.

$$V_{tot} = \frac{V_{max}(S + S^*)}{K_m + S + S^*}$$

Figure 2.11 – Rearrangement of the Michaelis-Mention equation to account for the radioactive and unlabelled substrate.

3 Choice of expression system

3.1 Introduction

There are several methods available for the *in vitro* expression of OATPs. Owing to the difficulties of transporter crystal structure determination, *in vitro* expression systems are one of the main techniques used to study transporters. The aim of this project was to explore the structural characteristics of OATPs and therefore a model system was needed to express OATPs and their mutants in isolation. *X. laevis* oocytes and cell lines have been used most extensively as over expression systems, to assess the effects of mutations on transport and membrane targeting. Therefore these systems were assessed and validated for OATP transport. A primary rat plasma membrane vesicle method was also investigated as a novel way to detect endogenous transport of compounds known to be OATP substrates.

3.1.1 *X. laevis* oocyte model

The *X. laevis* oocyte system is an established method for the expression of membrane proteins (Gurdon *et al.*, 1973), including OATPs (Geyer *et al.*, 2004; Leuthold *et al.*, 2009). Oocytes are approximately 1-1.2mm in diameter (Heikkila *et al.*, 2007), thus large enough to permit direct micro-injection of RNA into the cytoplasm or nucleus (figure 3.1). A mature oocyte also contains high volumes of expression machinery such as ribosomes and RNA polymerases, ensuring that a high level of expression occurs. However, oocyte quality and expression levels can vary considerably between oocyte batches. *SLCO1A2*, *SLCO1B1*, *SLCO1B3* and *SLCO2B1* were sub-cloned into the *X. laevis* specific vector pXT7 and transport assessed using *X. laevis* oocytes (refer to methods section 2.3).

A B

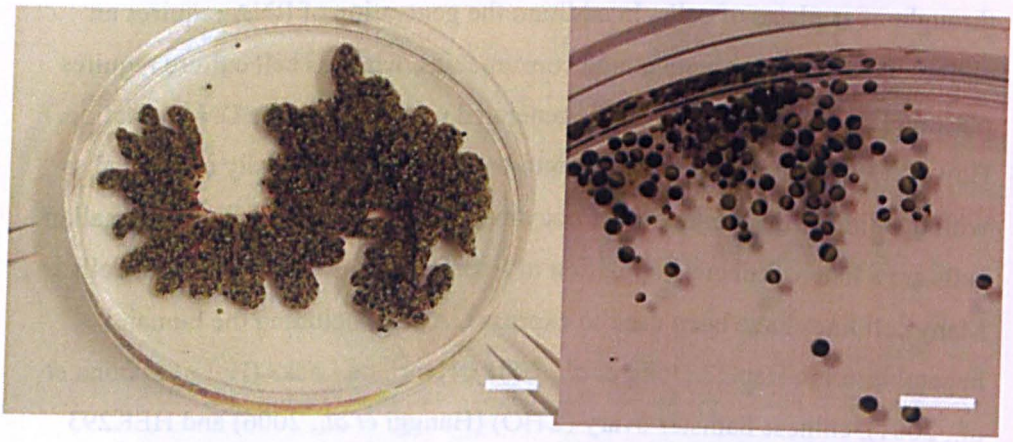

Figure 3.1 – Photographs of *X. laevis* oocytes A) in ovaries removed from the frog and B) individually before micro-injection. Scale bar = 1cm

3.1.2 HEK293T cell model

Cell culture is also an established method for studying the characteristics of transport proteins and is a simple and reproducible technique. Cell lines minimise whole animal studies and can be manipulated to focus on precise experimental conditions. Therefore like the *X. laevis* model, the system is useful for analysing the kinetic parameters of specific proteins. The advantage of cell line models compared to *X. laevis* oocytes lies in the ease of culture. Oocytes require extensive preparation and individual oocytes are not as high throughput as plates of cells. In addition the generation of RNA requires an extremely sterile environment and consumables, whereas cell culture requires plasmid DNA which can be easily generated using large scale DNA isolation. However, the transfection of DNA into cells cannot be as easily controlled as with the direct micro-injection of oocytes – transiently transfected mammalian cells are a heterogeneous population of transfected and non-transfected cells. Many cell lines have been used to express OATPs, including the human hepatoblastoma HepG2 (Jung *et al.*, 2001), Henrietta Lacks (HeLa) (Tirona *et al.*, 2001), chinese hamster ovary (CHO) (Hanggi *et al.*, 2006) and HEK293 cells (Fischer *et al.*, 2010).

HEK293T cells (figure 3.2) were the chosen cell line for comparison with the *X. laevis* model. This cell line is suitable for specific OATP protein expression as endogenous expression of the transporters is low, unlike in a hepatocyte cell line (Kullak-Ublick *et al.*, 1996). HEK293T cells are engineered from their original HEK293 counterparts by the addition of the SV40 large T-antigen. It has been shown that when transfecting HEK293T cells with a vector containing an SV40 origin of replication, the SV40 T-antigen induces replication of the plasmid (Mahon, 2011). The mammalian vector pcDNA3.1/Hygro(-) (to which the OATPs were sub-cloned, section 2.2.14) contains this SV40 origin of replication. Therefore this cell line exhibits a high level of protein expression. Cells were transiently transfected as expressed proteins could be analysed after several days and the process amenable to mutagenesis studies. The transfection

method was performed by nucleofection (Lonza, Preston, UK), an electroporation method chosen for the specially adapted HEK293 transfection kit (see methods section 2.5).

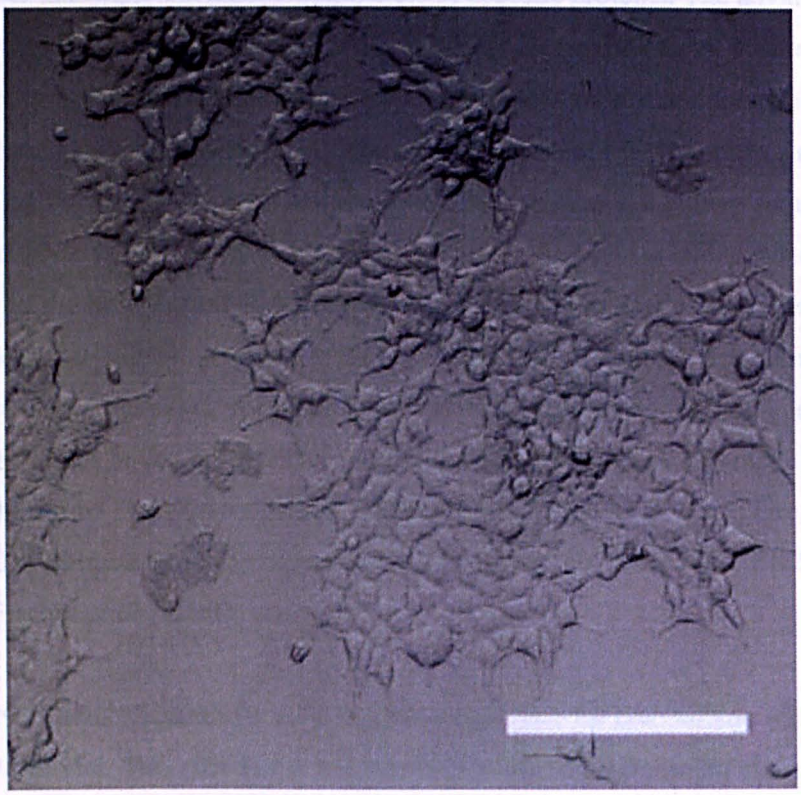

Figure 3.2 – Bright field image of non-transfected HEK293T cells obtained by confocal microscopy. Scale bar = 100μM.

3.1.3 Vesicular transport model

Vesicular transport assays form another model which can be explored for the functional analysis of transport proteins. The method involves forming enclosed vesicles from crude plasma membrane extract, adapted from an original method involving purified 'inside-out' vesicles from red blood cells (Steck *et al.*, 1970). This is where the inside of the membrane faces outwards, following incubation in alkaline buffer. Inside out vesicles are now commercially available for vesicular transport assays, in order to study a specific transporter of interest, such as the ABC efflux transporters (Krumpochova *et al.*, 2012).

Membrane vesicles are useful for studying the overall transport and inhibition of endogenously expressed membrane proteins, however there are very few studies conducted with OATPs. 'Right side out' vesicles (Palmgren *et al.*, 1990) are required to study the uptake of OATPs, whereby the extracellular side of the membrane remains facing the extracellular environment (figure 3.3). Previously, vesicles have been prepared from HEK293 cell membranes over-expressing OATP2B1 (Sai *et al.*, 2006), but this has not been conducted with primary tissues.

Primary rat kidney membrane vesicles were investigated as a tool for characterising endogenous OATP expression. Little is known about the functioning of OATPs in the kidney and it is likely that they play an important role in the absorption and elimination of xenobiotics. In humans, there are several OATPs that are expressed (table 3.1), however, the localisation of most is unknown. In the rat kidney several Oatps are also localised (table 3.1), although only Oatp1a1 and Oatp4c1 are homologues to the human OATP1A2 and OATP4C1. Interestingly it is not known as to whether rat Oatp4c1 is localised to the basolateral membrane of proximal tubule (PT) cells (Mikkaichi *et al.*, 2004), or to the apical membrane (Kuo *et al.*, 2012), as both have been reported. It is likely, however, that the human homologue is present on the same membrane. OATP4C1 is kidney specific and rat Oatp4c1 is

predominantly expressed in the kidney. Both transport the cardiac glycoside digoxin, and therefore could be the main influence on digoxin elimination from the kidney (Mikkaichi *et al.*, 2004).

Oatp1a1 and Oatp4c1 both transport E3S (Kuo *et al.*, 2012; Yang *et al.*, 2009), like their human homologues (Kullak-Ublick *et al.*, 1995; Yamaguchi *et al.*, 2010). To gain an insight into E3S transport by these transporters in the kidney, vesicles were isolated from rat kidney cortex, containing the PT and distal tubule (DT) (see methods section 2.4). Because rat Oatp1a1 shares 67% amino acid identity with OATP1A2 (Westholm *et al.*, 2008) and Oatp4c1 shares 80.4% amino acid identity with OATP4C1 (Kuo *et al.*, 2012), it is likely that these transporters may play a similar role in the kidney. Therefore approximate correlations between rat and human transport could be made. Transport, if detected, could provide physiologically relevant knowledge of drug uptake systems in the kidney, and be a useful screening tool for the transport and inhibition of novel compounds.

The results in this chapter include the E3S transport results by OATP1A2, OATP1B1, OATP1B3 and/or OATP2B1 using *X. laevis* oocytes and HEK293T cells. Rat kidney membrane vesicles were also evaluated as a tool for detecting endogenous OATP expression. The most reliable and reproducible method was then used for future experiments.

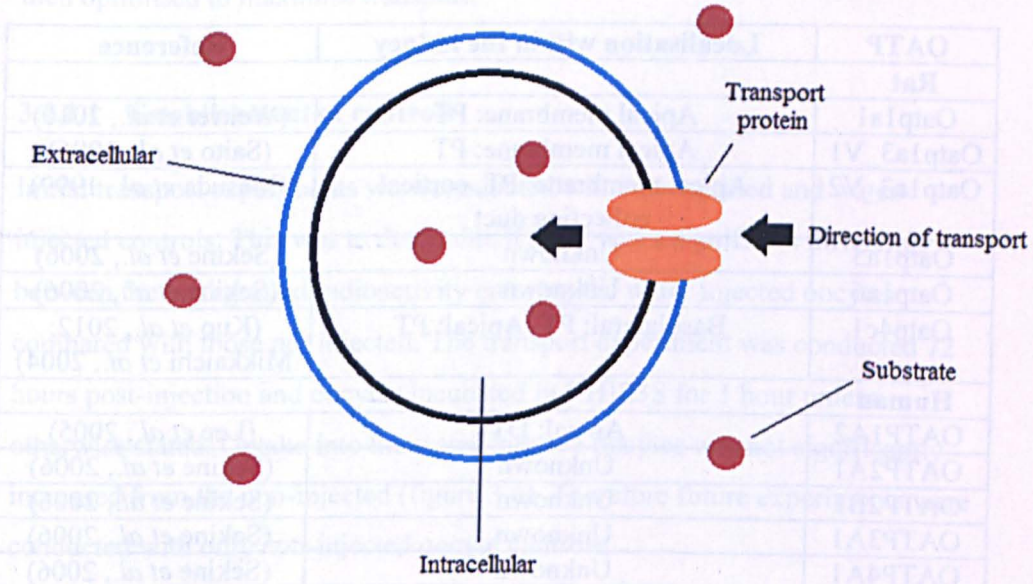

Figure 3.3 – Schematic representation of a 'right side out' vesicle, whereby vesicles are produced with the extracellular part of the membrane facing the extracellular environment.

Table 3.1 – Human and rat OATPs expressed in the kidney

OATP	Localisation within the kidney	Reference
Rat		
Oatp1a1	Apical membrane: PT	(Weaver *et al.*, 2010)
Oatp1a3_V1	Apical membrane: PT	(Saito *et al.*, 1996)
Oatp1a3_V2	Apical membrane: PT, cortical collecting duct	(Masuda *et al.*, 1999)
Oatp1a5	Unknown	(Sekine *et al.*, 2006)
Oatp1a6	Unknown	(Sekine *et al.*, 2006)
Oatp4c1	Basolateral: PT /Apical: PT	(Kuo *et al.*, 2012; Mikkaichi *et al.*, 2004)
Human		
OATP1A2	Apical: DT	(Lee *et al.*, 2005)
OATP2A1	Unknown	(Sekine *et al.*, 2006)
OATP2B1	Unknown	(Sekine *et al.*, 2006)
OATP3A1	Unknown	(Sekine *et al.*, 2006)
OATP4A1	Unknown	(Sekine *et al.*, 2006)
OATP4C1	Basolateral: PT	(Mikkaichi *et al.*, 2004)

PT: Proximal tubule, DT: Distal tubule

3.2 Results

3.2.1 *X. laevis* oocyte transport results

The *X. laevis* oocyte model was used to express OATP1A2, OATP1B1, OATP1B3 and OATP2B1. Controls were initially established and the experiment validated using a positive control. The transport experiment was then optimised to maximise transport.

3.2.1.1 Establishment of controls

Initial transport experiments were conducted with non-injected and water-injected controls. This was to determine if there was a significant difference between the background radioactivity entering the water injected oocytes compared with those not injected. The transport experiment was conducted 72 hours post-injection and oocytes incubated in [^{3}H]E3S for 1 hour unless otherwise stated. Uptake into the water-injected oocytes was not significantly increased from the non-injected (figure 3.4). Therefore future experiments were conducted with only non-injected oocyte controls.

3.2.1.2 Initial OATP transport results

The OATP clones purchased were contained within different vectors. *SLCO1A2* was contained within pBluescriptR, *SLCO1B1* in PCR-BluntII-TOPO, *SLCO1B3* in pENTR223.1 and *SLCO2B1* in pCMV-Sport6. Initially pBluescriptR/*SLCO1A2* cRNA was synthesised and injected to confirm detectable transport in oocytes. Uptake of OATP1A2 was not significant from the non-injected controls (figure 3.5 A).

To validate the transport experiment, cRNA for the rabbit peptide transporter PepT1 (*Slc15a1*) in the *X. laevis* vector pXT7 was injected into oocytes from the same frog as *SLCO1A2*. PepT1 has been successfully expressed in oocytes in the same lab (Pieri *et al.*, 2008). Uptake of the substrate [^{3}H]D-phenylalanyl-

L-glutamine (D-Phe-L-Gln) was significant for PepT1 but not for [^{3}H]E3S into OATP1A2 (figure 3.5 B).

As it was possible that the pBluescriptR vector did not facilitate suitable expression of the gene, the four OATP genes were also sub-cloned into pXT7 (section 2.2.14.1); a vector that facilitates *X. laevis* expression (Dominguez *et al.*, 1995). The pXT7 vector contains *X. laevis* untranslated β-globin regions that are detected by the oocyte's expression machinery

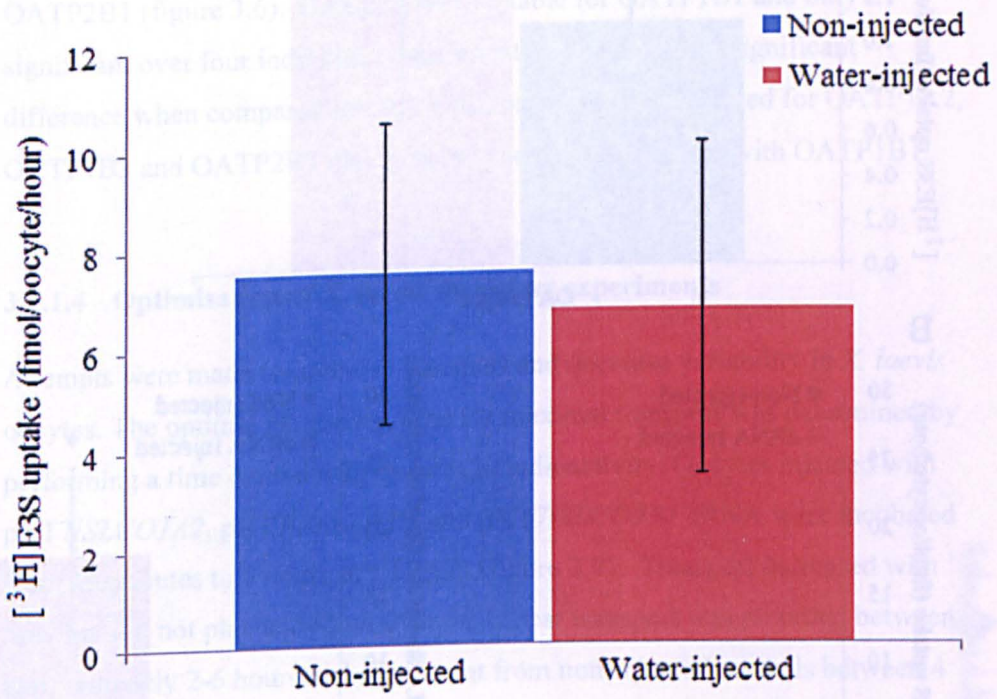

Figure 3.4 – Uptake of [^{3}H]E3S into non-injected and water-injected oocytes. Each bar is the mean ± SE of 10 individual experiments with 5 oocyte replicates.

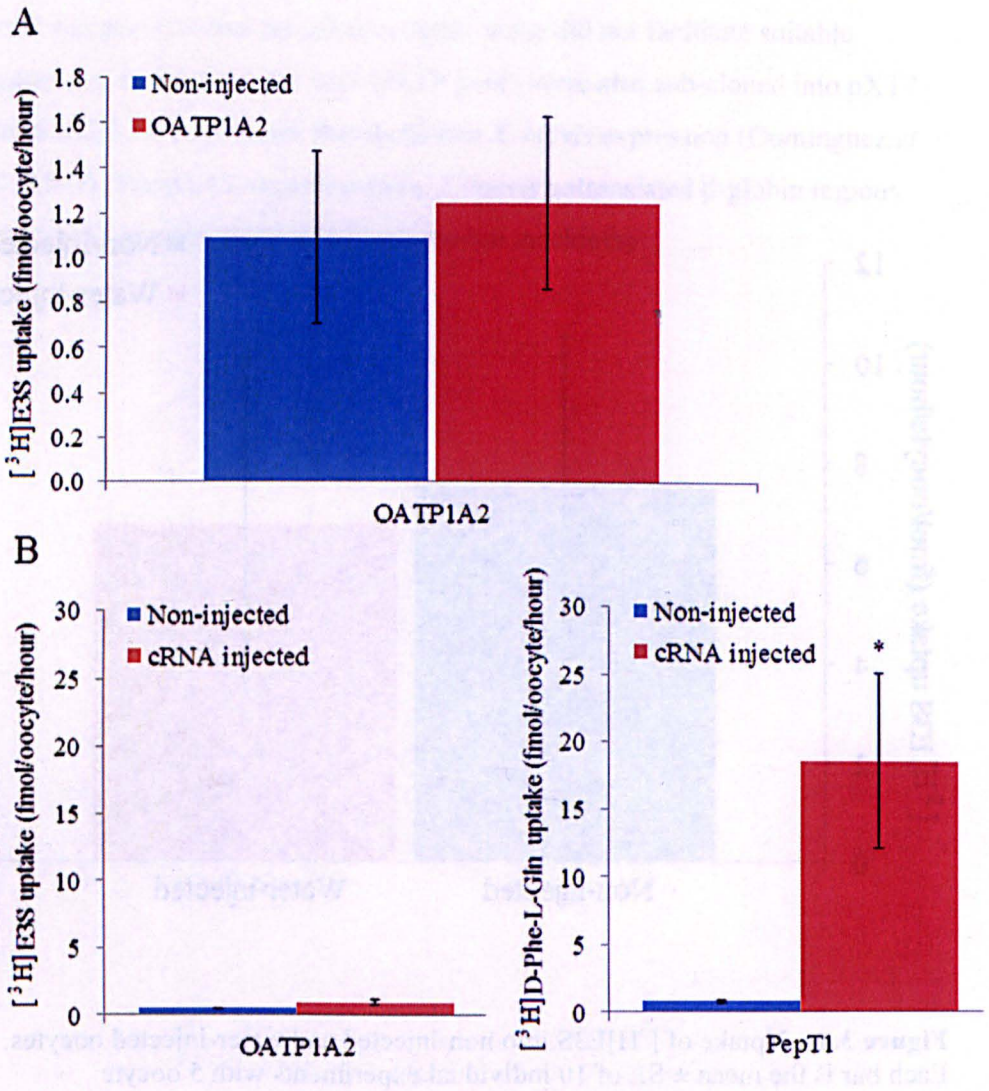

Figure 3.5 – A) Uptake of [^{3}H]E3S into non-injected and pBluescriptR/*SLCO1A2* cRNA injected oocytes. Each bar is the mean ± SE of 3 individual experiments with 5 oocyte replicates. B) Uptake of [^{3}H]E3S into non-injected and pBluescriptR/*SLCO1A2* cRNA injected oocytes, with [^{3}H]D-Phe-L-Gln into non-injected and pXT7/*Slc15a1* cRNA injected oocytes from the same frog. Data are representative of one experiment with 5 oocyte replicates. Asterisks (*) indicate a significant increase using an unpaired Student's t-test ($P<0.05$).

3.2.1.3 Transport by OATPs cloned into the pXT7 vector

The four *SLCO* genes cloned into the pXT7 vector were synthesised into cRNA and injected into oocytes. Uptake experiments were performed 72 hours post-injection, following a one hour incubation in [^{3}H]E3S. Transport of [^{3}H]E3S was significant from the non-injected controls for OATP1A2, OATP1B3 and OATP2B1 (figure 3.6). Transport was variable for OATP1B1 and only significant over four individual experiments, resulting in no significant difference when compared overall. Optimisation was performed for OATP1A2, OATP1B3 and OATP2B1 owing to the variability observed with OATP1B1.

3.2.1.4 Optimisation of *X. laevis* transport experiments

Attempts were made to optimise transport and decrease variability in *X. laevis* oocytes. The optimal incubation time for maximal transport was determined by performing a time course with oocytes in radioactivity. Oocytes injected with pXT7/*SLCO1A2*, pXT7/*SLCO1B3* and pXT7/*SLCO2B1* cRNA were incubated from 30 minutes to 6 hours in [^{3}H]E3S (figure 3.7). Transport increased with time but did not plateau within 6 hours. Linear transport was recorded between approximately 2-6 hours and significant from non-injected controls between 4 and 6 hours, thus future experiments were performed at 4 hour time points.

Transport experiments were performed at 3 and 4 days post-injection, to determine if transport or expression could be increased with an extra day; however, there was no significant increase (figure 3.8). Furthermore, oocyte membranes were more susceptible to rupture following the increased time post-injection.

Oocyte transport experiments were variable and depended on the quality of the oocytes week by week. This is highlighted in figure 3.9, whereby transport variability for OATP2B1 is displayed over several experiments. Over time the oocyte method for expressing OATPs did not reveal itself to be reliable.

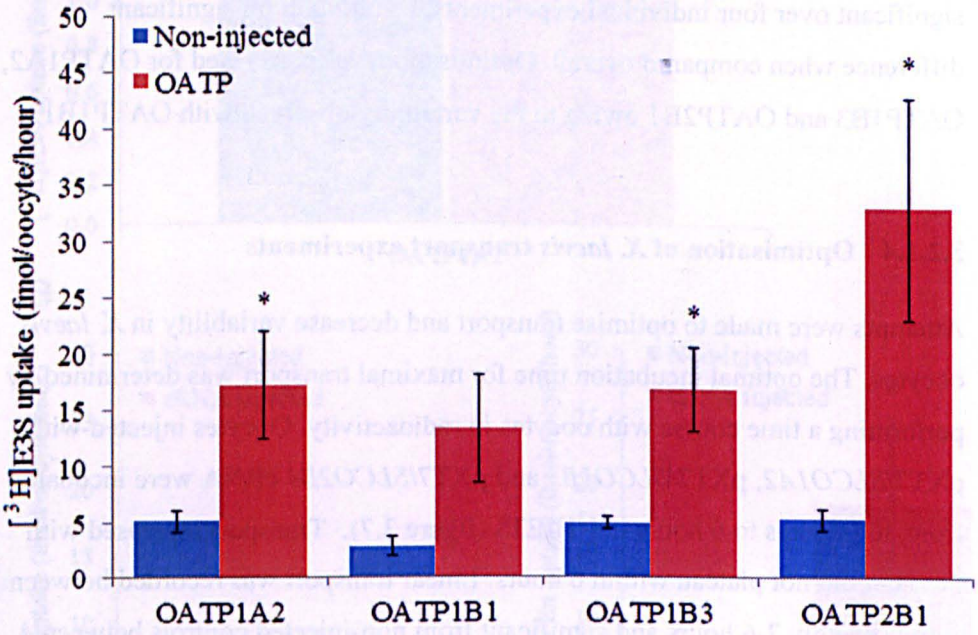

Figure 3.6 – Uptake of [^{3}H]E3S into non-injected and pXT7/*SLCO1A2*, pXT7/*SLCO1B1*, pXT7/*SLCO1B3* and pXT7/*SLCO2B1* cRNA injected oocytes. Each bar is the mean ± SE of 4-13 individual experiments with 5 oocyte replicates. *Unpaired t-test $P<0.05$.

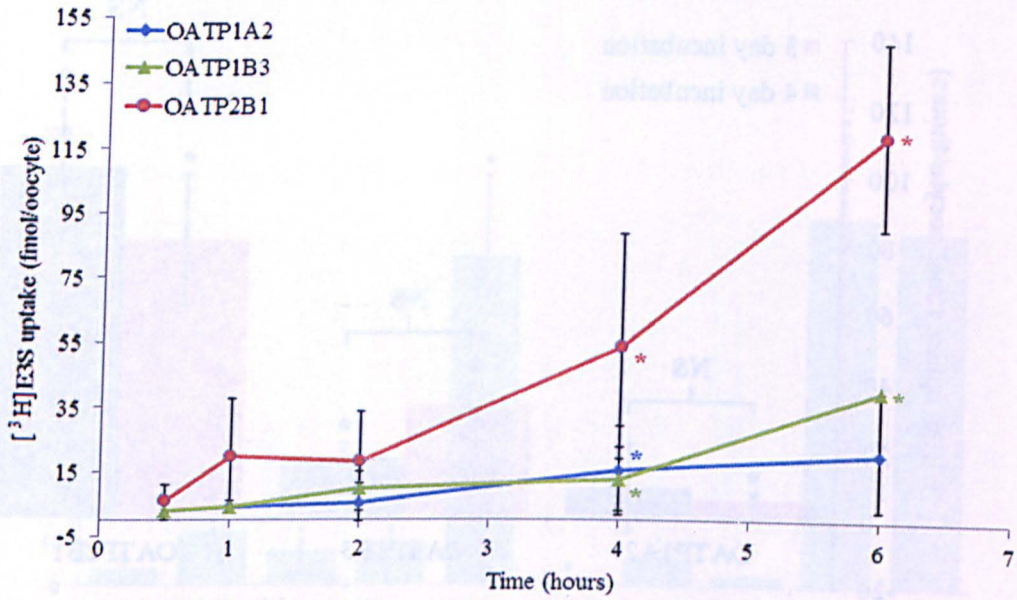

Figure 3.7 – Mediated uptake of [^{3}H]E3S into pXT7/*SLCO1A2*, pXT7/*SLCO1B3* and pXT7/*SLCO2B1* cRNA injected oocytes. Non-injected control uptake was subtracted. Each point is the mean ± SE of 3-6 experiments with 5 oocyte replicates. *Unpaired t-test $P<0.05$ (colour coded).

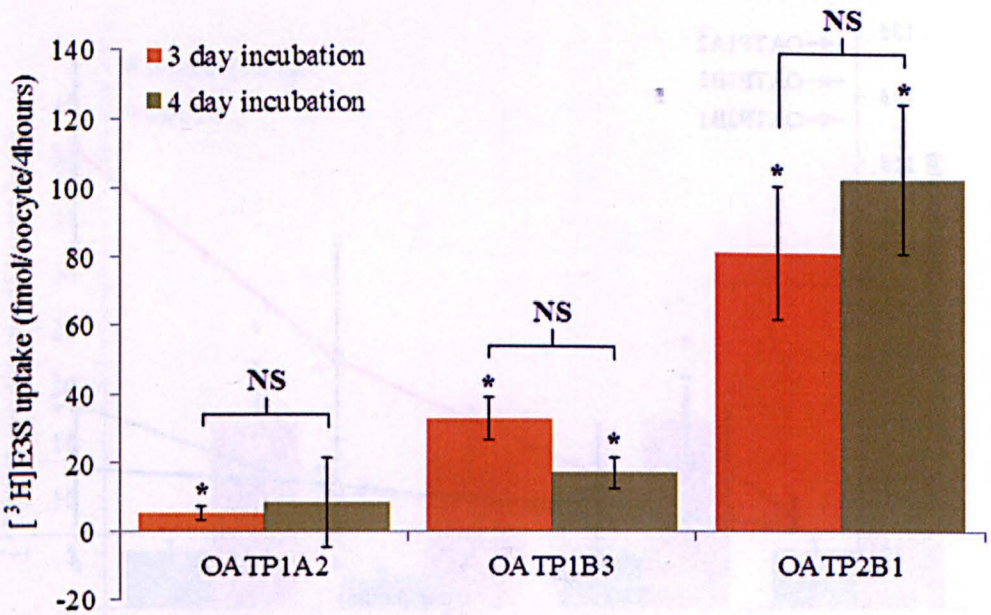

Figure 3.8 – Mediated uptake of [^{3}H]E3S into pXT7/*SLCO1A2*, pXT7/*SLCO1B3* and pXT7/*SLCO2B1* cRNA injected oocytes. Non-injected control uptake was subtracted. Each bar is the mean ± SE of one experiment with 5 oocyte replicates. *Unpaired t-test; $P<0.05$ from pcDNA control. NS=No significance.

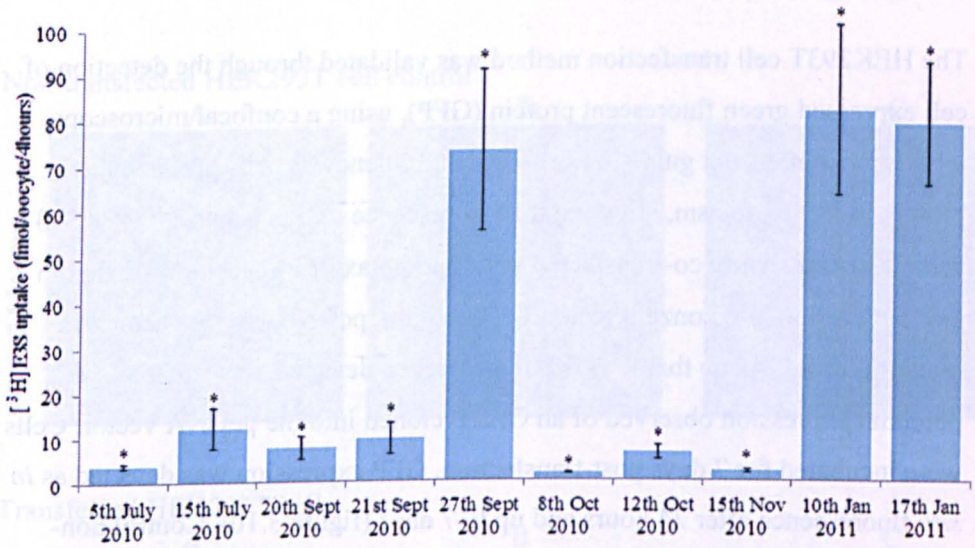

Figure 3.9 - Inter-assay variability of [^{3}H]E3S mediated uptake into pXT7/*SLCO2B1* cRNA injected oocytes. Non-injected oocyte controls were subtracted. Each bar is the mean ± SE of one experiment with 5 oocyte replicates. *Unpaired t-test $P<0.05$.

3.2.2 HEK293T cell experiment results

HEK293T cells were evaluated as another method for studying the characteristics of OATPs. *SLCO1A2*, *SLCO1B1* and *SLCO1B3* were sub-cloned from the pXT7 vector into the mammalian expression vector pcDNA3.1/Hygro(-) (section 2.2.14.2). The transfection and transport experiments were optimised for maximum transport.

3.2.2.1 Optimisation of HEK293T cell transfection

The HEK293T cell transfection method was validated through the detection of cell expressed green fluorescent protein (GFP), using a confocal microscope. GFP is a useful visual guide to transfection efficiency as cells produce the protein in the cytoplasm, allowing the fluorescence to be visualised. HEK293T cells were transiently co-transfected with 2µg pmaxGFP® vector provided in the transfection kit (Lonza, Preston UK) and 5µg pcDNA empty vector. An assumption was made that the GFP fluorescence detected was equal to the potential expression observed of an OATP cloned into the pcDNA vector. Cells were incubated for 7 days post-transfection. GFP expression was detected as *in situ* fluorescence after 24 hours and up to 7 days (figure 3.10). Control non-transfected cells did not express GFP. This provided a time frame for plasmid expression by the transiently expressing cells.

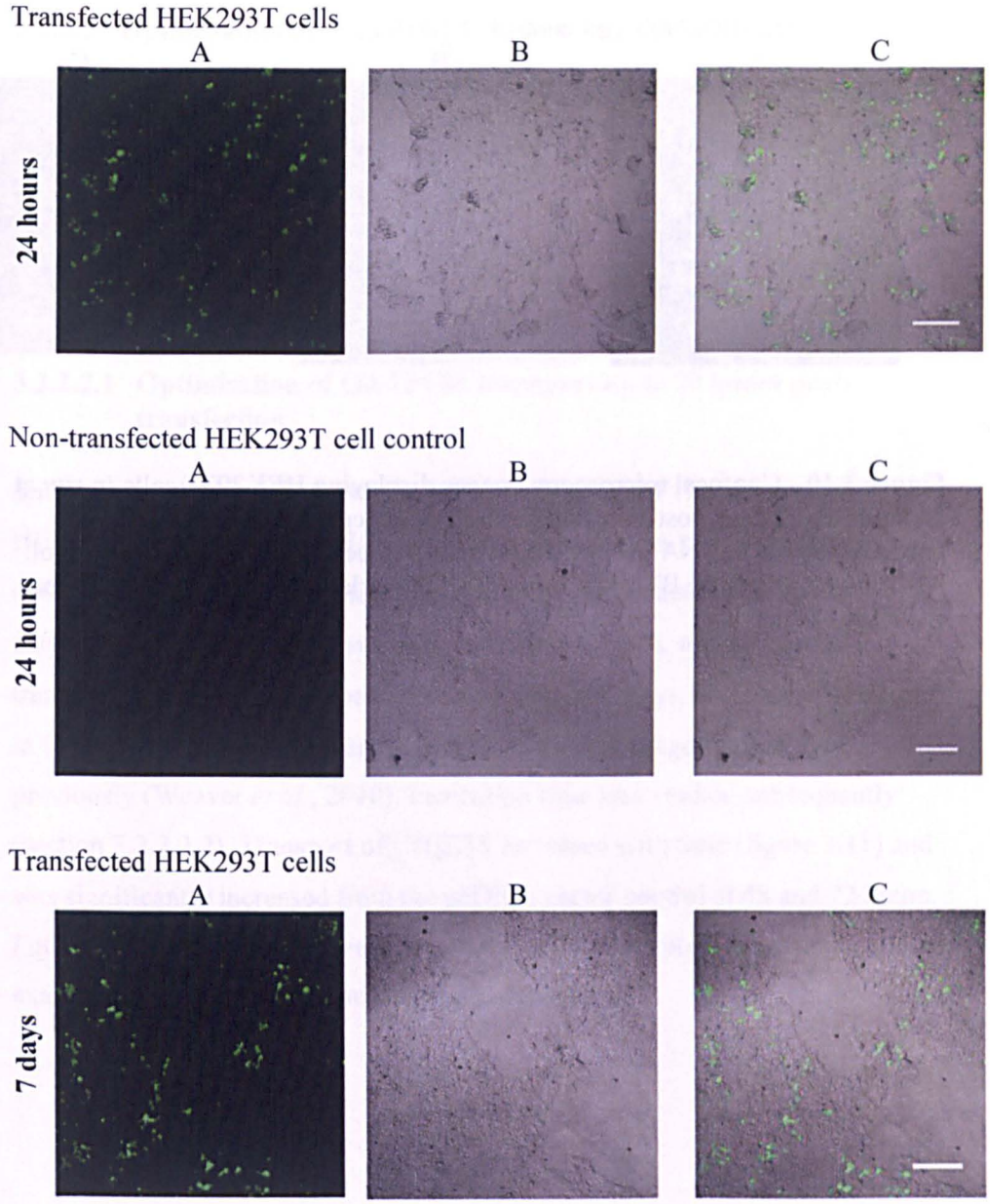

Figure 3.10 – continued on next page

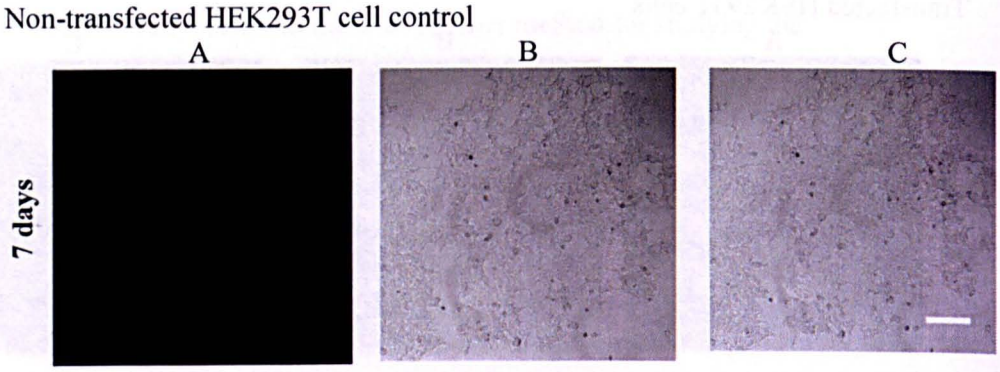

Figure 3.10 - Confocal microscopy images displaying HEK293T cells *in situ* at 24 hours and 7 days post-transfection. Cells were co-transfected with pmaxGFP® and pcDNA vector. Non-transfected cells were plated as a control. A) GFP only (488nm) B) bright field only C) overlay of both images. Scale bar = 200μm.

3.2.2.2 Optimisation of OATP1B1 transport in HEK293T cells

OATP1B1 was initially optimised in HEK293T cells with the aim that the experimental conditions could then be used as a basis for optimising the other transporters. The optimal incubation time for protein expression and transport were selected and the kinetics determined.

3.2.2.2.1 Optimisation of OATP1B1 transport up to 72 hours post-transfection

Substrate uptake experiments were performed on OATP1B1 expressing HEK293T cells at 24, 48 and 72 hours post-transfection, to determine the optimal incubation time for detecting transport. Expression of GFP was detected up to 7 days post-transfection (section 3.2.2.1), suggesting that transport proteins may also be expressed for up to 7 days. Cells were incubated in [^{3}H]E3S for 1 minute, an approximate linear time range as described previously (Weaver *et al.*, 2010). Incubation time was studied subsequently (section 3.2.2.2.2). Transport of [^{3}H]E3S increased with time (figure 3.11) and was significantly increased from the pcDNA vector control at 48 and 72 hours. Future uptake experiments were performed at 72 hours post-transfection and an exact linear time range was subsequently determined.

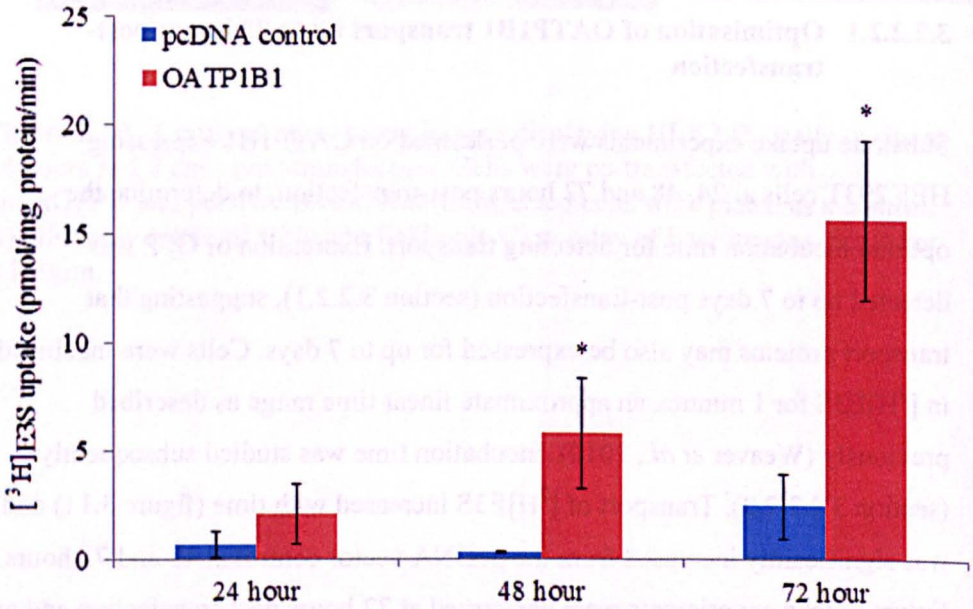

Figure 3.11 - Uptake of [^{3}H]E3S into pcDNA/*SLCO1B1* and pcDNA vector transfected HEK293T cells at 24, 48 and 72 hours post-transfection. Each bar is the mean ± SE of one experiment with 6 well replicates. *Unpaired t-test $P<0.05$.

3.2.2.2.2 Optimisation of the linear time frame for OATP1B1 transport

In order to detect the maximum transport by OATP1B1 expressing HEK293T cells the transport experiments should be conducted when the transport into the cell is linear. Therefore OATP1B1 transfected cells at 72 hours post-transfection were incubated in [^{3}H]E3S for various time points. Uptake experiments were performed at 0.5, 1, 2, 5, 10 and 20 minutes (figure 3.12). Uptake into the cells increased up until 5 minutes, then decreased. The linear range was between 2-5 minutes and therefore subsequent experiments were performed with 3 minute incubations in radioactivity.

3.2.2.2.3 Determination of OATP1B1 transport kinetics

The kinetics of [^{3}H]E3S transport into OATP1B1 expressing HEK293T cells were determined by calculating the K_m and V_{max}. A total of 6 different E3S concentrations: 0, 0.15, 0.3, 0.5, 1.0 and 1.5μM were tested using the optimised conditions described above. Uptake experiments were performed alongside the pcDNA control and control values subtracted. Values were fitted to the Michaelis-Menten equation as described in section 2.7.1 and the equation used to fit a Michaelis-Menten curve (figure 3.13). The K_m was 0.105 ± 0.008μM and the V_{max} 50.1 ± 10.9 pmol/mg protein/3min. The protein did not demonstrate biphasic kinetics as described by some other groups (0.23μM & 45μM, (Noe *et al.*, 2007), (67 ± 31nM & 7 ± 2μM, (Tamai *et al.*, 2001); however, not all groups have detected biphasic properties (Cui *et al.*, 2001; Hirano *et al.*, 2004; Miyagawa *et al.*, 2009). In comparison with the findings of others, the K_m found in this system may be the high affinity binding site. These kinetics will be used as a WT value for comparing with the kinetics of FLAG tagged and mutant isoforms.

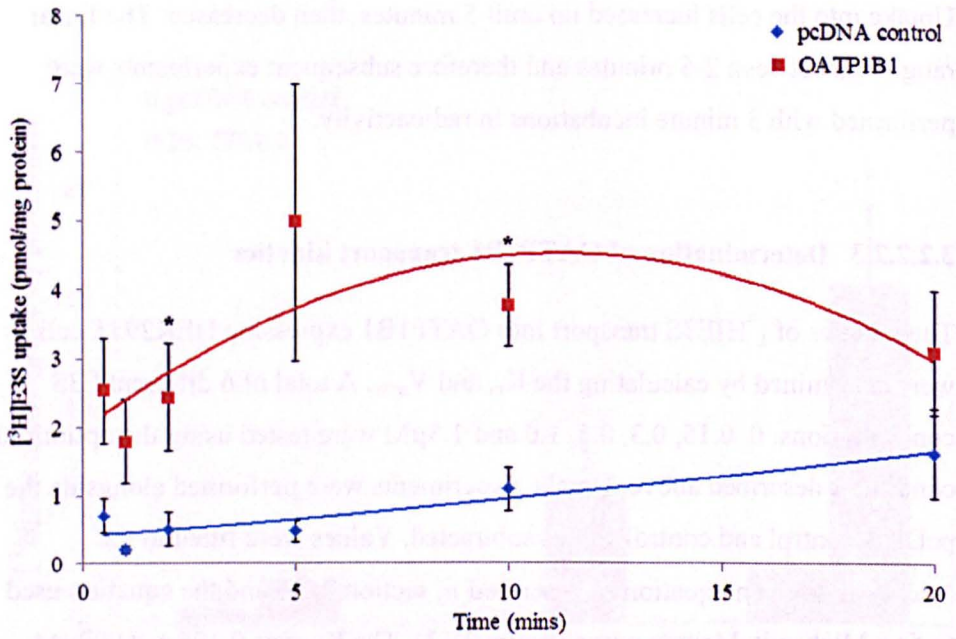

Figure 3.12 - Uptake of [^{3}H]E3S into pcDNA/*SLCO1B1* and pcDNA vector transfected HEK293T cells following 0.5, 1, 2, 5, 10 and 20 minute incubations with radioactivity. Points are the mean ± SE of one experiment with 3 well replicates. *Unpaired t-test $P<0.05$.

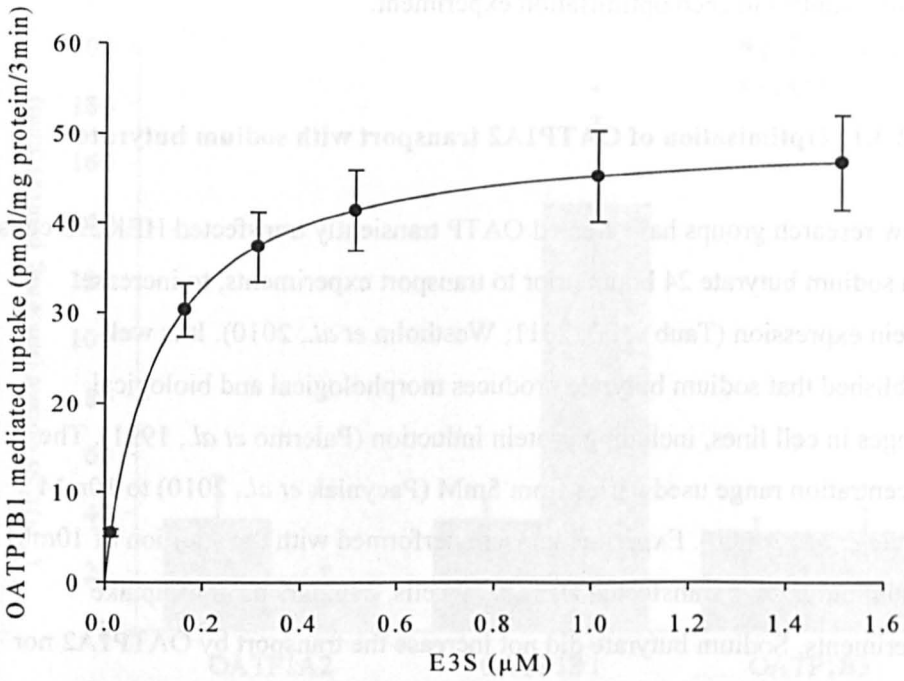

Figure 3.13 – Kinetics of pcDNA/OATP1B1 mediated transport of E3S. Uptake of increasing concentrations of E3S were measured. The line is the Michaelis-Menten equation fitted to the K_m and V_{max}. $K_m = 0.105 \pm 0.008\mu M$, $V_{max} = 50.1 \pm 10.9$ pmol/mg/3min. Each point is the mean ± SE of 5 individual experiments with 3 well replicates.

3.2.2.3 OATP1A2 and OATP1B3 transport results

The optimised conditions established for OATP1B1 were applied to OATP1A2 and OATP1B3 transport experiments. Transport by OATP1A2 and OATP1B3 in HEK293T cells was in contrast to OATP1B1 very low (figure 3.14), and not significant from the pcDNA vector control. Various parameters were changed in an attempt to increase the low levels of expression. OATP1B1 was used as a positive control in each optimisation experiment.

3.2.2.3.1 Optimisation of OATP1A2 transport with sodium butyrate

A few research groups have treated OATP transiently transfected HEK293 cells with sodium butyrate 24 hours prior to transport experiments, to increase protein expression (Taub *et al.*, 2011; Westholm *et al.*, 2010). It is well established that sodium butyrate produces morphological and biological changes in cell lines, including protein induction (Palermo *et al.*, 1991). The concentration range used varies from 5mM (Pacyniak *et al.*, 2010) to 10mM (Konig *et al.*, 2000b). Experiments were performed with the addition of 10mM sodium butyrate to transfected HEK293T cells, 24 hours prior to uptake experiments. Sodium butyrate did not increase the transport by OATP1A2 nor OATP1B3, and the observed effect on OATP1B1 was not significant (figure 3.15).

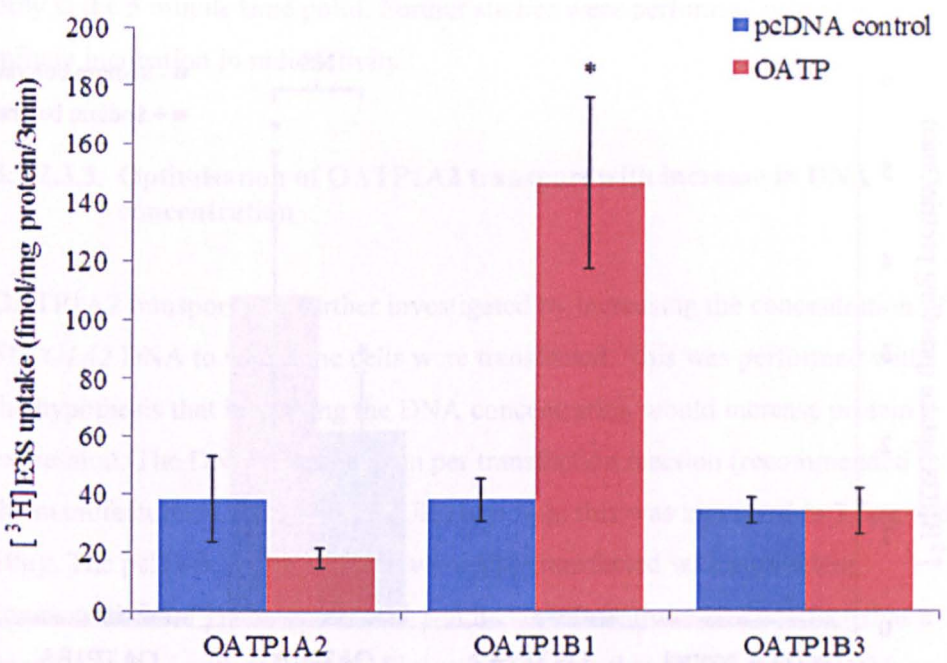

Figure 3.14 - Uptake of [^{3}H]E3S into pcDNA/*SLCO1A2*, pcDNA/*SLCO1B1*, pcDNA/*SLCO1B3* and pcDNA vector transfected HEK293T cells. Each bar is the mean ± SE of one experiment with 6 well replicates. *Unpaired t-test $P<0.05$.

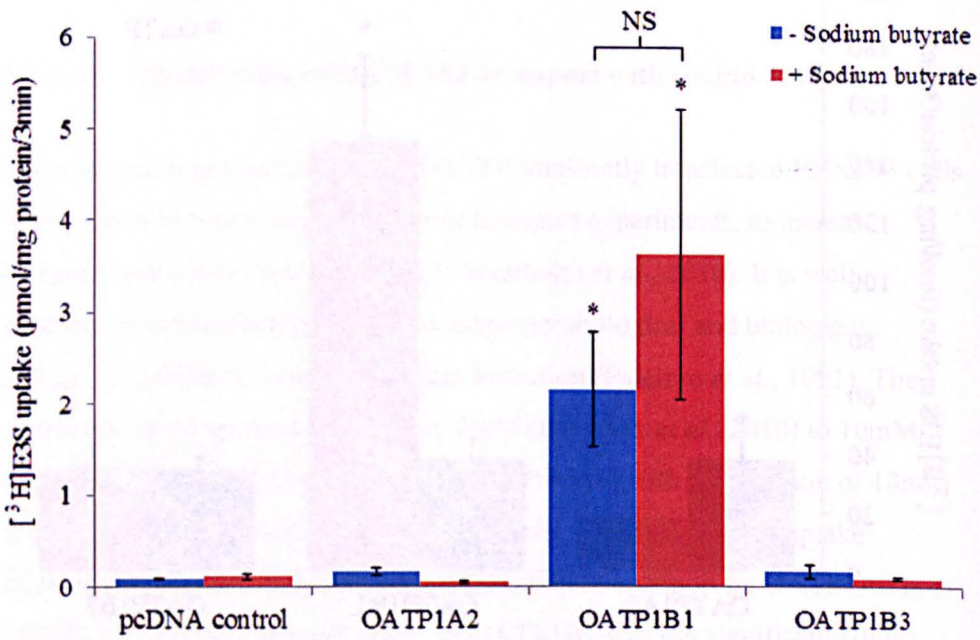

Figure 3.15 - Uptake of [^{3}H]E3S into pcDNA/*SLCO1A2*, pcDNA/*SLCO1B1*, pcDNA/*SLCO1B3* and pcDNA vector transfected HEK293T cells, in the presence/absence of sodium butyrate. Each bar is the mean ± SE of one experiment with 6 well replicates. *Unpaired t-test; $P<0.05$ from pcDNA control. NS = No significance.

3.2.2.3.2 Optimisation of the linear time frame for OATP1A2 transport

A time course was performed to determine the time range at which OATP1A2 transport was in the linear phase. Uptake experiments were performed following 1, 2, 3, 4, 5 and 10 minute incubations with radioactivity. Figure 3.16 shows that like OATP1B1, transport increased up to 5 minutes. However transport was marginally higher than the vector only control and significant only at the 5 minute time point. Further studies were performed using the 3 minute incubation in radioactivity.

3.2.2.3.3 Optimisation of OATP1A2 transport with increase in DNA concentration

OATP1A2 transport was further investigated by increasing the concentration of *SLCO1A2* DNA to which the cells were transfected. This was performed with the hypothesis that increasing the DNA concentration would increase protein expression. The DNA concentration per transfection reaction (recommended by the manufacturer; Lonza, Preston UK) was 5μg; this was increased to 7.5μg and 10μg. The pcDNA vector controls were also transfected with equivalent concentrations of DNA. OATP1B1 and its vector control were transfected as a positive control with 5μg DNA. Figure 3.17 shows that an increase in DNA concentration did not significantly increase transport for OATP1A2. The addition of 10μg DNA just failed to reach significance (P=0.06) for increasing transport by OATP1A2.

3.2.2.3.4 Optimisation of OATP1A2 transport by sub-cloning into the pCI-neo vector

An increase in OATP1A2 protein expression was further attempted by sub-cloning the *SLCO1A2* gene from pcDNA into another mammalian expression vector pCI-neo. pCI-neo is similar to pcDNA by containing a mammalian CMV promoter, however, pCI-neo also contains a chimeric intron derived from human β-globin and immunoglobulin genes. The insertion of introns flanking a

DNA insert has been shown to increase gene expression by up to 20-fold (Buchman and Berg, 1988), as the intron facilitates gene splicing. However gene expression is not always increased, owing to lack of recognition of the intron or inefficient splicing. *SLCO1A2* was cloned into pCI-neo in an attempt to increase gene expression. Figure 3.18, however, confirmed that the presence of the intron in pCI-neo did not increase expression of OATP1A2. Uptake of [^{3}H]E3S was not significantly increased in the OATP1A2 expressing cells compared with the vector control.

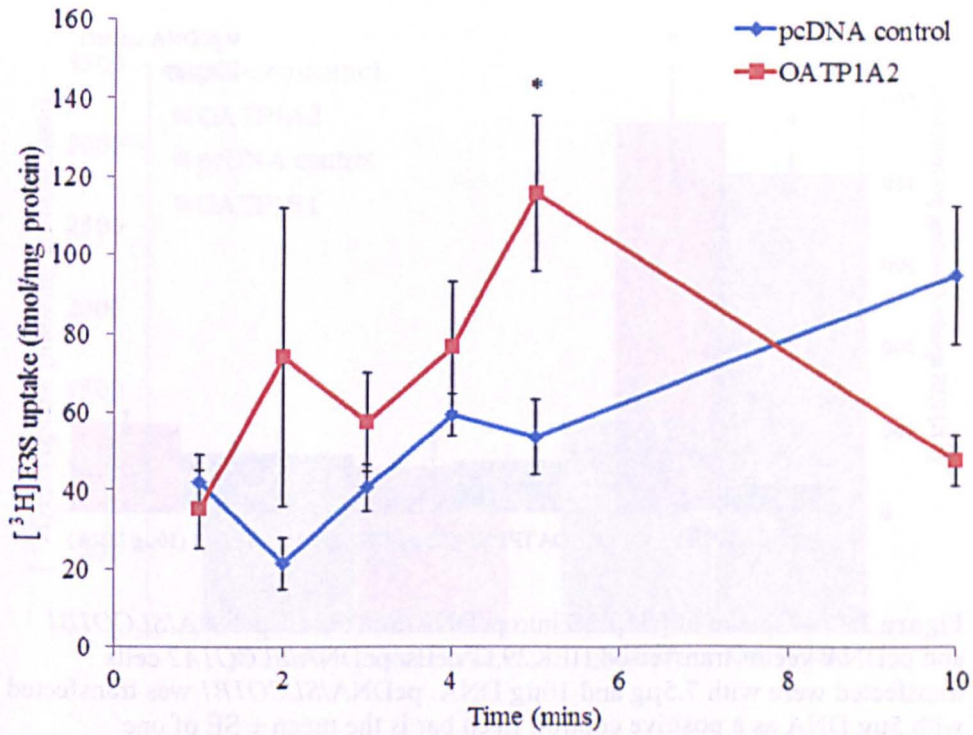

Figure 3.16 - Uptake of [^{3}H]E3S into pcDNA/*SLCO1A2* and pcDNA vector transfected HEK293T cells following 1, 2, 3, 4, 5, and 10 minute incubations in radioactivity. Each point is mean ± SE of one experiment with 3 well replicates. *Unpaired t-test $P<0.05$.

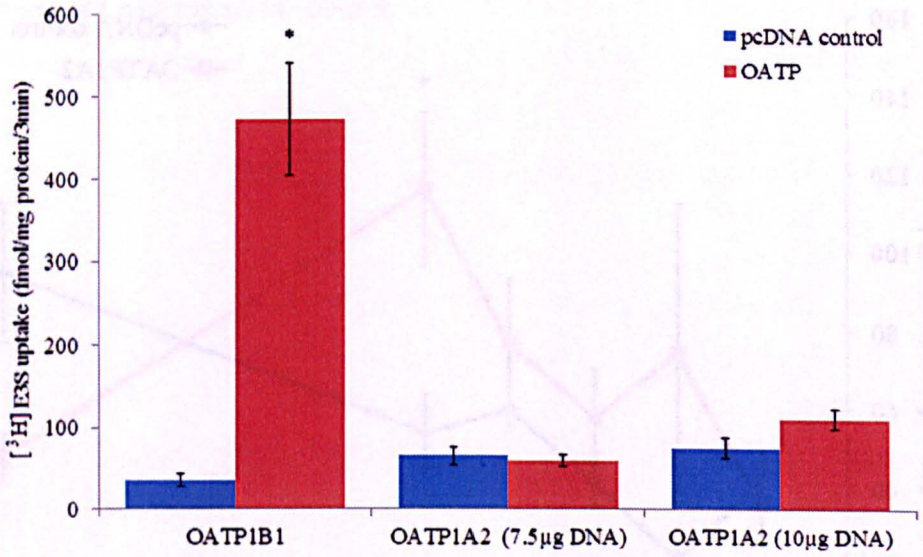

Figure 3.17 - Uptake of [^{3}H]E3S into pcDNA/*SLCO1A2*, pcDNA/*SLCO1B1* and pcDNA vector transfected HEK293T cells. pcDNA/*SLCO1A2* cells transfected were with 7.5µg and 10µg DNA. pcDNA/*SLCO1B1* was transfected with 5µg DNA as a positive control. Each bar is the mean ± SE of one experiment with 6 well replicates. *Unpaired t-test $P<0.05$.

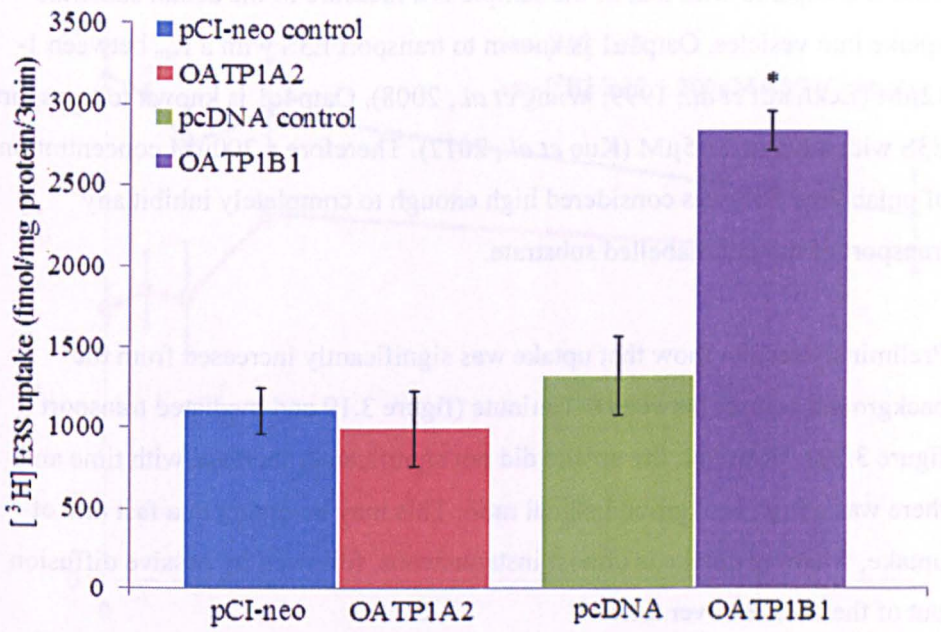

Figure 3.18 - Uptake of [^{3}H]E3S into pCI-neo control vector, pCI-neo/*SLCO1A2*, pcDNA control vector and pcDNA/*SLCO1B1* transfected HEK293T cells. Each bar is the mean ± SE of one experiment with 6 well replicates. *Unpaired t-test $P<0.05$.

3.2.3 Rat kidney membrane vesicle results

Membrane vesicles prepared from rat kidney PT and DT were evaluated for endogenous [^{3}H]E3S transport by Oatp1a1 and Oatp4c1. A control of [^{3}H]E3S + 200μM unlabelled E3S was used. In the control, the unlabelled E3S competed with the radiolabelled substrate and inhibited transport of the radioactive substrate into the vesicle. Therefore the control values are a measure of the background radioactivity, and the difference between uptake observed in the control compared with that of the sample is a measure of the actual substrate uptake into vesicles. Oatp1a1 is known to transport E3S with a K_m between 1-12μM (Eckhardt *et al.*, 1999; Wang *et al.*, 2008). Oatp4c1 is known to transport E3S with a K_m of 21.5μM (Kuo *et al.*, 2012). Therefore a 200μM concentration of unlabelled E3S was considered high enough to completely inhibit any transport of the radiolabelled substrate.

Preliminary results show that uptake was significantly increased from the background control between 0-1 minute (figure 3.19 and mediated transport figure 3.20). However, the uptake did not significantly increase with time and there was a high background:signal ratio. This may be owing to a fast rate of uptake, whereby uptake is almost instantaneous, followed by passive diffusion out of the vesicles over time.

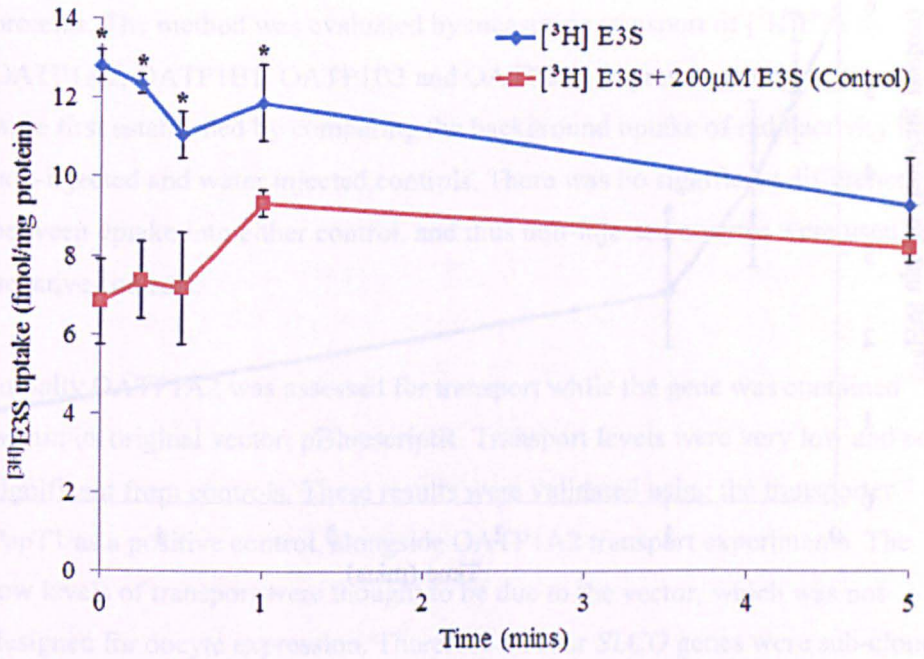

Figure 3.19 - Uptake of [^{3}H]E3S and control [^{3}H]E3S + 200µM E3S into rat kidney membrane vesicles. Each point is the mean ± SE of 2 individual experiments with 6 well replicates. *Unpaired t-test ($P<0.05$).

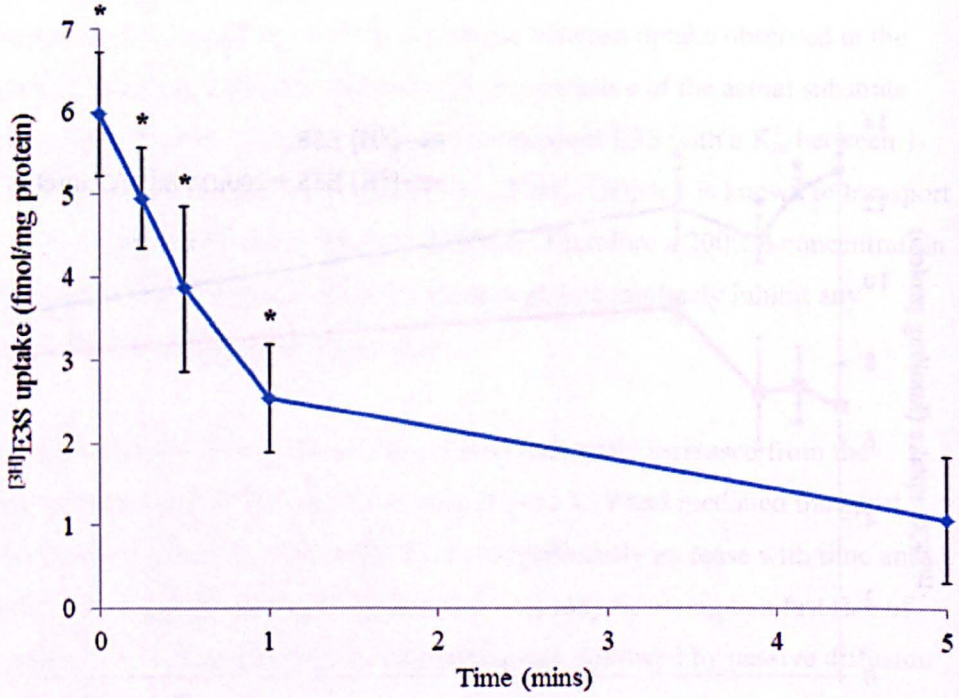

Figure 3.20 – Mediated uptake of [^{3}H]E3S into rat kidney membrane vesicles. Control [^{3}H]E3S + 200μM E3S values were subtracted. Each point is the mean ± SE of 2 individual experiments with 6 well replicates. *Unpaired t-test ($P<0.05$).

3.3 Conclusion

Two over-expression systems were evaluated for the expression of OATPs; *X. laevis* oocytes and HEK293T cells. Plasma membrane vesicles were also evaluated as an alternative tool for studying endogenous transport in primary tissue.

The *X. laevis* oocyte model is an established method for expressing transport proteins. The method was evaluated by measuring transport of [^{3}H]E3S by OATP1A2, OATP1B1, OATP1B3 and OATP2B1 expressing oocytes. Controls were first established by comparing the background uptake of radioactivity into non-injected and water injected controls. There was no significant difference between uptake into either control, and thus non-injected oocytes were used as negative controls.

Initially OATP1A2 was assessed for transport while the gene was contained within its original vector, pBluescriptR. Transport levels were very low and not significant from controls. These results were validated using the transporter PepT1 as a positive control, alongside OATP1A2 transport experiments. The low levels of transport were thought to be due to the vector, which was not designed for oocyte expression. Therefore all four *SLCO* genes were sub-cloned from their vectors into the *X. laevis* expression vector pXT7.
OATP1A2, OATP1B3 and OATP2B1 transported [^{3}H]E3S consistently over >6 independent experiments. OATP1B1 however only transported over 4 experiments and transport was generally low in comparison with the other OATPs. Therefore oocyte transport experiments with OATP1B1 were not continued.
Over time however, transport demonstrated by the other OATPs was variable, most likely owing to the variability in expression demonstrated by the oocytes. Many factors affected the oocytes, including the age and/or batch of frogs, adequate defolliculation of ovaries, accurate micro-injection and health of the oocytes post-injection. The oocyte system was therefore optimised in an

attempt to determine the best experimental conditions for OATP transport. The linear time frame for transport was assessed through a time course of incubations, from 30 minutes to 6 hours in radioactivity. Transport increased with time, but did not plateau within 6 hours. The linear time frame was estimated to be between 4-6 hours, although a longer time course would have been required to accurately determine this time. This however was not conducted as the increased incubation resulted in higher oocyte fatality. Transport experiments were also conducted over 3-4 days to determine if OATP expression increased when incubated for an extra day. Transport was not significantly increased and again there was increased oocyte death. These optimisation experiments did not improve the variation observed.

Cell lines have been used extensively for the characterisation of transport proteins, including OATPs (Roth *et al.*, 2011). The HEK293T cell model was utilised and OATP1B1 displayed a high and consistent level of transport. The experimental conditions chosen for OATP1B1-HEK293T expression were determined by optimising the transfection and substrate uptake experiments. Cells were grown up to 7 days post-transfection to determine the length of time to which the cells retained the temporary plasmid. Transfection experiments with GFP showed that cells were still expressing the fluorescent protein 7 days post-transfection, providing a 7 day time frame for which to perform uptake experiments. The nucleofection method was optimised from 6 well plates as described in the manufacturer's instructions to 12 well plates, which allowed for more replicate samples and wells which were practical for viewing under the microscope. Once the transfection method was established the optimal incubation time for protein expression was established.
Results showed that 24 hours did not provide the cells enough time to sufficiently express OATP1B1, however there was significant substrate transport at 48 and 72 hours. As maximal uptake was required, future experiments were performed 72 hours post-transfection. Other groups have also reported performing HEK293/OATP transport experiments at 48 (Kobayashi *et al.*, 2003) and 72 hours post-transfection (Sai *et al.*, 2006). In order to ensure a

maximal level of substrate uptake, a time course was performed to determine the phase at which transport was linear. Transport was linear between 2-5 minutes, therefore further experiments were conducted after 3 minute incubations in radioactivity. Using these experimental parameters, the K_m and V_{max} for OATP1B1 were determined as 0.105 ± 0.008μM and 50.1 ± 10.9 pmol/mg protein/3min.

Determination of these values validated the OATP1B1 transport and verified that the protein was functioning as described by other groups (0.23μM (Noe *et al.*, 2007), (0.21 ± 0.02μM, 25.6 ± 4.6 pmol/mg protein/2min (Li *et al.*, 2012). Determination of the K_m also set the suitable range of concentrations for future experiments which were performed with the following concentrations of unlabelled E3S: 0, 0.05, 0.1, 0.5, 1.0, 1.5μM. In addition, these values provided an important control value for later experiments with mutant isoforms, whereby the change in K_m and V_{max} were assessed.

OATP1A2 and OATP1B3 did not transport to a significant level from controls, despite several optimisation experiments. The reason for the low transport is surprising as both proteins have been expressed in HEK293 cells previously (Hu *et al.*, 2008). Sodium butyrate was shown to increase gene expression in HEK293 cells when supplemented 24 hours before uptake experiments, however this was not the case for this model. Further optimisation experiments with an uptake time course, increasing concentrations of DNA during transfection and even sub-cloning into another vector did not significantly increase transport of E3S by OATP1A2. OATP2B1 transport in HEK293T cells was not analysed.

Plasma membrane vesicles have been previously utilised for assessing endogenous membrane transport (Koopen *et al.*, 1997; Meredith and Laynes, 1996), but not for OATPs. Rat kidney cortex vesicles of PT and DT cells were assessed as a potential model for determining the endogenous uptake of substrates in the kidney. The substrate [^{3}H]E3S was used as it is a substrate for rat Oatp1a1 and Oatp4c1. Vesicle [^{3}H]E3S uptake was significantly higher than

the background control in the first minute, suggesting that vesicular transport was occurring. However, transport was not significantly increased over time, as expected with an increased incubation in radioactivity. It is possible that transport into the vesicles was extremely rapid, followed by a decrease over time. Or it may be that some of the radioactivity was retained on the filter, as shown by the high fmol detected at the zero timepoint (~13fmol).
The vesicle system was not explored further for several reasons. The availability of rat kidney was limited, which would have limited the amount of experiments. In addition, the overlapping substrate specificities of transporters for uptake and efflux in the kidney cause limitations when detecting endogenous transport. Many transporters are present in the PT and DT apart from OATPs, including the OATs and ABCs. Some of these transporters also transport E3S, including Oat3, which is present on the basolateral PT membrane (Sweet *et al.*, 2003). Therefore, the transport detected may have been the result of several transporters. Furthermore, gender differences occur between male and female kidney regulation. Oatp1a1 has a sex-dependent renal clearance, with female rats demonstrating a faster clearance of compounds than males (Yang *et al.*, 2009). Therefore both male and female rat kidneys would need to be analysed and compared. This gender difference has not been studied in the human homologues, making extrapolations from rat to human difficult.

In summary, rat kidney membrane vesicles, *X. laevis* oocytes and the HEK293T cell line were all evaluated as potential models for studying OATPs. OATP1B1 transported significantly and consistently in HEK293T cells and thus this cell model was used for further experiments. The vesicle experiment had a number of limitations and the oocyte system was not consistently reliable. Therefore the structural characteristics evaluated in chapters 4 and 5 were determined in OATP1B1 and compared to the WT type results generated here.

4 Investigation of the OATP1B1 topology

4.1 Introduction

The structural knowledge of transmembrane proteins is lagging behind that of most other protein families owing to the difficulties with structure determination. The exact structural properties of the OATPs are therefore yet to be determined.

The position of a protein within the membrane, along with the number and orientation of the TMs, is known as the topology (Wallin and von Heijne, 1998). All members of the SLC superfamily contain multiple TMs (He *et al.*, 2009) and the OATPs have been previously predicted by topology prediction analysis to contain 12TMs with a large fifth extracellular loop (Chang *et al.*, 2005; Hagenbuch, 2003; Konig *et al.*, 2000a; Li *et al.*, 2012). The N and C termini are putatively internal, facing the cytoplasmic space (Hanggi *et al.*, 2006; Meier-Abt *et al.*, 2005). So far only rat Oatp1a1 has been experimentally investigated as a potential 12TM protein (Wang *et al.*, 2008) and the orientation of the N and C termini was not elucidated.

OATP1B1 was the isoform chosen to study the topology of the human OATPs. OATP1B1 plays an important role in the transport of endogenous and xenobiotic compounds into the liver, and is implicated in many DDIs. Protein dysfunction and genetic variation are also implicated in disease and drug disposition (Niemi *et al.*, 2011; van de Steeg *et al.*, 2012).
Therefore OATP1B1 is an important candidate for which to determine the structure. Like all of the OATPs, OATP1B1 has been predicted as a 12TM protein with a large extracellular loop and internal N and C termini (Konig *et al.*, 2000b), as well as the OATP superfamily signature at the border with TM6 (Niemi *et al.*, 2011), but unlike some other OATPs it does not contain a C terminal PDZ sequence (Wang *et al.*, 2005a). OATP1B1 also contains glycosylation sites in extracellular loops 2 and 5 (N134, N503, N516) (Yao *et*

al., 2012), and the apparent molecular mass is reduced from 84 kDa to 58 kDa upon deglycosylation (Konig *et al.*, 2000b). Several of the TMs are shown to be important for substrate binding (Gui and Hagenbuch, 2009; Li *et al.*, 2012; Miyagawa *et al.*, 2009), as are positive amino acids R57, K361 and R580 (Weaver and Hagenbuch, 2010), which are predicted to line the putative pore of the protein (Meier-Abt *et al.*, 2005).

The topology of OATP1B1 was studied using a FLAG epitope tag and luminometry approach using the previously established OATP1B1/HEK293T system (section 3.2.3). FLAG epitope tags were inserted into putative extracellular and intracellular plus the N and C terminal regions of OATP1B1, as directed by topology prediction analysis. Sixteen topology prediction programs and 9 signal peptide prediction programs were used to evaluate the number of TMs, orientation of the N and C termini and presence of a signal peptide. Detection of the FLAG epitope was achieved by a quantitative luminometry experiment, using a FLAG antibody coupled to a chemiluminescent substrate.

The hypothesis was that extracellular tags would be detected by luminometry as the epitope was exposed; intracellular tags would not be detectable unless cells were permeabilised. Therefore the topology could be inferred from these results. The luminometry method was validated using the established PeptT1-FLAG transporter as positive control. Luminometry results were supported by a qualitative immunofluorescence method; the fluorescent cell membrane was visualised using confocal microscopy. Transport experiments were also performed on the FLAG mutants to ensure correct functioning of the mutant FLAG proteins. A new OATP1B1 topological model is proposed, based on the luminometry findings.

4.2 Results

4.2.1 OATP1B1 topology prediction

Topology modelling is an invaluable *in silico* approach to predicting the number and orientation of TMs in a membrane protein. The results provide a framework with which to base experimental analyses. A collection of programs with different algorithms were chosen to predict the topology of OATP1B1 (table 4.1), to ensure the most accurate prediction from the results. The programs SOSUI (Hirokawa *et al.*, 1998) and PRED-TMR (Pasquier *et al.*, 1999) use the hydropathy index and charge of the amino acid, whereas TMHMM (Krogh *et al.*, 2001), Phobius (Kall *et al.*, 2004), HMMTOP (Tusnady and Simon, 2001a) and Philius (Reynolds *et al.*, 2008) use the Hidden-Markov model as a statistical approach. TMpred (Hofman and Stoffel, 1993) and TSeg (Kihara *et al.*, 1998) compare the protein sequence with a TM protein database, using segment orientation and taxonomic classification in the analysis. ConPredII and TOPCONS use a consensus approach, predicting the structure based on the results of several programs.

The prediction programs predicted between 11-12TMs, with 10 programs predicting 12TMs and 6 programs predicting 11TMs (table 4.1). Of these, 11 programs predicted the positions of the termini (table 4.2). The programs predicting 12TMs all predicted the N and C termini to be internal. This same analysis was also performed on OATP1A2, OATP1B3 and OATP2B1 (appendix I-V). Interestingly, the results varied considerably, predicting 7-9TMs, 9-12TMs, 8-13TMs respectively. The proteins were also mainly predicted to contain internal N and C termini, however, there was more variation in the results. In particular, almost half of programs predicted OATP1A2 to contain extracellular termini.

OATP1B1 was also homology modelled on the MFS protein glycerol-3-phosphate using the modelling program Phyre2 (Kelley and Sternberg, 2009).

OATP1B3 has been modelled in a similar way (Meier-Abt *et al.*, 2005) (discussed in section 1.3.4). The glycerol-3-phosphate transporter contains 12TMs, internal N and C termini and functions with a rocker-switch mechanism (Huang *et al.*, 2003). The program modelled 65% of OATP1B1 residues with >90% confidence, displaying 12TMs and internal N and C termini (figure 4.1). This modelling supports the consensus results from the topology prediction programs and the TM predictions are comparable (data not shown). However, this is not surprising as both analyses match the putative TMs to regions of hydrophobicity. A limitation of this method however, is that homology modelling is only able to model residues onto a known template. As only 65% of residues were modelled with high confidence, 35% could not be modelled, suggesting that these regions may form a different structure. Furthermore, the glycerol-3-phosphate transporter contains only one binding site, unlike OATP1B1 which may have two binding sites, as discussed previously (section 1.3.4).

The presence of an OATP1B1 signal peptide sequence was also investigated. A signal peptide is a region of up to 70 hydrophobic amino acids at the N-terminus that is cleaved by signal peptidases, as part of the secretory pathway (Davis *et al.*, 2006). Some membrane proteins do not have a signal peptide as one of the TMs acts as an anchor within the membrane, but is not cleaved (Davis *et al.*, 2006). Signal peptides can be difficult to detect, as they can be mistaken for TMs owing to their hydrophobic nature (Kall *et al.*, 2004). Little is known about the presence of signal peptides in OATPs. A total of 9 signal peptide prediction programs were evaluated to assess the presence of an OATP1B1 signal peptide sequence (table 4.3). It is likely that OATP1B1 does not contain a signal peptide site as 6 programs did not report a signal sequence. The remaining 3 programs reported a signal sequence at cleavage site 44. Signal peptide analysis was also performed for OATP1A2, OATP1B3 and OATP2B1 (appendix V). OATP1B3 and OATP2B1 did not contain a signal peptide sequence, with detection from only 3/9 and 1/9 programs respectively.

However 7/9 programs reported OATP1A2 to contain an N-terminal signal peptide sequence, with a cleavage site at amino acid position 16.

Therefore the topology prediction analyses performed on OATP1B1 predicted a consensus of a 12TM protein with internal N and C termini, which did not contain a signal peptide sequence. This supports previous prediction analysis conducted by other groups (Hagenbuch and Meier, 2004; Meier-Abt *et al.*, 2005). Experimental analysis was driven by these prediction results.

Table 4.1 – Summary of OATP1B1 amino acid topology predictions

Name of program	Length of TM	TM1	TM2	TM3	TM4	TM5	TM6	TM7	TM8	TM9	TM10	TM11	TM12
ConPredII (Arai *et al.*, 2004)	**20**	29-49	63-86	95-115	209-229	259-279	332-352	375-395	409-429	537-557	576-596	626-646	-
SOSUI (Hirokawa *et al.*, 1998)	**23**	29-51	64-86	96-118	206-228	257-279	337-359	374-396	405-427	538-560	576-598	623-645	-
TopPredII (von Heijne, 1992)	**20**	28-48	71-91	96-116	165-185	211-231	262-282	336-356	376-396	410-430	534-554	580-600	627-647
TMpred (Hofman and Stoffel, 1993)	**21-28**	25-48	65-88	96-121	169-196	207-230	259-279	332-356	376-397	410-430	536-560	570-595	624-647
TMHMM (Krogh *et al.*, 2001)	**23**	30-52	67-89	96-118	208-230	257-279	332-354	375-397	407-429	536-558	573-595	624-646	-
TSeg (Kihara *et al.*, 1998)	**23-30**	27-52	65-89	95-117	208-234	258-281	331-357	372-397	406-435	531-558	574-599	625-648	-
MemBrain (Shen and Chou, 2008)	**13-29**	28-49	73-87	96-115	169-181	208-232	257-278	331-359	373-396	406-429	533-558	572-595	623-646
PHDhtm (Rost *et al.*, 1996)	**6-23**	29-45	74-88	98-113	175-180	211-231	259-277	332-356	378-396	410-428	536-558	577-594	628-645

Split 4.0 (Juretic *et al.*, 2002)	**15-36**	28-54	73-88	95-119	168-183	206-229	252-278	334-362	374-396	406-430	533-552	565-601	622-644
Phobius (Kall *et al.*, 2004)	**19-26**	29-48	68-89	96-117	170-195	207-230	258-279	337-356	376-395	407-428	534-560	572-595	624-646
Philius (Reynolds *et al.*, 2008)	**19-23**	29-48	66-87	96-118	177-196	207-230	257-279	337-356	376-397	406-429	539-560	572-594	625-646
HMMTOP (Tusnady and Simon, 2001b)	**17-27**	29-48	65-87	96-113	170-194	207-230	257-279	324-347	374-397	410-429	536-560	569-593	624-647
TOPCONS (Bernsel *et al.*, 2009)	**20**	27-47	68-88	97-117	173-193	207-227	259-279	336-356	376-396	410-430	536-556	574-594	627-647
PRED-TMR (Pasquier *et al.*, 1999)	**17-21**	29-48	65-84	96-113	207-226	254-271	339-360	376-397	410-429	534-552	577-595	624-644	-
MEMSAT3 (Jones, 2007)	**19-24**	29-48	65-87	96-120	207-230	258-279	337-360	376-397	410-429	536-560	570-594	624-646	-
SVMtm (Yuan *et al.*, 2004)	**14-21**	29-48	72-86	98-114	168-182	209-230	259-277	337-356	378-395	411-428	536-557	572-593	631-645

Table 4.2 - Predicted N and C terminal orientation for OATP1B1

Name of program	Number of TMs	N terminal position	C terminal position
ConPredII (Arai *et al.*, 2004)	11	Internal	External
SOSUI (Hirokawa *et al.*, 1998)	11	External	Internal
TopPredII (von Heijne, 1992)	12	Internal	Internal
TMpred (Hofman and Stoffel, 1993)	12	Internal	Internal
TMHMM (Krogh *et al.*, 2001)	11	Internal	External
TSeg (Kihara *et al.*, 1998)	11	Not predicted	Not predicted
MemBrain (Shen and Chou, 2008)	12	Not predicted	Not predicted
PHDhtm (Rost *et al.*, 1996)	12	Not predicted	Not predicted
Split 4.0 (Juretic *et al.*, 2002)	12	Internal	Internal
Phobius (Kall *et al.*, 2004)	12	Internal	Internal
Philius (Reynolds *et al.*, 2008)	12	Internal	Internal
HMMTOP (Tusnady and Simon, 2001b)	12	Internal	Internal
TOPCONS (Bernsel *et al.*, 2009)	12	Internal	Internal
PRED-TMR (Pasquier *et al.*, 1999)	11	Not predicted	Not predicted
MEMSAT3 (Jones, 2007)	11	External	Internal
SVMtm (Yuan *et al.*, 2004)	12	Not predicted	Not predicted

Table 4.3 - Signal peptide and cleavage position predictions for OATP1B1

Program	Signal peptide?	Cleavage position
iPSORT (Bannai *et al.*, 2002)	No	-
Phobius (Kall *et al.*, 2004)	Yes	44
PrediSi (Hiller *et al.*, 2004)	Yes	44
PSORT II (Nakai and Horton, 1999)	No	-
Sigcleave (von Heijne, 1986)	No	-
SignalP 4.0 (Petersen *et al.*, 2011)	Yes	44
SIG-Pred (Bradford, 2001)	No	-
SOSUIsignal (Gomi *et al.*, 2004)	No	-
SPEPLip (Fariselli *et al.*, 2003)	No	-

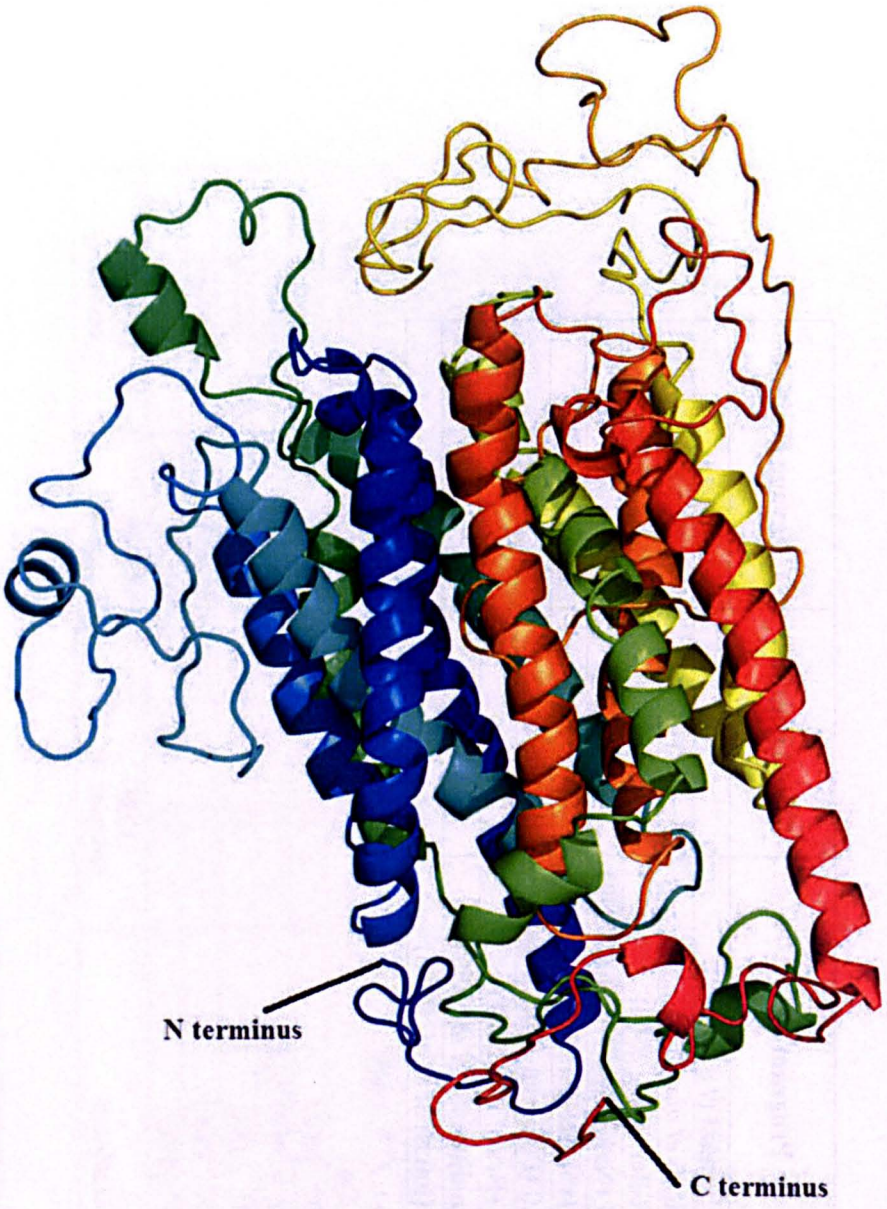

Figure 4.1 – Predicted tertiary structure of OATP1B1, produced by homology modelling with the glycerol-3-phosphate transporter, using Phyre2 (Kelley and Sternberg, 2009) and rendered using PyMOL (DeLano, 2002). The TMs are depicted as rainbow coloured springs, extracellular and intracellular regions as fine lines. The N and C termini are labelled.

4.2.2 Insertion of the OATP1B1 FLAG epitope tags

The topology prediction results (section 4.2.1) were used to map the internal/external loops for insertion of the FLAG epitope tags. OATP1B1 was predicted by the majority of programs to contain 12TMs with internal N and C termini. The protein does not have a C terminal PDZ sequence (Wang *et al.*, 2005a), and the consensus from predictions was an absence of an N terminal signal peptide, facilitating the addition of the tag at the terminals of the protein.

The range of the topology prediction results generated in section 4.2.1 was used to determine the amino acid range for each internal/external loop. Regions were predicted to be internal or external either side of the predicted TMs (table 4.4). The FLAG epitope (DYKDDDDK) was cloned into the amino acid sequence within or close to these regions at the positions described in table 4.4 (cloning described in section 2.2.14.4). The positions of the epitope tags are shown graphically in figure 4.2. A total of 13 individually tagged mutants were generated.

Table 4.4 – Predicted OATP1B1 amino acid regions for the internal/external loops and amino acid FLAG insertions

FLAG Tag number	Predicted orientation	Predicted amino acid region	Amino acid insertion of tag
1	Internal (N-terminus)	1-25	2
2	External (between TM 1-2)	54-63	58
3	Internal (between TM 2-3)	91-95	93
4	External (between TM 3-4)	121-165	142
5	Internal (between TM 4-5)	203-226	215
6	External (between TM 5-6)	248-286	265
7	Internal (between TM 6-7)	308-349	329
8	External (between TM 7-8)	371-387	379
9	Internal (between TM 8-9)	408-456	433
10	External (between TM 9-10)	477-549	514
11	Internal (between TM 10-11)	560-570	565
12	External (between TM 11-12)	614-625	620
13	Internal (C-terminus)	647-691	690

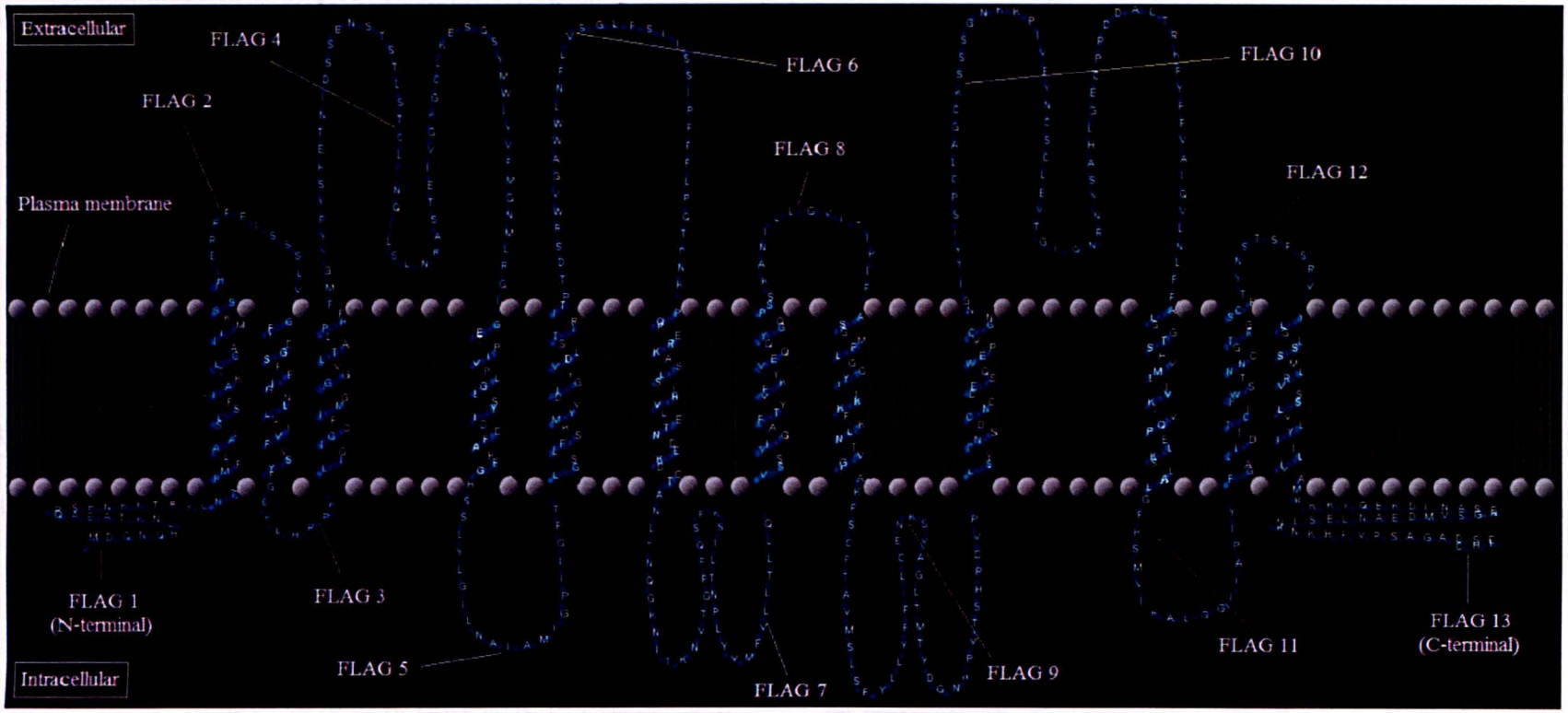

Figure 4.2 - Predicted topology of OATP1B1 displaying the locations of the inserted FLAG epitope tags. The model was rendered using TMRPres2D (Spyropoulos *et al.*, 2004).

4.2.3 OATP1B1-FLAG transport results

Transport experiments were performed on the 13 OATP1B1-FLAG mutants (termed F1-F13 hereafter) to confirm that the epitope tag did not affect transport function. All transport experiments were performed with the FLAG tagged mutant, WT as positive control and pcDNA vector as negative control. WT uptake was significant from the pcDNA control for each mutant, validating the experiment (figure 4.3). OATP1B1-F1, F4 and F13 were consistently significant from the pcDNA control and uptake increased, but not significantly, from that of the WT. This suggests that OATP1B1-F1, F4 and F13 were functioning normally following the addition of the FLAG. The remaining FLAG mutants exhibited markedly reduced transport, suggesting that the position of the FLAG disrupted transport.

Some of the FLAG mutants did exhibit significant transport in individual experiments, however it was variable. Figure 4.4 shows the individual uptake experiments for OATP1B1-F3, F6, F10 and F11. The graphs show an increasing trend in uptake from the vector control and several independent experiments are significant. It also highlights the inter-assay variability, which masks the overall statistical significance. OATP1B1-F3 and F10 revealed some transport as 3/4 experiments were significant from the vector controls. OATP1B1-F6 and F11 were much more variable, with F6 transporting a particularly low rate compared with the WT. It is likely that the position of the tag disrupted the function of these mutants.

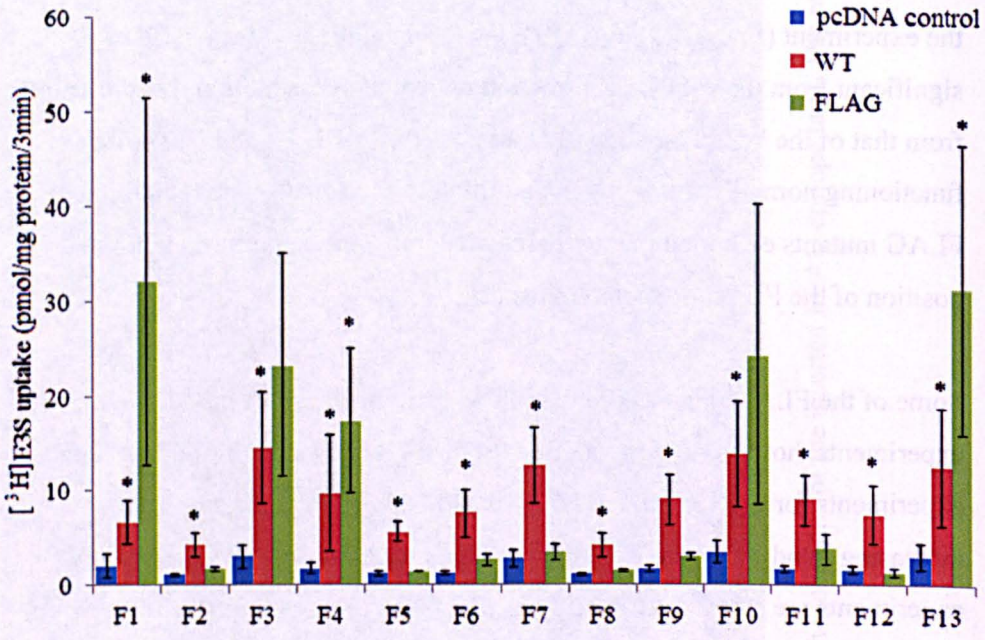

Figure 4.3 - Uptake of [^{3}H]E3S into pcDNA/*SLCO1B1*-F1-13, pcDNA/*SLCO1B1* WT and pcDNA vector transfected HEK293T cells. Each bar is the mean ± SE of 3-6 experiments with 6 well replicates. *Unpaired t-test; $P<0.05$ from the pcDNA control.

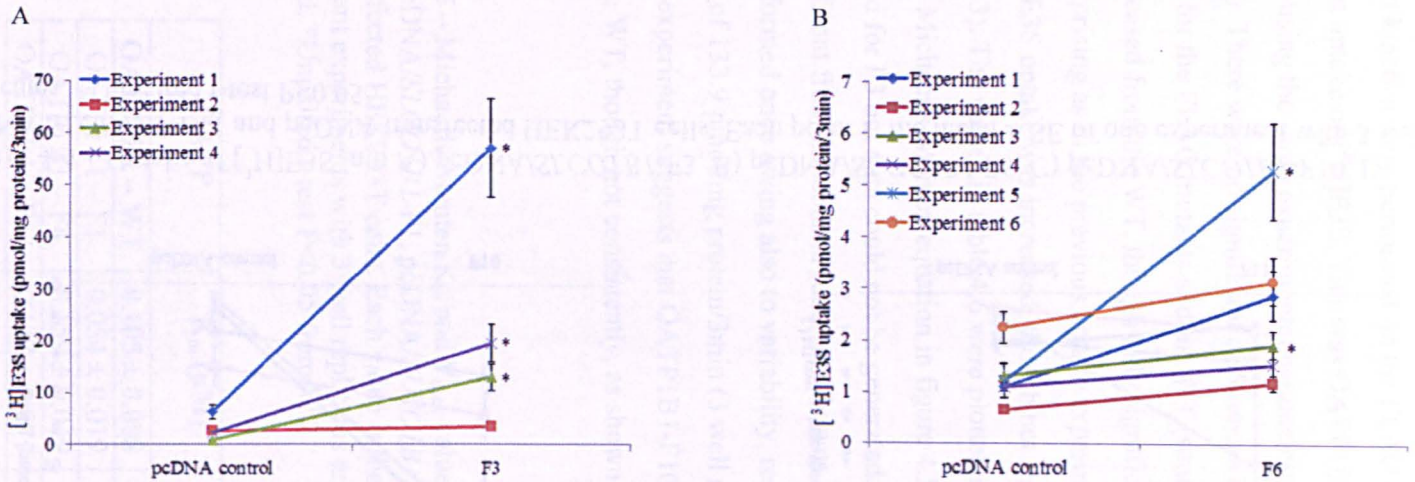

Figure 4.4 – continued on next page

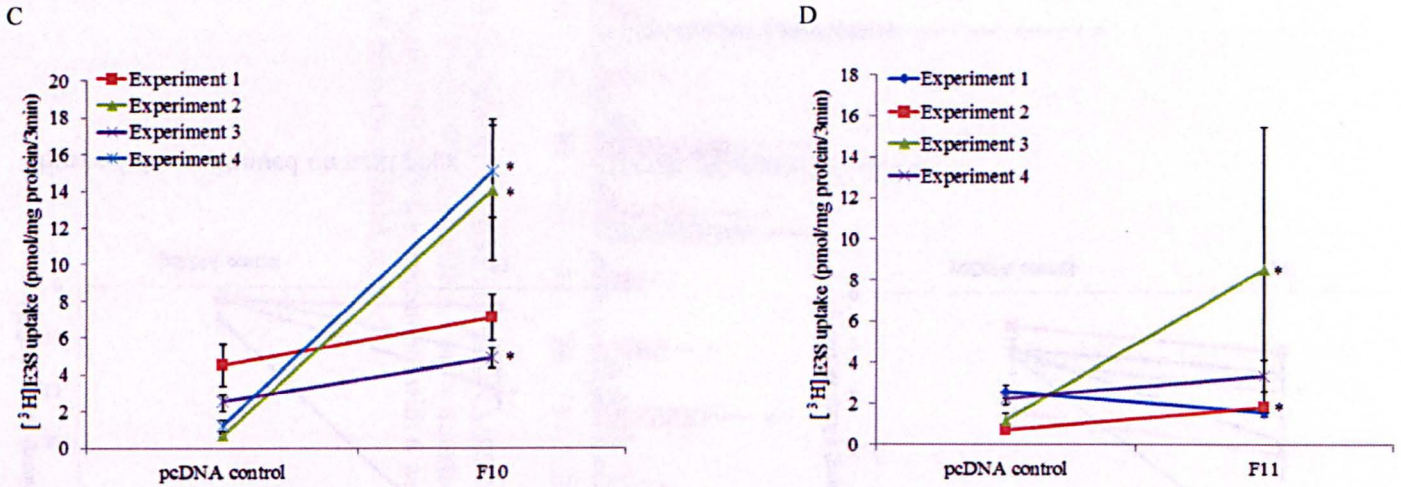

Figure 4.4 – Uptake of [^{3}H]E3S into A) pcDNA/*SLCO1B1*-F3, B) pcDNA/*SLCO1B1*-F6, C) pcDNA/*SLCO1B1*-F10, D) pcDNA/*SLCO1B1*-F11 and pcDNA transfected HEK293T cells. Each point is the mean ± SE of one experiment with 3 well replicates. *Unpaired t-test $P<0.05$.

4.2.3.1 OATP1B1-FLAG transport kinetics

Transport kinetics were performed on the FLAG mutants that demonstrated consistent uptake of [^{3}H]E3S. This was OATP1B1-F1, F4 and F13. Data were obtained using the same experimental parameters as for the WT (section 3.2.3.2.3). There were no significant differences between the K_m values obtained for the FLAG mutants and the WT (summarised in table 4.6). The V_{max} increased from the WT, though only significantly for OATP1B1-F1. This is not surprising as in the previous uptake experiments OATP1B1-F1, F4 and F13 [^{3}H]E3S uptake was increased, though not significantly, from the WT (figure 4.3). The values in table 4.6 were plotted as Michaelis-Menten curves using the Michaelis-Menten equation in figure 4.5. Transport kinetics were performed for F3 but data could not be generated as the uptake was variable and not significant from the control (data not shown). Kinetics for OATP1B1-F10 were performed once owing also to variability, resulting in a K_m of 0.111μM and V_{max} of 133.9 pmol/mg protein/3min (3 well replicates) (data not shown). This one experiment suggests that OATP1B1-F10 is transporting at a similar rate to the WT, though not consistently, as shown by the variable transport results.

Table 4.5 – Michaelis-Menten K_m and V_{max} values from pcDNA/*SLCO1B1* WT (bold), pcDNA/*SLCO1B1*-F1, pcDNA/*SLCO1B1*-F4 and pcDNA/*SLCO1B1*-F13 transfected HEK293T cells. Each value is the mean ± SE of 3-5 independent experiments with 3 well replicates and the pcDNA uptake subtracted. *Unpaired t-test P<0.05 from WT

OATP	K_m (μM)	V_{max} (pmol/mg protein/3min)
OATP1B1 – WT	**0.105 ± 0.008**	**50.1 ± 10.9**
OATP1B1 – F1	0.054 ± 0.019	103.8 ± 14.1*
OATP1B1 – F4	0.159 ± 0.049	79.6 ± 6.5
OATP1B1 – F13	0.147 ± 0.071	97.7 ± 21.3

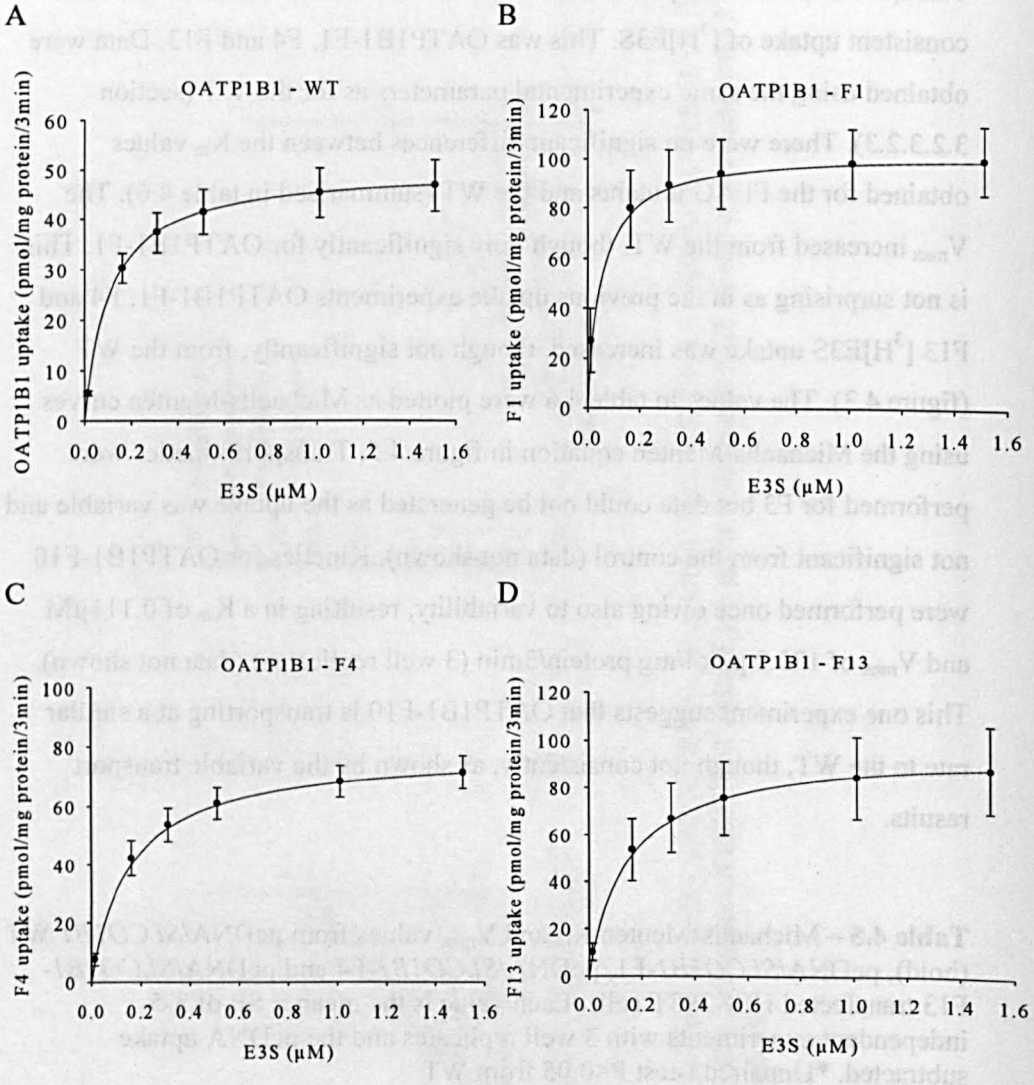

Figure 4.5 – E3S transport kinetics from A) pcDNA/*SLCO1B1* WT, B) pcDNA/*SLCO1B1*-F1, C) pcDNA/*SLCO1B1*-F4 and D) pcDNA/*SLCO1B1*-F13 transfected HEK293T cells. The line is the Michaelis-Menten equation fitted to the kinetic parameters in table 4.6. Each point is the mean ± SE of 3-4 individual experiments with 3 well replicates and the pcDNA uptake subtracted.

4.2.4 Luminometry results

4.2.4.1 Validation of the luminometry experiment

The luminometry experiment was validated using the rabbit PepT1 (*Slc15a1*) transport protein, containing a previously tested external FLAG tag (PepT1-FLAG) (Panitsas *et al.*, 2006). The *Slc15a1* gene with the FLAG epitope was cloned into the pcDNA3.1/Hygro(-) vector for expression in HEK293T cells (section 2.2.14). The construct was transfected simultaneously with the vector control. Surface expression of PepT1-FLAG was detected using luminometry and values were significantly increased from the vector control (figure 4.6). This validated the luminometry method and led to subsequent analysis of OATP1B1-FLAG surface expression.

4.2.4.2 OATP1B1-FLAG luminometry results

The 13 OATP1B1-FLAG mutants were analysed for surface expression using luminometry. OATP1B1-F1 and OATP1B1-F13 were the FLAG tagged N and C termini respectively. FLAG tags attached to external loops could be detected by luminometry as the FLAG antibody would attach to the externally accessible epitope. Those that were internal would require cell permeabilisation for the antibody to reach the epitope. Figure 4.7 shows a summary of the luminescence data generated from each tagged mutant. OATP1B1-F1, F4 and F13 were consistently significant from the WT in at least 3 independent experiments, suggesting that tags in these regions were external. OATP1B1-F4 and F13 however were not significant when the data were averaged owing to the inter-assay variation. The remaining FLAG mutants were not significant from the WT. These results are supported by the immunofluorescence detection in section 4.2.5.

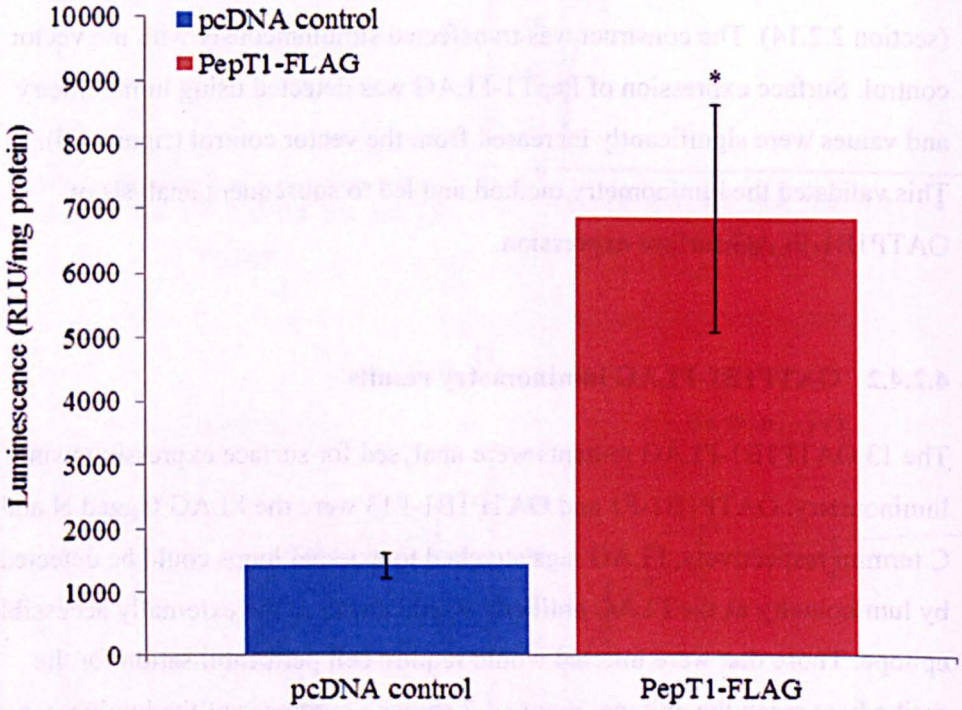

Figure 4.6 – Luminescence of pcDNA/*Slc15a1*-FLAG and pcDNA control transfected HEK293T cells. Each bar is the mean ± SE of one experiment with 4 dish replicates. *Unpaired t-test $P<0.05$.

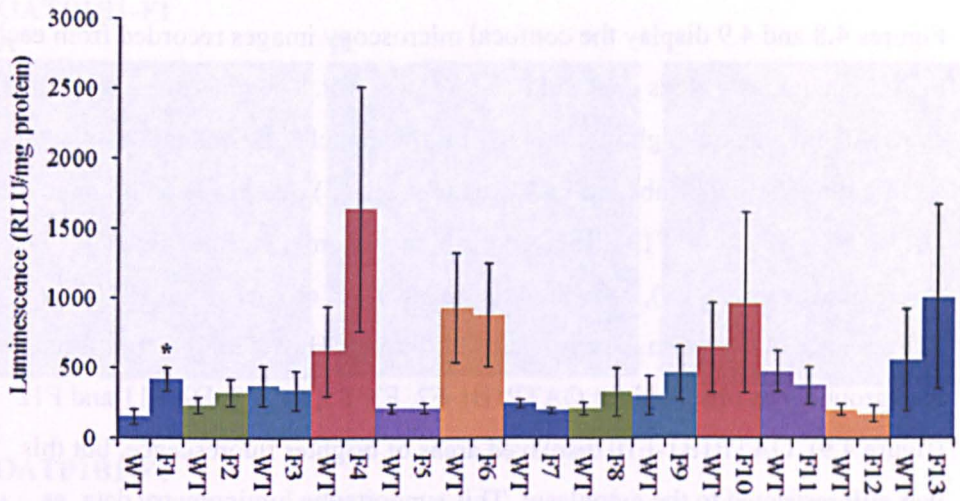

Figure 4.7 – Luminescence of pcDNA/*SLCO1B1*/F1-F13 and pcDNA/*SLCO1B1* WT transfected HEK293T cells. Each bar is the mean ± SE of 3-8 experiments with 3 dish replicates. *Unpaired t-test $P<0.05$.

4.2.5 OATP1B1-FLAG immunofluorescence results

Immunofluorescence was performed on HEK293T cells transfected with the pcDNA/*SLCO1B1*-FLAG mutants as a qualitative epitope detection method. Cells were fixed to cover slips and incubated with a primary anti-FLAG and secondary-FITC antibody that detected the FLAG epitope. Cells were also incubated with the nucleic acid stain DAPI to visualise the nucleus. The presence of intact nuclei combined with the visualisation of cells under the bright field confirmed that fixation did not disrupt cellular morphology.

Figures 4.8 and 4.9 display the confocal microscopy images recorded from each FLAG mutant, as well as the OATP1B1 WT control. The images are displayed as A) 405nm channel highlighting DAPI stained nuclei, B) 488nm channel highlighting the FITC labelled FLAG epitope and C) overlay of both images. OATP1B1-F1, F4 and F13 displayed distinctive membrane specific fluorescence (figure 4.8), compared to the low level of background FITC fluorescence observed in the cytoplasm of the WT. However, only non-specific background was observed for OATP1B1-F2, F3, F5, F7, F8, F9, F11 and F12 (figure 4.9). OATP1B1-F10 displayed areas of brighter fluorescence, but this was still restricted to the cytoplasm. This supports the luminometry data, as OATP1B1-F1, F4 and F13 demonstrated significant luminescence, whereas the other mutants did not.

OATP1B1 WT

A B C

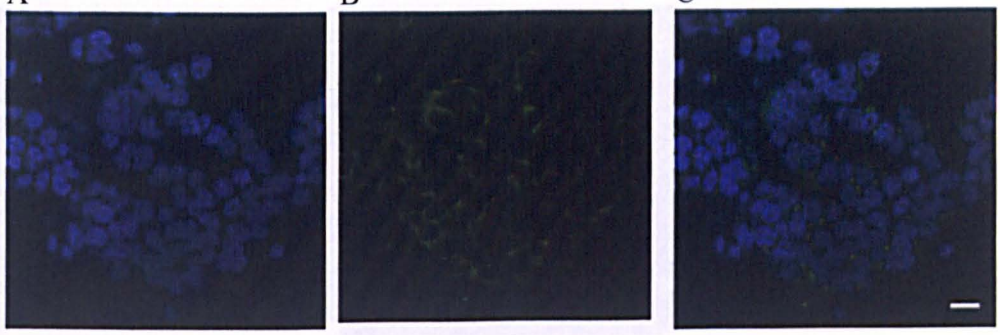

OATP1B1-F1

A B C

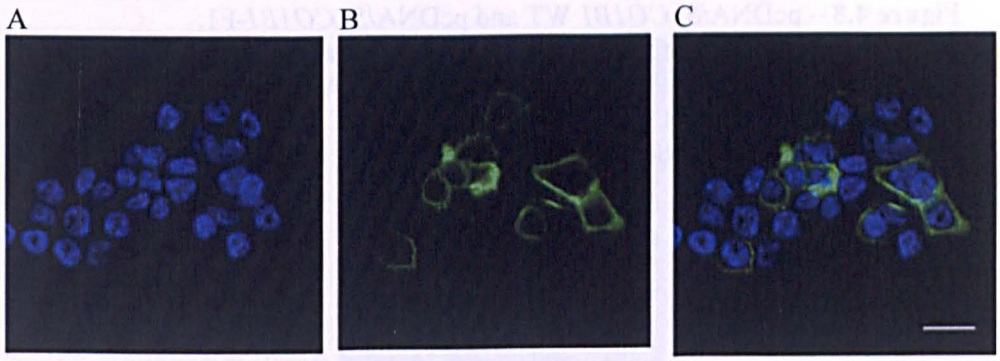

OATP1B1-F4

A B C

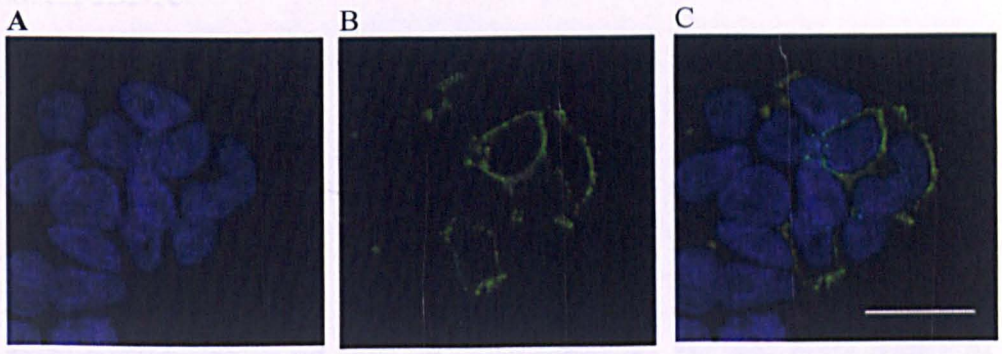

Figure 4.8 – continued on next page

OATP1B1-F13

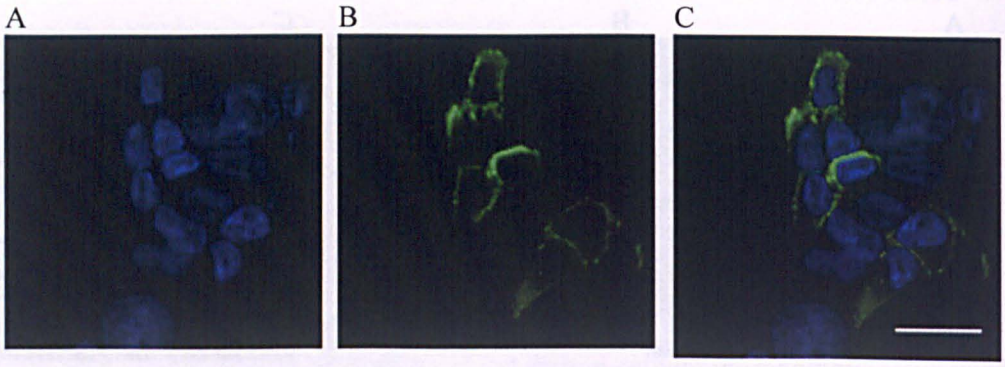

Figure 4.8 – pcDNA/*SLCO1B1* WT and pcDNA/*SLCO1B1*-F1, pcDNA/*SLCO1B1*-F4 and pcDNA/*SLCO1B1*-F13 transfected HEK293T cell immunofluorescence by confocal microscopy. A) DAPI (blue) localised to the nucleus (504nm) B) FITC (green) localised to the FLAG epitope (488nm) C) overlay of both images. Scale bar = 20µM.

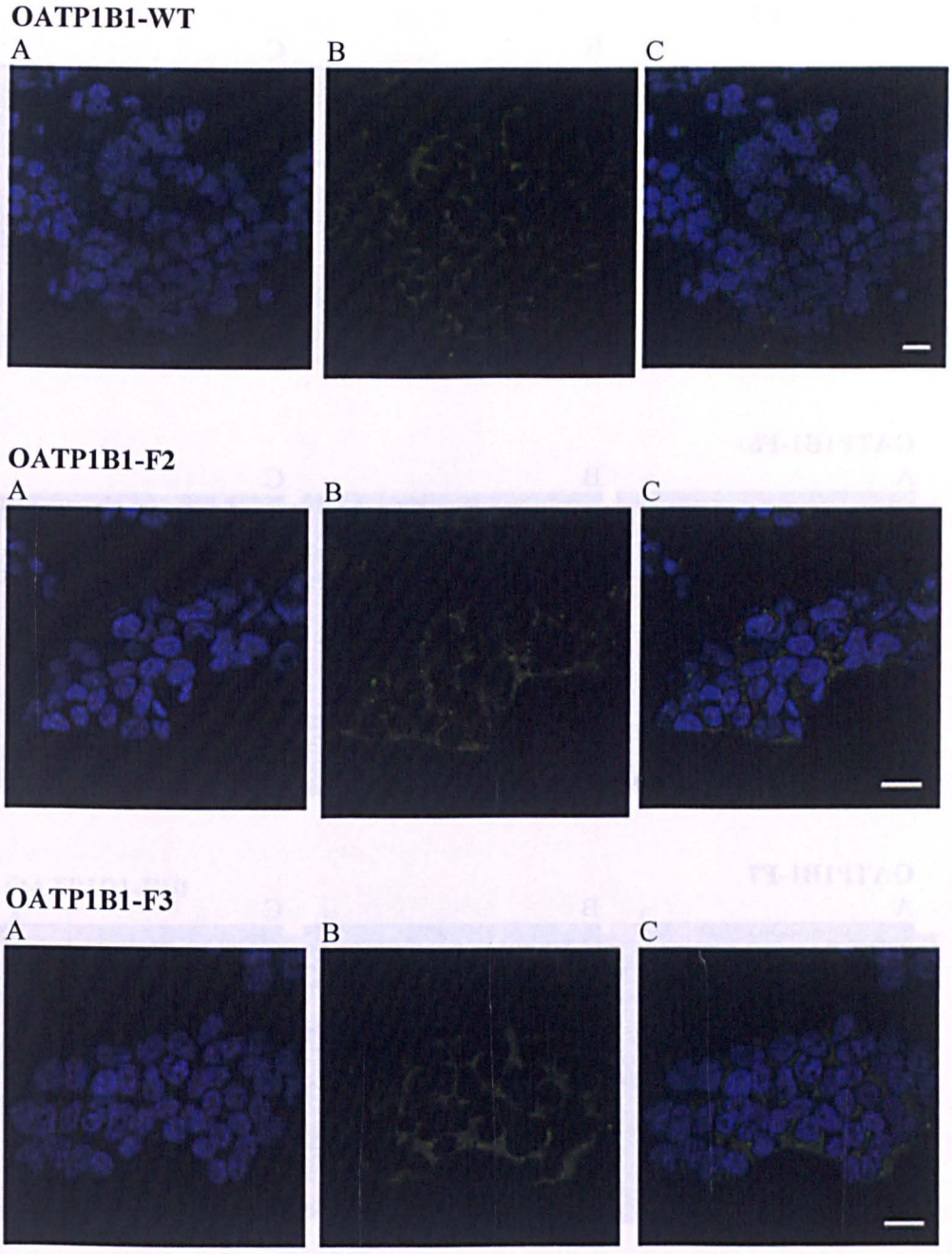

Figure 4.9 – continued on next page

OATP1B1-F5

A B C

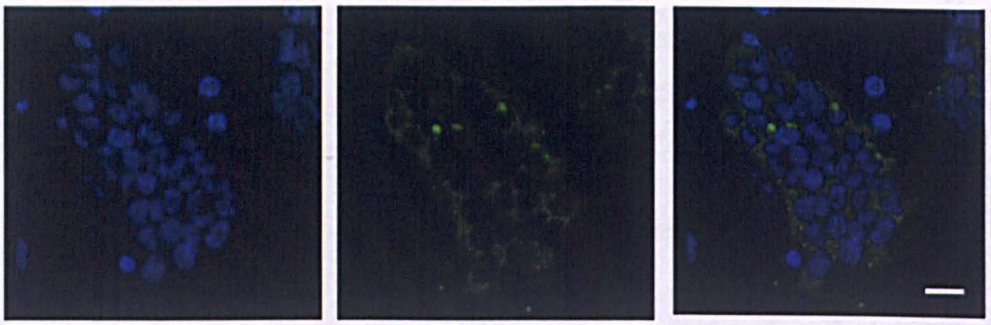

OATP1B1-F6

A B C

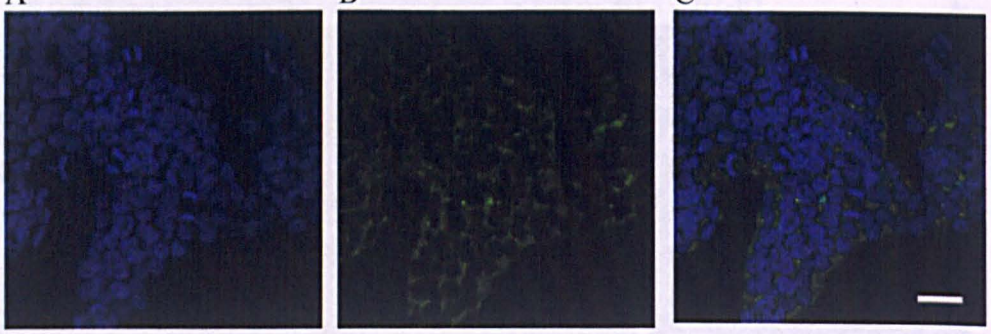

OATP1B1-F7

A B C

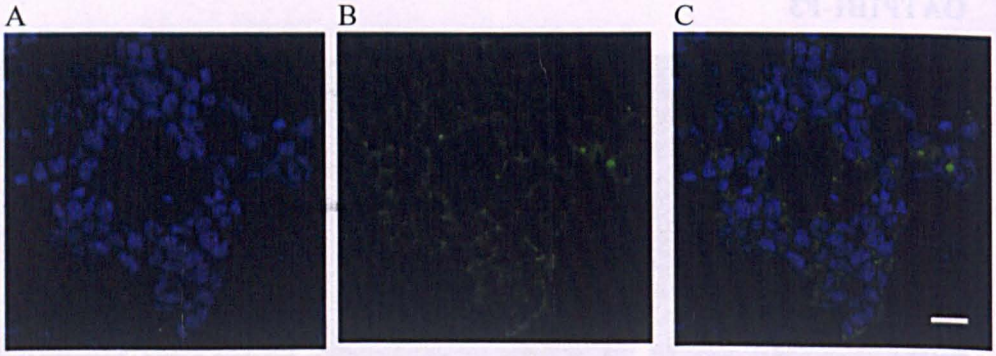

Figure 4.9 – continued on next page

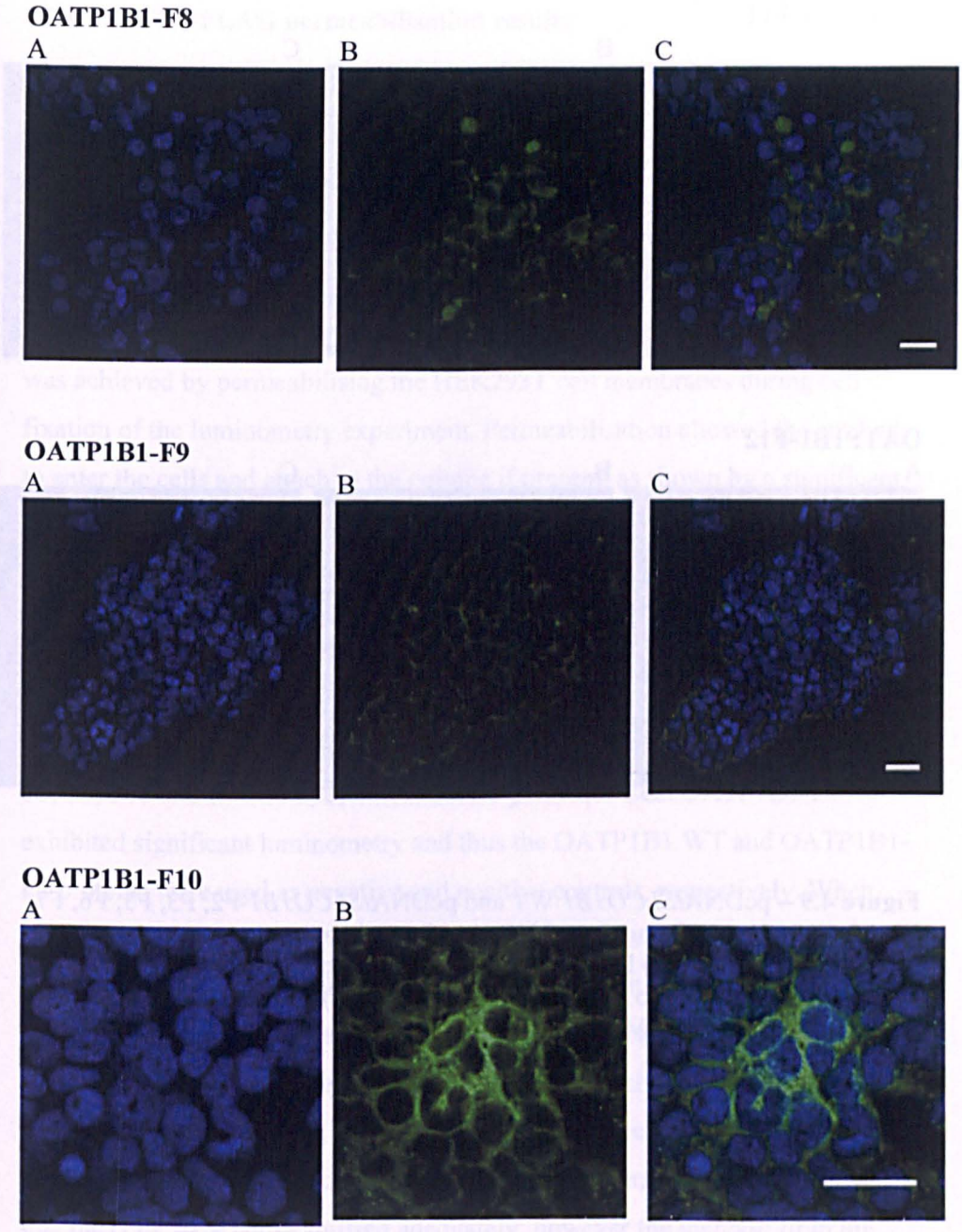

Figure 4.9 – continued on next page

OATP1B1-F11

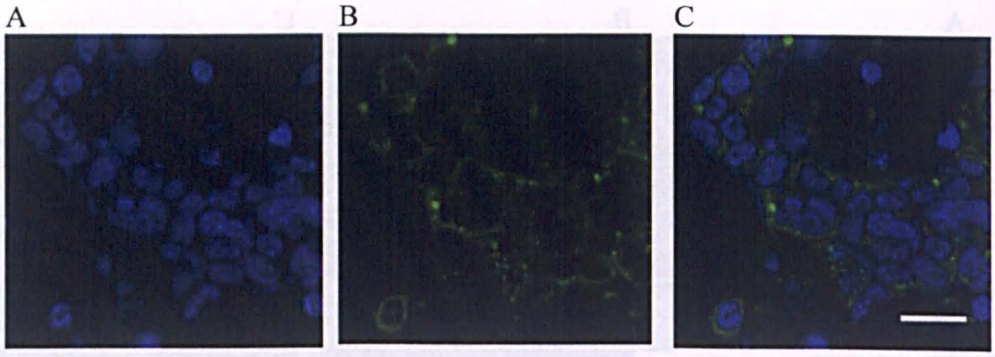

OATP1B1-F12

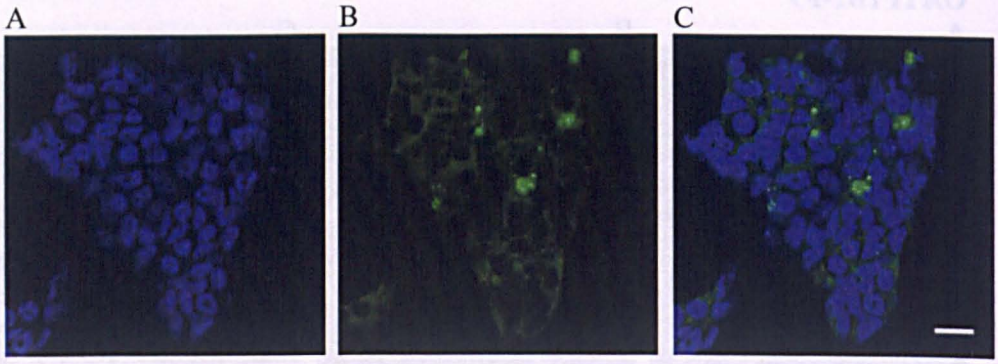

Figure 4.9 – pcDNA/*SLCO1B1* WT and pcDNA/*SLCO1B1*-F2, F3, F5, F6, F7, F8, F9, F10, F11, F12 transfected HEK293T cell immunofluorescence by confocal microscopy. A) DAPI (blue) localised to the nucleus (504nm) B) FITC (green) localised to the FLAG epitope (488nm) C) overlay of both images. Scale bar = 20μM.

4.2.6 OATP-FLAG permeabilisation results

FLAG mutants that did not exhibit significant luminescence but did exhibit low levels of transport were investigated as containing potential internal tags. OATP1B1-F3, F6, F10 and F11 did not show significant luminescence but did exhibit some transport of [^{3}H]E3S (section 4.2.3), albeit not significant overall. These FLAG mutants were chosen for permeabilisation experiments to determine whether the epitope was on the internal side of the membrane. This was achieved by permeabilising the HEK293T cell membranes during cell fixation of the luminometry experiment. Permeabilisation allowed the antibody to enter the cells and attach to the epitope if present, as shown by a significant increase in luminescence.

Permeabilised luminescence was normalised to non-permeabilised luminescence and significance was denoted using a one sample t-test. Normalised values were expressed as a percentage in figure 4.10. Results showed that luminescence increased, but not significantly, when the OATP1B1-F3, F6, F10 and F11 transfected cells were permeabilised. OATP1B1-F1 exhibited significant luminometry and thus the OATP1B1 WT and OATP1B1-F1 proteins were used as negative and positive controls, respectively. When these control cells were permeabilised, however, luminescence also increased (figure 4.10). An increase from the OATP1B1-F1 positive control was expected owing to the presence of transporters in the cytoplasm and organelles, however, there was a large signal from the OATP1B1 WT negative control which did not contain any tagged protein, most likely due to non-specific binding of the antibody. The increase in luminescence following permeabilisation suggests that the cells were permeabilised adequately; however the increase from the permeabilised FLAG mutants was not significantly higher than the background observed in the controls.

Immunofluorescence was also performed with permeabilised HEK293T cells transfected with pcDNA/*SLCO1B1*-F3, pcDNA/*SLCO1B1*-F6, pcDNA/*SLCO1B1*-F10 and pcDNA/*SLCO1B1*-F11 (figure 4.11). However

permeabilisation did not localise the antibody to the epitope on the membrane. Rather, large areas of non-specific fluorescence were observed. This, combined with presence of intact nuclei, suggests that cell permeabilisation was effective, but that there was non-specific binding of the antibody. This supports the results obtained from the luminometry experiments performed with permeabilised cells. These FLAG mutants did not display a high and consistent level of transport, which may be owing to disruption of protein expression from addition of the tag. This would also explain why the luminometry and immunofluorescence following permeabilisation did not indicate an internal tag.

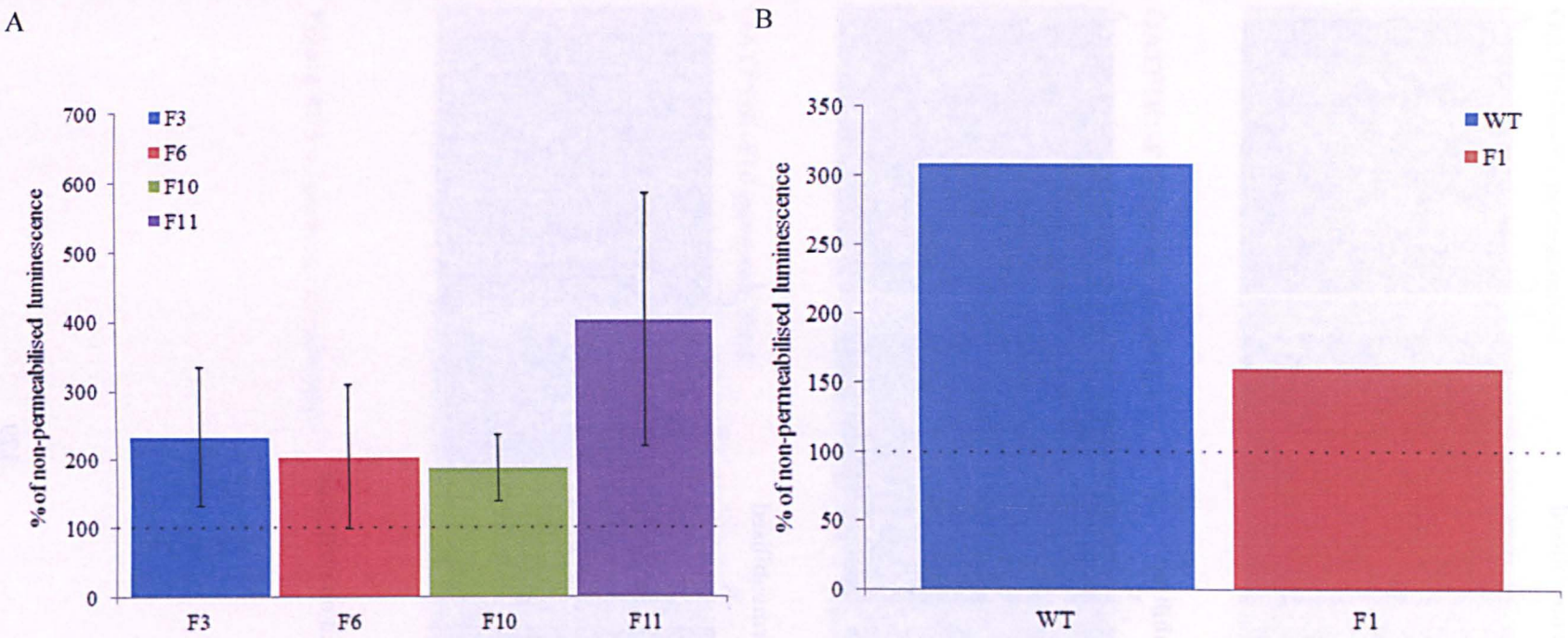

Figure 4.10 –Luminescence following permeabilisation. Permeabilised values are normalised to non-permeabilised values and expressed as a percentage A) pcDNA/*SLCO1B1*-F3, pcDNA/*SLCO1B1*-F6, pcDNA/*SLCO1B1*-F10 and pcDNA/*SLCO1B1*-F11 transfected HEK293T cells. Each bar is the mean ± SE of 2-5 experiments with 3 dish replicates. B) pcDNA/*SLCO1B1* WT negative control and positive pcDNA/*SLCO1B1*-F1 control transfected HEK293T cells. Each bar is representative of one experiment with 3 dish replicates.

OATP1B1-F3 non-permeabilised

A B C

OATP1B1-F3 permeabilised

A B C

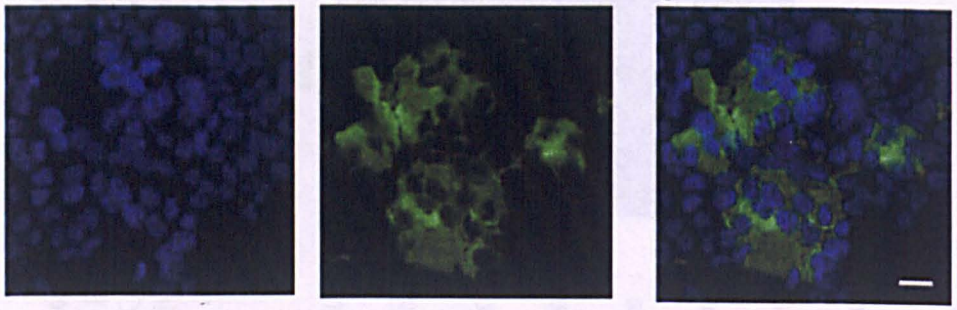

OATP1B1-F6 non-permeabilised

A B C

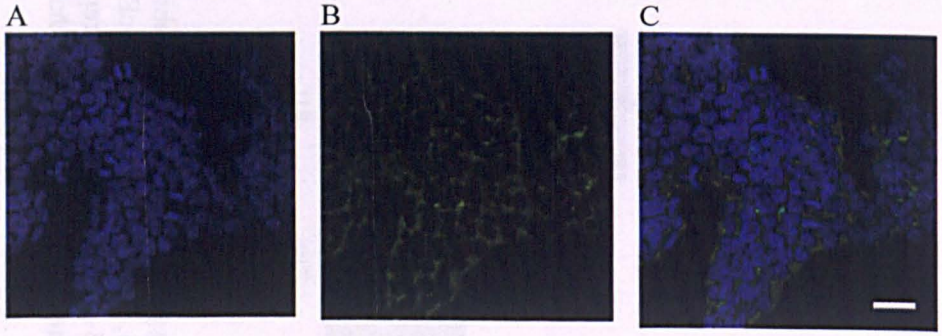

Figure 4.11 – continued on next page

OATP1B1-F6 permeabilised

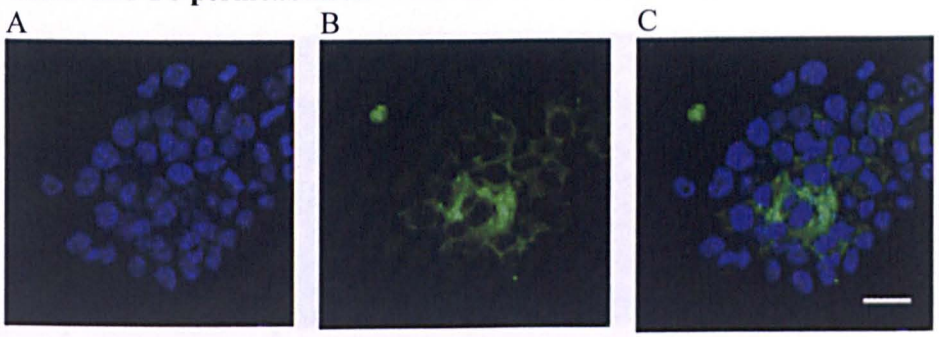

OATP1B1-F10 non-permeabilised

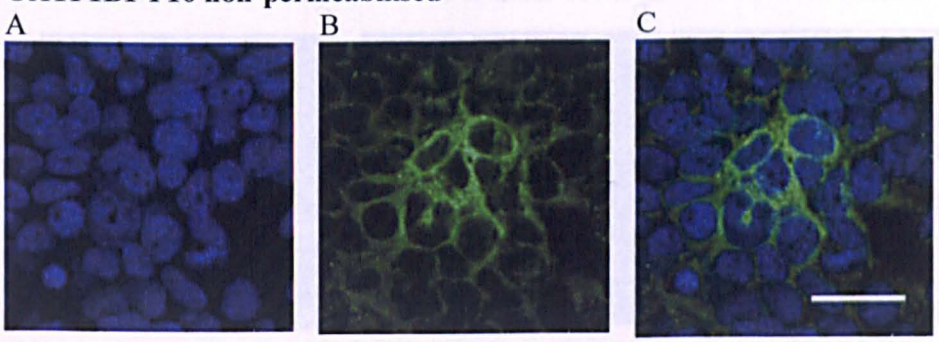

OATP1B1-F10 permeabilised

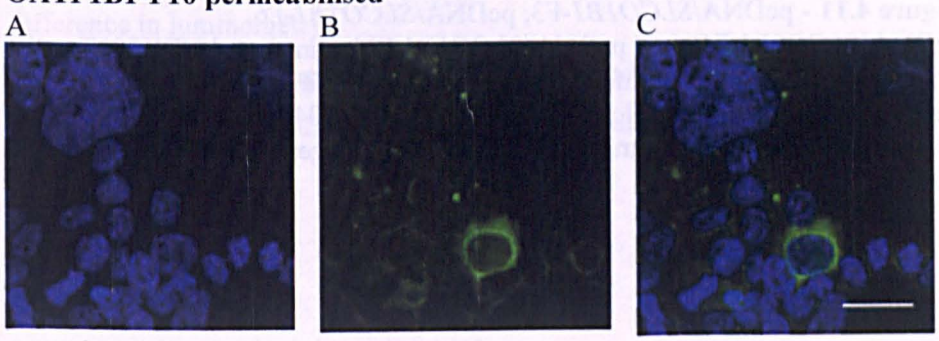

Figure 4.11 – continued on next page

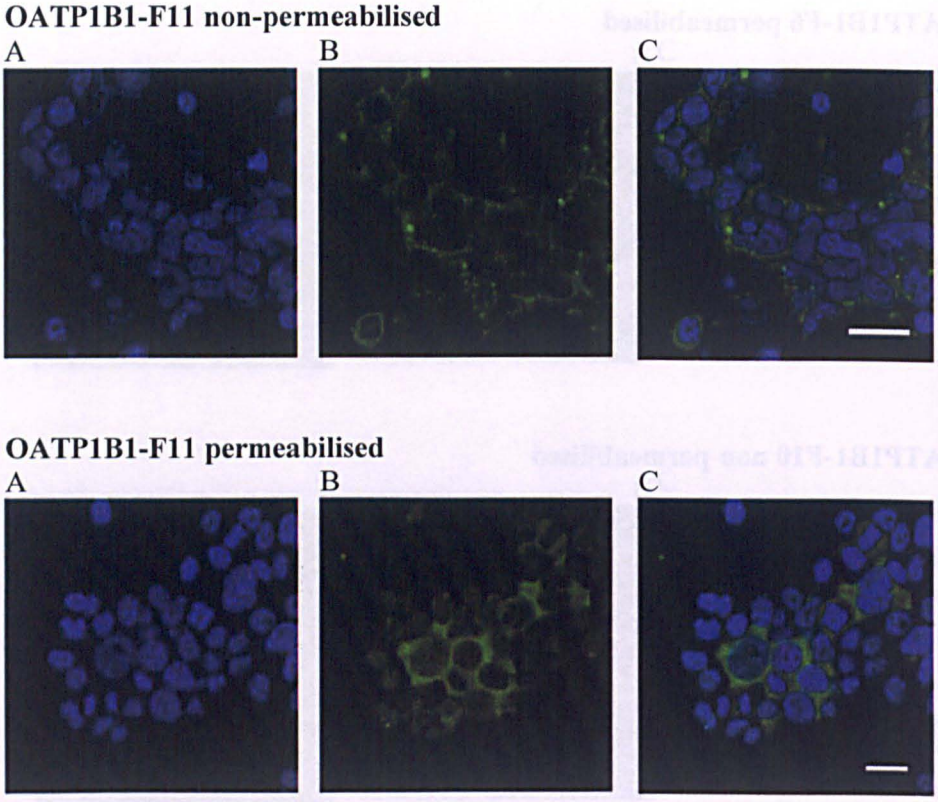

Figure 4.11 - pcDNA/*SLCO1B1*-F3, pcDNA/*SLCO1B1*-F6, pcDNA/*SLCO1B1*-F10 and pcDNA/*SLCO1B1*-F11 transfected HEK293T cell immunofluorescence by confocal microscopy, with and without cell permeabilisation. A) DAPI localised to the nucleus (504nm) B) FITC localised to the FLAG epitope (488nm) C) overlay of both images. Scale bar = 20μM.

4.2.7 Summary of OATP1B1 transport and luminometry results

Luminometry and transport experiments were performed with 3-6 replicates over at least 3 individual experiments. As discussed, there was some inter-assay variability, which masked the significance when the data were grouped together. To overcome this, the luminometry and uptake data for all FLAG mutants were normalised to the OATP1B1 WT in figure 4.12.

The pcDNA control uptake was subtracted from the sample uptake and the values normalised to those of the OATP1B1 WT. Similarly the sample luminometry values were normalised to those of the OATP1B1 WT. Values were expressed as a percentage and significance was denoted using a one sample t-test. Figure 4.12 highlights the significant luminometry and uptake for OATP1B1-F1, F4 and F13, observed in individual experiments. OATP1B1-F6 luminometry was also significantly increased from the OATP1B1 WT, though this is not supported by consistently significant transport and immunofluorescence experiments. OATP1B1-F2, F5, F6, F7, F8, F9, F11 and F12 all displayed a significant decrease in transport from the OATP1B1 WT. Furthermore, OATP1B1-F2, F5, F7, F8, F9, F11 and F12 showed no significant difference in luminometry.

Therefore, the epitope tagged OATP1B1-F1, F4 and F13 proteins retained transport function and will be used to make extrapolations and form a new OATP1B1 model.

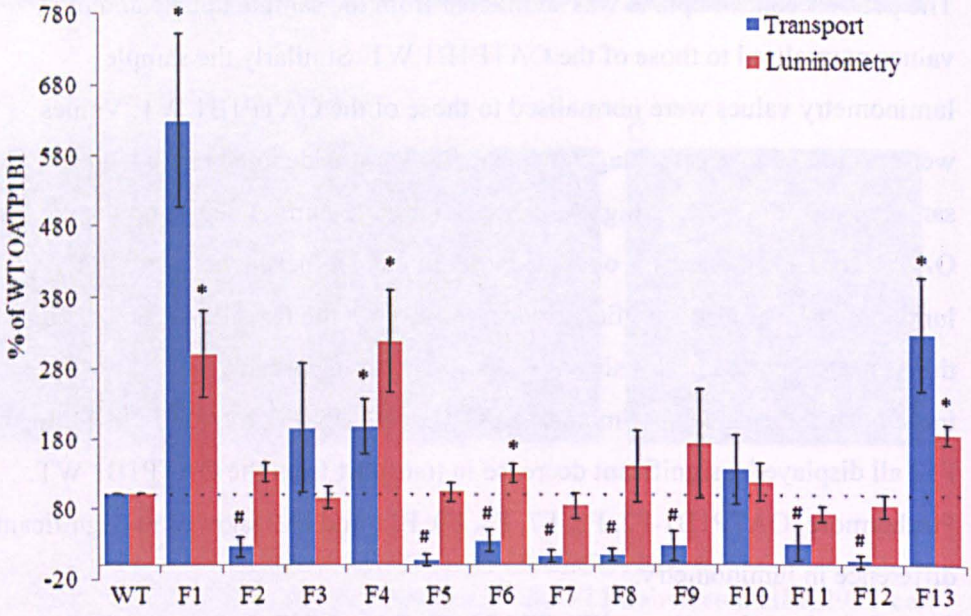

Figure 4.12 – Summary of [^{3}H]E3S transport and luminometry results from pcDNA/*SLCO1B1*-F1-F13 transfected HEK293T cells. Values are normalised to the WT and expressed as a percentage. Each bar is the mean ± SE of 3-8 experiments (luminometry = 3 dish replicates, transport = 6 well replicates). *P<0.05 increase from WT, #P<0.05 decrease from WT (Both one sample t-tests).

4.3 Conclusion

There is currently little understanding of the topological structure of OATPs. Knowledge of the structure is imperative to understanding how these proteins bind to and transport compounds. Therefore the topology of OATP1B1 was studied using topology prediction programs, epitope insertion, luminometry and immunofluorescence detection methods.
The topology prediction programs predicted OATP1B1 to contain between 11-12 domains with internal N and C termini. A 12TM model was chosen as more programs predicted 12TMs than 11, in line with the predictions of other groups (Gui and Hagenbuch, 2009; Konig *et al.*, 2000b). This was supported by the novel homology modelling of OATP1B1 on the glycerol-3-phosphate transporter, which revealed a 12TM protein with internal N and C termini.

Interestingly, OATP1A2 was predicted to be a 7-9TM protein by all the topology programs, which is not in keeping with the other predictions, nor that the OATPs are related to the MFS (Pao *et al.*, 1998). OATP1B3 and OATP2B1 were predicted with some variation but up to 12TMs were predicted. OATP1B3 shares 80% amino acid identity with OATP1B1 and thus it would be expected that the topology predictions were similar. However more variation was demonstrated for OATP1B3, predicting between 9-12TMs rather than 11-12. These predictions suggest that there may be a larger degree of TM variability between OATPs than previously recognised, and further experiments are required to confirm this topology.

A signal peptide was not predicted for OATP1B1. A small number of programs predicted a cleavage site at position 44, however later luminometry results from the N and C termini suggest that this is unlikely, as the tags at the N and C terminal ends were not cleaved/did not disrupt protein functioning. It is interesting also to note that OATP1A2 was predicted to contain a signal peptide site, whereas OATP1B3 and OATP2B1 were not. Why OATP1A2 contains a potential cleavage site and the others do not remains to be elucidated. However

some topology programs predicted the first 20 amino acids of OATP1A2 to be a TM, owing to their hydrophobic nature, so it is possible that the signal sequence predicted is in fact a TM. If so, this TM could be acting as an anchor, rather than a signal peptide. It is difficult for prediction programs to distinguish between a signal peptide sequence and a TM owing to their similarities in length and hydrophobicity, however several programs have adapted their algorithms to account for this (Kall *et al.*, 2007; Reynolds *et al.*, 2008). There is very little signal prediction data available for the OATP family and further research is required.

The FLAG epitope was cloned into the intracellular and extracellular regions of OATP1B1 based on the topology prediction results. A total of 13 tagged OATP1B1 proteins were generated; termed F1-F13.Transport experiments were performed on the FLAG mutants to ensure that inserting the epitope tag did not disrupt functioning. OATP1B1-F1 (N terminal), F4 and F13 (C terminal) all transported [^{3}H]E3S significantly and consistently. OATP1B1-F3, F6, F10 and F11 demonstrated some significant uptake but it was variable, as shown by the individual graphs. It is likely that the tag affected the functioning of these mutant proteins. The remaining FLAG mutants demonstrated very low transport, suggesting that insertion of the tag was detrimental to functioning or expression. Kinetic experiments were performed on OATP1B1-F1, F4, F10 and F13. The results showed that apart from the OATP1B1-F1 V_{max}, K_m and V_{max} were not significantly different from that of the WT.

Luminometry experiments were performed on the 13 mutants to detect the epitope on the membrane. A significant increase in luminescence was observed for OATP1B1-F1, F4 and F13. F1 and F13 as the N and C termini were predicted to be internal. Interestingly, the luminometry results revealed the terminals to be external. OATP1B1-F4 was also predicted to be external and confirmed by luminometry. OATP1B1-F6 displayed significant luminometry but this was not supported by immunofluorescence and transport experiments. The remaining luminometry results were not significant, in line with the low

transport results. OATP1B1-F3, F6, F10 and F11 demonstrated a small amount of transport and thus it was hypothesised that these epitopes may have been internal. Cell permeabilisation experiments were performed on these tagged proteins to determine whether the tag was on the inside of the membrane. Luminescence increased following permeabilisation but was not significantly increased from that of the non-permeabilised cells. Furthermore, the controls demonstrated a large increase in luminescence following permeabilisation, suggesting that the increase is due to non-specific binding.

Immunofluorescence experiments were performed in order to qualitatively validate the luminometry results. OATP1B1-F1, F4 and F13 displayed membrane specific fluorescence, confirming the significant luminometry. The other FLAG mutants were comparable to the background fluorescence observed for the OATP1B1 WT, suggesting that the epitope was not detectable. Furthermore, immunofluorescence of the permeabilised cells transfected with OATP1B1-F3, F6, F10 and F11 resulted in a large amount of fluorescence within the cell, but not on the membrane. This fluorescence increase, combined with the increase in luminescence following permeabilisation suggests that the cells were permeabilised adequately; however it is likely that the fluorescence was due to non-specific binding of the antibody.

These results reveal that the experimental evidence does not support the predicted topology for OATP1B1. The N and C termini were predicted to be facing the intracellular space, however the epitope tags attached to the N and C termini were detected as extracellular. The putative extracellular loop 2 containing F4 was also detected as external. However for both OATP1B1-F1 and F4 to be external, both TM2 and TM3 cannot exist, further contradicting the topology predictions. The epitope tags placed in the other predicted loops were not detectable by luminometry and/or did not function the same as the WT.

Further investigation is required to determine the exact number of TMs in OATP1B1, however this is the first experimental evidence to suggest that OATP1B1 and potentially the other human OATPs have extracellular N and C termini.

5 Mutagenesis of the OATP1B1 signature region

5.1 Introduction

The OATP superfamily signature is a highly conserved 13 amino acid sequence (D-X-RW-(I,V)-GAWW-XG-(F,L)-L), conserved across all known OATPs (Hagenbuch, 2003), the function of which is not known. A signature sequence is not uncommon among transporter families and sequences often play a pivotal role in the functioning of the transporter. For example, the ABC transporters contain the signature sequence 'LSGGQ' in their nucleotide binding domains, important for the ATP-hydrolysis required for driving transport (Ren *et al.*, 2004). The conserved nature of the OATP signature sequence suggests that it also plays a role in protein function.

The signature sequences for the 11 human OATPs are shown in table 5.1, highlighting the high degree of amino acid similarity within this region. This high degree of conservation and localisation within the protein family suggests an important role potentially for substrate binding, membrane targeting and/or membrane anchoring.

Table 5.1 – The human OATPs with each signature sequence region. Highly conserved amino acids are in bold/yellow. Source: NCBI (Benson *et al.*, 2012)

OATP	Signature sequence													Amino acid position
OATP1A2	**D**	T	**R**	**W**	V	**G**	**A**	**W**	**W**	F	**G**	F	**L**	218
OATP1B1	**D**	S	**R**	**W**	V	**G**	**A**	**W**	**W**	L	N	F	**L**	251
OATP1B3	**D**	S	**R**	**W**	V	**G**	**A**	**W**	**W**	L	**G**	F	**L**	251
OATP1C1	**D**	**P**	Q	**W**	V	**G**	**A**	**W**	**W**	L	**G**	Y	**L**	149
OATP2A1	**D**	**P**	**R**	**W**	I	**G**	**A**	**W**	**W**	L	**G**	L	**L**	250
OATP2B1	**D**	**P**	**R**	**W**	V	**G**	**A**	**W**	**W**	L	**G**	F	**L**	269
OATP3A1	**D**	**P**	**R**	**W**	I	**G**	**A**	**W**	**W**	G	**G**	F	**L**	199
OATP4A1	S	**P**	L	**W**	V	**G**	**A**	**W**	**W**	V	**G**	F	**L**	303
OATP4C1	**D**	**P**	**R**	**W**	L	**G**	**A**	**W**	**W**	I	**G**	F	**L**	307
OATP5A1	**D**	**P**	**R**	F	I	**G**	N	**W**	**W**	S	**G**	F	**L**	340
OATP6A1	S	**P**	E	**W**	L	W	T	**W**	**W**	I	N	F	**L**	307

The signature sequence is predicted to be between the external loop 3 and TM6, as determined by the topology analysis performed in chapter 4. This is in line with previous predictions (Hagenbuch, 2003).

The presence of the signature sequence at the interface between the TM and the extracellular loop suggests a potential role for stabilising or anchoring the protein in the membrane. This is supported by the presence of conserved tryptophan residues; residues which are relatively rare in proteins, normally constituting approximately 5% of the amino acid sequence (Lodish *et al.*, 2000).

Tryptophans are more prevalent in transmembrane proteins than soluble proteins (Schiffer *et al.*, 1992) and are often found in membrane proteins at the hydrophobic/hydrophilic interface of helices and TMs (Wallace and Janes, 1999). In the OATP1B1 sequence there are six tryptophan residues, three of which are present in the signature sequence. The preference of tryptophans for the interface has been linked to protein stability within the membrane. Clark and colleagues (Clark *et al.*, 2003) mutated the tryptophans in the transmembrane protein diacylglycerol kinase, finding that tryptophan tilted the residues at the end of the helix, linking them to the helix backbone. This stability may be because of hydrogen bonding from the unique indole ring, whereby hydrogen bonds are formed with the lipid heads of the membrane, whilst the hydrophobic rings are immersed within the bilayer (Schiffer *et al.*, 1992).

This hydrogen bonding was also found to be important for the correct folding of transmembrane gramicidin channels (Sun *et al.*, 2008b). Aromatic amino acids such as tryptophan can also undergo stacking interactions with other aromatic residues. This stacking of one amino acid on another stabilises the protein, and may suggest why there are three tryptophan residues in close proximity within the sequence.

A positively charged arginine is also found within the signature sequence and is highly conserved. Arginines and lysines that flank the membrane play an important role in anchoring the TM within the membrane. Positive amino acids are thought to interact with the negatively charged phospholipid head groups,

stabilising the hydrophobic regions within the membrane (Lodish *et al.*, 2000; Mandery *et al.*, 2011).
Therefore the presence of amino acids such as arginines and tryptophans and the localisation to the helix/TM interface suggest that the signature sequence region is important for protein anchoring and/or folding.

OATP1B1 was the chosen isoform to study the sequence with the OATP1B1-HEK293T model previously established (chapter 3). Furthermore, the topology of OATP1B1 has been evaluated, revealing extracellular loop 2 (F4) to be extracellular (chapter 4). The epitope in this position did not disrupt transport and kinetic values were comparable. Therefore this OATP1B1-F4 mutant isoform provided a suitable system for investigating the surface expression of the signature sequence.

The most conserved amino acids within the signature sequence were mutated conservatively to determine the importance of the charge and structure of the amino acid, for transport and surface expression. The mutations OATP1B1-F4-D251E, R253K, W254F, W258/259F (double mutant) and N261A were introduced using SDM. Each mutant was expressed in HEK293T cells and the effect on transport investigated using the previously validated [^{3}H]E3S transport experiment. In addition, luminometry and immunofluorescence experiments were performed to evaluate the effects of the mutations on surface expression. Values for each experiment were compared to OATP1B1-F4 as the WT.

The results from these experiments provided evidence for the importance of specific amino acids within the OATP signature sequence for transport and surface expression.

5.2 Results

5.2.1 OATP1B1 signature mutagenesis and rationale

The highly conserved OATP1B1 signature sequence was investigated using SDM. The topology predictions in section 4.2.1 were used to predict the location of the signature sequence in OATP1B1. The sequence was located between external loop 3 and TM6 (figure 5.2), in line with previous predictions (Hagenbuch, 2003).

Mutations were introduced to the validated F4 externally tagged OATP1B1 isoform to allow the quantification of surface expression following mutagenesis. Conservative mutations were made to 6 amino acids within the signature sequence of OATP1B1 (figure 5.1). These were D251E, R253K, W254F, W258/259F and N261A (mutagenesis method in section 2.2.14.5).

Aspartic acid was mutated to glutamic acid (D251E); both being negatively charged polar residues. Arginine, the only positively charged residue in the signature sequence, was mutated to the similarly positive and polar lysine (R253K). The tryptophans were mutated to phenylalanines; W254F and W258/259F as a double mutant. Phenylalanines and typtophans are non-polar with aromatic side chains, differing by the nitrogen containing indole ring of tryptophan and phenyl group of phenylalanine. Phenylalanine is also more hydrophobic than tryptophan but both are able to perform stacking interactions to stabilise the protein (Lieberman and Marks, 2012).

Interestingly, the first three residues of the signature sequence are polar, followed by a stretch of non-polar residues, with the exception of asparagine (figure 5.1). This asparagine is also not very conserved among the other OATPs, which are mostly non-polar glycines (table 5.1). Therefore asparagine was mutated to investigate the role of this amino acid in the sequence. Asparagine, as the amide of aspartic acid, does not carry a charge. Therefore it

was mutated to alanine (N261A), a residue similarly without a charge and lacking a reactive side group, so as not to mask the potential function of asparagine.

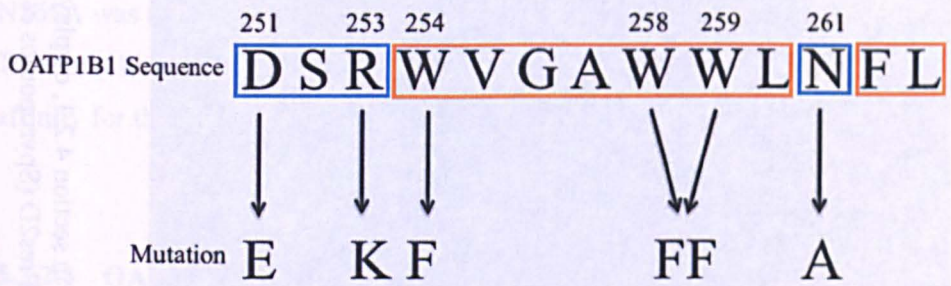

Figure 5.1 – OATP1B1 signature sequence with mutations and amino acid positions, polar amino acids highlighted in blue, non-polar in orange.

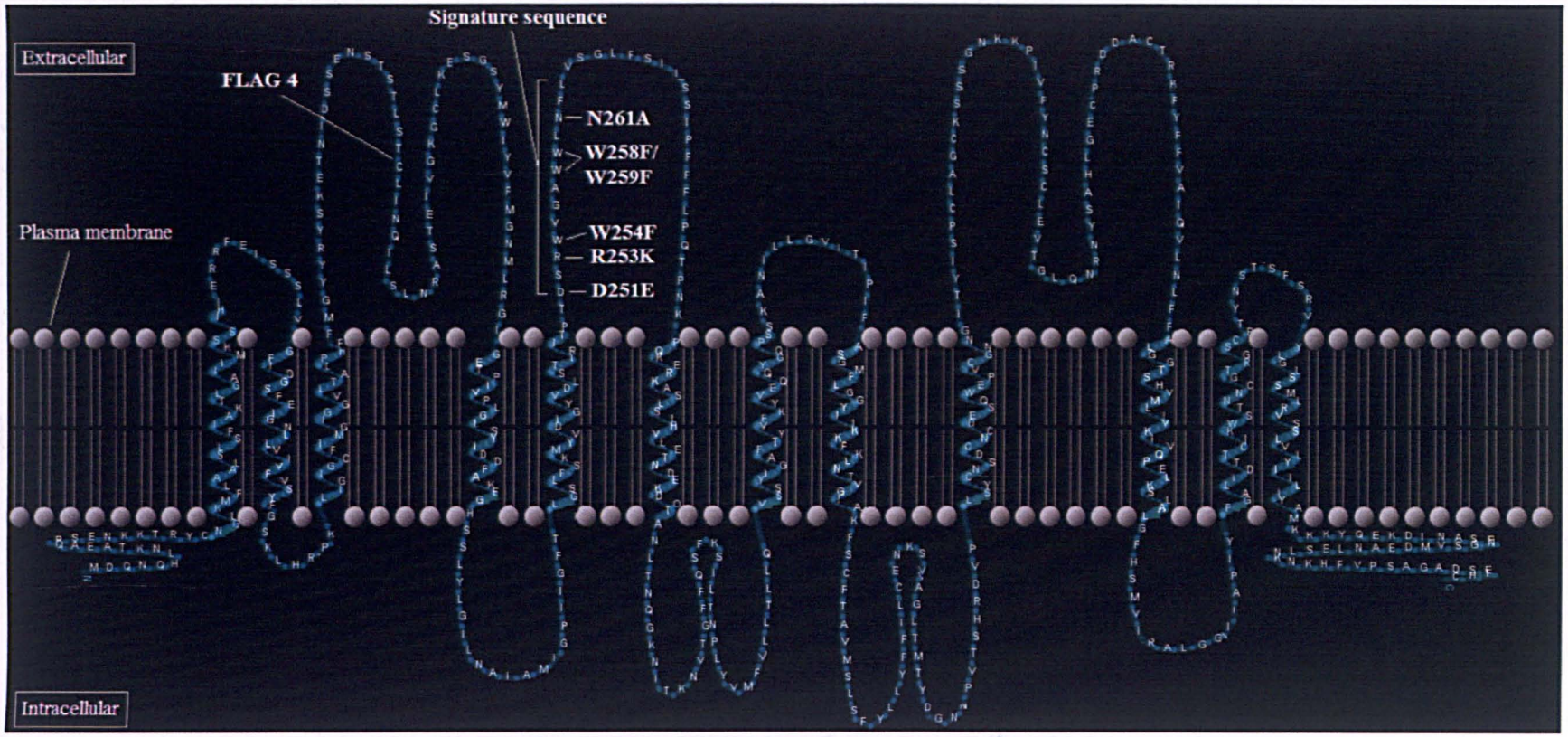

Figure 5.2 - Predicted topology of OATP1B1 from the prediction results in section 4.2.1, displaying the location of FLAG 4 and the signature sequence region (orange). The model was rendered using TMRPres2D (Spyropoulos *et al.*, 2004).

5.2.2 OATP1B1 signature mutant transport

Transport experiments were conducted with mutant transfected HEK293T cells and the substrate [^{3}H]E3S (figure 5.3). Experiments were performed simultaneously with the pcDNA vector negative control and OATP1B1-F4 WT (WT F4) positive control. All WT F4 transport was significant from the pcDNA control, validating the experiment. N261A was the only mutant to show a significant increase in transport from the pcDNA control, and was not significantly different from the WT F4. Mutants D251E, R253K, W254F and W258/259F were not significant from the negative control. This suggests that N261A was the only mutant to maintain significant transport function. Transport kinetics were performed on the mutants to ascertain whether the affinity for the substrate was changed (section 5.2.2.1).

5.2.2.1 OATP1B1 signature mutant transport kinetics

Transport kinetics were performed on the signature sequence mutants to investigate a change in K_m and/or V_{max} following mutagenesis. Initial transport experiments revealed that N261A was the only mutant to show significant transport from the pcDNA control (section 5.2.2), the remaining mutants were not significant.

Table 5.2 shows the K_m and V_{max} values obtained using the same experimental parameters as for the WT F4 (section 3.2.3.2.3). N261A transport kinetics were performed over three separate experiments and were not significantly different from the WT F4. Kinetic experiments with the remaining mutants were performed with one experiment owing to the low levels of transport. This small amount of data though not significant, does suggest that the K_m was increased and V_{max} slightly decreased from the WT F4. The values in table 5.2 were plotted as Michaelis-Menten curves using the Michaelis-Menten equation in figure 5.4.

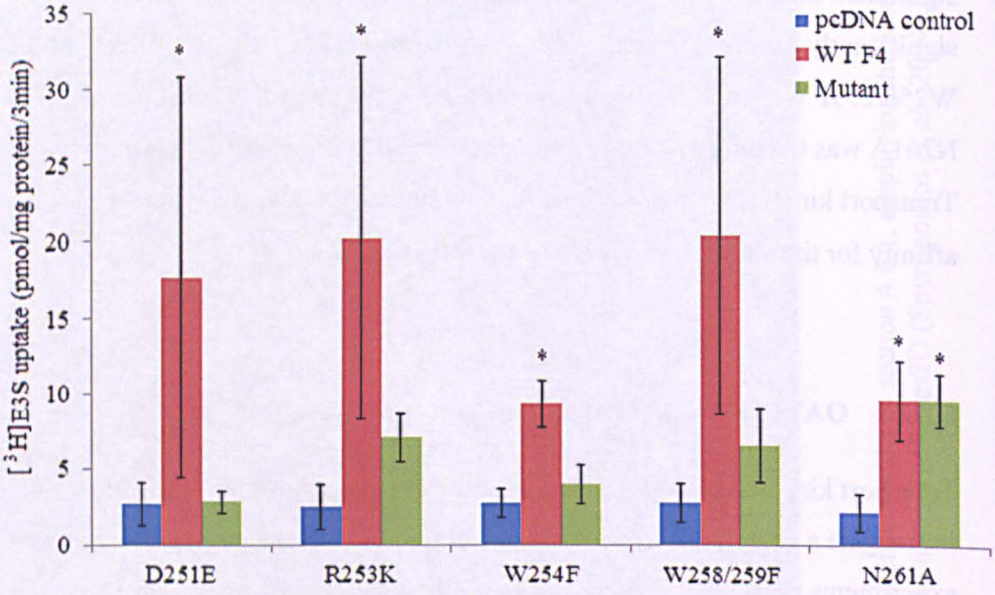

Figure 5.3 - Uptake of [^{3}H]E3S into pcDNA negative control, pcDNA/*SLCO1B1*-F4 WT and pcDNA/*SLCO1B1*-F4-D251E, pcDNA/*SLCO1B1*-F4-R253K, pcDNA/*SLCO1B1*-F4-W254F, pcDNA/*SLCO1B1*-F4-W258/259F and pcDNA/*SLCO1B1*-F4-N261 transfected HEK293T cells. Each bar is the mean ± SE of 3-5 experiments with 6 well replicates. *Unpaired t-test; $P<0.05$ from the pcDNA control.

Table 5.2 – Michaelis-Menten K_m and V_{max} values for pcDNA/*SLCO1B1*-F4 WT (bold), pcDNA/*SLCO1B1*-F4-D251E, pcDNA/*SLCO1B1*-F4-R253K, pcDNA/*SLCO1B1*-F4-W254F, pcDNA/*SLCO1B1*-F4-W258/259F and pcDNA/*SLCO1B1*-F4-N261A transfected HEK293T cells. Each value is the mean ± SE of 1-4 experiments with 3 well replicates and the pcDNA control subtracted.

OATP	K_m (μM)	V_{max} (pmol/mg protein/3min)
OATP1B1-F4 WT	**0.159 ± 0.049**	**79.6 ± 6.5**
OAT1B1-F4-D251E	0.886	74.6
OATP1B1-F4-R253K	0.303	76.7
OATP1B1-F4-W254F	0.772	76.7
OATP1B1-F4-W258/259F	0.424	76.6
OATP1B1-F4-N261A	0.084 ± 0.033	47.0 ± 19.4

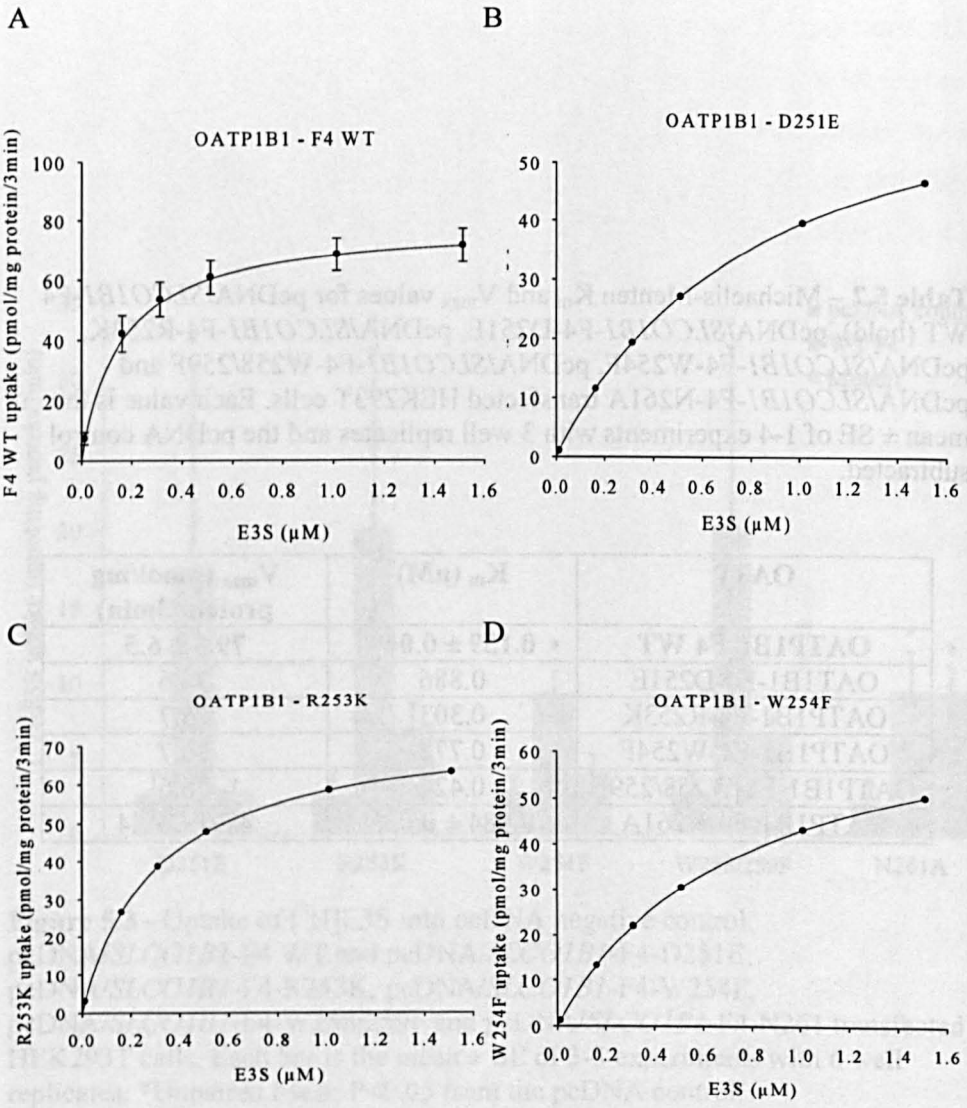

Figure 5.4 – continued on next page

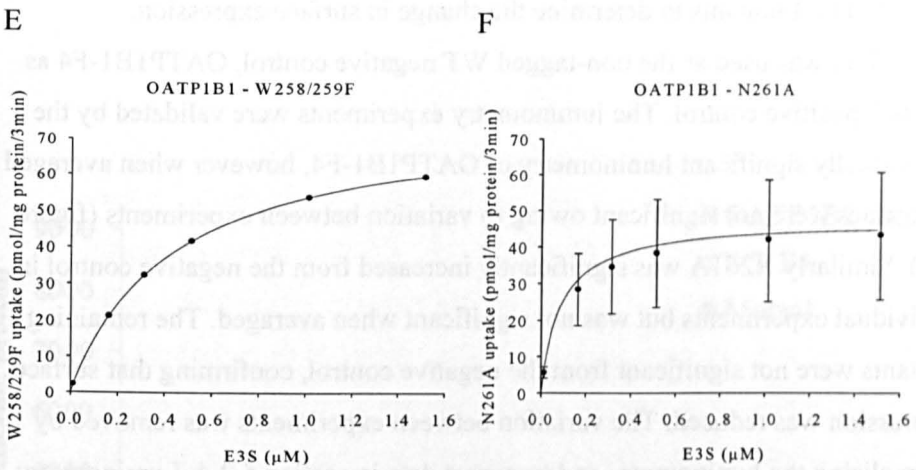

Figure 5.4 – E3S Michaelis-Menten curves of A) pcDNA/*SLCO1B1*-F4 WT, B) pcDNA/*SLCO1B1*-F4-D251E, C) pcDNA/*SLCO1B1*-F4-R253K, D) pcDNA/*SLCO1B1*-F4-W254F, E) pcDNA/*SLCO1B1*-F4-W258/259F and F) pcDNA/*SLCO1B1*-F4-N261A transfected HEK293T cells. The line is the Michaelis-Menten equation fitted to the kinetic parameters in table 5.2. Each point is the mean of 1 experiment, except for N261A where each point is the mean ± SE of 3 experiments and WT F4 which is the mean ± SE of 4 experiments. All were performed with 3 well replicates.

5.2.3 OATP1B1 signature mutant luminometry

Luminometry experiments were conducted with the signature sequence OATP1B1 F4 mutants to determine the change in surface expression. OATP1B1 was used as the non-tagged WT negative control, OATP1B1-F4 as the WT positive control. The luminometry experiments were validated by the individually significant luminometry of OATP1B1-F4, however when averaged the values were not significant owing to variation between experiments (figure 5.5). Similarly N261A was significantly increased from the negative control in individual experiments but was not significant when averaged. The remaining mutants were not significant from the negative control, confirming that surface expression was reduced. The variation between experiments was removed by normalising the luminometry and transport data in section 5.2.4. Luminometry results were supported by those of immunofluorescence experiments (section 5.2.5).

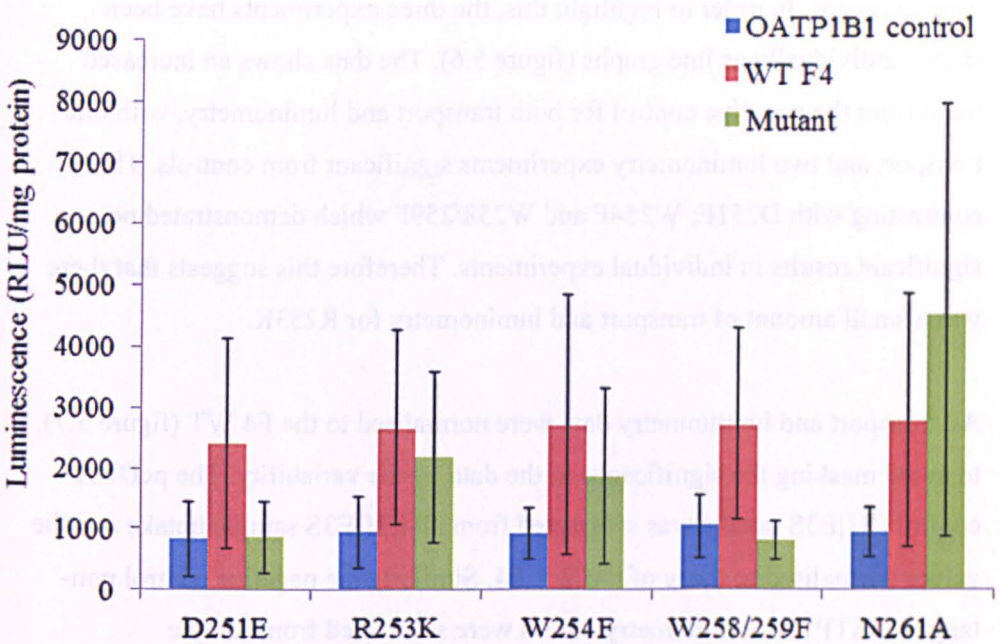

Figure 5.5 - Luminescence of pcDNA/*SLCO1B1* negative control, pcDNA/*SLCO1B1*-F4 WT and pcDNA/*SLCO1B1*-F4-D251E, pcDNA/*SLCO1B1*-F4-R253K, pcDNA/*SLCO1B1*-F4-W254F, pcDNA/*SLCO1B1*-F4-W258/259F and pcDNA/*SLCO1B1*-F4-N261 transfected HEK293T cells. Each bar is the mean ± SE of 3 experiments with 3 dish replicates.

5.2.4 Summary of OATP1B1 signature mutant transport and luminometry

The luminometry and transport experiments displayed some inter-assay variation as observed for the OATP1B1-FLAG experiments in section 4.2. This was particularly apparent for R253K. R253K demonstrated some significant transport and luminometry which were not significant when the experiments were averaged. In order to highlight this, the three experiments have been shown individually as line graphs (figure 5.6). The data shows an increased trend from the negative control for both transport and luminometry, with one transport and two luminometry experiments significant from controls. This is contrasting with D251E, W254F and W258/259F which demonstrated no significant results in individual experiments. Therefore this suggests that there was a small amount of transport and luminometry for R253K.

All transport and luminometry data were normalised to the F4 WT (figure 5.7), to avoid masking the significance in the data by the variability. The pcDNA control [^{3}H]E3S uptake was subtracted from all [^{3}H]E3S sample uptake and the values normalised to those of the WT F4. Similarly the negative control non-tagged OATP1B1 luminometry values were subtracted from sample luminometry values and values normalised to those of the WT F4. Significance was denoted using a one sample t-test and values were expressed as a percentage.

The normalised data displays a significant decrease in transport and luminometry for D251E, W254F and W258/259F. R253K was not significantly reduced from the WT F4. N261 was not significantly different from the WT F4 and was significant from controls, suggesting that this mutation did not affect the functioning of the protein.
The transport and luminometry values for D251E, R253K, W254F and W258/259F were not significant from one another, suggesting a relatively equal reduction in transport and surface expression. Therefore transport was most

likely reduced because there were fewer transporters on the membrane. These results are supported by immunofluorescence experiments (section 5.2.5).

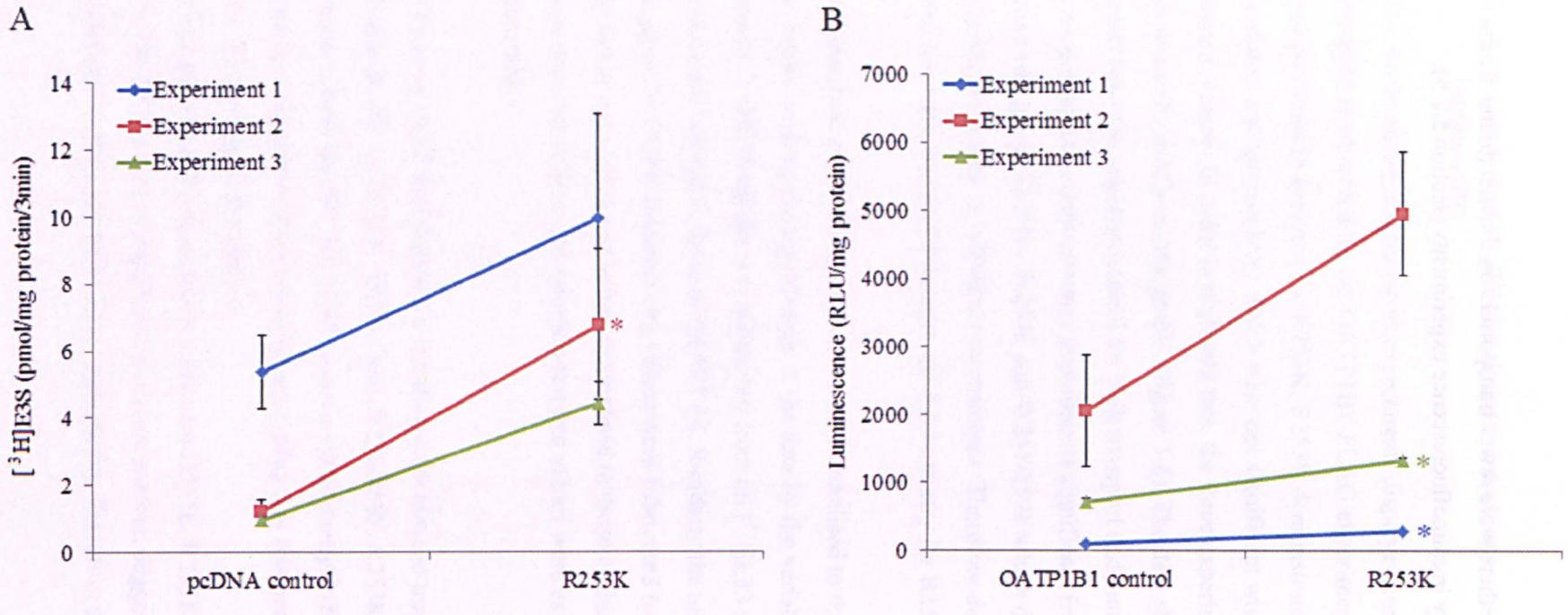

Figure 5.6 – Individual A) [^{3}H]E3S transport and B) luminometry experiments for pcDNA negative control, pcDNA/*SLCO1B1* negative control and pcDNA/*SLCO1B1*-F4-R253K transfected HEK293T cells. Each point is the mean ± SE of one experiment with 3 well replicates. *Unpaired t-test $P<0.05$.

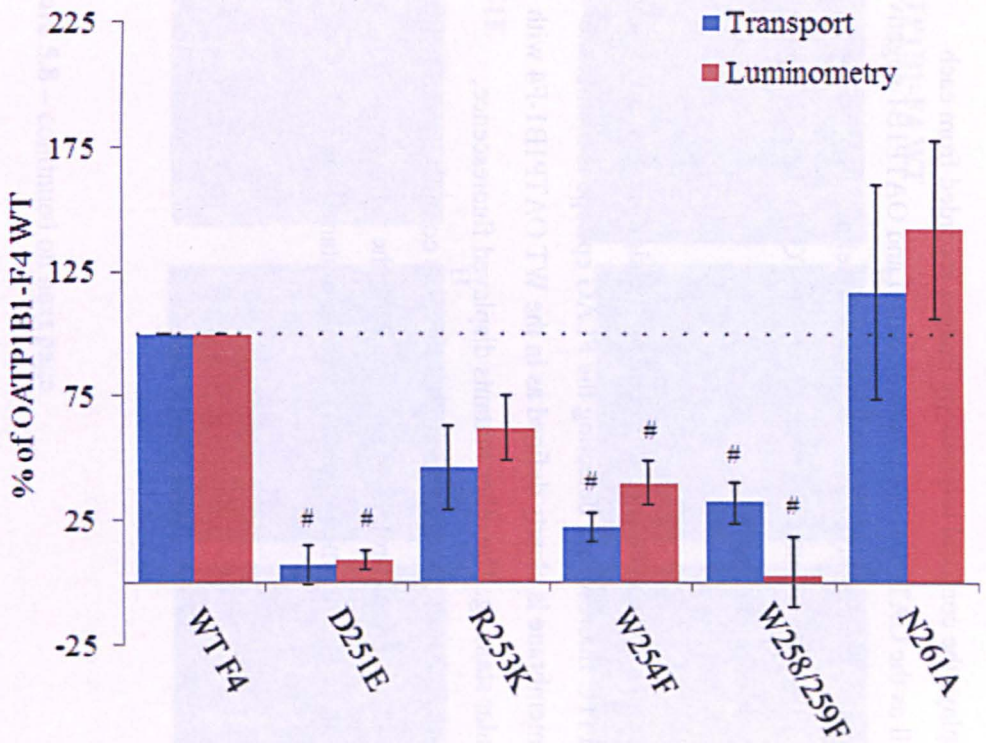

Figure 5.7 – Summary of transport and luminometry results for pcDNA/*SLCO1B1*-F4-D251E, pcDNA/*SLCO1B1*-F4-R253K, pcDNA/*SLCO1B1*-F4-W254F, pcDNA/*SLCO1B1*-F4-W258/259F and pcDNA/*SLCO1B1*-F4-N261A transfected HEK293T cells. Negative control values were removed and values normalised to the WT OATP1B1-F4, expressed as a percentage. Each bar is the mean ± SE of 3-5 experiments (luminometry = 3 dish replicates, transport = 6 well replicates). #P<0.05 decrease from WT (one sample t-test).

5.2.5 OATP1B1 signature mutant immunofluorescence

Immunofluorescence experiments were performed to qualitatively confirm the luminometry results displayed in section 5.2.3. The experiments were performed as previously described in section 4.2.5. To summarise, HEK293T cells expressing the protein were fixed to cover slips and incubated with a primary anti-FLAG and secondary-FITC antibody that detected the FLAG epitope. The nucleic acid stain DAPI was also used to visualise the DNA. Figure 5.8 displays the confocal microscopy images recorded from each mutant, as well as the OATP1B1-F4 positive control and OATP1B1 negative control. The images are displayed as A) 405nm channel highlighting the DAPI stained nuclei, B) 488nm channel highlighting the FITC labelled FLAG epitope and C) overlay of both images.

The N261A immunofluorescence results confirm the significant luminometry results as the FITC fluorescence detecting the FLAG epitope is membrane specific. The membrane is clearly defined as in the WT OATP1B1-F4 with little intracellular staining. The other mutants displayed fluorescence, suggesting that some protein was present, but this was completely throughout the cell, suggesting that the protein was not reaching the membrane. This supports the reduced luminometry values for these mutants.

OATP1B1 negative control

A B C

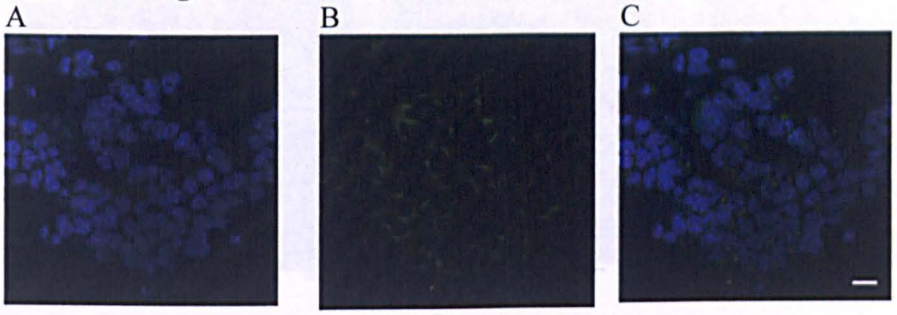

OATP1B1-F4 WT

A B C

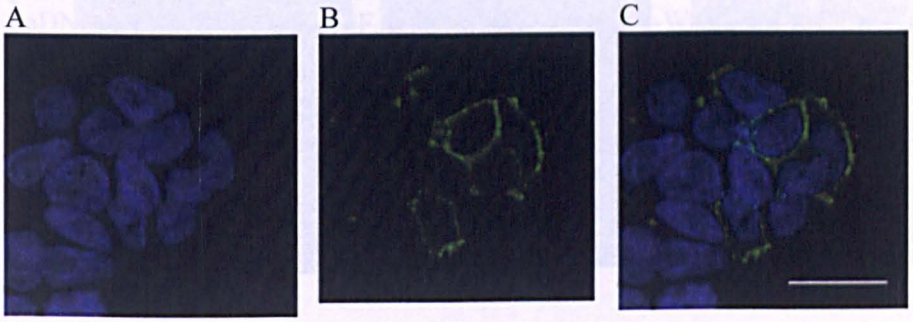

D251E

A B C

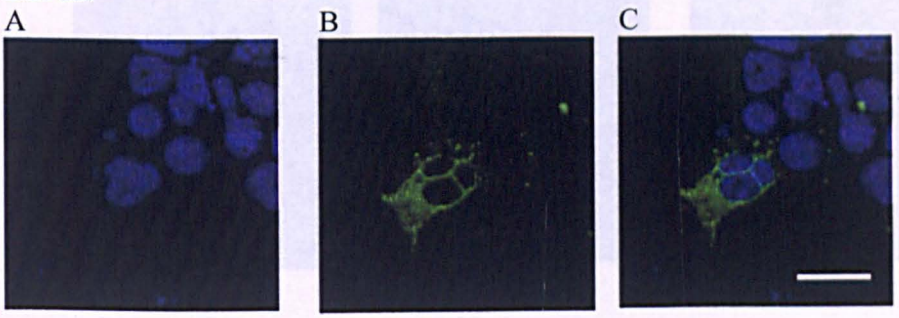

Figure 5.8 – continued on next page

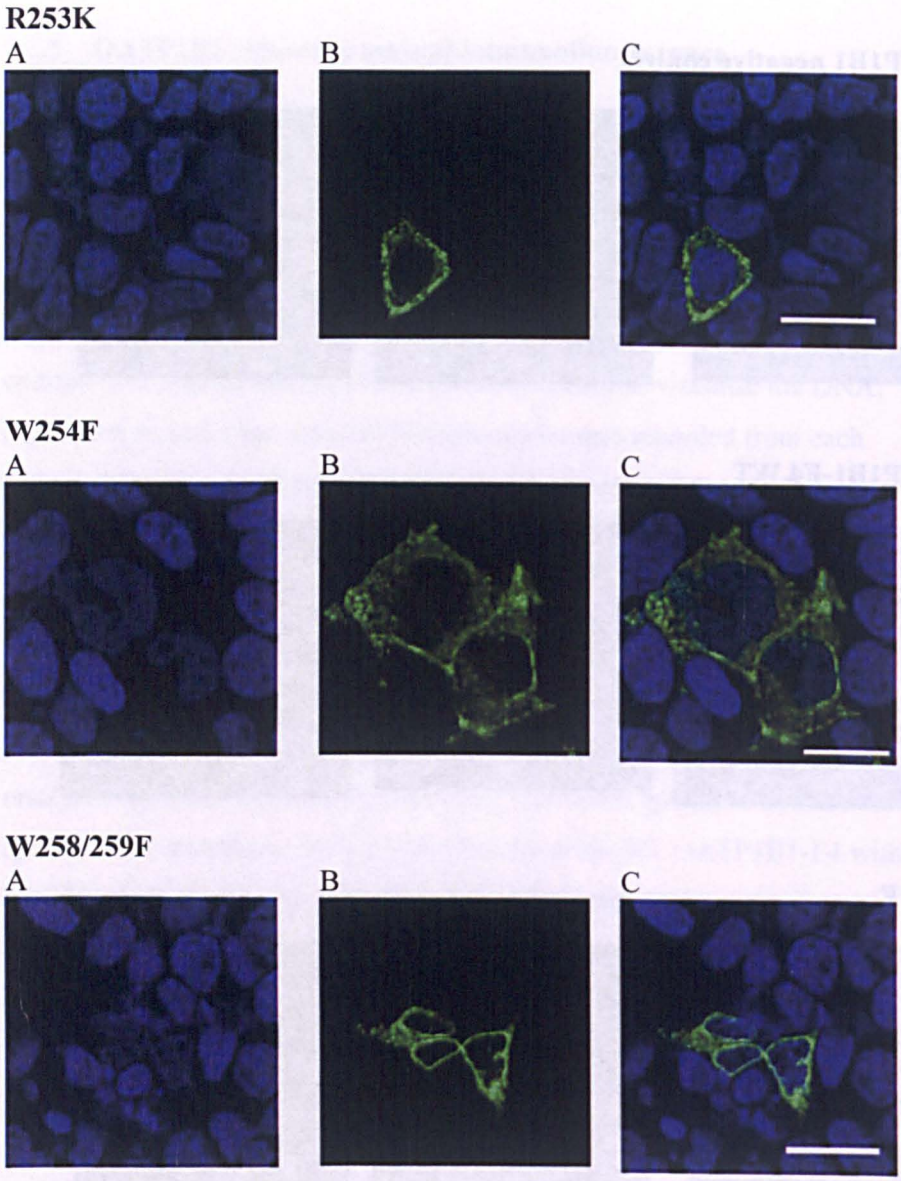

Figure 5.8 – continued on next page

N261A

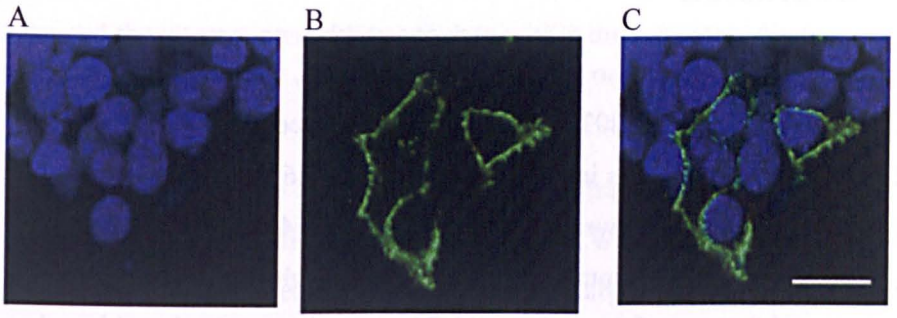

Figure 5.8 – pcDNA/*SLCO1B1* negative control, pcDNA/*SLCO1B1*-F4 WT, pcDNA/*SLCO1B1*-F4-D251E, pcDNA/*SLCO1B1*-F4-R253K, pcDNA/*SLCO1B1*-F4-W254F, pcDNA/*SLCO1B1*-F4-W258/259F and pcDNA/*SLCO1B1*-F4-N261A transfected HEK293T cell immunofluorescence by confocal microscopy. A) DAPI (blue) localised to the nucleus (504nm) B) FITC (green) localised to the FLAG epitope (488nm) C) overlay of both images. Scale bar = 20μM.

5.3 Conclusion

All OATPs contain a 13 amino acid signature sequence, the function of which is not known (Hagenbuch, 2003). The signature sequence of OATP1B1 (DSRWVGAWWLNFL) was investigated by mutating 6 highly conserved residues, using SDM. These were D251E, R253K, W254F, W258/259F and N261A. These conservative mutations were made to highlight the importance of the structural features of the amino acid. The mutations were cloned into the F4 externally tagged OATP1B1, which maintained WT transport kinetics and allowed changes in surface expression to be investigated.

Transport and luminometry results revealed that mutations D251E, W254F and W258/259F had dramatic effects on function and surface expression, reducing to less than 40% of the WT F4. R253K was reduced to approximately 50% of the WT F4 and displayed some significant transport and luminometry. The relatively equal reduction in transport and surface expression suggest that transport was reduced owing to fewer transporters present on the membrane. Transport kinetics, despite low experiment numbers and low transport, did show an increase in K_m and small reduction in V_{max}. N261A protein function was not significantly altered by the mutation. Immunofluorescence results supported the luminometry results, showing membrane specific fluorescence for N261A but throughout the cell for the other mutants. The presence of fluorescence suggests that some protein was present in the cell, but the intracellular staining was most likely the result of the antibody binding to incorrectly folded or retained protein.

Aspartic acid and glutamic acid are both negatively charged polar residues, therefore a substitution (D251E) was not expected to affect the protein. However a significant decrease in transport and luminometry to background levels was observed. This may be owing to the differing spacial preferences of the two amino acids. Aspartic acid interacts with tryptophan more frequently than glutamic acid, possibly because of the slightly differing chain lengths

(Jonson and Petersen, 2001). Therefore mutating to glutamic acid may have changed the interactions with tryptophan within the sequence, disrupting the structure.

Mutation of arginine to lysine (R253K) reduced transport and surface expression to approximately 50% of the WT F4, with a small amount of transport and luminometry. Positively charged arginine and lysine are thought to play a role in stabilising the membrane by interacting with negatively charged phospholipid head groups (Lodish *et al.*, 2000). The effects of this mutation on transport and surface expression suggest that a structurally different property of arginine is required for correct function. Arginine and lysine are both polar, positive amino acids, differing by their functional groups. The conformation of the guanidinium group of arginine is known to form more electrostatic interactions compared to the basic functional group of lysine. Arginine also has a higher pKa, potentially allowing for more stable ionic interactions (Sokalingam *et al.*, 2012). It may be for these reasons that arginine, rather than lysine, is required in this position, but that the positively charged property of lysine possibly rescued some of the function.

Tryptophan is a unique and versatile amino acid, exhibiting a large non-polar surface area, the capability for hydrogen bond formation from the indole N-H moiety and the greatest electrostatic potential for cation-π and other non-covalent interactions (Sanchez *et al.*, 2011). It is for these properties that the highly conserved tryptophans present in the sequence may be essential for stabilising OATP1B1 within the lipid bilayer. The reduction in function and surface expression from substituting tryptophan for phenylalanine (W254F, W258/259F) suggests that a feature within the tryptophan structure is required for the correct functioning of the signature sequence. This could be owing to the indole ring that only tryptophan possesses, previously shown as an important feature for hydrogen bonding and membrane stability (Sanchez *et al.*, 2011; Schiffer *et al.*, 1992). Westholm and colleagues however provide interestingly contrasting results (Westholm *et al.*, 2010). When the group

mutated the equivalent double tryptophans in rat Oatp1c1 (W277/278F) to phenylalanines, the protein retained WT transport kinetics and surface expression by immunofluorescence. It was only when replaced with small, non-aromatic alanines that function was abolished. This suggests that different OATPs may be folded or stabilised in the membrane slightly differently.

The mutation of asparagine to alanine (N261A) did not affect transport or surface expression. It may be that maintenance of a neutral charge at this position is sufficient to complete protein folding and function. Asparagine is able to perform hydrogen bond interactions with its side chain amide groups (Shimoni and Glusker, 1995), which is not possible with the hydrophobic side chain of alanine. Therefore hydrogen bonding is also unlikely to be required in this amino acid position.

Mutating residues within the signature sequence region has had a profound effect on protein transport and surface expression. Of the six amino acids mutated conservatively, four were severely affected. The relatively equal decrease in surface expression combined with transport suggests that there were less transporters present or that the protein was folded incorrectly on the membrane. This is supported by the intracellular fluorescence observed from the immunofluorescence experiments. However the presence of structurally important residues such as tryptophans and the putative position at the helix/TM interface suggest a role in stabilising or anchoring the protein within the membrane. It is possible that this sequence is an internal non-cleaved membrane-anchor sequence or stop-transfer anchor sequence, ensuring that the protein is anchored within the membrane at the correct position following translocation from the ER. However transmembrane proteins that contain an anchor sequence often also contain a cleavable signal peptide (Cooper, 2000), which is not predicted for OATP1B1. Further analysis would benefit from the investigation of L263 in the signature sequence, which is also conserved across all human OATPs.

6 Discussion

Membrane transport research has expanded significantly in the last decade; with the understanding that membrane transport contributes significantly to drug disposition. The OATPs are one such family of membrane proteins responsible for the transport of many varied endogenous and xenobiotic compounds. The presence of OATPs in the membranes of hepatocytes and renal cells highlights their influential role in the uptake of compounds for drug metabolism and excretion. Furthermore, the OATPs have been linked to disease and clinically relevant DDIs, emphasising the importance for understanding the structure and function of these proteins.

OATPs have been predicted to contain 12TMs with the N and C termini facing the cytoplasmic space (Hagenbuch and Meier, 2004; Hanggi *et al.*, 2006; Noe *et al.*, 1997; Roth *et al.*, 2011). *N*-glycosylation sites have been located in extracellular loops 2 and 5 (Lee *et al.*, 2003; Wang *et al.*, 2008; Yao *et al.*, 2012). The large extracellular loop 5 also contains cysteine residues linked by disulphide bonds, found to be essential for targeting to the cell surface in OATP2B1 (Hänggi *et al.* 2006). In addition, several residues within TMs are important for substrate binding (Gui and Hagenbuch, 2009; Li *et al.*, 2012; Miyagawa *et al.*, 2009). The OATPs are characterised by a signature sequence region (D-X-RW-(I,V)-GAWW-XG-(F,L)-L) located at the border between extracellular loop 3 and TM6, which is conserved across all species (Hagenbuch and Meier, 2004), but the function is not known. Meier-Abt and colleagues (Meier-Abt *et al.*, 2005) homology modelled OATP1B3 on two MFS proteins, revealing a pore like structure, to which substrates potentially translocate. Positive residues predicted to line the pore have been studied and are involved in transport (Glaeser *et al.*, 2010; Weaver and Hagenbuch, 2010). The aim of this research was to further this structural knowledge by validating the topology predictions experimentally and elucidate the role of the signature sequence.

OATP1A2, OATP1B1, OATP1B3 and OATP2B1 are functionally influential transporters that are present in the liver and kidney, linked to disease and implicated in DDIs. Therefore any/all of these isoforms were relevant candidates for evaluating the OATP structure/function. Several expression systems were investigated as potential models for studying these OATPs, using the substrate E3S. The *X. laevis* oocyte and HEK293T cell systems were evaluated as over-expression systems. *X. laevis* oocytes are used routinely to express membrane proteins and significant transport of E3S was observed for all four isoforms. However transport was variable, and so HEK293T cells were evaluated as an alternative cell culture model. OATP1B1 demonstrated consistent transport when expressed in HEK293T cells with an E3S K_m and V_{max} of 0.105 ± 0.008μM and 50.1 ± 10.9 pmol/mg protein/3min respectively. These values are in line with those published previously (0.23μM (Noe *et al.*, 2007), (0.21 ± 0.02μM, 25.6 ± 4.6 pmol/mg protein/2min (Li *et al.*, 2012).

Primary membrane vesicles were also evaluated as a potential tool for measuring endogenous Oatp1a1 and Oatp4c1 mediated E3S transport. Transport was significant from the control in the first minute, then decreased over time, suggesting that transport was either very rapid and/or that the radioactivity was potentially retained on the filter. This system requires further optimisation to determine whether it would be a suitable model for measuring endogenous OATP transport.

The validated OATP1B1/HEK293T cell system was used to further investigate the topology and OATP signature sequence region of the protein. There is very little supporting evidence for the topology of the OATPs, the only previously studied OATP is rat Oatp1a1 (Wang *et al.*, 2008). The authors used two prediction programs; TMPRED and TMHMM, which predicted 12 and 10TM proteins respectively. An epitope tag was inserted in a region that was external in the 10TM model and internal in the 12TM model to differentiate between the two. The region was found to be external, suggesting that the 10TM model may

not be correct. However further experiments were not performed to definitively confirm the 12TM topology and the orientation of the N and C termini.
The topology of OATP1B1 was predicted from the results of 16 topology prediction programs, including TMHMM and MEMSAT3, which were found in an independent comparison to be the most accurate (Moller *et al.*, 2001). Results predicted a consensus of 12TMs, internal N and C termini and no presence of a signal peptide sequence. A 12TM topology was therefore investigated, using FLAG epitope tags which were inserted into the predicted N and C termini plus extracellular/intracellular regions of the protein. The epitope was detected quantitatively using luminometry and qualitatively using immunofluorescence. Transport experiments were conducted to confirm that mutant proteins retained function. Results revealed that the N and C termini (F1 and F13) were external, as well as predicted extracellular loop 2 (F4). F6 demonstrated significant luminometry but this was not supported by the immunofluorescence experiments and transport was significantly reduced. The remaining internal and external tags disrupted the function of the protein. Therefore the topology predictions did not match the experimental data.

The lack of transport function from epitope insertion may be owing to the importance of the loops in protein folding; as the role of the intracellular/extracellular loops is not fully understood. Alternatively, the epitopes may have been inserted into TM regions of the protein. Topology prediction programs do have limitations which can often result in inaccurate predictions. Hydrophobic residues present in the external loops can skew the TM prediction results (Zhou and Zhou, 2003) predicting them as internal. Furthermore, fixed hydrophobicity thresholds present in programs such as TopPred can result in one or more TMs being missed because they are too small (Sonnhammer *et al.*, 1998). Also, TMs can span the membrane differently. For example, TMs1-3 in rabbit PepT1 do not span the membrane in a direct fashion, but are longer and potentially tilted (Meredith and Price, 2006). These domains could not be accurately predicted, nor epitope tagged because of this (Covitz *et al.*, 1998).

Predicted transmembrane proteins can also form re-entrant loops, whereby a TM enters the membrane and re-emerges on the same side (Viklund *et al.*, 2006). Approximately 10% of all transmembrane proteins are predicted to contain a re-entrant loop, some of which have been identified experimentally (Slotboom *et al.*, 1999). However when the OATP1B1 protein sequence was analysed using the re-entrant loop prediction programs Octopus (Viklund and Elofsson, 2008), ZPred (Granseth *et al.*, 2006) and PSI-Pred (Nugent and Jones, 2009), none identified a re-entrant loop (data not shown). However the accuracy of re-entrant loop prediction can be as low as 44% (Nugent and Jones, 2009). It may be that some of these structural characteristics are present in OATP1B1, resulting in inaccurate predictions.

A new OATP1B1 topological model has been generated based on the luminometry data and recent literature (figure 6.1). In this model, the F4 region (predicted extracellular loop 2), N and C termini are extracellular, as directed by the significant luminometry results. For both F1 and F4 to be extracellular, the protein is only able to span the membrane once. Therefore it is proposed that TM2 may be a re-entrant loop. In addition, F10 is in the putative large extracellular loop between TM9-10. The large size of the loop combined with the experimental evidence for OATP1B1 *N*-glycosylation sites (Yao *et al.*, 2012)and disulphide bonding in OATP2B1 (Hanggi *et al.*, 2006) (discussed below) suggest that this loop may be external. For F10 and F13 to be external, F11 may also be a re-entrant loop.

This model is supported by other structural studies conducted with OATP1B1 which match the model below (figure 6.1). OATP1B1 *N*-glycosylation sites have recently been identified as N134 in the extracellular loop between TM3-4 and N503 and N516 in the extracellular loop between TM9-10 (Yao *et al.*, 2012). This strongly supports the likelihood that these loops are extracellular, owing to the extracellular nature of these sites. The amino acids of TM/re-entrant loop 2 are highly conserved between different OATP members and four amino acids: D70, F73, E74 and G76 were found to be important for E3S

transport (Li *et al.*, 2012). Furthermore, surface expression was not reduced, suggesting that these residues play a functional rather than structural role, in accordance with being within a TM. These residues also fall within re-entrant loop 2 of the adapted model. The signature sequence predicted by the topology analysis here and previously as being between external loop 3/TM6 (Hagenbuch, 2003) is also located at the external/TM6 interface in the model. As discussed previously, homology modelling of OATP1B3 on the MFS transporters has been performed (Meier-Abt *et al.*, 2005), which revealed a number of positive residues that were solvent exposed. Of these, R57 is conserved between OATP1B1 and OATP1B3 and mutating the residue reduced transport function (Weaver and Hagenbuch, 2010). The homology modelling however was performed on 12TM MFS proteins with internal N and C termini, thus was predicted to be within extracellular loop 2. In this model this loop cannot be external as the N terminus is external, therefore it is intracellular. The equally conserved amino acids K361 and R580 predicted to be involved in substrate interactions also displayed reduced transport upon mutation (Weaver and Hagenbuch, 2010). In the model, these residues are in the positions as predicted by the homology modelling; extracellular between TM7-8 and within re-entrant loop 11 respectively. There is also evidence to suggest that TM10 is important for substrate binding, as shown by chimeric proteins made with OATP1B3 (Gui and Hagenbuch, 2009). The authors isolated four amino acids in TM10 that were critical for the transport of various OATP1B1 substrates; L545, F546, L550 and S554. These also are located in TM10 of the model below.

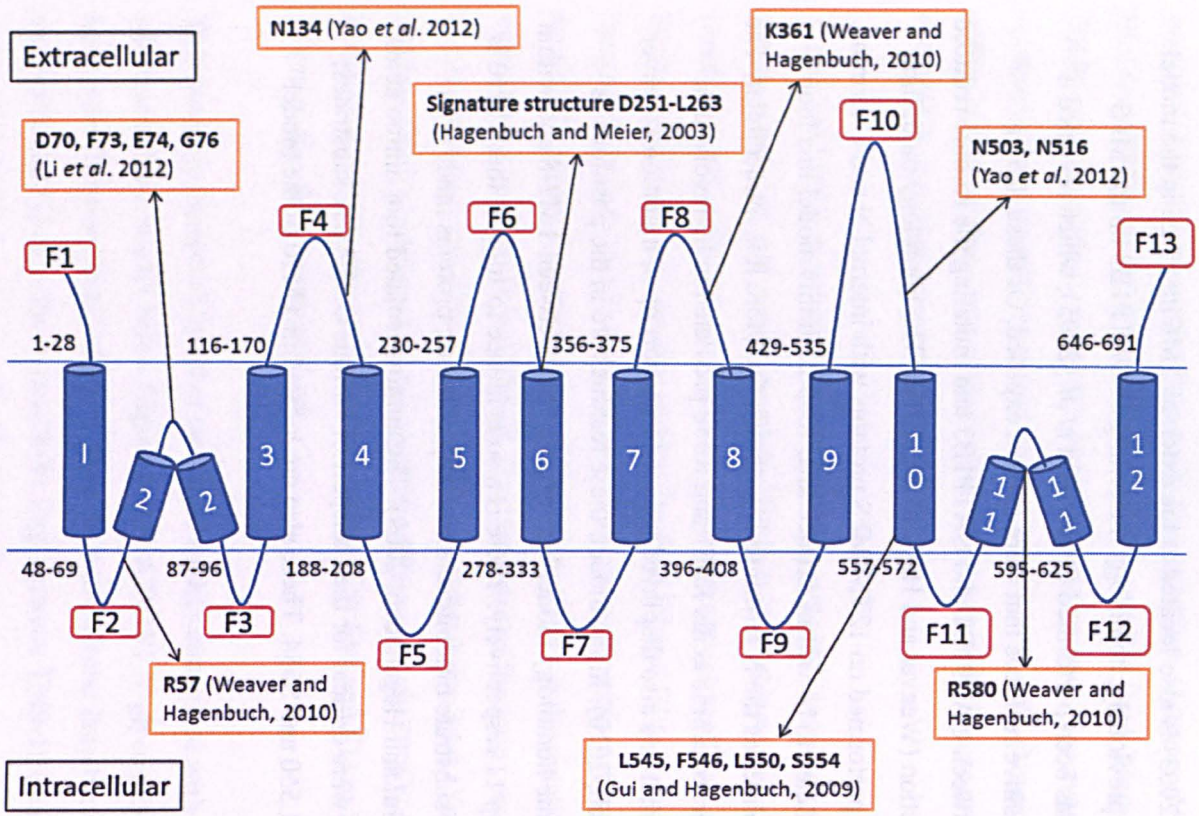

Figure 6.1 - Adapted OATP1B1 topology model based on luminometry results. Amino acid positions for the internal/external loops are displayed with FLAG epitope locations (red). TM2 and TM11 are displayed as re-entrant loops. Previously studied OATP1B1 structural features are highlighted in orange.

The structural features studied in other OATPs were also mapped onto OATP1B1 to evaluate their conservation and location within the new topology (figure 6.2). The large putative extracellular loop in OATP2B1 contains 10 cysteine residues (C489-C557), all found to be disulphide bonded (Hanggi *et al.*, 2006). When OATP2B1 was aligned with OATP1B1 using CLUSTALW2 (Larkin *et al.*, 2007) (data not shown), 7 of these cysteine residues were conserved (C489, C493, C495, C504, C516, C520, C557). The OATP1B1 extracellular loop (429-535) also contains 10 cysteine residues and overlaps with that of OATP2B1, suggesting that OATP1B1 also contains disulphide bonded cysteines in this region. This knowledge of OATP2B1, combined with the presence of OATP1B1 *N*-glycosylation sites strongly suggests that the large putative extracellular loop is external.

Rat Oatp1a1 contains 3 experimentally verified *N*-glycosylation sites (Lee *et al.*, 2003; Wang *et al.*, 2008). Of these three Oatp1a1 *N*-glycosylation sites, one is conserved in OATP1B1: N124. This is located within the extracellular loop between TM3-4, in the same location as OATP1B1 N134 (Yao *et al.*, 2012).

The model presented here serves to amalgamate the experimental findings described in this thesis with the previously reported structural knowledge. It may be that models such as those described here can be used in the future to aid *in silico* drug design, whereby a novel compound could be modelled on a computational binding site, potentially reducing the cost and time of drug discovery. Furthermore, developments in structural knowledge will provide important insights for the locations of functionally relevant SNPs. It is hoped that this will summarise and speculate on the current findings and drive further research.

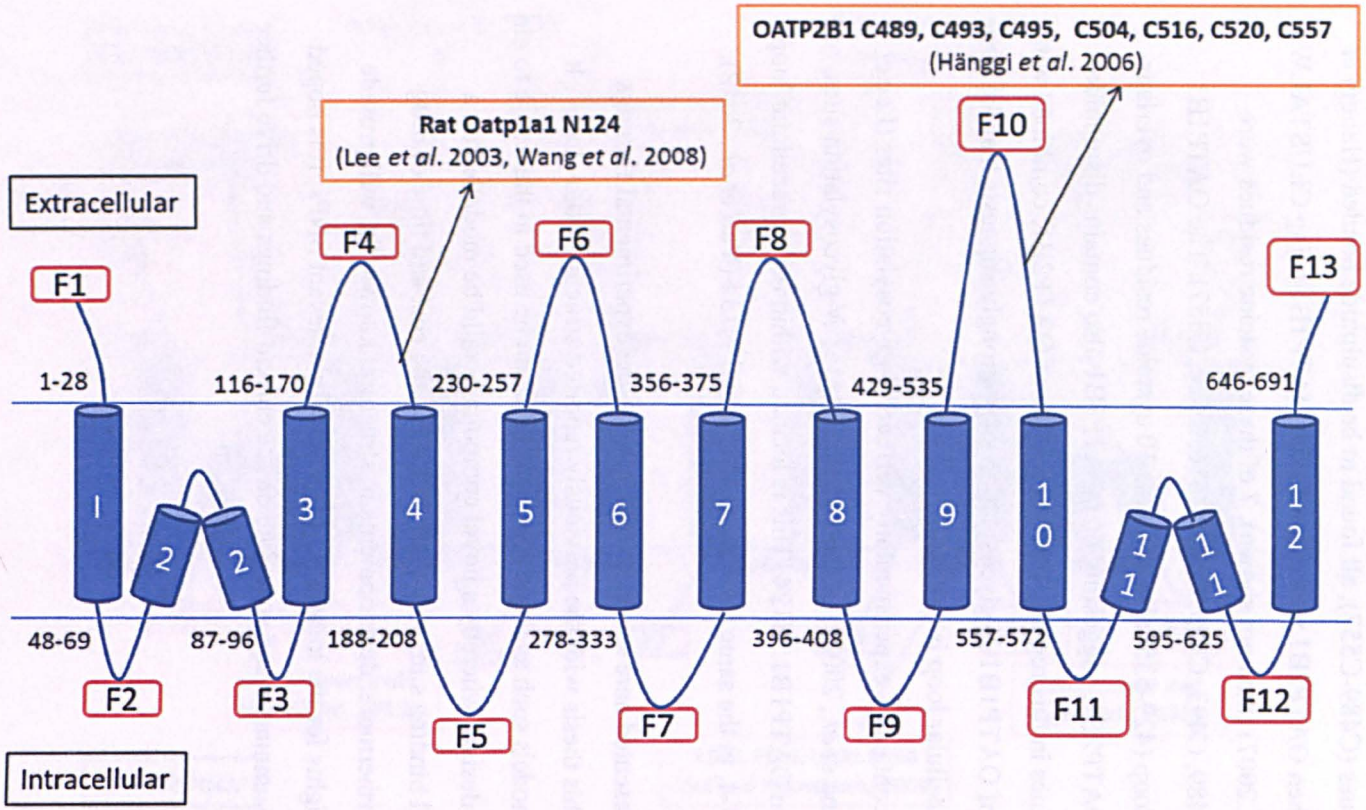

Figure 6.2 - Adapted OATP1B1 topology model based on luminometry results. Amino acid positions for the internal/external loops are displayed with FLAG epitope locations (red). TM2 and TM11 are displayed as re-entrant loops. Conserved OATP structural features are highlighted in orange.

The highly conserved signature sequence of OATP1B1 (DSRWVGGAWWLNFL) was investigated by SDM of the most highly conserved or unusual residues: D251E, R253K, W254F, W258/259F and N261A. Mutations were introduced to the previously validated OATP1B1-F4 which contained an external epitope tag and retained transport function. N261A was the only mutant to retain surface expression and transport kinetics. D251E, R253K, W254 and W258/259F surface expression and transport were reduced. The reduction in surface expression, combined with the intracellular staining observed from the immunofluorescence, suggests that the mutation caused the protein to be retained and/or not folded correctly in the membrane. These results, combined with the position of the signature sequence at the interface of the helix and TM, suggest that the sequence may have a role in stabilising the protein in the membrane. This is supported by the presence of an arginine and three tryptophan residues, amino acids which are known to anchor proteins via their charge, hydrogen bonding and/or stacking interactions.

This study has highlighted the effectiveness of luminometry methods for detecting surface expression and confirming the extracellular nature of different regions of a protein. It also is a useful tool for detecting the change in surface expression following the introduction of a mutation. Combined with immunofluorescence and transport detection methods, this approach provides a comprehensive analysis of structure/function effects in membrane transporters.

The structural knowledge of OATPs is required to understand how these transporters are targeted to and folded in the membrane, as well as how they bind and translocate compounds. This knowledge has great significance when attempting to understand how DDIs and drug toxicities arise from the competitive binding and inhibitory interactions between transporters and enzymes. Furthermore, understanding which residues are key to substrate binding or protein functionality will help understand how genetic variability in specific populations may affect drug disposition by the OATPs. This understanding is also transferrable to the knowledge of how OATP transport is

affected by disease, which has a broad relevance to many types of liver disease such as hepatitis, as well as cancer pathogenesis. With the advent of more sophisticated *in silico* prediction methods and advanced molecular biology and crystallography techniques, further investigation is required to study the intimate structure/function relationship of the OATPs.

7 Future perspectives

The specific future directions of this project are briefly described below. These include the optimisation of the primary membrane vesicle study, further OATP1B1 topology determination, additional characterisation of the OATP1B1 signature sequence and structural features identified during the course of this study which require further analysis.

The rat plasma membrane vesicle method requires further optimisation to determine whether it would be a reliable approach for investigating endogenous transport. The preliminary experiments described above suggest that some uptake by the vesicles was occurring. This would need to be confirmed by further experiments to determine the linear time frame for transport and the transport kinetics. Also, transport experiments would need to be performed with freshly prepared vesicles as well as frozen, to determine whether freeze thawing reduces transport capability. There is some evidence that freeze thawing produces more inside out rather than right side out vesicles (Palmgren *et al.*, 1990). The high background radioactivity observed at the zero timepoint may also be attributed to radioactivity being retained on the filter, and may be reduced by increased washing steps.

The topology of OATP1B1 was confirmed to have external N and C termini by luminometric methods; however the exact number of TMs was not elucidated owing to the disruption to function upon insertion of the epitope tags. Further investigations of the topology are required, which could include inserting the epitope tags elsewhere within the protein. The immunofluorescence technique in this case could be improved by the addition of a membrane specific marker, such as E-cadherin (Luo *et al.*, 2003), which would co-localise with the FLAG antibody in the membrane. This would clarify the membrane specific fluorescence. Other approaches could include cysteine scanning or *N*-glycosylation scanning mutagenesis.

Cysteine scanning mutagenesis is a strategy by which amino acid residues are substituted for cysteine residues. Chemical modifications of the introduced cysteine residues can provide information about the accessibility of a particular residue to the extracellular space, thereby locating the boundaries of the TM (Karlin and Akabas, 1998). This approach has been employed previously with transport proteins including the ABC transporters (Blott *et al.*, 1999). Scanning *N*-glycosylation employs a similar strategy, by introducing acceptor sites a minimum of 12-14 amino acids from the putative TMs (Cheung and Reithmeier, 2007). Therefore the TMs could be located by determining the limits to which extracellular regions can be glycosylated.

The topology predictions of OATP1A2, OATP1B3 and OATP2B1 require experimental verification, using the luminometry approach described for OATP1B1. OATP1A2 is particularly of interest, as it is predicted to contain between 7-9TMs, which is not in accordance with the predictions for the other OATPs, nor with the notion that the OATPs are related to the MFS. The topological analysis of OATP1A2 and OATP2B1 would however be more difficult than for OATP1B1, owing to the presence of a putative N terminal signal peptide sequence (OATP1A2) and C terminal PDZ sequence (OATP1A2 and OATP2B1), that would be cleaved or disrupted by the epitope. The results from these investigations would reveal whether all OATPs maintain a similar topology and contain external N and C termini.

The SDM of the OATP1B1 signature sequence revealed that the majority of the conserved residues are required for membrane targeting and/or protein anchoring. The remaining 7 residues in the sequence also require mutating to investigate their structure/function role, as they are also relatively conserved and likely to support the surrounding residues. This would in particular involve L263 which is a highly conserved amino acid at the end of the sequence. Leucine is an aliphatic, highly hydrophobic amino acid, possibly buried within a TM. Leucine could be substituted for valine or isoleucine, as both are also aliphatic hydrophobic amino acids (Barnes and Gray, 2003). In addition, more

investigation is required to determine the exact position of the signature region at the helix/TM interface. Cysteine scanning mutagenesis could also be employed for this purpose, and is particularly applicable for the signature sequence as it potentially spans an extracellular loop and a TM.

There are many further specific functional and structural OATP1B1 questions that still require answers, some of which have not been studied at all. These include the experimental identification and characterisation of the disulphide bonded cysteine residues in the large extracellular loop of OATP1B1, which have already been studied in OATP2B1. Seven of these cysteine residues in OATP2B1 are conserved in OATP1B1 and likely to be also disulphide bonded. Furthermore, serine phosphorylation sites have been identified and studied in Oatp1a1 but require identification and analysis in OATP1B1. The features described here are also applicable to characterisation in the other human OATPs.

The understanding of these structural features may help answer many of the general questions asked of OATPs. For example, what is the driving force for transport? There is currently conflicting evidence for the mechanism of transport and driving force. Electro-neutral exchange, bicarbonate, glutathione and pH have all been implicated. Do the OATPs function as multimers; i.e. do several monomer sub-units come together to form a complex required for function? Other transporters do function as multimers, such as the transporters PepT1 and the human copper transport Ctr1 (Guo *et al.*, 2004; Panitsas *et al.*, 2006). What is the exact 3D structure for OATPs and how do they bind to substrates in the membrane? Further mutagenesis and advances in crystallography are required to answer this question. Furthermore, there are many questions to be answered as to how OATPs are regulated, such as why some OATPs contain signal sequences whereas others do not.

These structural features are all required to determine how substrates are bound and translocated, and in turn how this causes disease and harmful DDIs. DDIs are caused by a complex collection of interactions, including interactions with the CYPs and ABCs, as well as genetic variation and inhibition. Therefore a

wealth of transporter knowledge is required to uncover these complex mechanisms. The above mentioned strategies will advance this knowledge for this influential family of multispecific OATP transporter proteins.

References

Abe, T., Unno, M., Onogawa, T., Tokui, T., Kondo, T. N., Nakagomi, R., Adachi, H., Fujiwara, K., Okabe, M., Suzuki, T., Nunoki, K., Sato, E., Kakyo, M., Nishio, T., Sugita, J., Asano, N., Tanemoto, M., Seki, M., Date, F., Ono, K., Kondo, Y., Shiiba, K., Suzuki, M., Ohtani, H., Shimosegawa, T., Iinuma, K., Nagura, H., Ito, S. and Matsuno, S. (2001). LST-2, a human liver-specific organic anion transporter, determines methotrexate sensitivity in gastrointestinal cancers. *Gastroenterology* 120 (7), pp.1689-1699.

Adachi, H., Suzuki, T., Abe, M., Asano, N., Mizutamari, H., Tanemoto, M., Nishio, T., Onogawa, T., Toyohara, T., Kasai, S., Satoh, F., Suzuki, M., Tokui, T., Unno, M., Shimosegawa, T., Matsuno, S., Ito, S. and Abe, T. (2003). Molecular characterization of human and rat organic anion transporter OATP-D. *Am J Physiol Renal Physiol* 285 (6), pp.F1188-1197.

Al Sarakbi, W., Mokbel, R., Salhab, M., Jiang, W. G., Reed, M. J. and Mokbel, K. (2006). The role of STS and OATP-B mRNA expression in predicting the clinical outcome in human breast cancer. *Anticancer Res* 26 (6C), pp.4985-4990.

Alberts, B., Johnson, A., Lewis, J., Raff, M., Roberts, K. and Walter, P. (2002). *Molecular Biology of The Cell.* 4th ed. New York: Garland Science.

Aller, S. G., Yu, J., Ward, A., Weng, Y., Chittaboina, S., Zhuo, R., Harrell, P. M., Trinh, Y. T., Zhang, Q., Urbatsch, I. L. and Chang, G. (2009). Structure of P-glycoprotein reveals a molecular basis for poly-specific drug binding. *Science* 323 (5922), pp.1718-1722.

Arai, M., Mitsuke, H., Ikeda, M., Xia, J. X., Kikuchi, T., Satake, M. and Shimizu, T. (2004). ConPred II: a consensus prediction method for obtaining transmembrane topology models with high reliability. *Nucleic Acids Res* 32 (Web Server issue), pp.W390-393.

Arakawa, H., Nakanishi, T., Yanagihara, C., Nishimoto, T., Wakayama, T., Mizokami, A., Namiki, M., Kawai, K. and Tamai, I. (2012). Enhanced expression of organic anion transporting polypeptides (OATPs) in androgen receptor-positive prostate cancer cells: Possible role of OATP1A2 in adaptive cell growth under androgen-depleted conditions. *Biochem Pharmacol* 84 (8), pp.1070-1077.

Arrese, M. and Accatino, L. (2002). From blood to bile: recent advances in hepatobiliary transport. *Ann Hepatol* 1 (2), pp.64-71.

Bachmakov, I., Glaeser, H., Fromm, M. F. and Konig, J. (2008). Interaction of oral antidiabetic drugs with hepatic uptake transporters: focus on organic anion transporting polypeptides and organic cation transporter 1. *Diabetes* 57 (6), pp.1463-1469.

Badagnani, I., Castro, R. A., Taylor, T. R., Brett, C. M., Huang, C. C., Stryke, D., Kawamoto, M., Johns, S. J., Ferrin, T. E., Carlson, E. J., Burchard, E. G. and Giacomini, K. M. (2006). Interaction of methotrexate with organic-anion transporting polypeptide 1A2 and its genetic variants. *J Pharmacol Exp Ther* 318 (2), pp.521-529.

Bannai, H., Tamada, Y., Maruyama, O., Nakai, K. and Miyano, S. (2002). Extensive feature detection of N-terminal protein sorting signals. *Bioinformatics* 18 (2), pp.298-305.

Barabote, R. D., Tamang, D. G., Abeywardena, S. N., Fallah, N. S., Fu, J. Y., Lio, J. K., Mirhosseini, P., Pezeshk, R., Podell, S., Salampessy, M. L., Thever, M. D. and Saier, M. H., Jr. (2006). Extra domains in secondary transport carriers and channel proteins. *Biochim Biophys Acta* 1758 (10), pp.1557-1579.

Barnes, M. R. and Gray, I. C. (2003). Amino acid properties and consequences of substitutions. In: Betts, M. J. and Russell, R. B. (eds.) *Bioinformatics for Geneticists*. Chichester, UK: John Wiley and Sons.

Benson, D. A., Karsch-Mizrachi, I., Clark, K., Lipman, D. J., Ostell, J. and Sayers, E. W. (2012). GenBank. *Nucleic Acids Res* 40 (Database issue), pp.D48-53.

Bernsel, A., Viklund, H., Hennerdal, A. and Elofsson, A. (2009). TOPCONS: consensus prediction of membrane protein topology. *Nucleic Acids Res* 37 (Web Server issue), pp.W465-468.

Bleasby, K., Castle, J. C., Roberts, C. J., Cheng, C., Bailey, W. J., Sina, J. F., Kulkarni, A. V., Hafey, M. J., Evers, R., Johnson, J. M., Ulrich, R. G. and Slatter, J. G. (2006). Expression profiles of 50 xenobiotic transporter genes in humans and pre-clinical species: a resource for investigations into drug disposition. *Xenobiotica* 36 (10-11), pp.963-988.

Blott, E. J., Higgins, C. F. and Linton, K. J. (1999). Cysteine-scanning mutagenesis provides no evidence for the extracellular accessibility of the nucleotide-binding domains of the multidrug resistance transporter P-glycoprotein. *EMBO J* 18 (23), pp.6800-6808.

Boelsterli, U. A. and Lim, P. L. (2007). Mitochondrial abnormalities--a link to idiosyncratic drug hepatotoxicity? *Toxicol Appl Pharmacol* 220 (1), pp.92-107.

Bradford, J. (2001). *SIG-Pred: Signal Peptide Prediction.* MRes Thesis. University of Leeds.

Bradford, M. M. (1976). A rapid and sensitive method for the quantitation of microgram quantities of protein utilizing the principle of protein-dye binding. *Anal Biochem* 72, pp.248-254.

Brondyk, B. (1994). pCI and pSI Mammalian Expression Vectors. *Promega Notes* 49, pp.7-11.

Brone, B. and Eggermont, J. (2005). PDZ proteins retain and regulate membrane transporters in polarized epithelial cell membranes. *Am J Physiol Cell Physiol* 288 (1), pp.C20-29.

Brunham, L. R., Lansberg, P. J., Zhang, L., Miao, F., Carter, C., Hovingh, G. K., Visscher, H., Jukema, J. W., Stalenhoef, A. F., Ross, C. J., Carleton, B. C., Kastelein, J. J. and Hayden, M. R. (2011). Differential effect of the rs4149056 variant in SLCO1B1 on myopathy associated with simvastatin and atorvastatin. *Pharmacogenomics J* 12 (3), pp.233-237.

Buchman, A. R. and Berg, P. (1988). Comparison of intron-dependent and intron-independent gene expression. *Mol Cell Biol* 8 (10), pp.4395-4405.

Cai, S. Y., Wang, W., Soroka, C. J., Ballatori, N. and Boyer, J. L. (2002a). An evolutionarily ancient Oatp: insights into conserved functional domains of these proteins. *American Journal of Physiology-Gastrointestinal and Liver Physiology* 282 (4), pp.G702-G710.

Cai, S. Y., Wang, W., Soroka, C. J., Ballatori, N. and Boyer, J. L. (2002b). An evolutionarily ancient Oatp: insights into conserved functional domains of these proteins. *Am J Physiol Gastrointest Liver Physiol* 282 (4), pp.G702-710.

Campbell, S. D., de Morais, S. M. and Xu, J. J. (2004). Inhibition of human organic anion transporting polypeptide OATP 1B1 as a mechanism of drug-induced hyperbilirubinemia. *Chem Biol Interact* 150 (2), pp.179-187.

Chandra, P. and Brouwer, K. L. (2004). The complexities of hepatic drug transport: current knowledge and emerging concepts. *Pharm Res* 21 (5), pp.719-735.

Chang, C., Pang, K. S., Swaan, P. W. and Ekins, S. (2005). Comparative pharmacophore modeling of organic anion transporting polypeptides: a meta-analysis of rat Oatp1a1 and human OATP1B1. *J Pharmacol Exp Ther* 314 (2), pp.533-541.

Chen, C., Mireles, R. J., Campbell, S. D., Lin, J., Mills, J. B., Xu, J. J. and Smolarek, T. A. (2005). Differential interaction of 3-hydroxy-3-methylglutaryl-coa reductase inhibitors with ABCB1, ABCC2, and OATP1B1. *Drug Metab Dispos* 33 (4), pp.537-546.

Chen, C., Stock, J. L., Liu, X., Shi, J., Van Deusen, J. W., DiMattia, D. A., Dullea, R. G. and de Morais, S. M. (2008). Utility of a novel Oatp1b2 knockout mouse model for evaluating the role of Oatp1b2 in the hepatic uptake of model compounds. *Drug Metab Dispos* 36 (9), pp.1840-1845.

Cheng, X. and Klaassen, C. D. (2009). Tissue distribution, ontogeny, and hormonal regulation of xenobiotic transporters in mouse kidneys. *Drug Metab Dispos* 37 (11), pp.2178-2185.

Cheng, X., Maher, J., Dieter, M. Z. and Klaassen, C. D. (2005). Regulation of mouse organic anion-transporting polypeptides (Oatps) in liver by prototypical microsomal enzyme inducers that activate distinct transcription factor pathways. *Drug Metab Dispos* 33 (9), pp.1276-1282.

Cheung, J. C. and Reithmeier, R. A. (2007). Scanning N-glycosylation mutagenesis of membrane proteins. *Methods* 41 (4), pp.451-459.

Chew, S. C., Sandanaraj, E., Singh, O., Chen, X., Tan, E. H., Lim, W. T., Lee, E. J. and Chowbay, B. (2011). Influence of SLCO1B3 haplotype-tag SNPs on docetaxel disposition in Chinese nasopharyngeal cancer patients. *Br J Clin Pharmacol* 73 (4), pp.606-618.

Chigutsa, E., Visser, M. E., Swart, E. C., Denti, P., Pushpakom, S., Egan, D., Holford, N. H., Smith, P. J., Maartens, G., Owen, A. and McIlleron, H. (2011). The SLCO1B1 rs4149032 polymorphism is highly prevalent in South Africans and is associated with reduced rifampin concentrations: dosing implications. *Antimicrob Agents Chemother* 55 (9), pp.4122-4127.

Choi, J. H., Murray, J. W. and Wolkoff, A. W. (2011). PDZK1 binding and serine phosphorylation regulate subcellular trafficking of organic anion transport protein 1a1. *Am J Physiol Gastrointest Liver Physiol* 300 (3), pp.G384-393.

Clark, E. H., East, J. M. and Lee, A. G. (2003). The role of tryptophan residues in an integral membrane protein: diacylglycerol kinase. *Biochemistry* 42 (37), pp.11065-11073.

Cooper, G. M. (2000). *The Cell: A Molecular Approach.* 2nd ed. Sunderland (MA): Sinauer Associates.

Covitz, K. M., Amidon, G. L. and Sadee, W. (1998). Membrane topology of the human dipeptide transporter, hPEPT1, determined by epitope insertions. *Biochemistry* 37 (43), pp.15214-15221.

Cui, Y., Konig, J., Leier, I., Buchholz, U. and Keppler, D. (2001). Hepatic uptake of bilirubin and its conjugates by the human organic anion transporter SLC21A6. *J Biol Chem* 276 (13), pp.9626-9630.

Cvetkovic, M., Leake, B., Fromm, M. F., Wilkinson, G. R. and Kim, R. B. (1999). OATP and P-glycoprotein transporters mediate the cellular uptake and excretion of fexofenadine. *Drug Metab Dispos* 27 (8), pp.866-871.

Davis, M. J., Zhang, F., Yuan, Z. and Teasdale, R. D. (2006). MemO: a consensus approach to the annotation of a protein's membrane organization. *In Silico Biol* 6 (5), pp.387-399.

Davis, M. W. (2012). *A Plasmid Editor (ApE). University of Utah.* Available at: http://biologylabs.utah.edu/jorgensen/wayned/ape/ (Accessed: 14th June 2012).

DeGorter, M. K., Ho, R. H., Leake, B. F., Tirona, R. G. and Kim, R. B. (2012). Interaction of three regiospecific amino acid residues is required for OATP1B1 gain of OATP1B3 substrate specificity. *Mol Pharm* 9 (4), pp.986-995.

DeLano, W. L. (2002). *The PyMOL Molecular Graphics System.* . DeLano Scientific, San Carlos, CA, USA. Available at: http://www.pymol.org (Accessed: 20th December 2012).

Dominguez, I., Itoh, K. and Sokol, S. Y. (1995). Role of glycogen synthase kinase 3 beta as a negative regulator of dorsoventral axis formation in Xenopus embryos. *Proc Natl Acad Sci U S A* 92 (18), pp.8498-8502.

Dresser, G. K., Bailey, D. G., Leake, B. F., Schwarz, U. I., Dawson, P. A., Freeman, D. J. and Kim, R. B. (2002). Fruit juices inhibit organic anion transporting polypeptide-mediated drug uptake to decrease the oral availability of fexofenadine. *Clin Pharmacol Ther* 71 (1), pp.11-20.

Eckhardt, U., Schroeder, A., Stieger, B., Hochli, M., Landmann, L., Tynes, R., Meier, P. J. and Hagenbuch, B. (1999). Polyspecific substrate uptake by the hepatic organic anion transporter Oatp1 in stably transfected CHO cells. *Am J Physiol* 276 (4 Pt 1), pp.G1037-1042.

Eiden, L. E., Schafer, M. K., Weihe, E. and Schutz, B. (2004). The vesicular amine transporter family (SLC18): amine/proton antiporters required for vesicular accumulation and regulated exocytotic secretion of monoamines and acetylcholine. *Pflugers Arch* 447 (5), pp.636-640.

Eloranta, J. J. and Kullak-Ublick, G. A. (2008). The role of FXR in disorders of bile acid homeostasis. *Physiology (Bethesda)* 23, pp.286-295.

Fallingborg, J. (1999). Intraluminal pH of the human gastrointestinal tract. *Dan Med Bull* 46 (3), pp.183-196.

Fariselli, P., Finocchiaro, G. and Casadio, R. (2003). SPEPlip: the detection of signal peptide and lipoprotein cleavage sites. *Bioinformatics* 19 (18), pp.2498-2499.

Fischer, A., Hoeger, S. J., Stemmer, K., Feurstein, D. J., Knobeloch, D., Nussler, A. and Dietrich, D. R. (2010). The role of organic anion transporting polypeptides (OATPs/SLCOs) in the toxicity of different microcystin congeners in vitro: a comparison of primary human hepatocytes and OATP-transfected HEK293 cells. *Toxicol Appl Pharmacol* 245 (1), pp.9-20.

Fischer, W. J., Altheimer, S., Cattori, V., Meier, P. J., Dietrich, D. R. and Hagenbuch, B. (2005). Organic anion transporting polypeptides expressed in liver and brain mediate uptake of microcystin. *Toxicol Appl Pharmacol* 203 (3), pp.257-263.

Franke, R. M., Scherkenbach, L. A. and Sparreboom, A. (2009). Pharmacogenetics of the organic anion transporting polypeptide 1A2. *Pharmacogenomics* 10 (3), pp.339-344.

Frisk, A. R., Diding, N. and Wallmark, G. (1952). Influence of probenecid on serum penicillin concentration after oral administration of penicillin. *Scand J Clin Lab Invest* 4 (2), pp.83-88.

Fuchikami, H., Satoh, H., Tsujimoto, M., Ohdo, S., Ohtani, H. and Sawada, Y. (2006). Effects of herbal extracts on the function of human organic anion-transporting polypeptide OATP-B. *Drug Metab Dispos* 34 (4), pp.577-582.

Fujiwara, K., Adachi, H., Nishio, T., Unno, M., Tokui, T., Okabe, M., Onogawa, T., Suzuki, T., Asano, N., Tanemoto, M., Seki, M., Shiiba, K., Suzuki, M., Kondo, Y., Nunoki, K., Shimosegawa, T., Iinuma, K., Ito, S., Matsuno, S. and Abe, T. (2001). Identification of thyroid hormone transporters in humans: different molecules are involved in a tissue-specific manner. *Endocrinology* 142 (5), pp.2005-2012.

Gao, B., Hagenbuch, B., Kullak-Ublick, G. A., Benke, D., Aguzzi, A. and Meier, P. J. (2000). Organic anion-transporting polypeptides mediate transport of opioid peptides across blood-brain barrier. *J Pharmacol Exp Ther* 294 (1), pp.73-79.

Gao, B., Huber, R. D., Wenzel, A., Vavricka, S. R., Ismair, M. G., Reme, C. and Meier, P. J. (2005). Localization of organic anion transporting polypeptides in the rat and human ciliary body epithelium. *Exp Eye Res* 80 (1), pp.61-72.

Geyer, J., Doring, B., Failing, K. and Petzinger, E. (2004). Molecular cloning and functional characterization of the bovine (Bos taurus) organic anion transporting polypeptide Oatp1a2 (Slco1a2). *Comp Biochem Physiol B Biochem Mol Biol* 137 (3), pp.317-329.

Gibson, G. G. and Skett, P. (2001). *Introduction to Drug Metabolism.* 3rd ed. Cheltenham, UK: Nelson Thornes.

Glaeser, H., Bailey, D. G., Dresser, G. K., Gregor, J. C., Schwarz, U. I., McGrath, J. S., Jolicoeur, E., Lee, W., Leake, B. F., Tirona, R. G. and Kim, R. B. (2007). Intestinal drug transporter expression and the impact of grapefruit juice in humans. *Clin Pharmacol Ther* 81 (3), pp.362-370.

Glaeser, H., Mandery, K., Sticht, H., Fromm, M. F. and Konig, J. (2010). Relevance of conserved lysine and arginine residues in transmembrane helices

for the transport activity of organic anion transporting polypeptide 1B3. *Br J Pharmacol* 159 (3), pp.698-708.

Glavy, J. S., Wu, S. M., Wang, P. J., Orr, G. A. and Wolkoff, A. W. (2000). Down-regulation by extracellular ATP of rat hepatocyte organic anion transport is mediated by serine phosphorylation of oatp1. *J Biol Chem* 275 (2), pp.1479-1484.

Gomi, M., Sonoyama, M. and Mitaku, S. (2004). High performance system for signal peptide prediction: SOSUIsignal. *Chem-Bio Informatics* 4 (4), pp.142-147.

Granseth, E., Viklund, H. and Elofsson, A. (2006). ZPRED: predicting the distance to the membrane center for residues in alpha-helical membrane proteins. *Bioinformatics* 22 (14), pp.e191-196.

Gui, C. and Hagenbuch, B. (2008). Amino acid residues in transmembrane domain 10 of organic anion transporting polypeptide 1B3 are critical for cholecystokinin octapeptide transport. *Biochemistry* 47 (35), pp.9090-9097.

Gui, C. and Hagenbuch, B. (2009). Role of transmembrane domain 10 for the function of organic anion transporting polypeptide 1B1. *Protein Sci* 18 (11), pp.2298-2306.

Gui, C., Miao, Y., Thompson, L., Wahlgren, B., Mock, M., Stieger, B. and Hagenbuch, B. (2008). Effect of pregnane X receptor ligands on transport mediated by human OATP1B1 and OATP1B3. *Eur J Pharmacol* 584 (1), pp.57-65.

Guo, G. L. and Klaassen, C. D. (2001). Protein kinase C suppresses rat organic anion transporting polypeptide 1- and 2-mediated uptake. *J Pharmacol Exp Ther* 299 (2), pp.551-557.

Guo, Y., Smith, K. and Petris, M. J. (2004). Cisplatin stabilizes a multimeric complex of the human Ctr1 copper transporter: requirement for the extracellular methionine-rich clusters. *J Biol Chem* 279 (45), pp.46393-46399.

Gurdon, J. B., Lingrel, J. B. and Marbaix, G. (1973). Message stability in injected frog oocytes: long life of mammalian alpha and beta globin messages. *J Mol Biol* 80 (3), pp.539-551.

Hagenbuch, B. (2007). Cellular entry of thyroid hormones by organic anion transporting polypeptides. *Best Pract Res Clin Endocrinol Metab* 21 (2), pp.209-221.

Hagenbuch, B. (2010). Drug uptake systems in liver and kidney: a historic perspective. *Clin Pharmacol Ther* 87 (1), pp.39-47.

Hagenbuch, B. and Gui, C. (2008). Xenobiotic transporters of the human organic anion transporting polypeptides (OATP) family. *Xenobiotica* 38 (7-8), pp.778-801.

Hagenbuch, B. and Meier, P. J. (2004). Organic anion transporting polypeptides of the OATP/ SLC21 family: phylogenetic classification as OATP/ SLCO superfamily, new nomenclature and molecular/functional properties. *Pflugers Arch* 447 (5), pp.653-665.

Hagenbuch, B. M., P. J. (2003). The superfamily of organic anion transporting polypeptides. *Biochim Biophys Acta* 1609 (1), pp.1-18.

Hamada, A., Sissung, T., Price, D. K., Danesi, R., Chau, C. H., Sharifi, N., Venzon, D., Maeda, K., Nagao, K., Sparreboom, A., Mitsuya, H., Dahut, W. L. and Figg, W. D. (2008). Effect of SLCO1B3 haplotype on testosterone transport and clinical outcome in caucasian patients with androgen-independent prostatic cancer. *Clin Cancer Res* 14 (11), pp.3312-3318.

Hanafy, F., El-Kadi, A. O. S. and Jamali, F. (2012). Effect of Inflammation on Molecular Targets and Drug Transporters. *Journal of Pharmacy and Pharmaceutical Sciences* 15 (3), pp.361-375.

Hanggi, E., Grundschober, A. F., Leuthold, S., Meier, P. J. and St-Pierre, M. V. (2006). Functional analysis of the extracellular cysteine residues in the human organic anion transporting polypeptide, OATP2B1. *Mol Pharmacol* 70 (3), pp.806-817.

Hartkoorn, R. C., Kwan, W. S., Shallcross, V., Chaikan, A., Liptrott, N., Egan, D., Sora, E. S., James, C. E., Gibbons, S., Bray, P. G., Back, D. J., Khoo, S. H. and Owen, A. (2010). HIV protease inhibitors are substrates for OATP1A2, OATP1B1 and OATP1B3 and lopinavir plasma concentrations are influenced by SLCO1B1 polymorphisms. *Pharmacogenet Genomics* 20 (2), pp.112-120.

He, L., Vasiliou, K. and Nebert, D. W. (2009). Analysis and update of the human solute carrier (SLC) gene superfamily. *Hum Genomics* 3 (2), pp.195-206.

Heckman, K. L. and Pease, L. R. (2007). Gene splicing and mutagenesis by PCR-driven overlap extension. *Nat Protoc* 2 (4), pp.924-932.

Hediger, M. A., Romero, M. F., Peng, J. B., Rolfs, A., Takanaga, H. and Bruford, E. A. (2004). The ABCs of solute carriers: physiological, pathological and therapeutic implications of human membrane transport proteins. *Pflugers Arch* 447 (5), pp.465-468.

Heikkila, J. J., Kaldis, A., Morrow, G. and Tanguay, R. M. (2007). The use of the Xenopus oocyte as a model system to analyze the expression and function of eukaryotic heat shock proteins. *Biotechnol Adv* 25 (4), pp.385-395.

Hiller, K., Grote, A., Scheer, M., Munch, R. and Jahn, D. (2004). PrediSi: prediction of signal peptides and their cleavage positions. *Nucleic Acids Res* 32 (Web Server issue), pp.W375-379.

Hirano, M., Maeda, K., Shitara, Y. and Sugiyama, Y. (2004). Contribution of OATP2 (OATP1B1) and OATP8 (OATP1B3) to the hepatic uptake of pitavastatin in humans. *J Pharmacol Exp Ther* 311 (1), pp.139-146.

Hirano, M., Maeda, K., Shitara, Y. and Sugiyama, Y. (2006). Drug-drug interaction between pitavastatin and various drugs via OATP1B1. *Drug Metab Dispos* 34 (7), pp.1229-1236.

Hirokawa, T., Boon-Chieng, S. and Mitaku, S. (1998). SOSUI: classification and secondary structure prediction system for membrane proteins. *Bioinformatics* 14 (4), pp.378-379.

Hofman, K. and Stoffel, W. (1993). Tmbase: a database of membrane spanning protein segments. *Biological Chemistry Hoppe Seyler* 374, pp.166-173.

Hsiang, B., Zhu, Y., Wang, Z., Wu, Y., Sasseville, V., Yang, W. P. and Kirchgessner, T. G. (1999). A novel human hepatic organic anion transporting polypeptide (OATP2). Identification of a liver-specific human organic anion transporting polypeptide and identification of rat and human hydroxymethylglutaryl-CoA reductase inhibitor transporters. *J Biol Chem* 274 (52), pp.37161-37168.

Hsu, A., Granneman, G. R., Cao, G., Carothers, L., el-Shourbagy, T., Baroldi, P., Erdman, K., Brown, F., Sun, E. and Leonard, J. M. (1998). Pharmacokinetic interactions between two human immunodeficiency virus protease inhibitors, ritonavir and saquinavir. *Clin Pharmacol Ther* 63 (4), pp.453-464.

Hu, S., Franke, R. M., Filipski, K. K., Hu, C., Orwick, S. J., de Bruijn, E. A., Burger, H., Baker, S. D. and Sparreboom, A. (2008). Interaction of imatinib with human organic ion carriers. *Clin Cancer Res* 14 (10), pp.3141-3148.

Huang, S. M., Zhang, L. and Giacomini, K. M. (2010). The International Transporter Consortium: a collaborative group of scientists from academia, industry, and the FDA. *Clin Pharmacol Ther* 87 (1), pp.32-36.

Huang, Y., Lemieux, M. J., Song, J., Auer, M. and Wang, D. N. (2003). Structure and mechanism of the glycerol-3-phosphate transporter from Escherichia coli. *Science* 301 (5633), pp.616-620.

Ismair, M. G., Stieger, B., Cattori, V., Hagenbuch, B., Fried, M., Meier, P. J. and Kullak-Ublick, G. A. (2001). Hepatic uptake of cholecystokinin octapeptide by organic anion-transporting polypeptides OATP4 and OATP8 of rat and human liver. *Gastroenterology* 121 (5), pp.1185-1190.

Iwai, M., Suzuki, H., Ieiri, I., Otsubo, K. and Sugiyama, Y. (2004). Functional analysis of single nucleotide polymorphisms of hepatic organic anion transporter OATP1B1 (OATP-C). *Pharmacogenetics* 14 (11), pp.749-757.

Jacquemin, E., Hagenbuch, B., Stieger, B., Wolkoff, A. W. and Meier, P. J. (1994). Expression cloning of a rat liver Na(+)-independent organic anion transporter. *Proc Natl Acad Sci U S A* 91 (1), pp.133-137.

Janneh, O., Hartkoorn, R. C., Jones, E., Owen, A., Ward, S. A., Davey, R., Back, D. J. and Khoo, S. H. (2008). Cultured CD4T cells and primary human lymphocytes express hOATPs: intracellular accumulation of saquinavir and lopinavir. *Br J Pharmacol* 155 (6), pp.875-883.

Jigorel, E., Le Vee, M., Boursier-Neyret, C., Bertrand, M. and Fardel, O. (2005). Functional expression of sinusoidal drug transporters in primary human and rat hepatocytes. *Drug Metab Dispos* 33 (10), pp.1418-1422.

Jones, D. T. (2007). Improving the accuracy of transmembrane protein topology prediction using evolutionary information. *Bioinformatics* 23 (5), pp.538-544.

Jonson, P. H. and Petersen, S. B. (2001). A critical view on conservative mutations. *Protein Eng* 14 (6), pp.397-402.

Jung, D., Hagenbuch, B., Gresh, L., Pontoglio, M., Meier, P. J. and Kullak-Ublick, G. A. (2001). Characterization of the human OATP-C (SLC21A6) gene promoter and regulation of liver-specific OATP genes by hepatocyte nuclear factor 1 alpha. *J Biol Chem* 276 (40), pp.37206-37214.

Juretic, D., Zoranic, L. and Zucic, D. (2002). Basic charge clusters and predictions of membrane protein topology. *J Chem Inf Comput Sci* 42 (3), pp.620-632.

Kall, L., Krogh, A. and Sonnhammer, E. L. (2004). A combined transmembrane topology and signal peptide prediction method. *J Mol Biol* 338 (5), pp.1027-1036.

Kall, L., Krogh, A. and Sonnhammer, E. L. (2007). Advantages of combined transmembrane topology and signal peptide prediction--the Phobius web server. *Nucleic Acids Res* 35 (Web Server issue), pp.W429-432.

Kalliokoski, A. and Niemi, M. (2009). Impact of OATP transporters on pharmacokinetics. *Br J Pharmacol* 158 (3), pp.693-705.

Kameyama, Y., Yamashita, K., Kobayashi, K., Hosokawa, M. and Chiba, K. (2005). Functional characterization of SLCO1B1 (OATP-C) variants, SLCO1B1*5, SLCO1B1*15 and SLCO1B1*15+C1007G, by using transient expression systems of HeLa and HEK293 cells. *Pharmacogenet Genomics* 15 (7), pp.513-522.

Karlgren, M., Vildhede, A., Norinder, U., Wisniewski, J. R., Kimoto, E., Lai, Y., Haglund, U. and Artursson, P. (2012). Classification of inhibitors of hepatic organic anion transporting polypeptides (OATPs): influence of protein expression on drug-drug interactions. *J Med Chem* 55 (10), pp.4740-4763.

Karlin, A. and Akabas, M. H. (1998). Substituted-cysteine accessibility method. *Methods Enzymol* 293, pp.123-145.

Kato, Y., Yoshida, K., Watanabe, C., Sai, Y. and Tsuji, A. (2004). Screening of the interaction between xenobiotic transporters and PDZ proteins. *Pharm Res* 21 (10), pp.1886-1894.

Kelley, L. A. and Sternberg, M. J. (2009). Protein structure prediction on the Web: a case study using the Phyre server. *Nat Protoc* 4 (3), pp.363-371.

Kempf, D. J., Marsh, K. C., Kumar, G., Rodrigues, A. D., Denissen, J. F., McDonald, E., Kukulka, M. J., Hsu, A., Granneman, G. R., Baroldi, P. A., Sun, E., Pizzuti, D., Plattner, J. J., Norbeck, D. W. and Leonard, J. M. (1997). Pharmacokinetic enhancement of inhibitors of the human immunodeficiency virus protease by coadministration with ritonavir. *Antimicrob Agents Chemother* 41 (3), pp.654-660.

Kibbe, W. A. (2007). OligoCalc: an online oligonucleotide properties calculator. *Nucleic Acids Res* 35 (Web Server issue), pp.W43-46.

Kihara, D., Shimizu, T. and Kanehisa, M. (1998). Prediction of membrane proteins based on classification of transmembrane segments. *Protein Eng* 11 (11), pp.961-970.

Kimoto, E., Chupka, J., Xiao, Y., Bi, Y. A. and Duignan, D. B. (2011). Characterization of digoxin uptake in sandwich-cultured human hepatocytes. *Drug Metab Dispos* 39 (1), pp.47-53.

Kindla, J., Muller, F., Mieth, M., Fromm, M. F. and Konig, J. (2011a). Influence of non-steroidal anti-inflammatory drugs on organic anion transporting polypeptide (OATP) 1B1- and OATP1B3-mediated drug transport. *Drug Metab Dispos* 39 (6), pp.1047-1053.

Kindla, J., Rau, T. T., Jung, R., Fasching, P. A., Strick, R., Stoehr, R., Hartmann, A., Fromm, M. F. and Konig, J. (2011b). Expression and localization of the uptake transporters OATP2B1, OATP3A1 and OATP5A1 in non-malignant and malignant breast tissue. *Cancer Biol Ther* 11 (6), pp.584-591.

Kirk, P., Wilson, M. C., Heddle, C., Brown, M. H., Barclay, A. N. and Halestrap, A. P. (2000). CD147 is tightly associated with lactate transporters MCT1 and MCT4 and facilitates their cell surface expression. *EMBO J* 19 (15), pp.3896-3904.

Kobayashi, D., Nozawa, T., Imai, K., Nezu, J., Tsuji, A. and Tamai, I. (2003). Involvement of human organic anion transporting polypeptide OATP-B (SLC21A9) in pH-dependent transport across intestinal apical membrane. *J Pharmacol Exp Ther* 306 (2), pp.703-708.

Kock, K., Koenen, A., Giese, B., Fraunholz, M., May, K., Siegmund, W., Hammer, E., Volker, U., Jedlitschky, G., Kroemer, H. K. and Grube, M. (2010). Rapid modulation of the organic anion transporting polypeptide 2B1 (OATP2B1, SLCO2B1) function by protein kinase C-mediated internalization. *J Biol Chem* 285 (15), pp.11336-11347.

Kohlrausch, F. B., de Cassia Estrela, R., Barroso, P. F. and Suarez-Kurtz, G. (2010). The impact of SLCO1B1 polymorphisms on the plasma concentration of lopinavir and ritonavir in HIV-infected men. *Br J Clin Pharmacol* 69 (1), pp.95-98.

Konig, J., Cui, Y., Nies, A. T. and Keppler, D. (2000a). Localization and genomic organization of a new hepatocellular organic anion transporting polypeptide. *J Biol Chem* 275 (30), pp.23161-23168.

Konig, J., Cui, Y., Nies, A. T. and Keppler, D. (2000b). A novel human organic anion transporting polypeptide localized to the basolateral hepatocyte membrane. *Am J Physiol Gastrointest Liver Physiol* 278 (1), pp.G156-164.

Koopen, N. R., Wolters, H., Muller, M., Schippers, I. J., Havinga, R., Roelofsen, H., Vonk, R. J., Stieger, B., Meier, P. J. and Kuipers, F. (1997). Hepatic bile salt flux does not modulate level and activity of the sinusoidal Na+-taurocholate cotransporter (ntcp) in rats. *J Hepatol* 27 (4), pp.699-706.

Kounnis, V., Ioachim, E., Svoboda, M., Tzakos, A., Sainis, I., Thalhammer, T., Steiner, G. and Briasoulis, E. (2011). Expression of organic anion-transporting polypeptides 1B3, 1B1, and 1A2 in human pancreatic cancer reveals a new class of potential therapeutic targets. *Onco Targets Ther* 4, pp.27-32.

Kozak, M. (1991). An analysis of vertebrate mRNA sequences: intimations of translational control. *J Cell Biol* 115 (4), pp.887-903.

Krogh, A., Larsson, B., von Heijne, G. and Sonnhammer, E. L. (2001). Predicting transmembrane protein topology with a hidden Markov model: application to complete genomes. *J Mol Biol* 305 (3), pp.567-580.

Krumpochova, P., Sapthu, S., Brouwers, J. F., de Haas, M., de Vos, R., Borst, P. and van de Wetering, K. (2012). Transportomics: screening for substrates of ABC transporters in body fluids using vesicular transport assays. *FASEB J* 26 (2), pp.738-747.

Kullak-Ublick, G. A., Beuers, U. and Paumgartner, G. (1996). Molecular and functional characterization of bile acid transport in human hepatoblastoma HepG2 cells. *Hepatology* 23 (5), pp.1053-1060.

Kullak-Ublick, G. A., Hagenbuch, B., Stieger, B., Schteingart, C. D., Hofmann, A. F., Wolkoff, A. W. and Meier, P. J. (1995). Molecular and functional characterization of an organic anion transporting polypeptide cloned from human liver. *Gastroenterology* 109 (4), pp.1274-1282.

Kullak-Ublick, G. A., Ismair, M. G., Stieger, B., Landmann, L., Huber, R., Pizzagalli, F., Fattinger, K., Meier, P. J. and Hagenbuch, B. (2001). Organic anion-transporting polypeptide B (OATP-B) and its functional comparison with three other OATPs of human liver. *Gastroenterology* 120 (2), pp.525-533.

Kullak-Ublick, G. A., Stieger, B. and Meier, P. J. (2004). Enterohepatic bile salt transporters in normal physiology and liver disease. *Gastroenterology* 126 (1), pp.322-342.

Kuo, K. L., Zhu, H., McNamara, P. J. and Leggas, M. (2012). Localization and functional characterization of the rat Oatp4c1 transporter in an in vitro cell system and rat tissues. *PLoS One* 7 (6), p.e39641.

Kurschat, C. E., Shmukler, B. E., Jiang, L., Wilhelm, S., Kim, E. H., Chernova, M. N., Kinne, R. K., Stewart, A. K. and Alper, S. L. (2006). Alkaline-shifted pHo sensitivity of AE2c1-mediated anion exchange reveals novel regulatory determinants in the AE2 N-terminal cytoplasmic domain. *J Biol Chem* 281 (4), pp.1885-1896.

Larkin, M. A., Blackshields, G., Brown, N. P., Chenna, R., McGettigan, P. A., McWilliam, H., Valentin, F., Wallace, I. M., Wilm, A., Lopez, R., Thompson, J. D., Gibson, T. J. and Higgins, D. G. (2007). Clustal W and Clustal X version 2.0. *Bioinformatics* 23 (21), pp.2947-2948.

Lee, S. Y., Williamson, B., Caballero, O. L., Chen, Y. T., Scanlan, M. J., Ritter, G., Jongeneel, C. V., Simpson, A. J. and Old, L. J. (2004). Identification of the gonad-specific anion transporter SLCO6A1 as a cancer/testis (CT) antigen expressed in human lung cancer. *Cancer Immun* 4, p.13.

Lee, T. K., Koh, A. S., Cui, Z., Pierce, R. H. and Ballatori, N. (2003). N-glycosylation controls functional activity of Oatp1, an organic anion transporter. *Am J Physiol Gastrointest Liver Physiol* 285 (2), pp.G371-381.

Lee, W., Glaeser, H., Smith, L. H., Roberts, R. L., Moeckel, G. W., Gervasini, G., Leake, B. F. and Kim, R. B. (2005). Polymorphisms in human organic anion-transporting polypeptide 1A2 (OATP1A2): implications for altered drug disposition and central nervous system drug entry. *J Biol Chem* 280 (10), pp.9610-9617.

Letschert, K., Komatsu, M., Hummel-Eisenbeiss, J. and Keppler, D. (2005). Vectorial transport of the peptide CCK-8 by double-transfected MDCKII cells stably expressing the organic anion transporter OATP1B3 (OATP8) and the export pump ABCC2. *J Pharmacol Exp Ther* 313 (2), pp.549-556.

Leuthold, S., Hagenbuch, B., Mohebbi, N., Wagner, C. A., Meier, P. J. and Stieger, B. (2009). Mechanisms of pH-gradient driven transport mediated by organic anion polypeptide transporters. *Am J Physiol Cell Physiol* 296 (3), pp.C570-582.

Li, L., Lee, T. K., Meier, P. J. and Ballatori, N. (1998). Identification of glutathione as a driving force and leukotriene C4 as a substrate for oatp1, the hepatic sinusoidal organic solute transporter. *J Biol Chem* 273 (26), pp.16184-16191.

Li, N., Hong, W., Huang, H., Lu, H., Lin, G. and Hong, M. (2012). Identification of amino acids essential for estrone-3-sulfate transport within transmembrane domain 2 of organic anion transporting polypeptide 1B1. *PLoS One* 7 (5), p.e36647.

Lieberman, M. and Marks, A. D. (2012). *Marks' Basic Medical Biochemistry.* 4th ed. Philadelphia: Lippincott, Williams & Wilkins.

Liedauer, R., Svoboda, M., Wlcek, K., Arrich, F., Ja, W., Toma, C. and Thalhammer, T. (2009). Different expression patterns of organic anion transporting polypeptides in osteosarcomas, bone metastases and aneurysmal bone cysts. *Oncol Rep* 22 (6), pp.1485-1492.

Lin, J. H. (2003). Drug-drug interaction mediated by inhibition and induction of P-glycoprotein. *Adv Drug Deliv Rev* 55 (1), pp.53-81.

Lockhart, A. C., Harris, E., Lafleur, B. J., Merchant, N. B., Washington, M. K., Resnick, M. B., Yeatman, T. J. and Lee, W. (2008). Organic anion transporting polypeptide 1B3 (OATP1B3) is overexpressed in colorectal tumors and is a predictor of clinical outcome. *Clin Exp Gastroenterol* 1, pp.1-7.

Lodish, H., Berk, A. and Zipursky, S. L. (2000). *Molecular Cell Biology.* New York: W. H Freeman.

Lu, W. J., Tamai, I., Nezu, J., Lai, M. L. and Huang, J. D. (2006). Organic anion transporting polypeptide-C mediates arsenic uptake in HEK-293 cells. *J Biomed Sci* 13 (4), pp.525-533.

Luo, Y., Vassilev, P. M., Li, X., Kawanabe, Y. and Zhou, J. (2003). Native polycystin 2 functions as a plasma membrane Ca2+-permeable cation channel in renal epithelia. *Mol Cell Biol* 23 (7), pp.2600-2607.

MacLennan, A. H., Wilson, D. H. and Taylor, A. W. (2002). The escalating cost and prevalence of alternative medicine. *Prev Med* 35 (2), pp.166-173.

Mahagita, C., Grassl, S. M., Piyachaturawat, P. and Ballatori, N. (2007). Human organic anion transporter 1B1 and 1B3 function as bidirectional carriers and do not mediate GSH-bile acid cotransport. *Am J Physiol Gastrointest Liver Physiol* 293 (1), pp.G271-278.

Mahon, M. J. (2011). Vectors bicistronically linking a gene of interest to the SV40 large T antigen in combination with the SV40 origin of replication enhance transient protein expression and luciferase reporter activity. *Biotechniques* 51 (2), pp.119-128.

Mandery, K., Bujok, K., Schmidt, I., Keiser, M., Siegmund, W., Balk, B., Konig, J., Fromm, M. F. and Glaeser, H. (2010). Influence of the flavonoids apigenin, kaempferol, and quercetin on the function of organic anion transporting polypeptides 1A2 and 2B1. *Biochem Pharmacol* 80 (11), pp.1746-1753.

Mandery, K., Sticht, H., Bujok, K., Schmidt, I., Fahrmayr, C., Balk, B., Fromm, M. F. and Glaeser, H. (2011). Functional and structural relevance of conserved positively charged lysine residues in organic anion transporting polypeptide 1B3. *Mol Pharmacol* 80 (3), pp.400-406.

Martinez-Becerra, P., Briz, O., Romero, M. R., Macias, R. I., Perez, M. J., Sancho-Mateo, C., Lostao, M. P., Fernandez-Abalos, J. M. and Marin, J. J. (2011). Further characterization of the electrogenicity and pH sensitivity of the human organic anion-transporting polypeptides OATP1B1 and OATP1B3. *Mol Pharmacol* 79 (3), pp.596-607.

Masuda, S., Ibaramoto, K., Takeuchi, A., Saito, H., Hashimoto, Y. and Inui, K. I. (1999). Cloning and functional characterization of a new multispecific organic anion transporter, OAT-K2, in rat kidney. *Mol Pharmacol* 55 (4), pp.743-752.

Meier-Abt, F., Faulstich, H. and Hagenbuch, B. (2004). Identification of phalloidin uptake systems of rat and human liver. *Biochim Biophys Acta* 1664 (1), pp.64-69.

Meier-Abt, F., Mokrab, Y. and Mizuguchi, K. (2005). Organic anion transporting polypeptides of the OATP/SLCO superfamily: identification of new members in nonmammalian species, comparative modeling and a potential transport mode. *J Membr Biol* 208 (3), pp.213-227.

Meier, P. J., Eckhardt, U., Schroeder, A., Hagenbuch, B. and Stieger, B. (1997). Substrate specificity of sinusoidal bile acid and organic anion uptake systems in rat and human liver. *Hepatology* 26 (6), pp.1667-1677.

Meredith, D. and Laynes, R. W. (1996). Dipeptide transport in brush-border membrane vesicles (BBMV) prepared from human full-term placentae. *Placenta* 17 (2-3), pp.173-179.

Meredith, D. and Price, R. A. (2006). Molecular modeling of PepT1-towards a structure. *J Membr Biol* 213 (2), pp.79-88.

Meyer zu Schwabedissen, H. E., Tirona, R. G., Yip, C. S., Ho, R. H. and Kim, R. B. (2008). Interplay between the nuclear receptor pregnane X receptor and

the uptake transporter organic anion transporter polypeptide 1A2 selectively enhances estrogen effects in breast cancer. *Cancer Res* 68 (22), pp.9338-9347.

Mikkaichi, T., Suzuki, T., Onogawa, T., Tanemoto, M., Mizutamari, H., Okada, M., Chaki, T., Masuda, S., Tokui, T., Eto, N., Abe, M., Satoh, F., Unno, M., Hishinuma, T., Inui, K., Ito, S., Goto, J. and Abe, T. (2004). Isolation and characterization of a digoxin transporter and its rat homologue expressed in the kidney. *Proc Natl Acad Sci U S A* 101 (10), pp.3569-3574.

Miyagawa, M., Maeda, K., Aoyama, A. and Sugiyama, Y. (2009). The eighth and ninth transmembrane domains in organic anion transporting polypeptide 1B1 affect the transport kinetics of estrone-3-sulfate and estradiol-17beta-D-glucuronide. *J Pharmacol Exp Ther* 329 (2), pp.551-557.

Moller, S., Croning, M. D. and Apweiler, R. (2001). Evaluation of methods for the prediction of membrane spanning regions. *Bioinformatics* 17 (7), pp.646-653.

Muto, M., Onogawa, T., Suzuki, T., Ishida, T., Rikiyama, T., Katayose, Y., Ohuchi, N., Sasano, H., Abe, T. and Unno, M. (2007). Human liver-specific organic anion transporter-2 is a potent prognostic factor for human breast carcinoma. *Cancer Sci* 98 (10), pp.1570-1576.

Nagai, M., Furihata, T., Matsumoto, S., Ishii, S., Motohashi, S., Yoshino, I., Ugajin, M., Miyajima, A. and Chiba, K. (2012). Identification of a new organic anion transporting polypeptide 1B3 mRNA isoform primarily expressed in human cancerous tissues and cells. *Biochem Biophys Res Commun* 418 (4), pp.818-823.

Nakai, D., Nakagomi, R., Furuta, Y., Tokui, T., Abe, T., Ikeda, T. and Nishimura, K. (2001). Human liver-specific organic anion transporter, LST-1, mediates uptake of pravastatin by human hepatocytes. *J Pharmacol Exp Ther* 297 (3), pp.861-867.

Nakai, K. and Horton, P. (1999). PSORT: a program for detecting sorting signals in proteins and predicting their subcellular localization. *Trends Biochem Sci* 24 (1), pp.34-36.

Nam, H. J., Jeon, J. and Kim, S. (2009). Bioinformatic approaches for the structure and function of membrane proteins. *BMB Rep* 42 (11), pp.697-704.

Nicholas, K. B., Nicholas H.B. Jr. and Deerfield, D. W. I. (1997). GeneDoc: Analysis and Visualization of Genetic Variation. *EMBNEW. news* 4 (14), pp.1-4.

Niemi, M., Pasanen, M. K. and Neuvonen, P. J. (2011). Organic anion transporting polypeptide 1B1: a genetically polymorphic transporter of major importance for hepatic drug uptake. *Pharmacol Rev* 63 (1), pp.157-181.

Noe, B., Hagenbuch, B., Stieger, B. and Meier, P. J. (1997). Isolation of a multispecific organic anion and cardiac glycoside transporter from rat brain. *Proc Natl Acad Sci U S A* 94 (19), pp.10346-10350.

Noe, J., Portmann, R., Brun, M. E. and Funk, C. (2007). Substrate-dependent drug-drug interactions between gemfibrozil, fluvastatin and other organic anion-transporting peptide (OATP) substrates on OATP1B1, OATP2B1, and OATP1B3. *Drug Metab Dispos* 35 (8), pp.1308-1314.

Nomura, T., Lu, R., Pucci, M. L. and Schuster, V. L. (2004). The two-step model of prostaglandin signal termination: in vitro reconstitution with the prostaglandin transporter and prostaglandin 15 dehydrogenase. *Mol Pharmacol* 65 (4), pp.973-978.

Nozawa, T., Imai, K., Nezu, J., Tsuji, A. and Tamai, I. (2004a). Functional characterization of pH-sensitive organic anion transporting polypeptide OATP-B in human. *J Pharmacol Exp Ther* 308 (2), pp.438-445.

Nozawa, T., Minami, H., Sugiura, S., Tsuji, A. and Tamai, I. (2005). Role of organic anion transporter OATP1B1 (OATP-C) in hepatic uptake of irinotecan and its active metabolite, 7-ethyl-10-hydroxycamptothecin: in vitro evidence and effect of single nucleotide polymorphisms. *Drug Metab Dispos* 33 (3), pp.434-439.

Nozawa, T., Nakajima, M., Tamai, I., Noda, K., Nezu, J., Sai, Y., Tsuji, A. and Yokoi, T. (2002). Genetic polymorphisms of human organic anion transporters OATP-C (SLC21A6) and OATP-B (SLC21A9): allele frequencies in the Japanese population and functional analysis. *J Pharmacol Exp Ther* 302 (2), pp.804-813.

Nozawa, T., Sugiura, S., Nakajima, M., Goto, A., Yokoi, T., Nezu, J., Tsuji, A. and Tamai, I. (2004b). Involvement of organic anion transporting polypeptides in the transport of troglitazone sulfate: implications for understanding troglitazone hepatotoxicity. *Drug Metab Dispos* 32 (3), pp.291-294.

Nugent, T. and Jones, D. T. (2009). Transmembrane protein topology prediction using support vector machines. *BMC Bioinformatics* 10, p.159.

Obaidat, A., Roth, M. and Hagenbuch, B. (2012). The expression and function of organic anion transporting polypeptides in normal tissues and in cancer. *Annu Rev Pharmacol Toxicol* 52, pp.135-151.

Ogasawara, K., Terada, T., Katsura, T., Hatano, E., Ikai, I., Yamaoka, Y. and Inui, K. (2010). Hepatitis C virus-related cirrhosis is a major determinant of the expression levels of hepatic drug transporters. *Drug Metab Pharmacokinet* 25 (2), pp.190-199.

Olszewski-Hamilton, U., Svoboda, M., Thalhammer, T., Buxhofer-Ausch, V., Geissler, K. and Hamilton, G. (2011). Organic Anion Transporting Polypeptide

5A1 (OATP5A1) in Small Cell Lung Cancer (SCLC) Cells: Possible Involvement in Chemoresistance to Satraplatin. *Biomarkers in Cancer* 3 (2703-BIC-Organic-Anion-Transporting-Polypeptide-5A1-(OATP5A1)-in-Small-Cell-Lun.pdf), p.31.

Oostendorp, R. L., van de Steeg, E., van der Kruijssen, C. M., Beijnen, J. H., Kenworthy, K. E., Schinkel, A. H. and Schellens, J. H. (2009). Organic anion-transporting polypeptide 1B1 mediates transport of Gimatecan and BNP1350 and can be inhibited by several classic ATP-binding cassette (ABC) B1 and/or ABCG2 inhibitors. *Drug Metab Dispos* 37 (4), pp.917-923.

Oswald, M., Kullak-Ublick, G. A., Paumgartner, G. and Beuers, U. (2001). Expression of hepatic transporters OATP-C and MRP2 in primary sclerosing cholangitis. *Liver* 21 (4), pp.247-253.

Paavola, K. J., Stephenson, J. R., Ritter, S. L., Alter, S. P. and Hall, R. A. (2011). The N terminus of the adhesion G protein-coupled receptor GPR56 controls receptor signaling activity. *J Biol Chem* 286 (33), pp.28914-28921.

Pacyniak, E., Roth, M., Hagenbuch, B. and Guo, G. L. (2010). Mechanism of polybrominated diphenyl ether uptake into the liver: PBDE congeners are substrates of human hepatic OATP transporters. *Toxicol Sci* 115 (2), pp.344-353.

Paine, M. F., Widmer, W. W., Hart, H. L., Pusek, S. N., Beavers, K. L., Criss, A. B., Brown, S. S., Thomas, B. F. and Watkins, P. B. (2006). A furanocoumarin-free grapefruit juice establishes furanocoumarins as the mediators of the grapefruit juice-felodipine interaction. *Am J Clin Nutr* 83 (5), pp.1097-1105.

Palermo, D. P., DeGraaf, M. E., Marotti, K. R., Rehberg, E. and Post, L. E. (1991). Production of analytical quantities of recombinant proteins in Chinese hamster ovary cells using sodium butyrate to elevate gene expression. *J Biotechnol* 19 (1), pp.35-47.

Palmgren, M. G., Askerlund, P., Fredrikson, K., Widell, S., Sommarin, M. and Larsson, C. (1990). Sealed inside-out and right-side-out plasma membrane vesicles : optimal conditions for formation and separation. *Plant Physiol* 92 (4), pp.871-880.

Palmieri, F. (2004). The mitochondrial transporter family (SLC25): physiological and pathological implications. *Pflugers Arch* 447 (5), pp.689-709.

Palmiter, R. D. and Huang, L. (2004). Efflux and compartmentalization of zinc by members of the SLC30 family of solute carriers. *Pflugers Arch* 447 (5), pp.744-751.

Panitsas, K. E., Boyd, C. A. and Meredith, D. (2006). Evidence that the rabbit proton-peptide co-transporter PepT1 is a multimer when expressed in Xenopus laevis oocytes. *Pflugers Arch* 452 (1), pp.53-63.

Pao, S. S., Paulsen, I. T. and Saier, M. H., Jr. (1998). Major facilitator superfamily. *Microbiol Mol Biol Rev* 62 (1), pp.1-34.

Parker, A. J. and Houston, J. B. (2008). Rate-limiting steps in hepatic drug clearance: comparison of hepatocellular uptake and metabolism with microsomal metabolism of saquinavir, nelfinavir, and ritonavir. *Drug Metab Dispos* 36 (7), pp.1375-1384.

Pasanen, M. K., Neuvonen, P. J. and Niemi, M. (2008). Global analysis of genetic variation in SLCO1B1. *Pharmacogenomics* 9 (1), pp.19-33.

Pasquier, C., Promponas, V. J., Palaios, G. A., Hamodrakas, J. S. and Hamodrakas, S. J. (1999). A novel method for predicting transmembrane segments in proteins based on a statistical analysis of the SwissProt database: the PRED-TMR algorithm. *Protein Eng* 12 (5), pp.381-385.

Paumgartner, G. and Pusl, T. (2008). Medical treatment of cholestatic liver disease. *Clin Liver Dis* 12 (1), pp.53-80, viii.

Petersen, T. N., Brunak, S., von Heijne, G. and Nielsen, H. (2011). SignalP 4.0: discriminating signal peptides from transmembrane regions. *Nat Methods* 8 (10), pp.785-786.

Pieri, M., Hall, D., Price, R., Bailey, P. and Meredith, D. (2008). Site-directed mutagenesis of Arginine282 suggests how protons and peptides are co-transported by rabbit PepT1. *Int J Biochem Cell Biol* 40 (4), pp.721-730.

Pizzagalli, F., Hagenbuch, B., Stieger, B., Klenk, U., Folkers, G. and Meier, P. J. (2002). Identification of a novel human organic anion transporting polypeptide as a high affinity thyroxine transporter. *Mol Endocrinol* 16 (10), pp.2283-2296.

Pressler, H., Sissung, T. M., Venzon, D., Price, D. K. and Figg, W. D. (2011). Expression of OATP family members in hormone-related cancers: potential markers of progression. *PLoS One* 6 (5), p.e20372.

Psaty, B. M., Furberg, C. D., Ray, W. A. and Weiss, N. S. (2004). Potential for conflict of interest in the evaluation of suspected adverse drug reactions: use of cerivastatin and risk of rhabdomyolysis. *JAMA* 292 (21), pp.2622-2631.

Quastel, J. H. (1965). Molecular transport at cell membranes. *Proc R Soc Lond B Biol Sci* 163 (991), pp.169-196.

Regazzi, M. B., Iacona, I., Campana, C., Raddato, V., Lesi, C., Perani, G., Gavazzi, A. and Vigano, M. (1993). Altered disposition of pravastatin

following concomitant drug therapy with cyclosporin A in transplant recipients. *Transplant Proc* 25 (4), pp.2732-2734.

Reitman, M. L., Chu, X., Cai, X., Yabut, J., Venkatasubramanian, R., Zajic, S., Stone, J. A., Ding, Y., Witter, R., Gibson, C., Roupe, K., Evers, R., Wagner, J. A. and Stoch, A. (2011). Rifampin's acute inhibitory and chronic inductive drug interactions: experimental and model-based approaches to drug-drug interaction trial design. *Clin Pharmacol Ther* 89 (2), pp.234-242.

Ren, X. Q., Furukawa, T., Haraguchi, M., Sumizawa, T., Aoki, S., Kobayashi, M. and Akiyama, S. (2004). Function of the ABC signature sequences in the human multidrug resistance protein 1. *Mol Pharmacol* 65 (6), pp.1536-1542.

Reynolds, S. M., Kall, L., Riffle, M. E., Bilmes, J. A. and Noble, W. S. (2008). Transmembrane topology and signal peptide prediction using dynamic bayesian networks. *PLoS Comput Biol* 4 (11), p.e1000213.

Romaine, S. P., Bailey, K. M., Hall, A. S. and Balmforth, A. J. (2010). The influence of SLCO1B1 (OATP1B1) gene polymorphisms on response to statin therapy. *Pharmacogenomics J* 10 (1), pp.1-11.

Rost, B., Fariselli, P. and Casadio, R. (1996). Topology prediction for helical transmembrane proteins at 86% accuracy. *Protein Sci* 5 (8), pp.1704-1718.

Roth, M., Obaidat, A. and Hagenbuch, B. (2011). OATPs, OATs and OCTs: The organic anion and cation transporters of the SLCO and SLC22A gene superfamilies. *Br J Pharmacol.*

Sai, Y., Kaneko, Y., Ito, S., Mitsuoka, K., Kato, Y., Tamai, I., Artursson, P. and Tsuji, A. (2006). Predominant contribution of organic anion transporting polypeptide OATP-B (OATP2B1) to apical uptake of estrone-3-sulfate by human intestinal Caco-2 cells. *Drug Metab Dispos* 34 (8), pp.1423-1431.

Saier, M. H., Jr. (2000). A functional-phylogenetic classification system for transmembrane solute transporters. *Microbiol Mol Biol Rev* 64 (2), pp.354-411.

Saier, M. H., Jr., Tran, C. V. and Barabote, R. D. (2006). TCDB: the Transporter Classification Database for membrane transport protein analyses and information. *Nucleic Acids Res* 34 (Database issue), pp.D181-186.

Saito, H., Masuda, S. and Inui, K. (1996). Cloning and functional characterization of a novel rat organic anion transporter mediating basolateral uptake of methotrexate in the kidney. *J Biol Chem* 271 (34), pp.20719-20725.

Sakoda, M. and Hiromi, K. (1976). Determination of the best-fit values of kinetic parameters of the Michaelis-Menten equation by the method of least squares with the Taylor expansion. *J Biochem* 80 (3), pp.547-555.

Samanta, U., Pal, D. and Chakrabarti, P. (2000). Environment of tryptophan side chains in proteins. *Proteins* 38 (3), pp.288-300.

Sanchez, K. M., Kang, G., Wu, B. and Kim, J. E. (2011). Tryptophan-lipid interactions in membrane protein folding probed by ultraviolet resonance Raman and fluorescence spectroscopy. *Biophys J* 100 (9), pp.2121-2130.

Sandhu, P., Lee, W., Xu, X., Leake, B. F., Yamazaki, M., Stone, J. A., Lin, J. H., Pearson, P. G. and Kim, R. B. (2005). Hepatic uptake of the novel antifungal agent caspofungin. *Drug Metab Dispos* 33 (5), pp.676-682.

Sanna, S., Busonero, F., Maschio, A., McArdle, P. F., Usala, G., Dei, M., Lai, S., Mulas, A., Piras, M. G., Perseu, L., Masala, M., Marongiu, M., Crisponi, L., Naitza, S., Galanello, R., Abecasis, G. R., Shuldiner, A. R., Schlessinger, D., Cao, A. and Uda, M. (2009). Common variants in the SLCO1B3 locus are associated with bilirubin levels and unconjugated hyperbilirubinemia. *Hum Mol Genet* 18 (14), pp.2711-2718.

Satlin, L. M., Amin, V. and Wolkoff, A. W. (1997). Organic anion transporting polypeptide mediates organic anion/HCO3- exchange. *J Biol Chem* 272 (42), pp.26340-26345.

Satoh, H., Yamashita, F., Tsujimoto, M., Murakami, H., Koyabu, N., Ohtani, H. and Sawada, Y. (2005a). Citrus juices inhibit the function of human organic anion-transporting polypeptide OATP-B. *Drug Metab Dispos* 33 (4), pp.518-523.

Satoh, J., Takahashi, K., Takizawa, Y., Ishihara, H., Hirai, M., Katagiri, H., Hinokio, Y., Suzuki, S., Tsuji, I. and Oka, Y. (2005b). Secondary sulfonylurea failure: comparison of period until insulin treatment between diabetic patients treated with gliclazide and glibenclamide. *Diabetes Res Clin Pract* 70 (3), pp.291-297.

Schiffer, M., Chang, C. H. and Stevens, F. J. (1992). The functions of tryptophan residues in membrane proteins. *Protein Eng* 5 (3), pp.213-214.

Schipani, A., Egan, D., Dickinson, L., Davies, G., Boffito, M., Youle, M., Khoo, S. H., Back, D. J. and Owen, A. (2012). Estimation of the effect of SLCO1B1 polymorphisms on lopinavir plasma concentration in HIV-infected adults. *Antivir Ther* 17 (5), pp.861-868.

Schuetz, E. G., Schinkel, A. H., Relling, M. V. and Schuetz, J. D. (1996). P-glycoprotein: a major determinant of rifampicin-inducible expression of cytochrome P4503A in mice and humans. *Proc Natl Acad Sci U S A* 93 (9), pp.4001-4005.

Schuster, V. L. (1998). Molecular mechanisms of prostaglandin transport. *Annu Rev Physiol* 60, pp.221-242.

Sciara, G. and Mancia, F. (2012). Highlights from recently determined structures of membrane proteins: a focus on channels and transporters. *Curr Opin Struct Biol* 22 (4), pp.476-481.

Seal, R. L., Gordon, S. M., Lush, M. J., Wright, M. W. and Bruford, E. A. (2011). genenames.org: the HGNC resources in 2011. *Nucleic Acids Res* 39 (Database issue), pp.D514-519.

Sebaugh, J. L. (2011). Guidelines for accurate EC50/IC50 estimation. *Pharm Stat* 10 (2), pp.128-134.

Seithel, A., Eberl, S., Singer, K., Auge, D., Heinkele, G., Wolf, N. B., Dorje, F., Fromm, M. F. and Konig, J. (2007). The influence of macrolide antibiotics on the uptake of organic anions and drugs mediated by OATP1B1 and OATP1B3. *Drug Metab Dispos* 35 (5), pp.779-786.

Sekine, T., Miyazaki, H. and Endou, H. (2006). Molecular physiology of renal organic anion transporters. *Am J Physiol Renal Physiol* 290 (2), pp.F251-261.

Sharma, P., Butters, C. J., Smith, V., Elsby, R. and Surry, D. (2012). Prediction of the in vivo OATP1B1-mediated drug-drug interaction potential of an investigational drug against a range of statins. *Eur J Pharm Sci* 47 (1), pp.244-255.

Shen, H. and Chou, J. J. (2008). MemBrain: improving the accuracy of predicting transmembrane helices. *PLoS One* 3 (6), p.e2399.

Shimoni, L. and Glusker, J. P. (1995). Hydrogen bonding motifs of protein side chains: descriptions of binding of arginine and amide groups. *Protein Sci* 4 (1), pp.65-74.

Shirasaka, Y., Mori, T., Shichiri, M., Nakanishi, T. and Tamai, I. (2012). Functional Pleiotropy of Organic Anion Transporting Polypeptide OATP2B1 Due to Multiple Binding Sites. *Drug Metab Pharmacokinet* 27 (3), pp.360-364.

Shitara, Y., Hirano, M., Sato, H. and Sugiyama, Y. (2004). Gemfibrozil and its glucuronide inhibit the organic anion transporting polypeptide 2 (OATP2/OATP1B1:SLC21A6)-mediated hepatic uptake and CYP2C8-mediated metabolism of cerivastatin: analysis of the mechanism of the clinically relevant drug-drug interaction between cerivastatin and gemfibrozil. *J Pharmacol Exp Ther* 311 (1), pp.228-236.

Shitara, Y., Itoh, T., Sato, H., Li, A. P. and Sugiyama, Y. (2003). Inhibition of transporter-mediated hepatic uptake as a mechanism for drug-drug interaction between cerivastatin and cyclosporin A. *J Pharmacol Exp Ther* 304 (2), pp.610-616.

Sigrist, C. J., Cerutti, L., de Castro, E., Langendijk-Genevaux, P. S., Bulliard, V., Bairoch, A. and Hulo, N. (2010). PROSITE, a protein domain database for

functional characterization and annotation. *Nucleic Acids Res* 38 (Database issue), pp.D161-166.

Simon, M. I. (1998). *Neurotransmitter Transporters.* Methods in Enzymology. California: Academic Press.

Singer, S. J. and Nicolson, G. L. (1972). The fluid mosaic model of the structure of cell membranes. *Science* 175 (4023), pp.720-731.

Slotboom, D. J., Sobczak, I., Konings, W. N. and Lolkema, J. S. (1999). A conserved serine-rich stretch in the glutamate transporter family forms a substrate-sensitive reentrant loop. *Proc Natl Acad Sci U S A* 96 (25), pp.14282-14287.

Sokalingam, S., Raghunathan, G., Soundrarajan, N. and Lee, S. G. (2012). A study on the effect of surface lysine to arginine mutagenesis on protein stability and structure using green fluorescent protein. *PLoS One* 7 (7), p.e40410.

Sonnhammer, E. L., von Heijne, G. and Krogh, A. (1998). A hidden Markov model for predicting transmembrane helices in protein sequences. *Proc Int Conf Intell Syst Mol Biol* 6, pp.175-182.

Spyropoulos, I. C., Liakopoulos, T. D., Bagos, P. G. and Hamodrakas, S. J. (2004). TMRPres2D: high quality visual representation of transmembrane protein models. *Bioinformatics* 20 (17), pp.3258-3260.

Sreedharan, S., Stephansson, O., Schioth, H. B. and Fredriksson, R. (2011). Long evolutionary conservation and considerable tissue specificity of several atypical solute carrier transporters. *Gene* 478 (1-2), pp.11-18.

St-Pierre, M. V., Hagenbuch, B., Ugele, B., Meier, P. J. and Stallmach, T. (2002). Characterization of an organic anion-transporting polypeptide (OATP-B) in human placenta. *J Clin Endocrinol Metab* 87 (4), pp.1856-1863.

St-Pierre, M. V., Stallmach, T., Freimoser Grundschober, A., Dufour, J. F., Serrano, M. A., Marin, J. J., Sugiyama, Y. and Meier, P. J. (2004). Temporal expression profiles of organic anion transport proteins in placenta and fetal liver of the rat. *Am J Physiol Regul Integr Comp Physiol* 287 (6), pp.R1505-1516.

Steck, T. L., Weinstein, R. S., Straus, J. H. and Wallach, D. F. (1970). Inside-out red cell membrane vesicles: preparation and purification. *Science* 168 (3928), pp.255-257.

Stenesh, J. (1998). *Biochemistry.* New York: Plenum Press.

Su, Y., Zhang, X. and Sinko, P. J. (2004). Human organic anion-transporting polypeptide OATP-A (SLC21A3) acts in concert with P-glycoprotein and multidrug resistance protein 2 in the vectorial transport of Saquinavir in Hep G2 cells. *Mol Pharm* 1 (1), pp.49-56.

Sun, A. Q., Ponamgi, V. M., Boyer, J. L. and Suchy, F. J. (2008a). Membrane trafficking of the human organic anion-transporting polypeptide C (hOATPC). *Pharm Res* 25 (2), pp.463-474.

Sun, H., Greathouse, D. V., Andersen, O. S. and Koeppe, R. E., 2nd (2008b). The preference of tryptophan for membrane interfaces: insights from N-methylation of tryptophans in gramicidin channels. *J Biol Chem* 283 (32), pp.22233-22243.

Suzuki, T., Onogawa, T., Asano, N., Mizutamari, H., Mikkaichi, T., Tanemoto, M., Abe, M., Satoh, F., Unno, M., Nunoki, K., Suzuki, M., Hishinuma, T., Goto, J., Shimosegawa, T., Matsuno, S., Ito, S. and Abe, T. (2003). Identification and characterization of novel rat and human gonad-specific organic anion transporters. *Mol Endocrinol* 17 (7), pp.1203-1215.

Svoboda, M., Riha, J., Wlcek, K., Jaeger, W. and Thalhammer, T. (2011a). Organic anion transporting polypeptides (OATPs): regulation of expression and function. *Curr Drug Metab* 12 (2), pp.139-153.

Svoboda, M., Wlcek, K., Taferner, B., Hering, S., Stieger, B., Tong, D., Zeillinger, R., Thalhammer, T. and Jager, W. (2011b). Expression of organic anion-transporting polypeptides 1B1 and 1B3 in ovarian cancer cells: relevance for paclitaxel transport. *Biomed Pharmacother* 65 (6), pp.417-426.

Sweet, D. H., Chan, L. M., Walden, R., Yang, X. P., Miller, D. S. and Pritchard, J. B. (2003). Organic anion transporter 3 (Slc22a8) is a dicarboxylate exchanger indirectly coupled to the Na+ gradient. *Am J Physiol Renal Physiol* 284 (4), pp.F763-769.

Tamai, I., Nezu, J., Uchino, H., Sai, Y., Oku, A., Shimane, M. and Tsuji, A. (2000). Molecular identification and characterization of novel members of the human organic anion transporter (OATP) family. *Biochem Biophys Res Commun* 273 (1), pp.251-260.

Tamai, I., Nozawa, T., Koshida, M., Nezu, J., Sai, Y. and Tsuji, A. (2001). Functional characterization of human organic anion transporting polypeptide B (OATP-B) in comparison with liver-specific OATP-C. *Pharm Res* 18 (9), pp.1262-1269.

Taub, M. E., Mease, K., Sane, R. S., Watson, C. A., Chen, L., Ellens, H., Hirakawa, B., Reyner, E. L., Jani, M. and Lee, C. A. (2011). Digoxin is not a substrate for organic anion-transporting polypeptide transporters OATP1A2, OATP1B1, OATP1B3, and OATP2B1 but is a substrate for a sodium-dependent transporter expressed in HEK293 cells. *Drug Metab Dispos* 39 (11), pp.2093-2102.

Tirona, R. G., Leake, B. F., Merino, G. and Kim, R. B. (2001). Polymorphisms in OATP-C: identification of multiple allelic variants associated with altered

transport activity among European- and African-Americans. *J Biol Chem* 276 (38), pp.35669-35675.

Tirona, R. G., Leake, B. F., Wolkoff, A. W. and Kim, R. B. (2003). Human organic anion transporting polypeptide-C (SLC21A6) is a major determinant of rifampin-mediated pregnane X receptor activation. *J Pharmacol Exp Ther* 304 (1), pp.223-228.

Treiber, A., Schneiter, R., Hausler, S. and Stieger, B. (2007). Bosentan is a substrate of human OATP1B1 and OATP1B3: inhibition of hepatic uptake as the common mechanism of its interactions with cyclosporin A, rifampicin, and sildenafil. *Drug Metab Dispos* 35 (8), pp.1400-1407.

Trevino, L. R., Shimasaki, N., Yang, W., Panetta, J. C., Cheng, C., Pei, D., Chan, D., Sparreboom, A., Giacomini, K. M., Pui, C. H., Evans, W. E. and Relling, M. V. (2009). Germline genetic variation in an organic anion transporter polypeptide associated with methotrexate pharmacokinetics and clinical effects. *J Clin Oncol* 27 (35), pp.5972-5978.

Tusnady, G. E. and Simon, I. (2001a). The HMMTOP transmembrane topology prediction server. *Bioinformatics* 17 (9), pp.849-850.

Tusnady, G. E. and Simon, I. (2001b). Topology of membrane proteins. *J Chem Inf Comput Sci* 41 (2), pp.364-368.

van de Steeg, E., Stranecky, V., Hartmannova, H., Noskova, L., Hrebicek, M., Wagenaar, E., van Esch, A., de Waart, D. R., Oude Elferink, R. P., Kenworthy, K. E., Sticova, E., al-Edreesi, M., Knisely, A. S., Kmoch, S., Jirsa, M. and Schinkel, A. H. (2012). Complete OATP1B1 and OATP1B3 deficiency causes human Rotor syndrome by interrupting conjugated bilirubin reuptake into the liver. *J Clin Invest* 122 (2), pp.519-528.

van Montfoort, J. E., Hagenbuch, B., Fattinger, K. E., Muller, M., Groothuis, G. M., Meijer, D. K. and Meier, P. J. (1999). Polyspecific organic anion transporting polypeptides mediate hepatic uptake of amphipathic type II organic cations. *J Pharmacol Exp Ther* 291 (1), pp.147-152.

Vavricka, S. R., Jung, D., Fried, M., Grutzner, U., Meier, P. J. and Kullak-Ublick, G. A. (2004). The human organic anion transporting polypeptide 8 (SLCO1B3) gene is transcriptionally repressed by hepatocyte nuclear factor 3beta in hepatocellular carcinoma. *J Hepatol* 40 (2), pp.212-218.

Vavricka, S. R., Van Montfoort, J., Ha, H. R., Meier, P. J. and Fattinger, K. (2002). Interactions of rifamycin SV and rifampicin with organic anion uptake systems of human liver. *Hepatology* 36 (1), pp.164-172.

Viklund, H. and Elofsson, A. (2008). OCTOPUS: improving topology prediction by two-track ANN-based preference scores and an extended topological grammar. *Bioinformatics* 24 (15), pp.1662-1668.

Viklund, H., Granseth, E. and Elofsson, A. (2006). Structural classification and prediction of reentrant regions in alpha-helical transmembrane proteins: application to complete genomes. *J Mol Biol* 361 (3), pp.591-603.

Vincze, T., Posfai, J. and Roberts, R. J. (2003). NEBcutter: A program to cleave DNA with restriction enzymes. *Nucleic Acids Res* 31 (13), pp.3688-3691.

Vlahakos, D. V., Manginas, A., Chilidou, D., Zamanika, C. and Alivizatos, P. A. (2002). Itraconazole-induced rhabdomyolysis and acute renal failure in a heart transplant recipient treated with simvastatin and cyclosporine. *Transplantation* 73 (12), pp.1962-1964.

von Heijne, G. (1986). A new method for predicting signal sequence cleavage sites. *Nucleic Acids Res* 14 (11), pp.4683-4690.

von Heijne, G. (1992). Membrane protein structure prediction. Hydrophobicity analysis and the positive-inside rule. *J Mol Biol* 225 (2), pp.487-494.

Wallace, B. A. and Janes, R. W. (1999). Tryptophans in membrane proteins. X-ray crystallographic analyses. *Adv Exp Med Biol* 467, pp.789-799.

Wallin, E. and von Heijne, G. (1998). Genome-wide analysis of integral membrane proteins from eubacterial, archaean, and eukaryotic organisms. *Protein Sci* 7 (4), pp.1029-1038.

Wang, H., Yan, Z., Dong, M., Zhu, X. and Wang, Z. (2012). Alteration in placental expression of bile acids transporters OATP1A2, OATP1B1, OATP1B3 in intrahepatic cholestasis of pregnancy. *Arch Gynecol Obstet* 285 (6), pp.1535-1540.

Wang, P., Hata, S., Xiao, Y., Murray, J. W. and Wolkoff, A. W. (2008). Topological assessment of oatp1a1: a 12-transmembrane domain integral membrane protein with three N-linked carbohydrate chains. *Am J Physiol Gastrointest Liver Physiol* 294 (4), pp.G1052-1059.

Wang, P., Wang, J. J., Xiao, Y., Murray, J. W., Novikoff, P. M., Angeletti, R. H., Orr, G. A., Lan, D., Silver, D. L. and Wolkoff, A. W. (2005a). Interaction with PDZK1 is required for expression of organic anion transporting protein 1A1 on the hepatocyte surface. *J Biol Chem* 280 (34), pp.30143-30149.

Wang, X., Wolkoff, A. W. and Morris, M. E. (2005b). Flavonoids as a novel class of human organic anion-transporting polypeptide OATP1B1 (OATP-C) modulators. *Drug Metab Dispos* 33 (11), pp.1666-1672.

Weaver, Y. M., Ehresman, D. J., Butenhoff, J. L. and Hagenbuch, B. (2010). Roles of rat renal organic anion transporters in transporting perfluorinated carboxylates with different chain lengths. *Toxicol Sci* 113 (2), pp.305-314.

Weaver, Y. M. and Hagenbuch, B. (2010). Several conserved positively charged amino acids in OATP1B1 are involved in binding or translocation of different substrates. *J Membr Biol* 236 (3), pp.279-290.

Wendel, C., Becker, H. M. and Deitmer, J. W. (2008). The sodium-bicarbonate cotransporter NBCe1 supports glutamine efflux via SNAT3 (SLC38A3) co-expressed in Xenopus oocytes. *Pflugers Arch* 455 (5), pp.885-893.

Westholm, D. E., Marold, J. D., Viken, K. J., Duerst, A. H., Anderson, G. W. and Rumbley, J. N. (2010). Evidence of evolutionary conservation of function between the thyroxine transporter Oatp1c1 and major facilitator superfamily members. *Endocrinology* 151 (12), pp.5941-5951.

Westholm, D. E., Rumbley, J. N., Salo, D. R., Rich, T. P. and Anderson, G. W. (2008). Organic anion-transporting polypeptides at the blood-brain and blood-cerebrospinal fluid barriers. *Curr Top Dev Biol* 80, pp.135-170.

Westholm, D. E., Salo, D. R., Viken, K. J., Rumbley, J. N. and Anderson, G. W. (2009a). The blood-brain barrier thyroxine transporter organic anion-transporting polypeptide 1c1 displays atypical transport kinetics. *Endocrinology* 150 (11), pp.5153-5162.

Westholm, D. E., Stenehjem, D. D., Rumbley, J. N., Drewes, L. R. and Anderson, G. W. (2009b). Competitive inhibition of organic anion transporting polypeptide 1c1-mediated thyroxine transport by the fenamate class of nonsteroidal antiinflammatory drugs. *Endocrinology* 150 (2), pp.1025-1032.

Wlcek, K., Svoboda, M., Riha, J., Zakaria, S., Olszewski, U., Dvorak, Z., Sellner, F., Ellinger, I., Jager, W. and Thalhammer, T. (2011). The analysis of organic anion transporting polypeptide (OATP) mRNA and protein patterns in primary and metastatic liver cancer. *Cancer Biol Ther* 11 (9), pp.801-811.

Wlcek, K., Svoboda, M., Thalhammer, T., Sellner, F., Krupitza, G. and Jaeger, W. (2008). Altered expression of organic anion transporter polypeptide (OATP) genes in human breast carcinoma. *Cancer Biol Ther* 7 (9), pp.1450-1455.

Wu, W., Baker, M. E., Eraly, S. A., Bush, K. T. and Nigam, S. K. (2009). Analysis of a large cluster of SLC22 transporter genes, including novel USTs, reveals species-specific amplification of subsets of family members. *Physiol Genomics* 38 (2), pp.116-124.

Yamaguchi, H., Sugie, M., Okada, M., Mikkaichi, T., Toyohara, T., Abe, T., Goto, J., Hishinuma, T., Shimada, M. and Mano, N. (2010). Transport of estrone 3-sulfate mediated by organic anion transporter OATP4C1: estrone 3-sulfate binds to the different recognition site for digoxin in OATP4C1. *Drug Metab Pharmacokinet* 25 (3), pp.314-317.

Yamashiro, W., Maeda, K., Hirouchi, M., Adachi, Y., Hu, Z. and Sugiyama, Y. (2006). Involvement of transporters in the hepatic uptake and biliary excretion

of valsartan, a selective antagonist of the angiotensin II AT1-receptor, in humans. *Drug Metab Dispos* 34 (7), pp.1247-1254.

Yang, C. H., Glover, K. P. and Han, X. (2009). Organic anion transporting polypeptide (Oatp) 1a1-mediated perfluorooctanoate transport and evidence for a renal reabsorption mechanism of Oatp1a1 in renal elimination of perfluorocarboxylates in rats. *Toxicol Lett* 190 (2), pp.163-171.

Yang, M., Xie, W., Mostaghel, E., Nakabayashi, M., Werner, L., Sun, T., Pomerantz, M., Freedman, M., Ross, R., Regan, M., Sharifi, N., Figg, W. D., Balk, S., Brown, M., Taplin, M. E., Oh, W. K., Lee, G. S. and Kantoff, P. W. (2011). SLCO2B1 and SLCO1B3 may determine time to progression for patients receiving androgen deprivation therapy for prostate cancer. *J Clin Oncol* 29 (18), pp.2565-2573.

Yao, J., Hong, W., Huang, J., Zhan, K., Huang, H. and Hong, M. (2012). N-Glycosylation dictates proper processing of organic anion transporting polypeptide 1B1. *PLoS One* 7 (12), p.e52563.

Yuan, Z., Mattick, J. S. and Teasdale, R. D. (2004). SVMtm: support vector machines to predict transmembrane segments. *J Comput Chem* 25 (5), pp.632-636.

Zhang, D., Chando, T. J., Everett, D. W., Patten, C. J., Dehal, S. S. and Humphreys, W. G. (2005). In vitro inhibition of UDP glucuronosyltransferases by atazanavir and other HIV protease inhibitors and the relationship of this property to in vivo bilirubin glucuronidation. *Drug Metab Dispos* 33 (11), pp.1729-1739.

Zhang, Z., Xia, W., He, J., Ke, Y., Yue, H., Wang, C., Zhang, H., Gu, J., Hu, W., Fu, W., Hu, Y., Li, M. and Liu, Y. (2012). Exome sequencing identifies SLCO2A1 mutations as a cause of primary hypertrophic osteoarthropathy. *Am J Hum Genet* 90 (1), pp.125-132.

Zheng, Q. L., Sheng, Q. and Zhang, Y. Z. (2006). Progresses in the structure and function of Kazal-type proteinase inhibitors. *Sheng Wu Gong Cheng Xue Bao* 22 (5), pp.695-700.

Zhou, F., Lee, A. C., Krafczyk, K., Zhu, L. and Murray, M. (2011). Protein kinase C regulates the internalization and function of the human organic anion transporting polypeptide 1A2. *Br J Pharmacol* 162 (6), pp.1380-1388.

Zhou, H. and Zhou, Y. (2003). Predicting the topology of transmembrane helical proteins using mean burial propensity and a hidden-Markov-model-based method. *Protein Sci* 12 (7), pp.1547-1555.

Zsembery, A., Thalhammer, T. and Graf, J. (2000). Bile Formation: a Concerted Action of Membrane Transporters in Hepatocytes and Cholangiocytes. *News Physiol Sci* 15, pp.6-11.

Appendix

Appendix I: Summary of OATP1A2 amino acid TM predictions by 16 topology prediction programs

Name	Length of TM	TM1	TM2	TM3	TM4	TM5	TM6	TM7	TM8	TM9	TM10	TM11	TM12
ConPredII (Arai *et al.*, 2004)	**21**	36-56	65-85	134-154	179-199	226-246	292-312	335-355	370-390	-	-	-	-
SOSUI (Hirokawa *et al.*, 1998)	**22-23**	1-23	35-57	64-86	130-152	178-200	226-248	297-319	336-357	368-390	-	-	-
TopPredII (von Heijne, 1992)	**20**	1-21	43-63	66-86	181-201	226-246	296-316	334-354	370-390	-	-	-	-
TMpred (Hofman and Stoffel, 1993)	**18-29**	2-20	40-61	67-85	136-164	182-202	223-240	297-316	334-357	362-388	-	-	-
TMHMM (Krogh *et al.*, 2001)	**23**	35-57	67-89	174-196	224-246	297-319	334-356	368-390	-	-	-	-	-
TSeg (Kihara *et al.*, 1998)	**22-27**	37-60	63-87	177-203	224-249	291-317	333-358	370-391	-	-	-	-	-
MemBrain (Shen and Chou, 2008)	**13-56**	6-21	45-59	68-87	136-148	175-199	224-245	291-319	333-356	366-389	-	-	-

PHDhtm (Rost *et al.*, 1996)	**2-29**	11-12	42-61	69-88	138-151	175-201	223-245	291-319	336-358	367-390	-	-	-
Split 4.0 (Juretic *et al.*, 2002)	**15-26**	45-60	65-88	133-149	176-200	223-246	293-319	334-359	368-391	-	-	-	-
Phobius (Kall *et al.*, 2004)	**18-27**	40-60	67-85	137-163	175-202	222-246	297-319	334-356	368-388	-	-	-	-
Philius (Reynolds *et al.*, 2008)	**19-23**	36-58	66-85	176-198	223-246	297-318	334-356	369-389	-	-	-	-	-
HMMTOP (Tusnady and Simon, 2001b)	**20-23**	37-60	67-90	138-161	174-197	224-247	285-307	334-357	370-390	-	-	-	-
TOPCONS (Bernsel *et al.*, 2009)	**20**	3-23	39-59	69-89	140-160	175-195	222-242	297-317	336-356	370-390	-	-	-
PRED-TMR (Pasquier *et al.*, 1999)	**18-22**	37-56	67-85	182-202	225-246	297-316	335-356	370-388	-	-	-	-	-
MEMSAT3 (Jones, 2007)	**16-23**	37-59	66-82	174-196	225-246	297-319	334-357	367-388	-	-	-	-	-
SVMtm (Yuan *et al.*, 2004)	**14-21**	44-58	68-82	136-150	178-197	224-245	297-313	336-356	373-387	-	-	-	-

Appendix II: Summary of OATP1B3 amino acid TM predictions by 16 topology prediction programs

Name	Length of TM	TM1	TM2	TM3	TM4	TM5	TM6	TM7	TM8	TM9	TM10	TM11	TM12
ConPredII (Arai *et al.*, 2004)	**21**	29-49	68-88	96-116	211-231	258-278	332-352	375-395	408-428	534-554	575-595	625-645	-
SOSUI (Hirokawa *et al.*, 1998)	**23**	29-51	210-232	256-278	337-359	374-396	406-428	536-558	574-596	624-646	-	-	-
TopPredII (von Heijne, 1992)	**20**	28-48	71-91	96-116	135-155	211-231	259-279	337-357	376-396	410-430	542-562	576-596	627-647
TMpred (Hofman and Stoffel, 1993)	**20-27**	24-44	68-88	96-121	170-196	215-234	256-280	340-360	376-397	411-430	534-560	570-595	624-647
TMHMM (Krogh *et al.*, 2001)	**23**	30-52	67-89	96-118	208-230	255-277	332-354	375-397	407-429	534-556	576-595	624-646	-
TSeg (Kihara *et al.*, 1998)	**22-29**	28–52	65–89	95-116	210-236	257-281	331-358	373-397	406-431	532-558	574-598	522-650	-
MemBrain (Shen and Chou, 2008)	**13-29**	28-49	73-87	96-115	169-181	208-232	257-278	331-359	373-396	406-429	533-558	572-595	623-646
PHDhtm (Rost *et al.*, 1996)	**14-24**	31-45	74-88	98-112	211-233	258-277	332-356	378-397	409-428	536-559	577-594	628-646	-

lit 4.0 (Juretic *et al.*, 2002)	**14-29**	28-57	73-87	94-114	168-183	207-232	253-277	334-358	374-395	403-429	533-548	566-595	619-646
Phobius (Kall *et al.*, 2004)	**19-28**	29-52	64-84	96-117	170-195	207-235	255-279	337-356	376-397	404-425	534-558	570-591	624-647
Philius (Reynolds *et al.*, 2008)	**19-24**	27-48	66-87	96-118	177-196	207-231	257-279	337-359	376-397	405-426	538-560	576-595	625-647
HMMTOP (Tusnady and Simon, 2001b)	**19-24**	29-52	65-87	96-118	170-194	207-230	257-279	324-347	374-397	410-429	534-558	571-595	626-645
TOPCONS (Bernsel *et al.*, 2009)	**20**	27-47	68-88	97-117	173-193	208-228	259-279	336-356	376-396	410-430	540-560	573-593	625-645
PRED-TMR (Pasquier *et al.*, 1999)	**17-22**	29-48	99-120	214-231	254-271	339-360	376-397	402-421	534-556	577-595	624-645	-	-
MEMSAT3 (Jones, 2007)	**17-24**	29-48	96-120	207-231	258-279	337-360	376-397	404-426	534-558	578-595	624-647	-	-
SVMtm (Yuan *et al.*, 2004)	**14-25**	29-48	72-86	98-113	210-231	258-275	336-356	376-397	406-426	535-558	572-592	621-646	-

Appendix III: Summary of OATP2B1 amino acid TM predictions by 16 topology prediction programs

Name	Length of TM	TM1	TM2	TM3	TM4	TM5	TM6	TM7	TM8	TM9	TM10	TM11	TM12	TM13
ConPredII (Arai *et al.*, 2004)	**21**	47-67	90-110	117-137	187-207	226-246	276-296	371-391	410-430	442-462	562-582	595-615	654-674	-
SOSUI (Hirokawa *et al.*, 1998)	**23**	44-66	117-139	189-211	226-248	275-297	375-397	409-431	441-463	-	-	-	-	-
TopPredII (von Heijne, 1992)	**21**	49-69	88-108	117-137	156-176	186-206	225-245	272-292	371-391	411-431	445-465	559-579	596-616	653-673
TMpred (Hofman and Stoffel, 1993)	**16-27**	50-68	91-112	117-138	188-214	225-244	277-298	371-390	411-432	441-466	562-578	597-622	656-672	-
TMHMM (Krogh *et al.*, 2001)	**23**	88-110	117-139	192-214	227-249	275-297	372-394	409-431	443-465	565-587	600-622	651-673	-	-
TSeg (Kihara *et al.*, 1998)	**21-32**	48-68	118-140	185-208	224-250	275-299	365-394	406-435	438-469	554-584	653-676	-	-	-
MemBrain (Shen and Chou, 2008)	**14-29**	48-69	94-108	117-136	186-199	226-250	276-296	366-394	408-431	440-464	560-585	599-622	649-672	-
PHDhtm (Rost *et al.*, 1996)	**8-24**	50-66	96-109	119-133	191-199	229-249	277-295	368-392	412-431	445-463	561-585	603-621	655-671	-

lit 4.0 (Juretic *et al.*, 2002)	**22-36**	49-71	119-142	185-212	223-250	272-297	370-395	399-430	438-471	555-591	593-628	648-675	-	-
Phobius (Kall *et al.*, 2004)	**19-28**	50-69	89-110	117-138	188-213	225-253	273-297	372-394	406-432	444-464	560-587	608-631	651-673	-
Philius (Reynolds *et al.*, 2008)	**18-24**	51-69	89-108	117-138	188-211	225-249	275-297	372-394	408-432	440-463	560-583	598-622	652-673	-
HMMTOP (Tusnady and Simon, 2001b)	**17-24**	50-69	86-108	117-134	188-212	225-248	275-298	371-394	411-432	441-463	564-587	596-620	651-673	-
TOPCONS (Bernsel *et al.*, 2009)	**20**	48-68	89-109	117-137	186-206	225-245	276-296	372-392	411-431	443-463	560-580	598-618	653-673	-
PRED-TMR (Pasquier *et al.*, 1999)	**17-22**	117-134	188-206	229-249	272-292	372-394	411-432	445-463	566-587	597-617	651-673	-	-	-
MEMSAT3 (Jones, 2007)	**16-23**	50-69	88-108	117-134	186-206	225-249	276-297	372-394	411-432	440-463	564-587	596-612	651-673	-
SVMtm (Yuan *et al.*, 2004)	**14-24**	50-64	94-108	119-133	187-201	226-248	276-294	371-391	408-431	442-466	560-574	601-615	657-671	-

Appendix IV – Table of predicted N and C terminal orientation for OATP1A2, OATP1B3 and OATP2B1

Name of program	OATP1A2		OATP1B3		OATP2B1	
	Number of TMs	N terminal position	Number of TMs	N terminal Position	Number of TMs	N terminal Position
ConPredII (Arai *et al.*, 2004)	8	Internal	11	Internal	12	Internal
SOSUI (Hirokawa *et al.*, 1998)	9	External	9	External	8	External
TopPredII (von Heijne, 1992)	8	External	12	Internal	13	Internal
TMpred (Hofman and Stoffel, 1993)	9	Internal	12	Internal	12	Internal
TMHMM (Krogh *et al.*, 2001)	7	Internal	11	Internal	11	External
TSeg (Kihara *et al.*, 1998)	7	Not predicted	11	Not predicted	10	Not predicted
MemBrain (Shen and Chou, 2008)	9	Not predicted	12	Not predicted	12	Not predicted
PHDhtm (Rost *et al.*, 1996)	9	Not predicted	11	Not predicted	12	Not predicted
Split 4.0 (Juretic *et al.*, 2002)	8	External	12	Internal	11	External
Phobius (Kall *et al.*, 2004)	8	External	12	Internal	12	Internal
Philius (Reynolds *et al.*, 2008)	7	Internal	12	Internal	12	Internal
HMMTOP (Tusnady and Simon, 2001b)	8	External	12	Internal	12	Internal
TOPCONS (Bernsel *et al.*, 2009)	9	Internal	12	Internal	12	Internal
PRED-TMR (Pasquier *et al.*, 1999)	7	Not predicted	10	Not predicted	10	Not predicted
MEMSAT3 (Jones, 2007)	7	Internal	11	External	12	Internal
SVMtm (Yuan *et al.*, 2004)	8	Not predicted	11	Not predicted	12	Not predicted

Appendix V – Table of signal peptide and cleavage position predictions for OATP1A2, OATP1B3 and OATP2B1

Program	OATP1A2		OATP1B3		OATP2B1	
	Signal peptide	Cleavage position	Signal peptide	Cleavage position	Signal peptide	Cleavage position
iPSORT (Bannai *et al.*, 2002)	No	-	No	-	No	-
Phobius (Kall *et al.*, 2004)	Yes	16	Yes	44	No	-
PrediSi (Hiller *et al.*, 2004)	Yes	16	Yes	351	No	-
PSORT II (Nakai and Horton, 1999)	No	-	No	-	No	-
Sigcleave (von Heijne, 1986)	Yes	16	No	-	Yes	384
SignalP 4.0 (Petersen *et al.*, 2011)	Yes	16	Yes	43	No	-
SIG-Pred (Bradford, 2001)	Yes	16	No	-	No	-
SOSUIsignal (Gomi *et al.*, 2004)	Yes	16	No	-	No	-
SPEPLip (Fariselli *et al.*, 2003)	Yes	16	No	-	No	-

Appendix VI: List of license agreements for copyrighted materials

License agreement for figure 1.3

License number: 2995521209255

License date: Sept 24, 2012

Licensed content publisher: Elsevier

Licensed content publication: Comparative Biochemistry and Physiology Part B: Biochemistry and Molecular Biology

Licensed content title: Molecular cloning and functional characterization of the bovine (*Bos taurus*) organic anion transporting polypeptide Oatp1a2 (Slco1a2)

Licensed content author: Joachim Geyer, Barbara Döring, Klaus Failing, Ernst Petzinger

Licensed content date: March 2004

Volume number: 137

Issue number: 3

Type of use: Thesis/Dissertation

Portion: Figures

Licence agreement for figure 1.4 (not required)

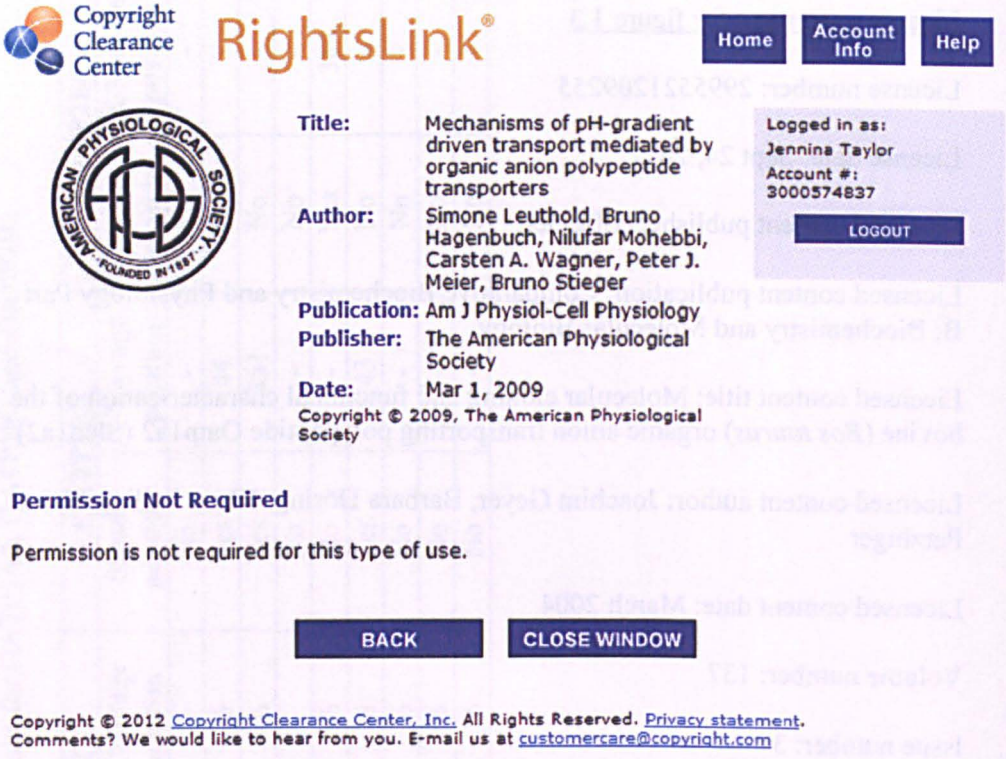

Copyright Clearance Center RightsLink®

Home | Account Info | Help

Logged in as:
Jennina Taylor
Account #:
3000574837
LOGOUT

Title: Mechanisms of pH-gradient driven transport mediated by organic anion polypeptide transporters
Author: Simone Leuthold, Bruno Hagenbuch, Nilufar Mohebbi, Carsten A. Wagner, Peter J. Meier, Bruno Stieger
Publication: Am J Physiol-Cell Physiology
Publisher: The American Physiological Society
Date: Mar 1, 2009
Copyright © 2009, The American Physiological Society

Permission Not Required

Permission is not required for this type of use.

BACK | CLOSE WINDOW

Copyright © 2012 Copyright Clearance Center, Inc. All Rights Reserved. Privacy statement.
Comments? We would like to hear from you. E-mail us at customercare@copyright.com

License agreement for figure 1.5

License number: 2998161206949

License date: Sept 29, 2012

Licensed content publisher: Springer

Licensed content publication: Journal of Membrane Biology

Licensed content title: Organic Anion Transporting Polypeptides of the OATP/ *SLCO* Superfamily: Identification of New Members in Nonmammalian Species, Comparative Modeling and a Potential Transport Mode

Licensed content author: Fabienne Meier-Abt

Licensed content date: Jan 1, 2006

Volume number: 208

Issue number: 3

Type of use: Thesis/dissertation

Portion: Figures

License agreement for figure 1.7

aspet

9650 Rockville Pike
Bethesda, MD 20814-3995

Phone: (301) 634-7060
Fax: (301) 634-7061

info@aspet.org
www.aspet.org

October 4, 2012

Jennina Taylor-Wells
Membrane Transport, Life Sciences
Oxford Brookes University
Gipsy Lane
Headington, Oxford OX3 0BP
UK

Email: jtaylorwells@brookes.ac.uk

Dear Ms. Taylor-Wells:

This is to grant you permission to reproduce the following figure in your thesis titled "Structural and functional determination of OATP1B1 utilising homology modeling and a HEK293T cell system" for Oxford Brookes University:

> Figure 2 from Mikko Niemi, Marja K. Pasanen, and Pertti J. Neuvonen, Organic Anion Transporting Polypeptide 1B1: a Genetically Polymorphic Transporter of Major Importance for Hepatic Drug Uptake, *Pharmacol Rev* March 2011 63:157-181

Permission to reproduce the figure is granted for worldwide use in all languages, translations, and editions, and in any format or medium including print and electronic. The authors and the source of the materials must be cited in full, including the article title, journal title, volume, year, and page numbers.

Sincerely yours,

Richard Dodenhoff

Richard Dodenhoff
Journals Director

American Society for Pharmacology and Experimental Therapeutics

License agreement for table 1.4

License number: 3005961121401

License date: Oct 11, 2012

Licensed content publisher: John Wiley & Sons

Licensed content publication: British Journal of Pharmacology

Licensed content title: Impact of OATP Transporters on Pharmacokinetics

Licensed content author: A Kalliokoski,M Niemi

Licensed content date: Sep 28, 2009

Volume number: 158

Issue number: 3

Type of use: Thesis/dissertation

Portion: Table